

**Isolation and Characterization
of New Antibacterial Active Secondary Metabolites
from Microorganisms
as Potential Starting Points for Drug Discovery**

DISSERTATION

zur Erlangung des akademischen Grades
Doktor der Naturwissenschaften
(Dr. rer. nat.)

dem Fachbereich 08 – Biologie und Chemie
der Justus-Liebig-Universität Gießen

vorgelegt von
Mona-Katharina Bill

Gießen, April 2021

Die vorliegende Arbeit wurde im Zeitraum von Dezember 2017 bis März 2021 am Fraunhofer-Institut für Molekularbiologie und Angewandte Ökologie IME-BR in Gießen unter der Betreuung von Prof. Dr. Peter Hammann angefertigt.

Dissertation eingereicht am: 07.04.2021

1. Gutachter: Prof. Dr. Peter E. Hammann

2. Gutachter: Prof. Dr. Till F. Schäberle

Tag der mündlichen Prüfung: 07.07.2021

Teile dieser Arbeit wurden vorab in folgenden Beiträgen veröffentlicht oder sind in Vorbereitung zur Veröffentlichung:

Publikationen

Bill, M.-K.; Brinkmann, S.; Oberpaul, M.; Patras, M.A.; Leis, B.; Marner, M.; Maitre, M.-P.; Hammann, P.E.; Vilcinskas, A.; Schuler, S.M.M.; Schäberle, T.F. Novel Glycerophospholipid, Lipo- and *N*-acyl Amino Acids from Bacteroidetes: Isolation, Structure Elucidation and Bioactivity. *Molecules* **2021**, *26*, 5195.

Bill, M.-K.; Kleiner, Y.; Flügel, J.L.; Kurz, M.; Spohn, M.; Marner, M.; Mihajlovic, S.; Vilcinskas, A.; Schäberle, T.F.; Hammann, P.E.; Patras, M.A.; Schuler, S.M.M. Isolation, characterization, and bioactivity profiling of oxazoline containing madurastatin siderophores from *Actinomadura* sp. (Manuskript eingereicht bei *J. Antibiot.*)

Tagungsbeiträge

Bill, M.-K.; Schuler, S.M.M.; Vilcinskas, A.; Hammann, P.E. Tackling the resistance crisis: What does the antibiotic pipeline look like? 9th HIPS Symposium, 2019, Saarbrücken, Germany. (Kurzvortrag/Poster)

Hiermit versichere ich, die vorgelegte Thesis selbstständig und ohne unerlaubte fremde Hilfe und nur mit den Hilfen angefertigt zu haben, die ich in der Thesis angegeben habe. Alle Textstellen, die wörtlich oder sinngemäß aus veröffentlichten Schriften entnommen sind, und alle Angaben die auf mündlichen Auskünften beruhen, sind als solche kenntlich gemacht. Bei den von mir durchgeführten und in der Thesis erwähnten Untersuchungen habe ich die Grundsätze guter wissenschaftlicher Praxis, wie sie in der „Satzung der Justus-Liebig-Universität zur Sicherung guter wissenschaftlicher Praxis“ niedergelegt sind, eingehalten. Gemäß § 25 Abs. 6 der Allgemeinen Bestimmungen für modularisierte Studiengänge dulde ich eine Überprüfung der Thesis mittels Anti-Plagiatssoftware.

Schöneiche, 07.04.2021

Ort, Datum

Unterschrift (Mona-Katharina Bill)

Our greatest weakness lies in giving up.
The most certain way to succeed is always to try just one more time.

Thomas A. Edison (1847–1931)

Acknowledgement

First of all, I wish to express my sincere respect and deep gratitude to my supervisor Prof. Dr. PETER HAMMANN for providing the ideal balance between challenging tasks and support to sustainably shape the scientist I have evolved into. The clear and unquestionable way of leading made it pleasant to follow. It has been a privilege to learn from your remarkable expertise and experiences on antibiotic research and drug development in the pharmaceutical industry.

Special thanks go to Prof. Dr. TILL SCHÄBERLE for officiating as second reviewer and being in charge of the natural products group at Fraunhofer IME-BR over the last year. In this regard, I would also like to thank predecessor Dr. JENS GLAESER and head of institute Prof. Dr. ANDREAS VILCINSKAS for giving me the opportunity to be part of this exciting research project.

To all former and present chemistry group leaders: The freedom of action you granted me significantly contributed to the growth I have experienced over the last three years on a professional as well as personal level. Thank you Dr. ARMIN BAUER and Dr. FLORIAN ZUBEIL especially for the assistance in the beginning of this new chapter and ever since despite changed circumstances. Thank you Dr. MARIA A. PATRAS for your cordiality, your unquestioning support at any given moment and sharing your inspiring MS skills with me. And thank you Dr. SÖREN SCHULER for the continuous encouragement and support without equal. Your understanding of teamwork and loyalty is most honorable and I appreciate any way it contributed to me mastering every single challenge along the way. Ever since the friendliest first job interview, I valued every *not* not read mail and all the weekends of *not* not working.

A special word of extraordinary thanks and appreciation to CHRISTOPH HARTWIG for the sheer countless questions answered, for everything I've learned and the mistakes you let me make in this regard, for the trust and responsibility I felt honored to have as well as for every fruitful discussion and idea. All the time spent in windowless, air-conditioned labs filled with the sound vacuum pumps has been a pleasure. Thank you for the glimpse I took below the surface and the imaginary princess crown to your MS kingdom I will take with me.

Huge thanks go to 'my' technical assistants ANGELIKA BROHL, JUDITH HÄRTER, MONA ABDULLAHI. Thank you for facing everyday 'miracles' of isolation wonderland with me, forming my less emotionally attached and more balanced counterpart and for all your very much appreciated assistance.

I tremendously thank JENNIFER KUHN, CHRISTINE WEHR and KIRSTEN BOMMERSHEIM for performing all fermentations/media variations and screenings, respectively. Your efforts marked starting point and finish line of my projects and your ever-helpful support made sure there is no one else I'd rather go to at times of euphoric hope or just after overcoming disappointment.

Furthermore, I would like to thank all supervising postdocs, Dr. BENEDIKT LEIS, Dr. MICHAEL MARNER, Dr. MARIUS SPOHN and Dr. SANJA MIHAJLOVIC, for their constant commitment and the valuable scientific input.

I also thank JANA L. FLÜGEL for the help and dedication during her bachelor thesis on the madurastatin project.

Apart from the Fraunhofer group, I have to express my special gratitude for the support I have received regarding NMR data acquisition and structure elucidation. My greatest respect and admiration go to MICHAEL KURZ. Your expertise and amazing skills beyond comparison still leave me in awe. Thank you MARC-PHILIPPE MAITRE for the provided assistance and guidance. And finally thanks go to the whole NMR team at the JLU Gießen, especially to Dr. HEIKE HAUSMANN for ever trying unremittingly to make the most of my provided samples.

Furthermore, I would like to thank Dr. CHRISTOPH PÖVERLEIN for contributing with his incredible expertise on natural product synthesis and providing more ideas than I could ever have put into practice; thank you YOLANDA KLEINER for helping to at least try.

I also appreciate very much all screenings that have been performed on Evotec side. Thank you to everyone involved in performing the assays and providing the resulting data.

Extra special heartfelt thanks to my PhD colleges for the epic group resilience getting through every day's madness: STEPHAN BRINKMANN, SANDRA SEMMLER, YOLANDA KLEINER and CELINE ZUMKELLER. I'm glad we agreed that the countless hours spent at work together were not enough so that I can now look back at the hilarious pub quiz Thursdays, our weekend in Dublin, games nights, delicious food and even more drinks, watching movies and soccer as well as at all the running and climbing we did.

To my closest family and friends: You are an army of few, yet making me invincible. It is your love and guarding, your faith and support that carries me towards becoming the best person I can be. Words have ever failed to express how deeply I adore you.

To my dad – dad – dad: Your unconditional love and support are fundamental and constant principles of my life. Leading by example, you have raised me knowing I can achieve anything I put my mind to. Thank you for being my father I cannot only look up to but can always come running to.

To my twin brother: I am your biggest fan and incredibly proud of the person you are. Thank you for caring, knowing and protecting me the way you do.

To my husband: You totally mesmerized me the moment we met. I love the way you look at me while trying to explain how I'm isolating 'peas from fresh fruit salad'. Thank you for easing my never-resting mind and for the celebration we call our life.

Abstract

Once considered the ‘magic bullet’, antibiotics no longer satisfy the wonder drug label as antimicrobial resistance (AMR) has largely eradicated the advantages given when first discovered more than 100 years ago.^[1] Stopped research efforts after ‘The Golden Age’ of antibiotics and the major challenges of antibacterial drug development (e.g., discovery of new compounds, performing clinical trials, economic value) resulted in the existing therapeutic gap contributing to the resistance crisis mankind is currently facing.^[2] As most large pharmaceutical companies dropped out of antibiotic research, small firms and research groups are left in the frontline. In order to prevent the 21st century from turning into the ‘post-antibiotic era’, innovative partnerships between academia and industry combining innovative research with expertise represent one promising strategy.^[3] For this purpose, the Public Private Partnership (PPP) between Fraunhofer IME and Sanofi (later Evotec) was established in 2014. The defined Target Product Profile (TPP) towards discovery of novel antibacterial compounds dictated a main focus on Gram-negative (GN) ESKAPE pathogens and *M. tuberculosis* (*Mtb*). Rising to the tremendous challenge based on natural product (NP) research, a discovery platform was built on the Sanofi-Fraunhofer strain collection harboring more than 120,000 different organisms further incorporating innovative screening approaches and focusing on underexplored phyla. Within this pipeline, isolation and structure elucidation of active metabolites focusing especially on novel chemistry remains a crucial part as it allows the identification of potential hit compounds for further hit expansion and lead generation.

In the present PhD thesis, four ‘active-extract-to-hit’ (AE2H) projects covering both GN and *Mtb*-active secondary metabolites from fungal and bacterial producers including the phylum Bacteroidetes were successfully accomplished. In total, the structures of all eight compounds identified by dereplication to cause the initial activity were elucidated comprising four so far unknown NPs. Additionally, 24 analogs were isolated including 14 new metabolites. Overall, the 32 compounds belong to four different NP classes: polyoxygenated and N-heterocyclic arenes, linear peptides as well as amino- and phospholipids. Diverse isolation protocols were developed utilizing various techniques to obtain compounds of interest in sufficient quantity and of adequate purity. Therefore, optimization of fermentation conditions was beneficial. Structure elucidation was achieved by conclusive NMR spectroscopy and strongly supported by ESI-QTOF-MS/MS analysis. Assignment of relative and absolute configuration employed analytical methods (e.g., 2D ROESY NMR analysis) as well as chemical derivatization (e.g., Marfey’s Analysis) and stereoselective total synthesis. Moreover, synthetic chemistry was used to perform first SAR studies. For hit confirmation, bioactivity properties of all isolated and synthesized compounds was extensively investigated (MIC determination, *in vitro* TLR2/TLR4 and cytotoxicity assays). Overall, generated data finally encourage further efforts as promising starting points for future projects were presented.

Table of Content

1. INTRODUCTION	1
1.1 The Antimicrobial Resistance Crisis	1
1.1.1 Historical Outline	2
1.1.2 Current medical need	4
1.1.3 Clinical Development Pipeline	5
1.1.4 Summary and Outlook	8
1.2 Natural Product Drug Discovery	8
1.2.1 Cultivation	9
1.2.2 Screening	10
1.2.3 Dereplication	10
1.2.3.1 Mass spectrometry in NP research	11
1.2.3.2 Molecular Networking	11
1.2.4 Isolation	12
1.2.5 Structure Elucidation	13
1.2.6 Assignment of Stereochemical Configuration	14
1.2.6.1 Relative Configuration	14
1.2.6.2 Absolute Configuration	15
1.3 Outline of this PhD thesis	16
2. GRAM-NEGATIVE ACTIVE METABOLITES FROM ASPERGILLUS TERREUS ST000934	18
2.1 Introduction	18
2.2 Gram-negative Activity against <i>E. coli</i>	19
2.3 Isolation	19
2.4 Structure Elucidation of Fungal Metabolites	20
2.4.1 SF005-B	20
2.4.2 Other Fungal Secondary Metabolites	24
2.5 Antibacterial Activity	26
2.6 Summary	27
3. OXAZOLINE-CONTAINING MADURASTATINS FROM ACTINOMADURA SP. ST100801	29
3.1 Introduction	29
3.2 Dereplication of Madurastatins	31
3.2.1 Gram-negative Activity against <i>E. coli</i> MHC	31
3.2.2 Molecular Networking	32
3.3 Isolation	33

3.4 Structure Elucidation	33
3.5 Assignment of Absolute Configuration by Marfey's Analysis	42
3.6 Stereoselective Synthesis of Madurastatin B1 and Derivatives	44
3.7 Antibacterial Activity	45
3.7.1 Isolated Madurastatins	45
3.7.2 Synthesized Madurastatin Derivatives	47
3.8 Iron Chelating Properties	48
3.9 Summary and Outlook	49
4. AMINO- AND PHOSPHOLIPIDS FROM OLIVIBACTER SP. FHG000416	51
<hr/>	
4.1 Introduction	51
4.2 Gram-negative Activity against <i>E. coli</i> MHC	51
4.3 Isolation	53
4.3.1 FE003 and FE004	53
4.3.2 FE005 and FE006	54
4.3.3 Additional compounds	54
4.4 Structure Elucidation	55
4.4.1 Aminolipids FE003 and FE004	55
4.4.2 Lysophospholipids FE005 and FE006	59
4.4.3 <i>N</i> -Acyl Amino Acids FE008, FE009 and FE010	61
4.4.4. Aminolipids Lipid 430 and FE002	64
4.5 Assignment of Absolute Configuration	65
4.6 Bioactivity Profiling	66
4.6.1 Antimicrobial Activity	66
4.6.2 TLR2/TLR4 Activity	68
4.7 Stereoselective Total Synthesis of FE004	69
4.7.1 Retrosynthetic Analysis: From D-Ribose towards 71a/ <i>ent</i> -71a and 71b/ <i>ent</i> -71b	71
4.7.2 Route Scouting using Ethyl and Butyl Model Systems	72
4.7.3 Synthesis towards 71a and 71b from D-Ribose	74
4.7.4 Retrosynthetic Analysis: From D-Glucose and D-Galactose towards <i>ent</i> -71c and 71d	76
4.7.5 Synthesis of the Julia-Kocienski Olefination Reagent	78
4.7.6 Synthesis towards <i>ent</i> -71c from D-Glucose	79
4.7.7 Synthesis towards 71d from D-Galactose	80
4.7.8 Summary and Outlook	81
4.8 Summary and Outlook	82
5. ANTIMYCOBACTERIAL ACTIVITY OF STREPTOMYCES SP. HAG010336	83
<hr/>	
5.1 Introduction	83
5.2 Antibacterial Activity against <i>M. smegmatis</i>	86

Table of Content

5.3 Media Variation	87
5.4 Isolation	88
5.4.1 Medium 5265	88
5.4.2 Medium SM25	89
5.5 Structure Elucidation	90
5.6 Tandem Mass Spectrometric Investigations	91
5.7 Total Synthesis of SF009 and Derivatives	93
5.8 Bioactivity Profiling	94
5.8.1 Antimicrobial Activity	94
5.8.2 Dereplication of Antimycobacterial Active Secondary Metabolites	95
5.8.3 Cytotoxicity	98
5.9 Summary	98
6. SUMMARY AND CONCLUSION	99
<hr/>	
7. EXPERIMENTAL	103
<hr/>	
8. APPENDIX	151
<hr/>	
9. REFERENCES	196
<hr/>	
10. PROJECT CONTRIBUTIONS	209

Abbreviations

<i>A. baumannii</i>	<i>Acinetobacter baumannii</i>	DIBAL-H	diisobutylaluminiumhydrid
ACN	acetonitrile	DMF	dimethylformamide
AMK	amikacin	DMP	Dess-Martin periodinane
AMR	antimicrobial resistance	DMSO	dimethyl sulfoxide
API	atmospheric pressure ionization	DNA	deoxyribonucleic acid
A2H	active-to-hit	<i>E. coli</i>	<i>Escherichia coli</i>
AUC	area under curve	<i>E. faecalis</i>	<i>Enterococcus faecalis</i>
<i>B. subtilis</i>	<i>Bacillus subtilis</i>	<i>E. faecium</i>	<i>Enterococcus faecium</i>
BDQ	bedaquiline	ECD	electronic circular dichroism
BLI	β -lactam inhibitor	EDC	1-ethyl-3-(3-dimethylamino- propyl)carbodiimide
BPC	base peak chromatogram	<i>ee</i>	enantiomeric excess
<i>C. albicans</i>	<i>Candida albicans</i>	EIC	extracted ion chromatogram
CC	column chromatography	ELSD	evaporative light scattering detector
CDA	chiral derivatizing agent	EMB	etambutol
CHCl ₃	chloroform	ESBL	extended-spectrum β -lactamases
CID	collision-induced dissociation	ESI	electrospray ionization
COSY	correlation spectroscopy	EtOAc	ethyl acetate
δ	chemical shift	FA	formic acid
Da	Dalton	FDA	Food and Drug Administration
DAD	diode array detector	FDAA	N α -(2,4-dinitro-5-fluoro- phenyl)alaninamide
DAST	diethylaminosulfur trifluoride	FDVA	N α -(2,4-dinitro-5-fluoro- phenyl)valinamide
dbe	double bond equivalent	GC	gas chromatography
DBO	diazabicyclooctane		
DCM	dichloromethane		
DIAD	diisopropyl azodicarboxylate		

Abbreviations

HEK	human embryonic kidney	<i>M. smegmatis</i>	<i>Mycobacterium smegmatis</i>
HETLOC	heteronuclear long-range coupling	<i>M tuberculosis</i> ,	<i>Mycobacterium tuberculosis</i>
HMBC	heteronuclear multiple-bond correlation	<i>Mtb</i>	
HPLC	high-performance liquid chromatography	<i>m/z</i>	mass-to-charge ratio
HR	high resolution	MABA	Microplate Alamar Blue Assay
HSQC	heteronuclear single quantum correlation	MBL	metallo- β -lactamases
IC _{50/80}	50%/80% inhibitory concentration	<i>m</i> -CPBA	<i>meta</i> -chloroperoxybenzoic acid
IEC	ion exchange chromatography	MDR	multidrug resistant
INH	isoniazid	MeOH	methanol
IR	infrared	MHC	Mueller-Hinton bicarbonate
<i>J</i>	coupling constant	MHB	Mueller-Hinton II broth
<i>K. pneumonia</i>	<i>Klebsiella pneumoniae</i>	MIC	minimum inhibitory concentration
KAN	kanamycin	MoA	mode of action
KHMDS	potassium bis(trimethylsilyl)amide	MRSA	methicillin/multi-resistant <i>Staphylococcus aureus</i>
LC	liquid chromatography	MS	mass spectrometry
LiHMDS	lithium bis(trimethylsilyl)amide	MsCl	methanesulfonyl chloride
LLE	liquid-liquid extraction	MSSA	methicillin-sensitive <i>Staphylococcus aureus</i>
LPE	lysophosphatidylethanolamine	MTBE	methyl <i>tert</i> -butyl ether
LPS	lipopolysaccharide	MTPA	α -methoxy- α -trifluoromethyl- α -phenylacetic acid
<i>M. catarrhalis</i>	<i>Moraxella catarrhalis</i>	NBE	new biological entry
<i>M. luteus</i>	<i>Micrococcus luteus</i>	NCE	new chemical entry
		NDM	New Delhi metallo- β -lactamase
		NMR	nuclear magnetic resonance

Abbreviations

NOE	nuclear Overhauser effect	RT	room temperature
NOESY	nuclear Overhauser effect spectroscopy	<i>S. aureus</i>	<i>Staphylococcus aureus</i>
NP	natural product	SAR	structure-activity relationship
OD	optical density	SEC	size exclusion chromatography
OR	optical rotation	sp.	species
ORD	optical rotatory dispersion	SPE	solid-phase extraction
OSMAC	'one strain many compounds'	TB	tuberculosis
Oxyma	ethyl cyanohydroxyimino acetate	TBAF	tetra- <i>n</i> -butylammonium fluoride
<i>P. aeruginosa</i>	<i>Pseudomonas aeruginosa</i>	TBS	<i>tert</i> -butyldimethylsilyl
PBP	penicillin-binding protein	TCCA	trichloroisocyanuric acid
ppm	parts per million	TEA	triethylamine
PPP	Public Private Partnership	TEMPO	(2,2,6,6-tetramethylpiperidin-1-yl)oxyl
PZA	pyrazinamide	THF	tetrahydrofuran
QIT	quadrupole ion trap	TIPS	triisopropylsilyl
QTOF	quadrupole time-of-flight	TLC	thin-layer chromatography
R	undefined substituent	TPP	Target Product Profile
R _f	retardation factor	<i>t_R</i>	retention time
RIF	rifampicin	Tr	trityl
RNA	ribonucleic acid	UPLC	ultra high-performance liquid chromatography
ROA	Raman optical activity	UV/vis	ultraviolet/visible light
ROE	rotating-frame nuclear Overhauser effect	VCD	vibrational circular dichroism
ROESY	rotating frame Overhauser effect spectroscopy	VRE	vancomycin-resistant <i>enterococci</i>
RP	reversed-phase	WHO	World Health Organization
RPT	rifapentine	XDR	extensively drug-resistant
RR	rifampicin-resistant		

1. Introduction

1.1 The Antimicrobial Resistance Crisis¹

The discovery of antibiotics is considered one of the greatest breakthroughs in the history of modern medicine. Ironically, it led to one of the most serious threats to human health only one century later as antimicrobial resistance (AMR) is an inevitable consequence of antibiotic chemotherapy.^[5] The resistance crisis of current times is the result of rapidly emerging and spreading AMR promoted by misuse of antibiotic drugs that are now no longer effective. Especially multidrug-resistant (MDR) ESKAPE pathogens (*Enterococcus faecium*, *Staphylococcus aureus*, *Klebsiella pneumoniae*, *Acinetobacter baumannii*, *Pseudomonas aeruginosa* and *Enterobacter* sp.) largely contribute to the alarming situation in which mankind is more and more often left with very few or even no options for the treatment of bacterial infections.^[6]

As evolutionary response to the selective pressure, bacteria have developed effective strategies to withstand the harmful effect of antibiotics. On genetic level, adaptation occurs either by mutation or horizontal gene transfer, which is possible even between different species. Resistance mechanisms involve inactivation of the antimicrobial compound by modification or degradation, preventing it from reaching its molecular target by restricted uptake or active extrusion *via* efflux mechanisms, modification of the antibiotic target as well as bypassing its essentiality. Notably, multiple pathways are most of the time simultaneously used to develop antibiotic resistance.^[7]

One outstandingly important example due to its clinical relevance is β -lactamase-mediated resistance to β -lactams, which are the most commonly used antibiotics.^[8] These bacterial enzymes hydrolyze the amide bond of the essential β -lactam pharmacophore and thereby inactivate this class of antibiotics mainly consisting of penicillins, cephalosporins, carbapenems and monobactams. According to Ambler, β -lactamases are divided into the classes A, C and D of active-site serine β -lactamases as well as the class B of zinc-dependent metallo- β -lactamases (MBLs). Increasing incidence of extended-spectrum β -lactamases (ESBLs) and carbapenemases, especially MBLs such as New Delhi metallo- β -lactamase 1 (NDM-1), represent major current problems, in particular true for Gram-negative bacteria. New β -lactamase inhibitors (BLIs) that rise up to these challenges could maintain the effectiveness of some of the most valuable antibiotics for now. In the long term however, only novel antibiotics with new mode of actions (MoAs) will manage to overcome the resistance crisis.^[9]

¹ If not states otherwise, all information resented in this chapter are based on a conference contribution.^[4]

Before starting research to tackle the challenges of AMR, it is crucial to define a Target Product Profile (TPP). The benchmark is one of the key questions that need to be answered thereto. This includes: i) the current medical need, ii) the clinical development pipeline and iii) recently approved drugs. These aspects will be discussed in the following chapter with a focus on novel systemic antibiotics used for treatment of community-acquired and nosocomial bacterial infections. For the reason of distinctly different pharmacokinetic and pharmacodynamic profiles, this excludes antibiotics that are: i) topically applied to treat e.g., skin or eye infections, ii) orally administered but not resorbed for the purpose of treating *Clostridium difficile* infections or iii) used for the treatment of *Mycobacterium tuberculosis* (*M. tuberculosis*) infections. The latter will be outlined in another chapter of this work (see chapter 5).

1.1.1 Historical Outline

The history of antibiotics started more than 100 years ago with the discovery of the synthetic salvarsan in 1909 and revolutionized modern medicine.^[10] Sulfamidochrysoidine (Prontosil) represented the sulfonamides as first clinical relevant class of antimicrobials that was introduced in the 1930s.^[11] In the 1940s, discovery of the first natural product (NP) antibiotic penicillin started an era of extensive research efforts towards finding new antibacterial drugs. In fact, 15 of the 22 antibiotic classes approved up to the present day were introduced in the following 30 years known as ‘The Golden Age’ of antibiotics (Fig. 1). Given the success, further research was considered groundless and therefore terminated. Additional reasons, such as economic value and challenges of discovering new antibiotics as well as performing clinical trials, resulted in the current therapeutical gap.^[2] For the rest of the millennium, no major novel class against Gram-positive pathogens was introduced until linezolid was discovered 40 years later. However, no major novel antibiotic was discovered ever since to treat Gram-negative infections.

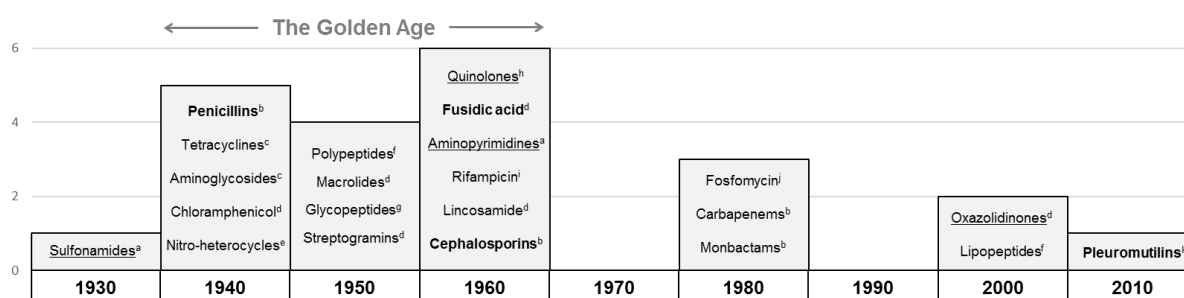


Fig. 1: Approved classes of antibiotics since 1930 sorted by the decade of introduction. Synthetic classes are underlined; fungal natural product classes are written in bold. Molecular targets: ^afolic acid metabolism, ^bpenicillin-binding proteins (PBPs), ^c30S ribosome, ^d50S ribosome, ^eDNA interaction, ^fmembrane, ^gpeptidoglycan precursors, ^hDNA synthesis, ⁱRNA synthesis, ^jMurA, ^k50S ribosome.

The number of approved antibiotics in relation to the overall approved New Chemical and Biological Entries (NCEs and NBEs) decreases constantly providing further evidence for the current therapeutic

1. Introduction

gap in the treatment of infectious diseases (Fig. 2). Moreover, most of these launched antibiotic drugs are only derivatives within the known compound classes.

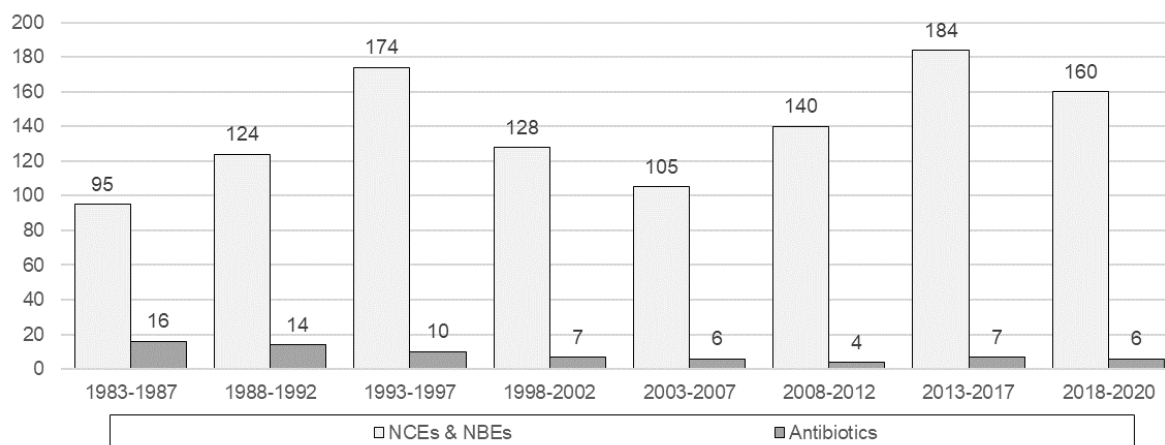


Fig. 2: Number of FDA approved NCEs and NBEs as well as antibiotics since 1983 in five year intervals.^[12]

In fact, since 2000 only three first-in-class systemic antibacterials were approved: i) oxazolidinone linezolid (2000), ii) lipopeptide daptomycin (2003) and iii) pleuromutilin lefamulin (2019). All exhibit either mainly or only Gram-positive activity.^[13] Although the introduction of a new class of Gram-negative antibiotics remains elusive, three recently launched novel structures within the known antibiotic classes are worth mentioning (Fig. 3). Diazabicyclooctane (DBO) avibactam (**1**) and boronate-type vaborbactam (**3**) represent two novel BLIs approved over the last decade (2015 and 2017). As for most BLIs, they lack direct antibiotic activity but in combination with β -lactams however, they can be used for treatment of Gram-negative infections and demonstrate an overall better profile against serine β -lactamases. With the approval of cefiderocol (**4**) in November 2019, a promising candidate had successfully completed clinical development. This cephalosporin was designed as ‘Trojan horse’ to utilize the iron transport pathway *via* siderophores for entering bacterial cells.^[14] Additionally, Gram-negative pathogens can be entered *via* a porin-mediated pathway which helps to balance the risk of a fast resistance development against the siderophore transporter. Surprisingly, the catechol siderophore moiety also increases the MBL stability by coordinating the metal atom of the enzyme.

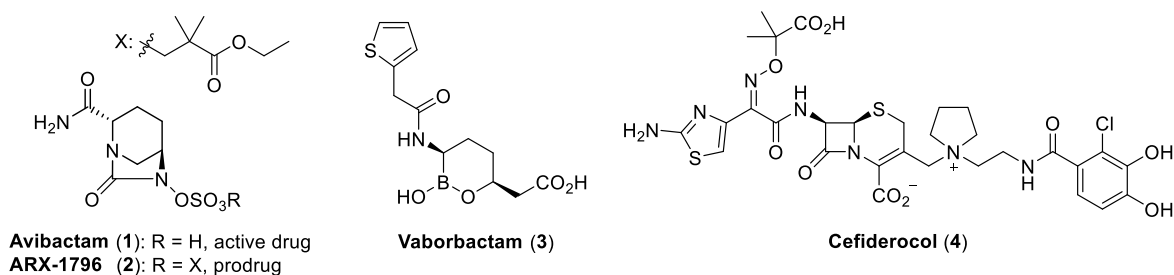


Fig. 3: Chemical structures of avibactam (**1**) and prodrug ARX-1796 (**2**), vaborbactam (**3**) and cefiderocol (**4**).

1.1.2 Current medical need

The most prominent example for multidrug-resistant pathogens is the Gram-positive MRSA (methicillin/multi-resistant *Staphylococcus aureus*). But in fact, various antibiotics are approved and available, for which no resistance occurs so far (Table 1).^[15] However, treatment frequently fails as a result of challenges other than resistance. For example, penetration issues and biofilm formation are causes that prevent antibiotics from either reaching the site of infections or taking full effect.^[16]

By far less treatment options are available for vancomycin-resistant *enterococci* (VRE) including

E. faecium and *E. faecalis*. Especially infective endocarditis is a major issue here as it requires penetration into the heart muscle and bactericidal activity which only daptomycin exhibits from the antibiotics investigated herein since tigecycline and linezolid are bacteriostatic agents (Table 1).^[17]

The examples of MRSA and VRE demonstrate that, when it comes to Gram-positive bacteria, penetration into tissue such as necrotic tissue or the heart muscle rather than resistance is the major challenge. Appropriate assays to investigate this issue as early as possible in the preclinical drug development would be highly advantageous and are acutely needed.

On top of penetration issues, resistance is a major challenge when it comes to Gram-negative bacteria. As pointed out above, resistance acquired by producing β -lactamases is a severe problem. In particular,

Table 2: Resistances of ESBL-forming *Klebsiella* sp. and *P. aeruginosa* against present antibiotics in Germany (status 2018; compared to 2017).^[15]

Resistance (%) in Germany [2018]		
Present Antibiotics	<i>Klebsiella</i> (ESBL)	<i>P. aeruginosa</i>
Cephalosporin (3rd generation)	12.9 (-1.7)	9.8 (-0.7) ^a
Piperacillin/Tazobactam	n.d. ^b	13.5 (-2.0)
Aminoglycosides	6.2 (-2.0)	3.6 (-1.2)
Carbapenems	0.4 (-0.1)	12.1 (-0.5)
Quinolones	13.3 (-2.0)	12.3 (-1.6)
Tigecycline	n.d. ^b	not active
Colistin	toxic	toxic

^aReferring to Ceftazidime as specific example.

^bNo data available.

is alarming and points out once more that novel antibiotics against Gram-negative bacterial infections are urgently needed.

Table 1: Resistances of MRSA and VRE against present antibiotics in Germany (status 2018).^[15]

Resistance in Germany [2018]		
Present Antibiotics	MRSA	VRE
Vancomycin	✓	× ^a
Daptomycin	✓	✓
Tigecycline	✓	✓
Linezolid	✓	✓
Synercid	✓	(✓) ^b
Telavancin	✓	×
Ceftaroline	✓	×

^a*E. faecium*: 23.8% (+ 7.3% since 2017).

^bSynercid only active against *E. faecium*, not *E. faecalis*.

this applies to MBLs due to their ability to hydrolyze carbapenems representing the last treatment option against ESBLs. A striking example for the severe consequences is *Pseudomonas aeruginosa*, an opportunistic pathogen noted for its inherent antibiotic resistance.^[18] In addition to that, diverse resistance mechanisms lead to MDR and result in depletion of the very few treatment options available at all. For the treatment of multidrug-resistant *P. aeruginosa* there is already only one toxic reserve antibiotic left, namely colistin (Table 2). This fact is

1. Introduction

1.1.3 Clinical Development Pipeline

Since recent approvals in 2019², the clinical development pipeline currently contains 28 compounds including three novel compounds with Gram-positive activity only and three new derivatives with remarkable properties and Gram-negative activity (Table 3).

Table 3: Compounds currently in clinical development according to their antibiotic class and clinical phase (status 03/2020). Compounds with novel structures are underlined; compounds possibly active or active against Gram-negative ESKAPE pathogens are written in bold.

Classification	Antibiotic class	Compound; active company			Total
		Phase III or beyond	Phase II	Phase I	
Known compound classes	Hybrids	Ceflavancin (TD-1792); R-Pharm/Theravance ^a	TNP-2092; TenNor	TNP-2198; TenNor ^b	3
	Aminoglycosides			Apramycin (EBL-1003, repurposed); Juvabis	1
	Ketolides		Nafithromycin (WCK-4873, OP-1068); Wockhardt		1
	Oxazolidinones	Contezolid (MRX-I); MicuRx			1
	Quinolones		Finafloxacin (BAY-35-3377); Merlion ^a		1
	Tetracyclines			KBP-7072 ; KBP Biosciences ^a TP-271 ; Tetraphase TP-6076 ; Tetraphase	3
	β -Lactams	Sulopenem ; Iterum	BOS-228 ; Boston Pharmaceuticals Benapenem; Sihuan	AIC-499 ; AiCuris ^a	4
Non-antibiotic active enhancers	β -Lactamase inhibitors (BLIs)	Enmetazobactam (AAI-101)/cefepime; Allegra		Nacubactam (OP-0595, RG-6080)/meropenem; Fedora/Meiji	8
		Durlobactam (ETX-2514)/sulbactam; Entasis		Zidebactam /cefepime; Wockhardt	
		Taniborbactam (VNRX-5133)/cefepime; VenatoRx		ETX0282CPDP /cefepime; Entasis	
				VNRX-7145 /ceftibuten; VenatoRx ARX-1796 (Avibactam prodrug); Arixa	
Novel compound classes	Peptides			SPR-741 /antibiotic; Northern Antibiotics SPR-206 ; Spero	2
	Other structures	<u>Gepotidacin</u> (GSK-2140944); GSK <u>Zoliflodacin</u> (EXT0914); Entasis	<u>Afabicin</u> (AFN-1252, Debio-1452); Debiopharm		3
unknown class/structure				BCM-0184; Biocidium	1
Total		8	6	14	28

^aCompounds likely to have been discontinued from clinical development.

^bStructure not publically disclosed; likely to be hybrid like TNP-2092.

One of Gram-positive active novel compounds is benzofuran naphthyridine afabycin (**5**). Currently in phase II, **5** is the prodrug of Debio-1452 (**6**) and targets the bacterial type I fatty acid biosynthesis. Molecular target of novel zoliflodacin (**7**) and gepotidacin (**8**) is the DNA replication. As gyrase inhibitors they share the mode of action with the quinolones, however no cross-resistance is observed. On this account, the potential of these phase III candidates lies in the treatment of quinolone-resistant *Neisseria gonorrhoea* infections in the community despite their activity mainly against Gram-positive pathogens (Fig. 4).

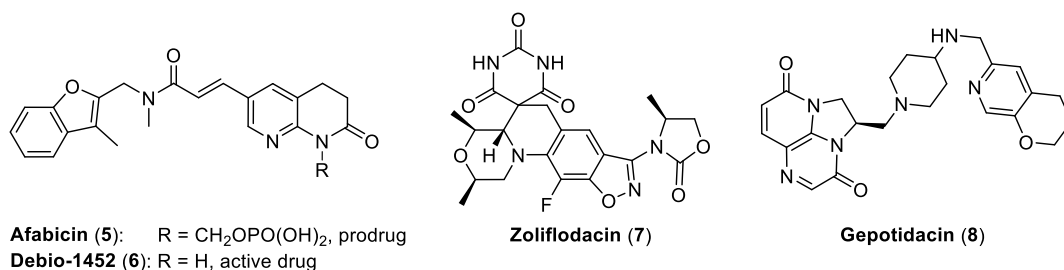


Fig. 4: Chemical structures of novel compounds currently in clinical development.

² Fluoroquinolones lascefloxacin (KYORIN; launched in Japan) and alalevonadifloxacin (WOCKHARDT; launched in India) as well as cephalosporin siderophore cefiderocol (SHIONOGI), pleuromutilin lefamulin (NABRIVA), and BLI relebactam (MERCCK) in combination with imipenem.

1. Introduction

In terms of the current medical need, there is no novel compound presently in clinical development exhibiting activity against Gram-negative pathogens. One of such clinical candidates that have most recently dropped out of the development pipeline is SPR719 (**9**). This novel gyrase inhibitor had previously been investigated in combination with the uptake enhancer SPR741 (**11**) by SPERO THERAPEUTICS. However, its phosphate prodrug SPR720 (**10**) is now being developed for the treatment of tuberculosis (see chapter 5). Furthermore, the company decided to continue with SPR206 (**12**) as its lead product candidate. Instead, originator company NORTHERN ANTIBIOTICS carried on with **11** in conjunction with a partner antibiotic since itself has no direct activity. Both compounds (**11** and **12**) are colistin derivatives and target the cell wall which leads to disruption of the outer membrane of Gram-negative bacteria. However, further clinical studies have to prove that the side effects of both candidates are tolerable for patients with severe infections (Fig. 5).

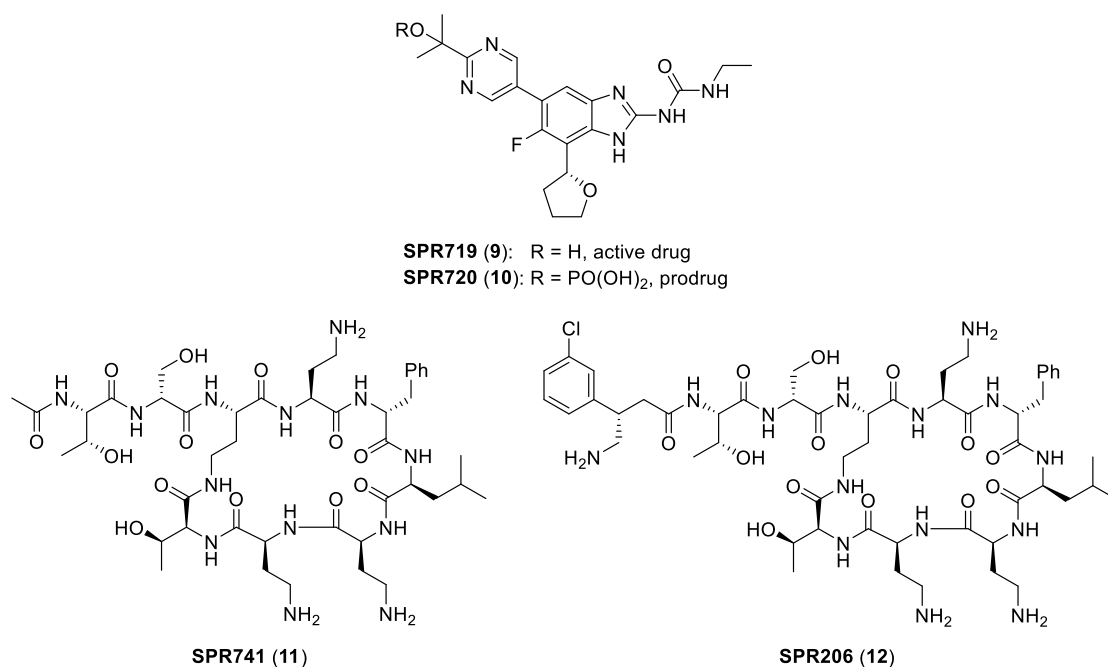


Fig. 5: Chemical structures of former and current SPR compounds **9–12** in clinical development.

The toxicity profile of macrocyclic peptides is often a major hurdle for drug approval which was proven once more when clinical development of murepavadin (**13**) was stopped in 2019 due to kidney toxicity. Now, **13** is under investigation in the context of a potential inhalative application (Fig. 6). However, since the termination of POLYPHOR's phase III candidate, there is no novel compound currently in the pipeline to meet the medical need by exhibiting activity especially against *Pseudomonas*.

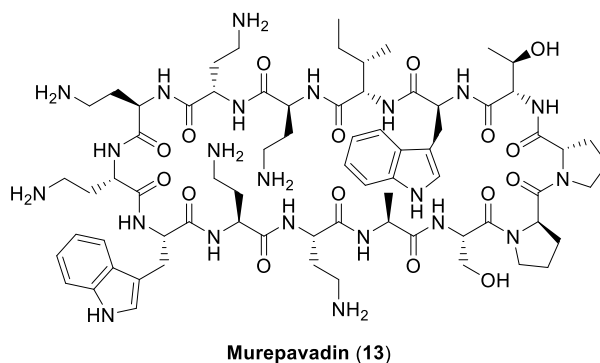


Fig. 6: Chemical structure of murepavadin (13).

With increasing cephalosporin resistance, carbapenems (such as benapenem currently in phase II, not shown) are the only treatment option left. But consequently, MBL-mediated resistance will increase in near future. Therefore, new derivatives of known compound classes with activity against MBLs expressing Gram-negative bacteria are an important contribution to the pipeline. This is true for three of the seven³ β -lactamase inhibitors currently under clinical investigation in combination with known β -lactam antibiotics (Fig. 7).

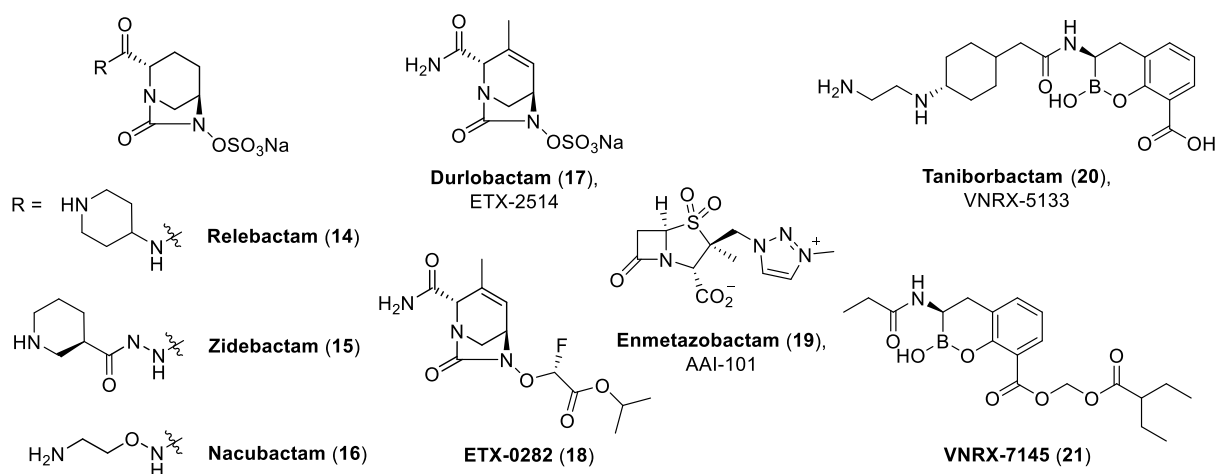


Fig. 7: Chemical structures of BLIs either marketed (14) or in clinical development (15–21).

The DBOs zidebactam (15) and nacubactam (16) are currently in phase I. They are combined with cephalosporins and act as BLIs for class A and C β -lactamases (Table 4). The activity also observed for class B β -lactamases is explained by a direct antibiotic activity inhibiting PBP2. The phase III boronate-type taniborbactam (20) in combination with cefepime is active against class A and C β -lactamases by covalent binding, whereas competitive binding is observed for MBLs. The structurally related VNRX-7145 (21), new to the pipeline, lacks this beneficial activity against class B β -lactamases. In combination with ceftibuten, the oral bioavailability of this phase I candidate is still advantageous.

³ ARX-1796 (2) as avibactam (1) prodrug is not included here.

1. Introduction

Table 4: Susceptibility of selected β -lactam antibiotics to all classes of β -lactamases and efficacy of marketed BLIs and those currently in clinical development.

β -lactamases		Suceptibility to		Marketed BLIs				BLIs in development						
		3 rd generation Cephalosporins	Carbapenems	Clavulanic acid	Avibactam (1)	Vaborbactam (3)	Relebactam (14)/ imipenem	Zidebactam (15)/ cefepime	Nacubactam (16)/ meropenem	Durlobactam (17)/ subbactam	ETX-0282 (18)/ cefpodoxime	Enmetazobactam (19)/ cefepime	Taniborbactam (20)/ cefepime	VNRX-7145 (21)/ cefibuten
Ambler class	Examples													
A	TEM, SHV (ESBL)	-	+	+	+	+	+	+	+	+	+	+	+	+
	KPC	-	-	+	+	+	+	+	+	+/-	+	+	+	+
B	NDM, IMP, VIM	-	-	-	-	+/-	-	+	+	-	-	-	+	-
C	AMP C	-	+	-	+	+	+	+	+	+	+	+	+	+
D	OXAs	+/-	+/-	+/-	+/-	+/-	+/-	+/-	+/-	+	+/-	+/-	+	+

1.1.4 Summary and Outlook

The prevalence of antimicrobial resistance has turned the treatment of Gram-negative infections into one of the major challenges of our time. Although this problem is predominantly observed in hospitals, its effect on community-acquired infections is most likely to increase as the black box warnings now strongly limits the indication of quinolones in this area.^[19] From that, yet another gap will emerge due to the oral application, tissue distribution and broad Gram-negative activity of this antibiotic class.

Recent advances and the current clinical development pipeline can only provide very limited advantage over present bacterial resistance. Novel approaches in academia and industry are urgently needed to close the existing gaps and overcome the resistance crisis in order to prevent the 21st century from turning into the ‘post-antibiotic era’.^[3] To meet this tremendous challenge, a strategic Public Private Partnership (PPP) was established between Fraunhofer IME and Sanofi (later Evotec) in 2014. This cooperation pursued the ambitious goal to discover and develop novel antimicrobial agents for the treatment of infectious diseases with a strong focus on Gram-negative infections. For this purpose, the Sanofi strain collection as well as extract libraries were extensively studied and further expanded to utilize natural products as fertile source for drug discovery.

1.2 Natural Product Drug Discovery

The importance of natural products as source for pharmaceutical drugs such as anti-infective agents is undeniable.^[20] As the ‘low-hanging fruits’ have already been picked, rediscovery of known compounds has become a major hurdle. New strategies are being pursued at all stages along the NP discovery process to ensure that efforts will continue to successfully explore the vast yet mostly untapped biological and chemical diversity of microbes and deliver new lead structures.^[21]

Based on their starting point, discovery processes can be divided into two categories. On the one hand, genomics-based approaches have been evolving rapidly since microbial whole-genome sequencing is available and becoming even more economical. Starting at DNA level, bioinformatics tools and gene manipulation techniques are used to identify and express gene clusters of interest in either native or heterologous hosts. The aim is to fully exploit biosynthetic potential and metabolic capabilities of any given microorganism.^[21] On the other hand, more traditional approaches start at microorganism level. Concepts and advances will be discussed below in more detail.

1.2.1 Cultivation

In order to find new active compounds, it is essential to access new natural resources.^[22] Therefore, in addition to commonly explored soil samples from terrestrial environment, other sources are being widely sampled for antibiotic producing microorganisms. This includes domains like oceans, rainforests and deserts besides other environmental niches. Symbiotic and endophytic microorganisms living associated with their hosts (e.g., plants^[23], insects and nematodes^[24]) are another example for potent sources that have only recently started to be explored.

Besides profound investigation of the microbial diversity in nature, it is also important to improve access to their full biosynthetic potential.^[22] Organisms cultivated under laboratory conditions face optimal growth conditions. In their natural habitat however, they are confronted with diverse environmental stress caused by e.g., interactions with other species or nutrient deficiency.^[21] Mimicking these conditions so that microorganisms are triggered to activate otherwise silent genes and express further metabolites in order to survive, is one approach that has successfully been implemented. This involves varying medium compositions (including minimal medium), different cultivation status (solid or liquid, dynamic or static), co-cultivation with other strains and adding epigenetic modifier or other factors such as enzyme inhibitors or biosynthetic precursors. This strategy is referred to as OSMAC ('one strain many compounds') approach.^[25]

Evaluation of any cultivation-dependent approach generally requires the extraction of a grown culture so that the obtained crude extract can be analyzed and subjected to primary *in vitro* bioassays for example. However, this principle is only applied to the very small fraction of microorganisms that can be grown in a laboratory.^[26] Yet, the vast majority is either uncultured or unculturable. This 'microbial dark matter' presents both challenges and opportunities.^[27] While certain techniques (e.g., metagenomics) do not require cultivation to provide information, it remains essential when aiming for true understanding of the diverse aspects and complex nature of a microbial species. Recent advances in innovative cultivation such as encapsulation of environmental cells in microdroplets raise hope that one day we will be up to the challenge with yet a long way to go.^[28]

1.2.2 Screening

Searching for new antibacterial compounds, bioactivity screening remains essential at various stages along the discovery process. Traditionally, target-based or phenotypic high-throughput screening (HTS) strategies are employed.^[2] The less relevant target-based approach directly tests against certain molecular targets represented by recombinant proteins. However, when translated into whole-cell screenings, permeability and efflux occur as major issues.^[29] Instead, the phenotype-based approach is widely used. On the one hand, *in vitro* antibiotic susceptibility testing (AST) of concentrated extracts obtained from diverse cultivation approaches represents the starting point for activity-guided isolation.^[2] However, interfering or synergistic effects within such complex mixtures may affect the validity of the results. Therefore, advanced strategies to simplify extracts include adapted extraction methods and pre-fractionation.^{[30][31]} Following isolation on the other hand, AST is also used to determine the minimal inhibitory concentration (MIC) of the purified compounds in order to evaluate the antibacterial potency.^[2] Covering both stages, advanced screening strategies have been developed to increase the active extract hit rate as well as to improve the prediction value towards *in vivo* efficiency in mouse models. This includes mimicking of environmental factors relevant for pathogenic bacteria during host infection e.g., by using NaHCO₃ supplemented Mueller-Hinton broth (MHC) screening medium since it has been shown that the host's bicarbonate buffer system disrupts the proton motive force across bacterial membranes by dissipating the transmembrane pH gradient.^{[32][33]} For phenotypic screenings in general however, toxicity and target identification remain the major challenges. In order to overcome general limitations, further improved approaches combine target-based and whole-cell screening methods using genetically modified screening strains either expressing reporter genes or differing from wild-type strains regarding engineered antibiotic resistance or gene deletion/overexpression.^[29]

1.2.3 Dereplication

Differentiation between previously described and novel metabolites is important to save a considerable amount of time and resources on re-isolation.^[34] Therefore, identification of known active compounds and potential analogues in crude extracts is a crucial part of NP discovery.^{[35][36]} This process is called dereplication and typically involves chromatographic techniques such as reversed-phase (RP) high-performance liquid chromatography (HPLC) or ultra high-performance liquid chromatography (UPLC) as well as spectroscopic and spectrometric methods in combination with bioactivity screening. Based on features such as retention time, UV/vis absorption, exact mass and MS/MS fragmentation pattern, compounds detected in active fractions are then evaluated by database search using either in-house or commercial databases like Antibase or Dictionary of Natural Products.^[37]

1.2.3.1 Mass spectrometry in NP research

Since the introduction of more gentle ionization techniques at atmospheric pressure (atmospheric pressure ionization, API) such as electrospray ionization (ESI), mass spectrometry (MS) became an indispensable analytical method in NP research.^[38] Besides the advantageous combinability with liquid chromatography (LC) extending the scope of application to non-volatile organic compounds, high sensitivity as well as continuously improving resolution and mass accuracy are major advantages of MS analysis.^[35] This allows the prediction of elemental composition of a given ion even for minor components in a complex mixture such as extracts of microbiological origin.^[37] However, complex and unpredictable fragmentation and adduct formation pattern complicate the identification of the parent ion and therefore the correct assignment of a molecular formula.^[35] Furthermore ionization efficiency and consequently sensitivity is strongly dependent on the compound's structure as well as co-eluting impurities. Their interfering in terms of ion suppression imposes another limitation to the method.^[39] For dereplication, ESI is commonly combined with hybrid quadrupole time-of-flight (QTOF) and quadrupole ion-trap (QIT) mass spectrometers due to their ability to perform untargeted tandem MS by collision-induced dissociation (CID) besides high mass accuracies.^[35] This way, MS/MS data is acquired in high-throughput manner without requiring additional effort but providing further useful information. Modern computational approaches like Molecular Networking are being increasingly exploited as tools for dereplication to support interpretation of the enormous MS/MS data sets.^[40]

1.2.3.2 Molecular Networking

Based on the fundamental assumption that structurally related compounds share a similar MS/MS fragmentation pattern, Molecular Networking is a tool to visualize the chemical similarity of all precursor ions detected and fragmented in large sample sets analyzed by tandem mass spectrometry.^[41] Preprocessing of the generated MS/MS data involves removal of precursor and low-intensity fragment ions as well as merging identical spectra sharing the same parent ion m/z value and fragmentation pattern into a single consensus spectrum (Fig. 8).^[42] For generation of the molecular network analysis, the simplified spectra are converted into multidimensional vectors taking m/z values and intensity of fragment ions into account.^[43] The similarity of these normalized vectors is calculated for every possible pair of consensus spectra. The resulting cosine scores represent the degree of spectral similarity ranging from 0 to 1 whereby a value of 1 indicates completely identical spectra. Programs like Cytoscape can be used to visualize the output of this algorithm-based analysis in form of so called Molecular Networks. All MS/MS consensus spectra are represented by nodes (typically labeled with the mass of the parent ions) while the thickness of edges connecting two nodes indicates the degree of similarity of the according pair.^[40]

Therefore, Molecular Networking is a powerful dereplication tool especially when database search is included in the analysis. It not only allows rapid identification of known molecules in complex

1. Introduction

mixtures but also identifies potential analogs and thus provides valuable information in regard to pursuing the isolation of individual compounds.

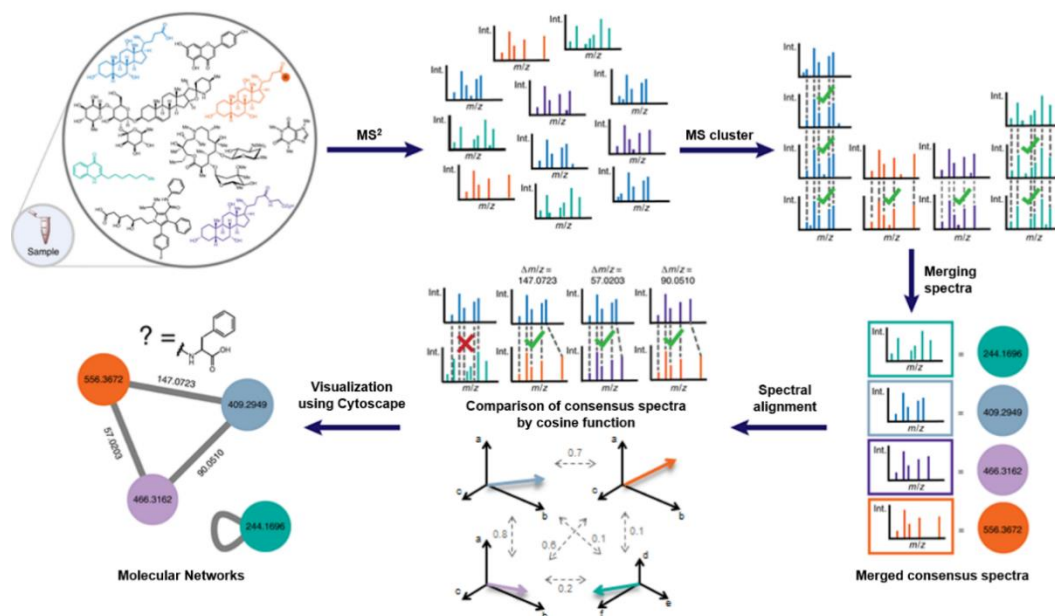


Fig. 8: Schematic representation of the process of generating a Molecular Network. Adapted and modified from ARON *et al.*^[44] and BOUDREAU *et al.*^[45]

1.2.4 Isolation

Once dereplication identified an active and potentially novel compound of interest, isolation takes place. The goal is to obtain a sufficient amount of the target compound pure enough for structure elucidation and further characterization. Despite continuous progress made in the development of extraction and purification techniques, this remains a major challenge. The complexity of most extracts as well as limited biosynthetic production of certain components complicates the task. Furthermore, isolation protocols need to be designed individually for each target compound. Information about general molecular features like stability, solubility, acid-base properties and charge are advantageous but usually not given.^[46] Therefore it is advisable to investigate the expediency of each isolation step by performing preliminary tests.

Fermentation of the producing microorganism represents the starting point for isolation. Optimization of cultivation conditions such as medium composition, salinity, pH, temperature, oxygen concentration and time of incubation can be an efficient approach to increase the production of the desired metabolite.^[47] The isolation process begins with extraction. The most popular method is solvent extraction of either the whole culture or after separation of cells and culture filtrate using filtration or centrifugation.^[48] Separation is advantageous when the target molecule is either secreted into the medium and can be separated from the biomass or solely associated with the cells so that extracellular material and media components can be removed immediately. For extraction of the usually lyophilized culture, various solvents of different polarities like e.g., MeOH or acetone can be

used. It is also possible to perform liquid-liquid extraction (LLE) of aqueous liquid cultures using EtOAc, ether or DCM for example or to carry out solid-phase extraction (SPE) using polymeric adsorbent resins (e.g., XAD).

Isolation of the target compound from the obtained crude extract and eliminating impurities at the same time usually requires several orthogonal purification steps. A variety of procedures employing different separation mechanisms are available for fractionation especially when it comes to widely used liquid chromatography. Thereby, the stationary phase is usually arranged as column. Normal-phase, reversed-phase and size exclusion chromatography (SEC) are just a few examples for column chromatography (CC) techniques. Due to major advantages regarding resolution, automation, speed and reproducibility, automated systems like HPLC are favored and mostly used to achieve final purification of the target compound.

The multistep isolation procedure should be closely monitored to prevent obtaining the compound in small yield or even losing it along the various purification steps. For many years, this was accomplished by activity-guided isolation.^[49] At each step, every fraction had to be subjected to an *in vitro* bioassay to detect the active fractions. This method is highly time-consuming and strongly dependent on the compound concentration in each sample. A faster and much more sensitive way is the detection of the target compound using spectroscopic and spectrometric analysis based on characteristics known from dereplication. Furthermore, this allows relative quantification and evaluation of the purity of each fraction at the same time.

The isolation process is considered successful when able to provide the target metabolite in sufficient quantity and purity for structure elucidation by nuclear magnetic resonance (NMR) spectroscopy. Ideally, bioactivity screening furthermore confirms that the initially observed activity was in fact caused by the isolated compound.

1.2.5 Structure Elucidation

Even with various spectroscopic methods available to provide useful information, conclusive structure elucidation of unknown, complex natural products normally requires significant expertise as well as experiences.^[46] Although X-ray crystallography is considered the ultimate tool for molecular structure determination, its application to natural product research is strongly limited by the requirement of suitable quality crystals.^[50] Instead, NMR spectroscopy now represents the most powerful tool to meet the challenges of structure determination. In terms of sensitivity, dramatic improvement has been made over the last decades by technical innovations like construction of high-field cryomagnets, cryoprobes minimizing thermal noise and small volume sample tubes significantly shorten acquisition time as well as requirements regarding sample quantity.^[51] This is essential because acquiring sufficient amounts of natural products by isolation remains a major challenge. Full characterization at sample concentrations down to 1 nM is now achievable in a practicable amount of time.^[52]

NMR spectroscopy is based on resonant interactions between atomic nuclei and electromagnetic radiation in the radio frequency range in a strong external magnetic field requiring a magnetic moment and therefore a spin quantum number l other than zero. Thus, NMR spectroscopy can provide information about number and type of nuclei such as ^1H , ^{13}C , ^{15}N and ^{31}P which are most important in NP chemistry as well as the relationships among them.^[53]

Practical structure elucidation successively combines all information of the various NMR experiments to identify structural fragments which are then connected to provide the entire molecular structure of a compound. The analysis starts based on the molecular formula predicted by HRMS. The elemental consumption can be used to calculate the degree of unsaturation and therefore provides the number of double bonds and rings present in the molecule. Examination of 1D ^1H and ^{13}C NMR spectra allows verification of the molecular formula and can also give information on functional groups based on the chemical shifts. In this context, IR and UV/vis spectroscopy can provide additional useful information. Nevertheless, homo- and heteronuclear 2D NMR experiments are indispensable to fully determine and link all individual fragments of a molecule. The ^1H - ^{13}C HSQC (heteronuclear single quantum correlation) experiment allows the detection of one-bond carbon-proton connectivities ($^1J_{\text{C,H}}$). If an even or odd number of protons is bound to the corresponding carbons can also be determined due to the phase sensitivity of this experiment. In the next step, ^1H - ^1H COSY (correlation spectroscopy) spectra provide information on the connectivity of those CH_n ($n = 1, 2, 3$) groups. Structural fragments can be deduced based on the homonuclear germinal ($^2J_{\text{H,H}}$), vicinal ($^3J_{\text{H,H}}$) or in some cases even long-range ($^4J_{\text{H,H}}$) coupling of adjacent protons. Finally, the ^1H - ^{13}C HMBC (heteronuclear multiple-bond correlation) experiment is used to combine all structural units. As it reveals heteronuclear long-range correlations (mainly $^2J_{\text{C,H}}$ and $^3J_{\text{C,H}}$) even through quaternary carbons and heteroatoms, the overall skeletal connectivity can be established revealing the whole planar structure of the molecule.^{[54][55]}

1.2.6 Assignment of Stereochemical Configuration

With elucidated two-dimensional structures in hand, the question of spatial arrangement remains for chiral compounds. Since the stereochemistry has a profound impact on physicochemical, biological and pharmaceutical properties of a molecule, determination of the relative and absolute configuration is of fundamental importance.^[56]

1.2.6.1 Relative Configuration

For elucidation of the relative configuration, once more NMR spectroscopy is a very powerful tool. Relatively rigid or cyclic molecules that predominantly exist in a single conformation provide reliable information. NMR parameters such as coupling constants (J) and the nuclear Overhauser effect (NOE) allow prediction of the relative stereochemistry.^[57]

Saturating the magnetic resonance of a particular proton by specific irradiation leads to a change in resonance intensity of a neighboring proton. This phenomenon is called NOE.^[58] Here, spin polarization transfer occurs *via* dipolar cross-relaxation and strongly depends on the internuclear distance ($\leq 5 \text{ \AA}$). These dipole interactions through space can be visualized in homonuclear NOESY (Nuclear Overhauser Effect Spectroscopy) and ROESY (Rotating-frame Overhauser Effect Spectroscopy) experiments.^[59] The NOE also depends on the motional character of molecules in solution and is characterized by the tumbling rate (or rotational correlation time) which in turn particularly depends on the molecular weight besides solvent viscosity, temperature and spectrometer frequency.^[60] For small molecules ($MW < 700 \text{ Da}$), the NOE is positive while a negative NOE is observed for large molecules ($MW > 2000 \text{ Da}$). Consequently the NOE for medium-sized molecules ($700 \text{ Da} > MW < 2000 \text{ Da}$) is very weak or even zero. In those cases, ROESY experiments are performed. Because the cross-relaxation occurs here in spin-locked magnetization, the rotating-frame NOE (or ROE) is always positive. Therefore, ROESY supplies very similar, additional information compared to NOESY.^[61]

Besides dipolar couplings through space, scalar couplings provide further stereochemical information in the form of coupling constant values. Especially homonuclear, vicinal coupling of protons ($^3J_{\text{H,H}}$) allows identification of 1,2-stereochemical relations. The J values can be extracted from 1D ^1H NMR spectra in a straightforward manner and their direct correlation to dihedral angles is defined by the Karplus equation.^[55] Further development of this method also allows heteronuclear $^nJ_{\text{C,H}}$ ($n = 2, 3$; only for $n = 2$ if electronegative substituent is attached to C_α) values obtained from 2D HETLOC (Heteronuclear Long-Range Coupling) experiments to provide stereochemical information in a similar manner.^[62]

Because J -based configurational analysis is applicable to acyclic, substituted carbon chains, coupling constants are an important and useful complement to the NOE-based analysis. Both NMR parameters collectively provide essential geometric information in regard to the relative configuration.

1.2.6.2 Absolute Configuration

A variety of different methods and techniques are available for absolute configuration assignment of natural products. This includes X-ray crystallography, chiroptical methods (e.g., optical rotation (OR) and optical rotatory dispersion (ORD), electronic and vibrational circular dichroism (ECD/VCD), Raman optical activity (ROA)) and NMR-based methods.^[63] In the latter case, chemical derivatization with a chiral derivatizing agent (CDA) is required which represents a major disadvantage over non-destructive techniques. α -Methoxy- α -trifluoromethylphenylacetic acid (MTPA; Mosher's reagent, Fig. 9) represents one of the most common CDAs used to determine the absolute configuration of monofunctional molecules such as secondary alcohols and amines in combination with NMR analysis.^[64]

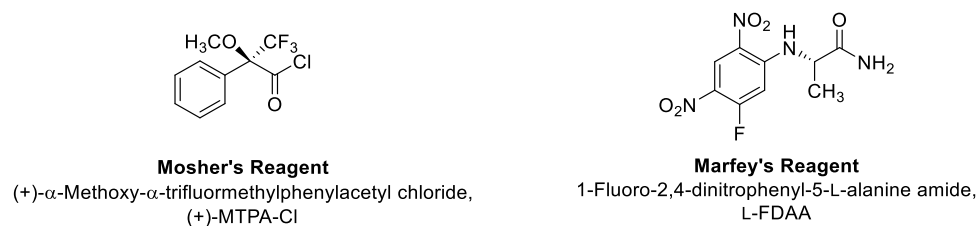


Fig. 9: Chemical structures of Mosher's Reagent and Marfey's Reagent as examples for CDAs.

The products of chemical degradation and/or chiral derivatization can also be analyzed by chromatography-based methods such as gas chromatography (GC) and chiral HPLC.^[65] This approach is applied in the widely used Marfey's method to determine the absolute configuration of amino acids e.g., in peptides.^[66] After acidic hydrolysis of the natural product to obtain the constituent amino acids, the hydrolysate is derivatized with Marfey's reagent as CDA in the next step. The most commonly used Marfey's reagent is 1-fluoro-2,4-dinitrophenyl-5-L-alanine amide (L-FDAA, Fig. 9).^[67] However, a variety of L- and D-amino acid amides can be attached to 1,5-difluoro-2,4-dinitrobenzene *via* synthesis or purchased commercially.^[68] The reaction of any given chiral Marfey's reagent with a racemic mixture of an amino acid results in two diastereomers that can be separated by HPLC and detected using UV absorption or MS. The retention time provides first evidence regarding the identification of both diastereomers. It has been shown various times that, on reversed-phase LC, the L-L diastereomer elutes first in most cases due to stronger intramolecular hydrogen bond formation than in the L-D diastereomer.^[69] However, final determination of the absolute configuration can only be achieved by comparing the retention time to enantiomerically pure standards that serve as reference.

Since all above-mentioned methods are limited in their scope regarding certain structural features, total synthesis remains gold standard to determine or confirm the absolute configuration.^[54] While also potentially giving access to a larger amount of compound, this approach most often represents a major challenge as true for many aspects within natural product drug discovery.

1.3 Outline of this PhD thesis

The present PhD thesis was prepared in the *Sanofi-Fraunhofer Natural Product Center of Excellence* later becoming the *Fraunhofer-Evotec Natural Products Excellence Center for Infectious Diseases* (FENPEC ID), a PPP established between Fraunhofer and Sanofi resp. Evotec in 2014. The focus of this collaboration was to tackle the antimicrobial resistance crisis by discovering novel active compounds for treatment of severe bacterial infections caused by Gram-negative pathogens and *M. tuberculosis*. Besides continued high-throughput screening of extracts originating from diverse microorganisms in

order to identify new antimycobacterial active metabolites, the following innovative approaches were pursued to achieve this objective as standard screening of the strain collection only delivered known Gram-negative active antibiotics: i) Adapted screening methods were implemented including the use of bicarbonate supplemented medium. Also applied to Actinobacteria broadly explored under common screening conditions, this approach implied an increased chance of identifying new and yet undetected active metabolites. ii) In order to discover novel NPs, exploration of rare and less-studied bacterial phyla such as Bacteroidetes and Acidobacteria represented another key aspect. Innovative cultivation techniques (e.g., microdroplets) were used to isolate corresponding producer strains from ecological niches such as termite nests.^[70] The goal of the current work is to demonstrate proof of concepts by directly translating these strategic efforts starting at the microbiology site of the group into chemistry and identifying new or even novel active metabolites based on isolation, structure elucidation and coordination of extensive bioactivity profiling. Thus, provided data then allow determination of potential hit compounds for further antibiotic drug discovery.

2. Gram-negative active metabolites from *Aspergillus terreus* ST000934

2.1 Introduction

Fungi are highly diverse microorganisms that form the second biggest kingdom behind bacteria.^[71] More than 1.5 million species are estimated to be living in almost every ecological niche across the planet with a maximum of only 10% that have been discovered so far.^[72] Natural products of fungal origin exhibit a wide range of pharmaceutically relevant activities. A variety of e.g., antiviral, anticancer, antidiabetic, antihypercholesterolemic and immunosuppressant drugs such as irofulven, lovastatin and cyclosporine A are in clinical development or approved for treatment.^[73] Ever since the discovery of penicillin G (**22**) from *Penicillium notatum* (later termed *P. chrysogenum*), the great importance of fungal NPs in the field of antibiotics is furthermore undeniable. Fusidic acid (**23**) as well as the classes of cephalosporins and pleuromutilins like lefamulin (**24**) represent further examples of antibiotics originating from fungi (Fig. 10). The latter has only recently been approved and is a good example for how advanced technologies of present days overcome challenges of earlier times in antibiotic research history. In contrast to fast-growing bacteria, receiving sufficient quantities of relevant compounds from fungi was considered more difficult and therefore neglected.^[74] For this reason, only a minority of natural product antibiotics in current clinical use is derived from fungal secondary metabolites.

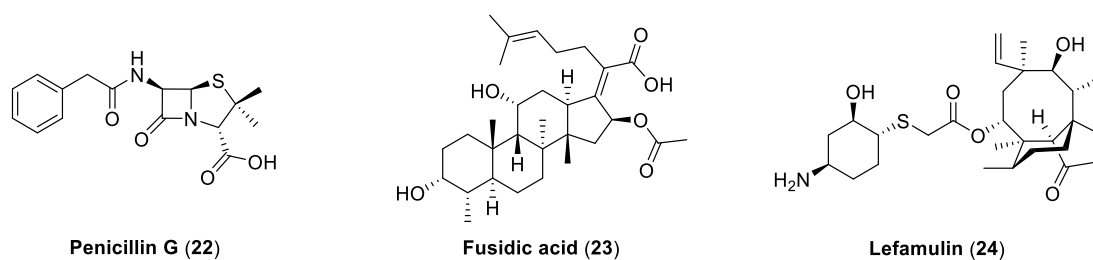


Fig. 10: Chemical structures of penicillin G (**22**), fusidic acid (**23**) and lefamulin (**24**).

However, as fungi remain a rich and yet widely underexplored source for novel antibiotics, their potential has been studied increasingly in recent years.^[75] Especially endophytic fungi from e.g., marine environment have been identified to produce a great variety of new secondary metabolites.^[71] In the Sanofi-Fraunhofer strain collection, fungi make up approximately 20% of all species which were exploited regarding the production of novel Gram-negative active secondary metabolites in the PPP.

2.2 Gram-negative Activity against *E. coli*

Within the standard process of screening the Sanofi-Fraunhofer strain collection for producer strains of Gram-negative active metabolites, the methanolic crude extract of *Aspergillus terreus* ST000934 inhibited the growth of *E. coli* (ATCC 35218) in the primary screening. Based on subsequent UPLC-MS/MS fractionation of the crude extract and screening of the obtained fractions, the antibacterial activity was assigned to a highly polar compound produced in large quantity by dereplication (Fig. 11).

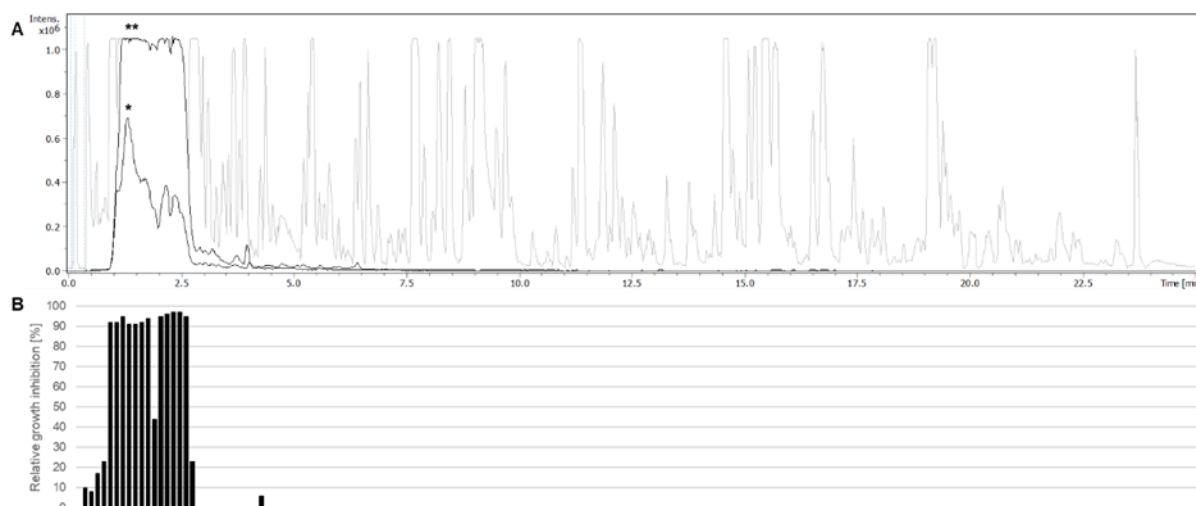
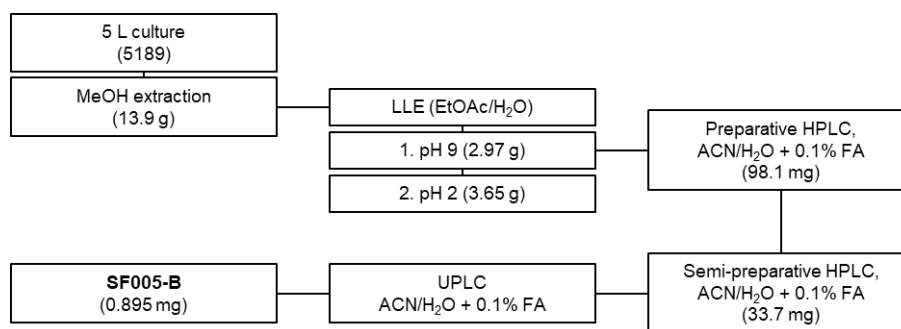


Fig. 11: Crude extract of ST000934. A: Base peak chromatogram (BPC, grey), extracted ion chromatogram (EIC, black) of $C_{18}H_{16}O_9$ * m/z 377.0867 \pm 0.005, $[M+H]^+$ and ** m/z 359.0761 \pm 0.005, $[M-H_2O+H]^+$; B: Relative growth inhibition [%] of fractions 1–159 against *E. coli* ATCC 35218, F-06–F-12 and F-14–F-18: > 90%.

According to the positive HRESIMS ion peak at m/z 377.0864 ($[M+H]^+$, Δ ppm 0.80), the molecular formula was assigned to $C_{18}H_{16}O_9$ retrieving seven hits in the Antibase database. However, none of them conclusively explained the observed molecular characteristics such as UV absorption and MS/MS fragmentation pattern (Fig. 12). Therefore, an isolation project was initiated purposing structure elucidation of the potentially new fungal metabolite and confirmation of the Gram-negative activity against *E. coli*. Henceforth, the compound will be referred to as SF005-B (25).

2.3 Isolation

Despite the relatively high production of SF005-B (25) by ST000934, isolation proved to be challenging due to the high polarity of the compound. Various techniques such as separation of cells and culture filtrate, pH effects, normal phase chromatography and size exclusion chromatography had been investigated throughout optimization of the isolation procedure. The most efficient protocol was established as described in the following (Scheme 1).



Scheme 1: Optimized isolation procedure of **25** from liquid culture of ST000934 in medium 5189.

The isolation started from 5 L fermentation of ST000934 in liquid medium 5189. After lyophilization of the whole broth and subsequent MeOH extraction, the crude extract was dissolved in H₂O to perform LLE. Therefore, the aqueous phase was first adjusted to pH 9 for the first round of ethyl acetate extraction and then acidified to pH 2 for the second round. Based on LC-MS analysis, only the extract obtained under alkaline conditions was further processed. Preparative HPLC using a C18 column (Synergi™ Fusion-RP 80 Å, 250 x 21.2 mm) and a linear gradient of 5–55% ACN in water was performed followed by semi-preparative HPLC (NUCLEODUR® Gravity-SB, 3 μm, 250 x 4.6 mm) with an adjusted gradient of 5–30% ACN in water. Final purification was achieved by UPLC fractionation (ACQUITY UPLC® BEH C18, 1.7 μm, 100 x 2.1 mm) yielding 0.895 mg of SF005-B (**25**) which was subjected to structure elucidation and bioactivity profiling.

2.4 Structure Elucidation of Fungal Metabolites

2.4.1 SF005-B

First indications regarding the structure of SF005-B (**25**) were provided by LC-MS/MS analysis. As noticed along the isolation process, an unusually broad peak was observed in the chromatogram (Fig. 12A). Reversible reactions (e.g., tautomerism, ring-opening/ring-closure) under acidic conditions during analysis were considered as potential explanation for this observation.^[76]

In agreement with dereplication, HRMS analysis of isolated **25** proved the molecular formula C₁₈H₁₆O₉ according to the positive ESIMS ion peak at m/z 377.0864 ([M+H]⁺, Δppm 0.80) further supported by the sodium adduct with m/z 399.0683 ([M+Na]⁺, Δppm 1.00) (Fig. 12C). From the sodium adduct however, a further water adduct was annotated (m/z 417.0791, [M+H₂O+Na]⁺, Δppm 0.24). Moreover, the fragment ion resulting from neutral loss of H₂O (m/z 359.0759, [M–H₂O+H]⁺, Δppm 0.56) represented the ion of highest intensity in the spectrum. Additionally, a certain dimeric structure was proposed by neutral losses of C₉H₈O₄ (180.0421 Da, Δppm 2.22) and C₉H₈O₅ (196.0370 Da, Δppm 2.04) resulted in the fragment ions C₉H₉O₅⁺ and C₉H₉O₄⁺, respectively. Yet, in the MS/MS spectrum of the [M+H]⁺ parent ion, only the former case was observed followed by neutral

losses of H₂O and CO/C₂H₄ (Fig. 12D). These findings suggested highly oxygenated aromatic structures for both monomeric units potentially linked *via* oxygen bridge.

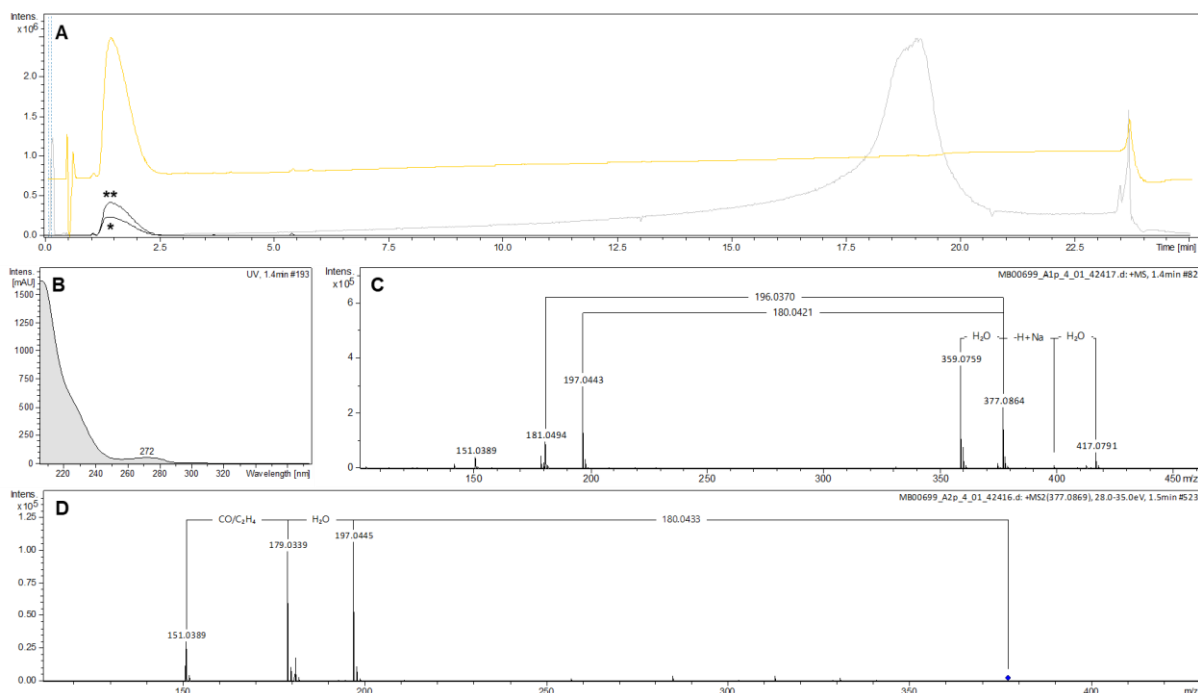


Fig. 12: LC-MS/MS analysis of SF005-B (**25**). A: BPC (grey), EIC (black) of C₁₈H₁₆O₉ * m/z 377.0867±0.005 [M+H]⁺ and ** m/z 359.0761±0.005 [M-H₂O+H]⁺, UV chromatogram 205–640 nm (yellow); B: UV spectrum of **25**; C: MS spectrum of **25**; D: MS/MS spectrum of [M+H]⁺ parent ion m/z 377.0869.

Consistent with these findings, the literature-known fungal metabolite eleganketal A (**26**)^[77] was considered as a potential structural candidate (Fig. 13). Yet, NMR analysis of purified **25** disproved this hypothesis as no methylene groups were detected. Conclusive structure elucidation however failed as multiple signal sets indicated a mixture of three highly similar compounds.

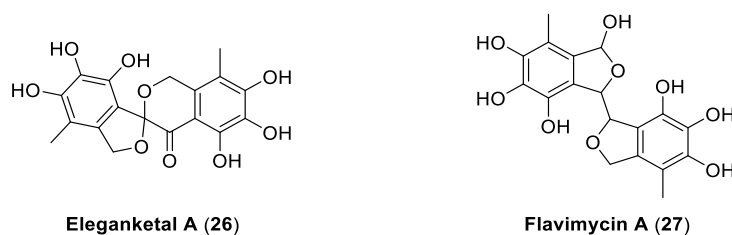
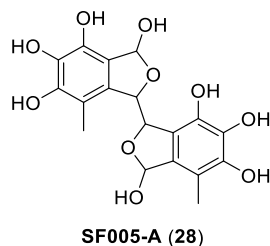
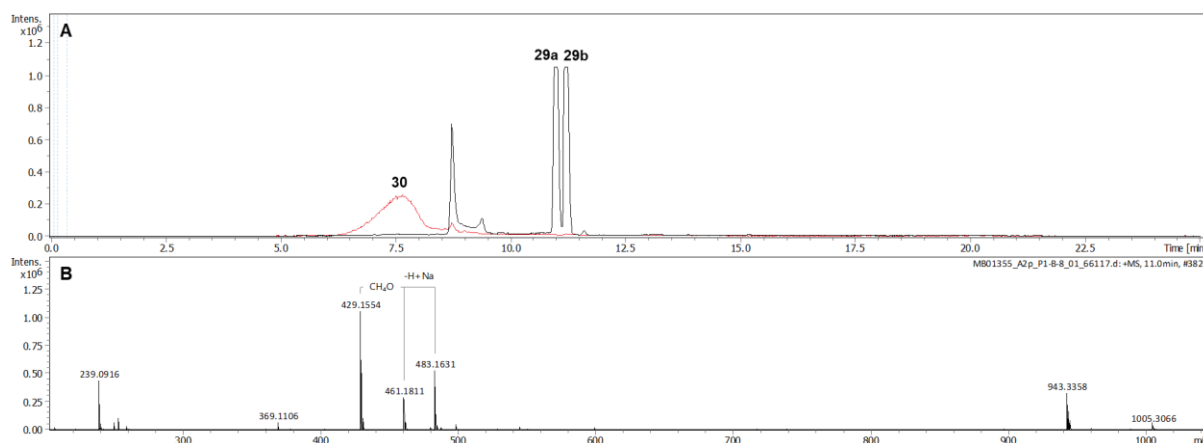


Fig. 13: Chemical structures of eleganketal A (**26**) and flavimycin A (**27**).

Yet, 1D and 2D NMR spectra still revealed the same aromatic system substituted with three hydroxyl groups and one methyl group as in **25** to be present. Furthermore, only methine groups with either one or two oxygen substituents (-OH, -OMe or -O-) were identified. This information strongly pointed towards a monooxygenated derivative of flavimycin A (**27**).^[78] With SF005-A (**28**), such a fungal metabolite had previously been isolated by PLAZA *et al.* from the strain ST005638 within the Sanofi-Fraunhofer collaboration in 2016 (Fig. 14). However, 1D NMR spectra did not match (data not shown).

Fig. 14: Chemical structure of SF005-A (**28**).

As for **26**, methylation had been reported to contribute to the structure elucidation of polyhydroxylated natural products.^[77] Moreover, restriction of intramolecular interactions most likely causing the characteristics observed in LC-MS and NMR analysis were considered advantageous in the particular case of SF005-B (**25**). Therefore, a pre-purified sample of **25** was methylated according to a modified protocol reported by CORNELLA *et al.*^[79] Two isomers of the 6-fold methylated product (**29a** and **29b**) were detected as sharp peaks in LC-MS analysis according to the pseudo-molecular ion at m/z 461.1806 ($C_{24}H_{29}O_9^+$, $[M+H]^+$) and its sodium adduct at m/z 483.1626 ($C_{24}H_{28}O_9Na^+$, $[M+Na]^+$). Similar to the most intensive $[M-H_2O+H]^+$ ion of **25**, the fragment ion at m/z 429.1544 ($C_{23}H_{25}O_8^+$, $[M-CH_4O+H]^+$) resulting from a neutral loss of CH_3OH was observed as most intensive in the MS spectrum of **29**. Both obtained isomers **29a** and **29b** were separated. Their conversion into compound **30** occurred constantly during purification under used conditions (Fig. 15). This aspect detected by LC-MS analysis of pure fractions will be further discussed below, however, contributed to the strongly limited amount obtained, especially for **29a**. Therefore, only **29b** was analyzed by NMR spectroscopy.

Fig. 15: Methylation products of SF005-B (**25**). A: EIC of **29** (black, m/z 429.1544 \pm 0.005, $C_{24}H_{28}O_9$ $[M-CH_4O+H]^+$) and **30** (red, m/z 447.1650 \pm 0.005, $C_{23}H_{26}O_9$ $[M+H]^+$); B: Annotated MS spectrum of **29b**.

Based on the NMR analysis results, the structure of **29b** was postulated according to 1H and 2D spectra as insufficient quantity did not allow ^{13}C analysis. The relative configuration was predicted based on ROESY experiments (Fig. 16). Clearly related to the flavimycins and SF005-A (**28**), the presence of an oxocane motif and two acetals was most prominent. Formation of the dioxabicyclic ring system only

during methylation reaction could not be excluded completely. Yet, based on this structure a variety of findings could be explained comprehensively.

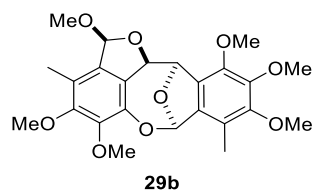


Fig. 16: Chemical structure of **29b** including relative configuration postulated by NMR analysis.

Firstly, even though acidic conditions had been avoided during purification, the conversion of **29a** and **29b** into the more polar compound **30** (m/z 447.1648, $C_{23}H_{27}O_9^+$, $[M+H]^+$, Δ ppm 0.45) accompanied by the formal loss of CH_2 had been observed as previously implied. Similar to the unmethylated metabolite **25**, **30** showed the very same broad peak in LC-MS at a shifted retention time between 6.4 min and 8.2 min (Fig. 15A, Fig. 17A). Furthermore, the MS spectrum was in accordance (Fig. 17B). As **30** had also been isolated, a mixture of highly similar compounds was again observed during NMR analysis not allowing valid structure elucidation. However, based on LC-MS/MS data and structural features of **29**, the chemical structure of **30** was postulated.

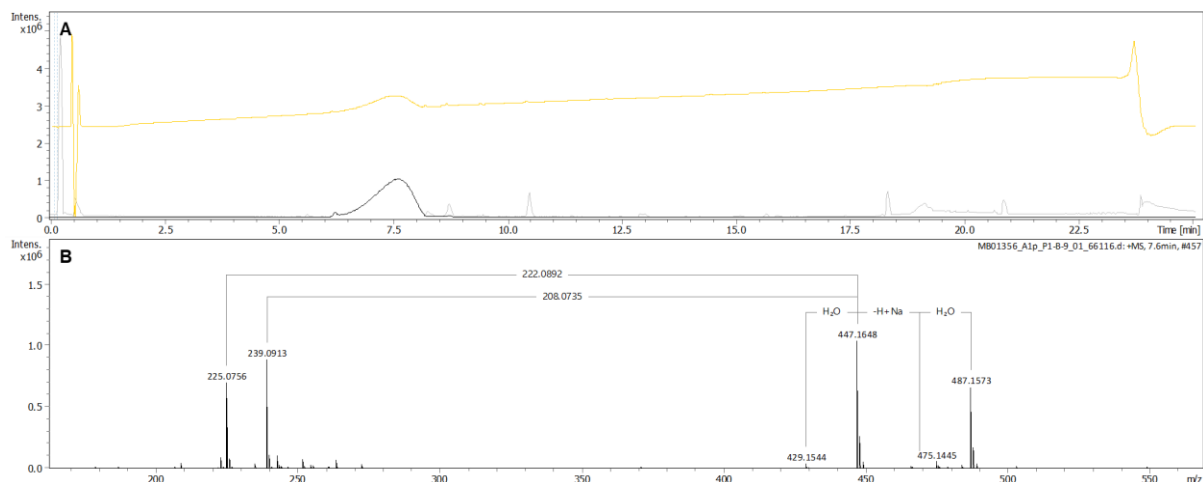


Fig. 17: LC-MS analysis of **30**. A: BPC (grey), EIC (black) of m/z 447.1648 \pm 0.005 ($C_{23}H_{26}O_9$ $[M+H]^+$), UV chromatogram 205–640 nm (yellow); B: Annotated MS spectrum of **30**.

While methylation had led to the sharp peak shape of acetals **29**, the structure still suggested the formation of the corresponding hemiacetal **30** explaining the observed formal loss of CH_2 . **30** can furthermore undergo oxo-cyclo tautomerism to **30'** potentially explaining the mixture of compounds observed in NMR analysis (Fig. 18). This interconversion moreover suggested **29a** being diastereomeric to **29b** with altered configuration most likely at the two stereogenic centers of the monocyclic methyl acetal.

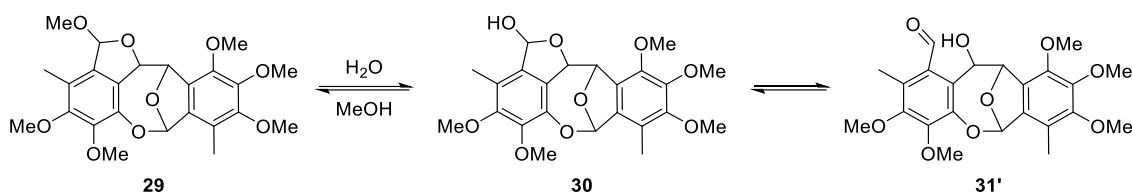


Fig. 18: Equilibrium of acetal **29** and hemiacetal **30** undergoing oxo-cyclo tautomerism leading to **30'**.

Accordingly, the structure of the unmethylated **29** represented by SF005-B (**25**) was proposed as depicted also able to undergo tautomerism to **25'** and most likely at equilibrium with hemiacetal **31**, a regioisomer of SF005-A (**28**) (Fig. 19). This also explained the sodium adduct of the $[M+H_2O+H]^+$ ion observed in LC-MS analysis (Fig. 12) and the mixture of highly similar compounds present in the NMR sample including diastereomeric forms of **25**. Furthermore, the MS/MS fragmentation pattern could be explained conclusively based on this structure for SF005-B (**25**) (Fig. S62).

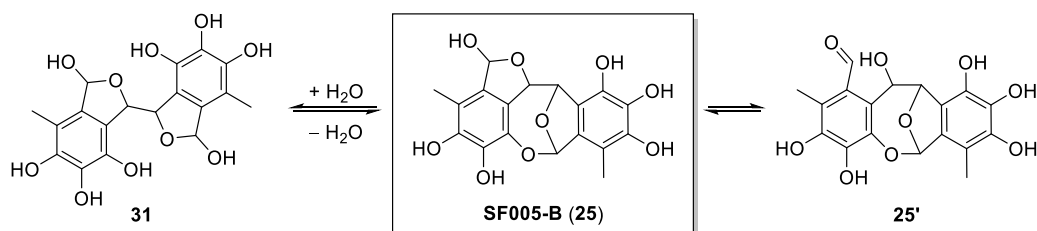


Fig. 19: Postulated structure of SF005-B (**25**) including equilibrium with hemiacetal **31** and oxo-cyclo tautomerism leading to **25'**.

Overall, the postulated structure of SF005-B (**25**) was brought into accordance with all findings observed in LC-MS/MS and NMR analysis including for the methylated derivatives **29** and **30** (Fig. S63, Fig. S64). However, the proposition remains theoretical as structural features clearly indicate a high level of isomerism hindering isolation of sufficient amounts of compound as well as structure elucidation. To the best of knowledge, **25** is being reported for the first time. Yet, several other bioactive natural products have been described also possessing the rare oxocane moiety even as unique dioxabicyclic ring system, e.g., arenaran B (**32**)^[80], integrastatin B (**33**)^[81], and isolaureatin (**34**)^[82] (Fig. 20).

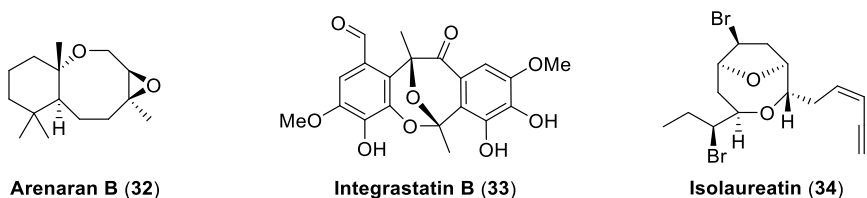


Fig. 20: Chemical structures of selected natural products containing dioxabicyclic ether moieties.

2.4.2 Other Fungal Secondary Metabolites

In the isolation campaign of SF005-B (**25**), eight additional secondary metabolites were isolated from *A. terreus* ST000934 including the three butyrolactones (**35–37**), flavipin (**38**), epicoccolide B (**39**),

dibefurin (**40**) as well as ethyl 2,4-dihydroxy-5,6-dimethyl benzoate (**41**) and its novel derivative **42** representing the only unknown compound. Similar to **25**, all structures feature highly oxygenated aromatic systems (Fig. 21).

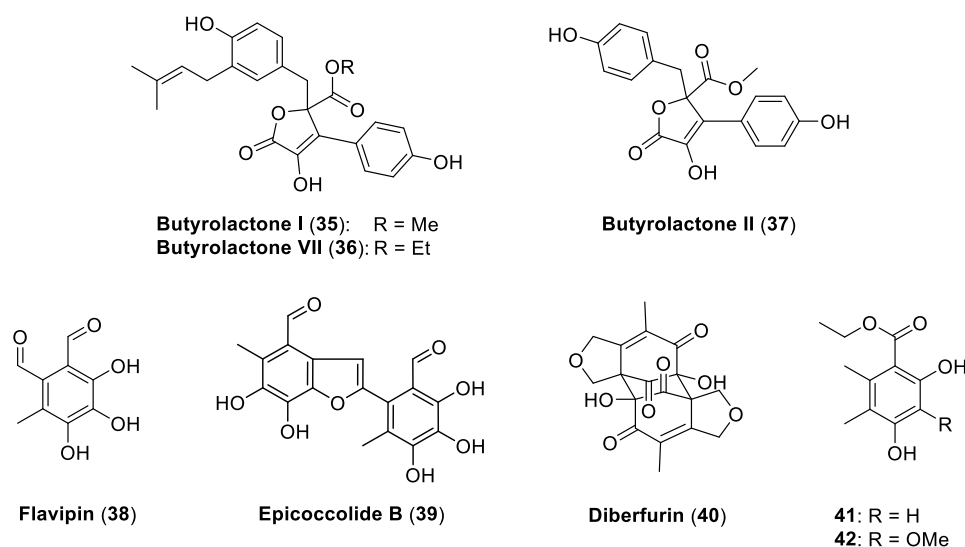
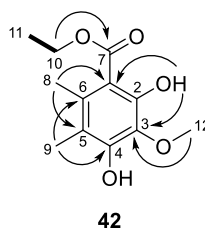


Fig. 21: Additional fungal secondary metabolites **35–42** isolated from *Aspergillus terreus* ST000934.

Butyrolactone I (**35**),^[83] II (**37**)^[84] and VII (**36**)^[85] are known fungal metabolites isolated from *Aspergillus terreus*. While lacking antibacterial and antiplasmodial activity, they are known to exhibit mild cytotoxicity.^{[85][86]} Various further derivatives have been described.^[87]

Flavipin (**38**) is a polyoxygenated fungal polyketide exhibiting broad bioactivity including antifungal^[88], nematocidal^[89] and antialgal^{[90][91]} properties. **38** was first isolated from *Aspergillus flavipes* and *Aspergillus terreus*^[92] but also found to be produced by other fungi such as *Chaetomium* sp.^[89] and *Epicoccum* sp.^[93] The latter case is also true for flavipin-derived epicoccolide B (**39**).^[94] Besides antibacterial (*S. aureus*, *E. coli*) and antifungal activity^[95], **39** showed inhibition of protein kinase and histone deacetylase activities as well as cytostatic effects.^[96] Isolation of **39** together with the biosynthetically related calcineurin inhibitor dibefurin (**40**) from the fungal culture AB 1650I-759 has also been published.^[97]

Ethyl 2,4-dihydroxy-5,6-dimethyl benzoate (**41**) was isolated from the endophytic fungus *Phomopsis cassia*.^[98] Antifungal activity against the phytopathogenic fungi *Cladosporium cladosporioides* and *Cladosporium sphaerospermum* was reported. However, the 3-methoxy derivative **42** has not yet been described in literature. HRMS data suggested the molecular formula C₁₂H₁₆O₅ (m/z 241.1070, [M+H]⁺, Δ ppm 0.42). The structure was elucidated by NMR analysis in comparison to **41** with 2D HMBC and NOESY experiments confirming the aromatic substitution pattern (Table 5).

Table 5: ^1H and ^{13}C data of **42** (^1H : 600 MHz, ^{13}C : 101 MHz, $\text{DMSO-}d_6$) including COSY and selected HMBC correlations in comparison to reported data for **41** (^1H : 500 MHz, ^{13}C : 125 MHz, $\text{DMSO-}d_6$).**42**

— COSY → HMBC (key)

position	41 ^[98]		42	
	δ_{H} (\mathcal{J} in Hz)	δ_{C} , type	δ_{H} (\mathcal{J} in Hz)	δ_{C} , type
1	–	112.2	–	112.4
2	–	154.5	–	147.5
2-OH	–	–	9.50, s	–
3	6.26, s	99.9	–	133.4
4	–	157.2	–	150.0
4-OH	–	–	9.09, s	–
5	–	113.8	–	115.1
6	–	135.9	–	130.2
7	–	169.2	–	168.9
8	2.10, s	17.1, CH_3	2.09, s	16.8, CH_3
9	1.95, s	11.1, CH_3	1.99, s	11.5, CH_3
10	4.22, q (7.0)	60.2, CH_2	4.25, q (7.1)	60.5, CH_2
11	1.26, t (7.0)	14.1, CH_3	1.28, t (7.2)	14.1, CH_3
12	–	–	3.63, s	60.2, CH_3

2.5 Antibacterial Activity

The antibacterial activity of all nine metabolites isolated from *A. terreus* ST000934 was evaluated by micro broth dilution assay against a selected panel of Gram-negative and Gram-positive pathogenic bacteria (Table 6). Overall, growth inhibition was observed for every compound against at least one of the screening strains due to the high test concentration of up to 256 $\mu\text{g/mL}$. However, considering clinical relevant ranges, very low antibacterial activity was only detected against the sensitive Gram-negative *M. catarrhalis*. With a MIC of 8–16 $\mu\text{g/mL}$, epicoccolide B (**39**) exhibited the highest activity and also represented the only compound for which antibacterial activity had been reported.^[95]

The structurally related SF005-B (**25**) and flavipin (**38**) showed a similar activity pattern. Both compounds revealed comparable polarity and eluted within the active fractions (Fig. 11). Their large quantity present in the crude extract of ST000934 most likely resulted in the originally observed activity against *E. coli* as the purified compounds exhibited very low MIC values of 256 $\mu\text{g/mL}$ and 128 $\mu\text{g/mL}$, respectively. Previously, the same MIC of 256 $\mu\text{g/mL}$ had also been determined for SF005-A (**28**).

Table 6: MICs [$\mu\text{g/mL}$] of isolated compounds **25** and **35–42**.

	25	35	36	37	38	39	40	41	42
<i>Escherichia coli</i> ATCC 35218 (MH-II)	256	> 256	> 256	> 256	128	256	> 256	> 256	> 256
<i>Escherichia coli</i> ATCC 35218 (MHC)	128	256	256	> 256	128	64–128	256	256	> 256
<i>Moraxella catarrhalis</i> ATCC 25238	16–32	64	32	256	16	8–16	32–128	64	256
<i>Mycobacterium smegmatis</i> ATCC 607	128	256	64	> 256	256	256	> 256	64	256
<i>Staphylococcus aureus</i> ATCC 25923	64	256	64	> 256	32	64	256	256	> 256

Considering the presented MIC values and cytotoxic or cytostatic properties reported for some compounds, the isolated metabolites overall lacked pharmacological potential for further antibiotic drug development. Also true for SF005-B (**25**), stability issues were an additional criterion leading to the decision not to follow up this project by the industrial partner.

2.6 Summary

Within the standard process of screening the Sanofi-Fraunhofer strain collection for novel Gram-negative active secondary metabolites, the crude extract of *Aspergillus terreus* ST000934 inhibited growth of *E. coli*. The activity was assigned to a novel compound named SF005-B (**25**). Structural features of **25** complicated its isolation. Yet, these challenges were overcome. However, structure elucidation required methylation of the natural product leading to profound postulation of the reported structure in conclusive agreement with the presented LC-MS/MS data. Additionally, a total of eight fungal metabolites were furthermore isolated. Among them, **42** had been described for the first time. The antibacterial activity of all isolated compounds was evaluated and revealed broad growth inhibition towards Gram-positive and Gram-negative bacteria. The initially observed activity against *E. coli* was attributed to the high concentration of **25** present in the extract. However, the

determined MIC values discouraged further efforts regarding antibiotic drug development. Yet, SF005-B (25) has successfully been characterized and will serve as valuable contribution to the in-house dereplication database, although no further development is planned.

3. Oxazoline-containing Madurastatins from *Actinomadura* sp. ST100801

3.1 Introduction

Iron is essential for optimal cellular growth of many microorganisms. Yet, the concentration of free Fe(III) in most microbial habitats is strongly limited due to its low solubility. Therefore, the production of siderophores represents a common strategy to counteract the restricted bioavailability. These small chelating molecules selectively bind extracellular ferric iron typically forming hexadentate complexes with high affinity. Affiliated uptake into the cell occurs *via* membrane transporters.^[99]

For complexing siderophores, a great structural variety has been reported with more than 500 known analogs. Normally, the mononuclear, hexadentate iron(III) coordination results from functional assembly of several bidentate ligands such as catecholates or phenolates, hydroxamates and α -hydroxy carboxylates. Hydroxyphenyloxazoline acts as less frequently occurring coordinating motif.^{[99][100]} Mycobactins (such as mycobactin S (**43a**) and mycobactin T (**43b**)) and the structurally related brasilibactin A (**44**), nocardimicins (such as nocardimicin B (**45**)) as well as oxachelin (**46**) exemplify this group of siderophores with hydroxamate units completing the chelating design (Fig. 22).^{[101][102][103][104]} Bioactive properties have been reported for these compounds, e.g., the antibacterial and antifungal activity of **46**.

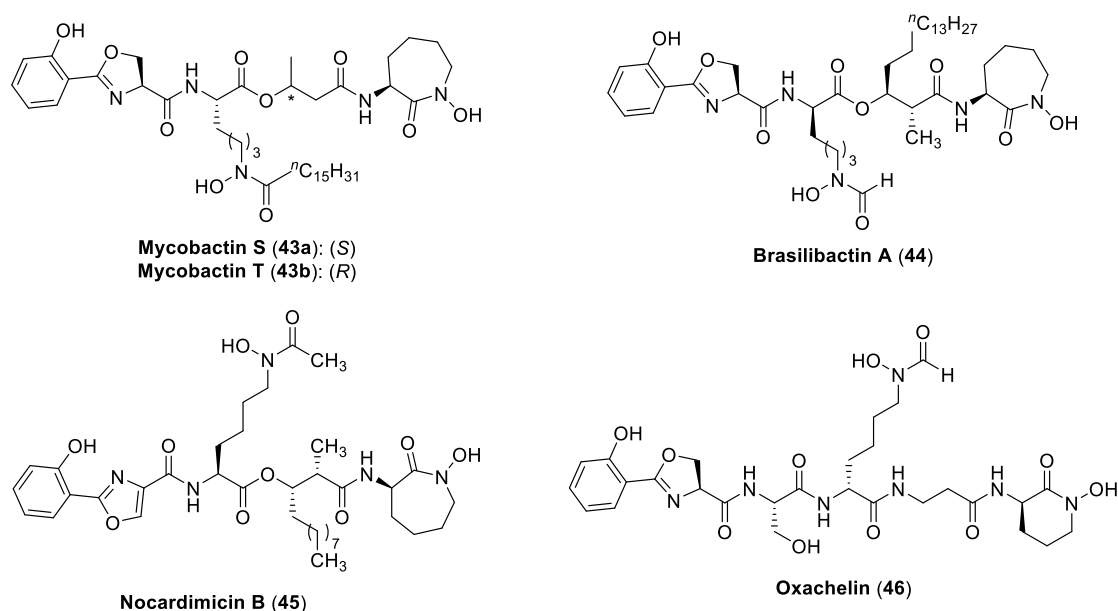


Fig. 22: Chemical structures of selected hydroxyphenyloxazoline siderophores and related analogs.

Another example is the group of madurastatins produced by *Actinomyces*. Various members of this class, such as madurastatin A1 (**47**), madurastatin C1 (**48**) (also designated as MBJ-0034) and

MBJ-0035 (**49**), have been isolated and identified as linear pentapeptides (Fig. 23).^{[105][106][107]} Other members of the madurastatin family like madurastatin B1 (**50**), B2 (**51**) and B3 (**52**) only consist of the characteristic core unit functionalized in position 4 of the oxazoline ring.^{[105][108]} The originally reported aziridine element (as depicted for madurastatin B3 (**52**)) has been revised for **47–50** by SHAABAN *et al.* and is further supported by the work of TYLER *et al.*^{[109][110]} The distinctive N-terminal 2-(2-hydroxyphenyl)oxazoline motif in combination with two hydroxamate moieties explains the siderophoric character responsible for the reported antibacterial activity. This hypothesis is further supported by the loss of activity accompanying ferric iron complex formation.^{[105][106]} Although breaking the hexadentate design, antibacterial activity is also described for madurastatin B1 (**50**) and B3 (**52**).^{[105][108]}

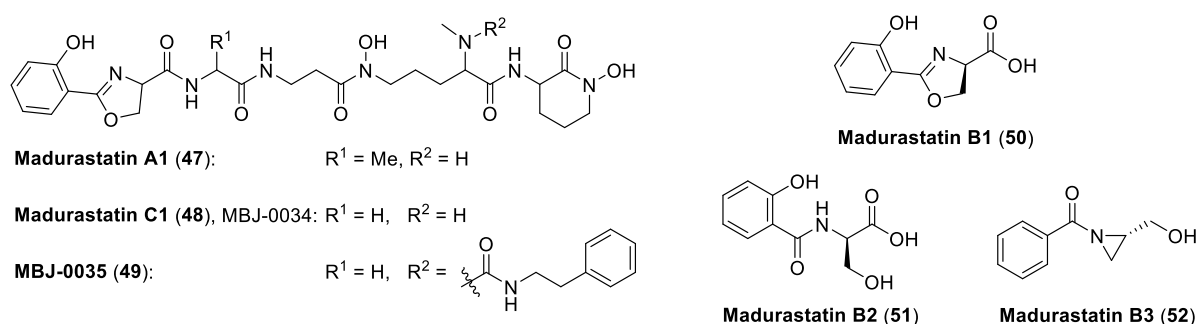


Fig. 23: Chemical structures of selected madurastatins described in literature.

Generally, the naturally evolved concept of iron chelation is being exploited for various applications in medicine (e.g., iron excess, malaria or cancer therapy) and agriculture (e.g., promoting plant growth and health).^[111] In antibiotic therapy, the ability of siderophores to cross the membrane barrier, especially of Gram-negative bacteria, is most relevant in terms of iron transport-mediated drug delivery. Covalently attached to an antibiotic, the siderophore serves as ‘Trojan horse’ to facilitate cellular uptake of the conjugate.^{[99][100]} The most current example of clinically relevant sideromycins is cefiderocol (**4**) approved in 2019 (Fig. 3). However, for other siderophore-antibiotic conjugates entering only *via* one type of siderophore transporter, rapid resistance development remains the major problem.^[112] Therefore, it is worth exploring siderophores regarding antibacterial activity potentially independent of the Fe(III) concentration as they may utilize additional uptake systems. Overall, the iron metabolism is a target of great potential for a large scope of applications emphasizing the importance of continuous research in the field of siderophore biology and chemistry for better understanding and superior drug development.

3.2 Dereplication of Madurastatins

3.2.1 Gram-negative Activity against *E. coli* MHC

Besides the Gram-negative pathogens included in the standard screening panel, *E. coli* (ATCC 35218) was additionally tested in Mueller-Hinton II broth supplemented with sodium bicarbonate (MHC) in order to mimic *in vivo* host physiology. These screening conditions are reported to improve the prediction value of *in vitro* antimicrobial susceptibility assays and to ensure the identification of otherwise undetected active compounds.^[33] Utilizing this procedure, *Actinomadura* sp. ST100801 was identified to produce active metabolites inhibiting growth of *E. coli*. Subsequently, the methanolic crude extract was fractionated *via* UPLC and dereplication was then performed using available MS/MS data in correlation with obtained screening data (Fig. 24).

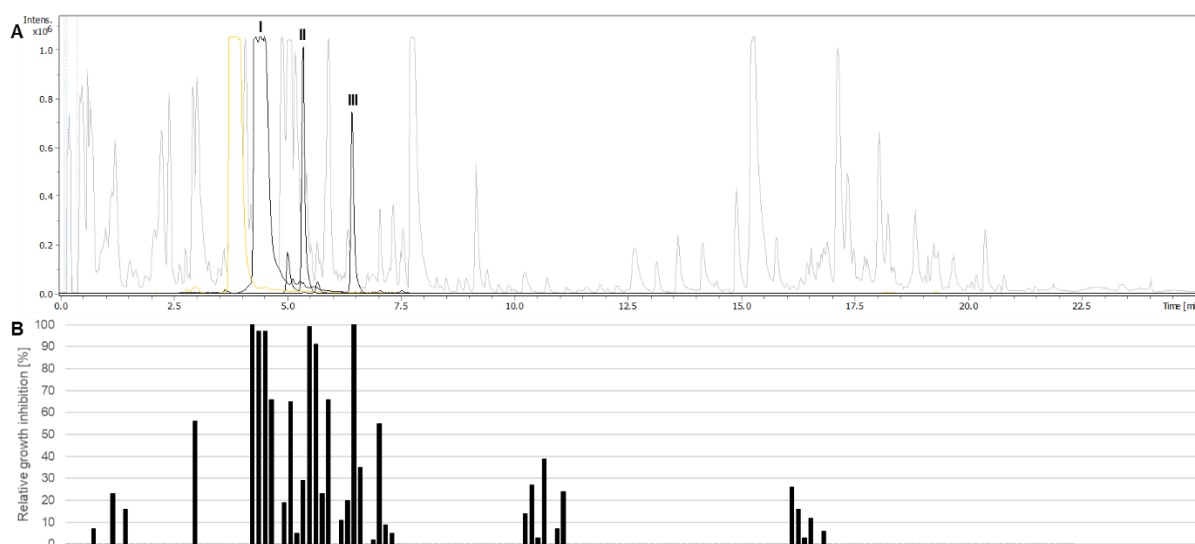


Fig. 24: Crude extract of ST100801. A: BPC (grey); EIC (black) of I: m/z 296.6399 \pm 0.005, $C_{26}H_{37}N_7O_9$, $[M+2H]^{2+}$, II: m/z 309.6477 \pm 0.005, $C_{28}H_{39}N_7O_9$, $[M+2H]^{2+}$ and III: m/z 316.6556 \pm 0.005, $C_{29}H_{41}N_7O_9$, $[M+2H]^{2+}$; EIC (yellow): m/z 208.0604 \pm 0.005, $C_{10}H_9NO_4$, $[M+H]^+$. B: Relative growth inhibition [%] of fractions 1–159 against *E. coli* ATCC 35218 in MHC medium; F-30–F-33, F-39+F-40 and F-46: > 90%.

Considering fractions with a relative growth inhibition above 90%, the activity of fractions F-30–F-33 was assigned to a compound with the molecular formula $C_{26}H_{37}N_7O_9$ (m/z 592.2705 $[M+H]^+$, Δ ppm 3.55). It was dereplicated as madurastatin C1 (**48**) for which antibacterial activity against *S. aureus*, *B. subtilis* and *M. luteus* had been described.^{[100][105]} The growth inhibition in F-39+F-40 and F-46 was presumed to be caused by $C_{28}H_{39}N_7O_9$ (**53**) (m/z 618.2862 $[M+H]^+$, Δ ppm 3.24) and $C_{29}H_{41}N_7O_9$ (**54**) (m/z 632.3024 $[M+H]^+$, Δ ppm 2.37), respectively. Similar molecular formulae and MS/MS fragmentation pattern compared to **48** suggested two unknown madurastatin derivatives (Fig. S72). An additional double bond equivalent (dbe) indicated a further double bond or ring to be present in these molecules.

Based on the occurrence of (un)known active madurastatins, the extract was furthermore examined regarding the presence of other reported derivatives. Thus, madurastatin B1 (**50**) was identified as

also being produced by ST100801 (Fig. 24A). Having identified various madurastatins gave occasion to perform Molecular Networking for fast identification of additional derivatives in the crude extract.

3.2.2 Molecular Networking

In order to identify more potential madurastatin derivatives with chemical similarities to the dereplicated compounds based on available ESI-QTOF-MS/MS data, Molecular Networking was performed. This well-established bioinformatics tool allows detection of analogs even when present in very limited concentrations.^[113] Potential growth inhibiting properties of compounds detected by this activity-independent approach need be determined following upscaled isolation campaigns. In general, isolation of several derivatives can potentially provide information about their common biosynthesis and can be used to investigate structure-activity relationships.

Within the Molecular Network of ST100801, the three compounds **48**, **53** and **54** to which activity had been assigned, were detected in three different clusters (cluster A–C, Fig. S73). Madurastatin C1 (**48**) arranged with either one of the dereplicated madurastatin derivatives in the $[2M+H/2M+Na]^+$ cluster A or the $[M+2H]^{2+}$ cluster C (Fig. S74) and with both of them in the $[M+H]^+$ cluster B (Fig. 25).

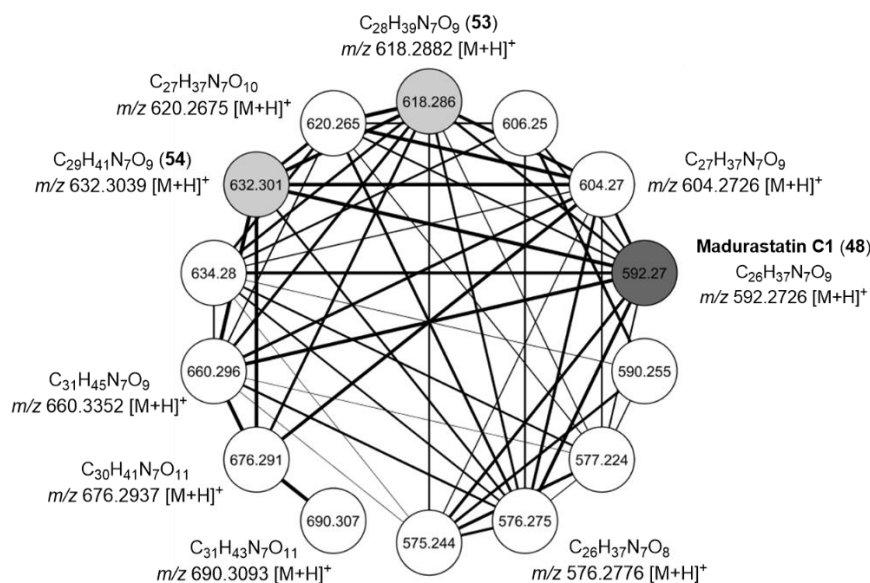
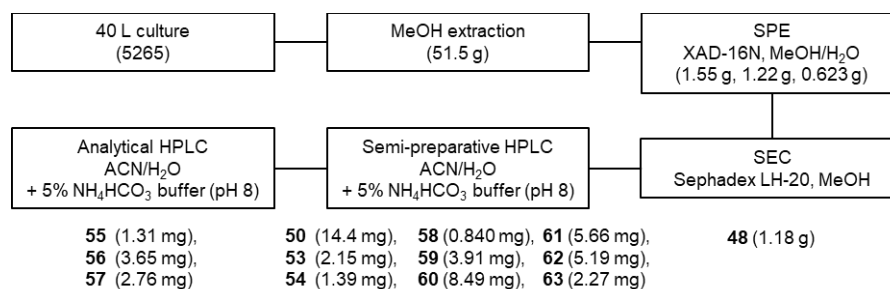


Fig. 25: Molecular Network of *Actinomadura* sp. ST100801: $[M+H]^+$ madurastatin cluster B. Nodes are labelled with m/z values of parent ions; width of edges correlates with cosine scores. Dark grey: madurastatin C1 (**48**); light grey: potential madurastatin derivatives **53** and **54** previously identified by activity-based dereplication. For the six further relevant derivatives, parent ion masses and molecular formulae are given.

In the latter case, eleven additional parent ions completed the cluster showing a high degree of similarity indicated by the large number of linkages and the corresponding cosine scores. Therefore, an isolation project was initiated in order to purify as many compounds as possible, elucidate their structure and study their antimicrobial activity.

3.3 Isolation

In regards to establishing an appropriate isolation protocol, acidic conditions were strictly avoided since oxazoline ring opening by acidic hydrolysis has been described before.^[114] This finding was additionally confirmed by the observation of water addition product formation during LC-MS analysis at pH 2.7. Furthermore, as indicated by **51** (Fig. 23), the hydrolyzed forms of **47**, **48** and **50** have been reported in literature most likely occurring during isolation.^{[105][106]} Thus, an NH_4HCO_3 buffer adjusted to pH 8 was used to prepare HPLC solvents.



Scheme 2: Isolation scheme of **48**, **50**, **53–63** from liquid culture of ST100801 in medium 5265.

Intending isolation and characterization of as many madurastatins as possible, strain ST100801 was fermented in 40 L scale in liquid medium 5265. After lyophilization and MeOH extraction, the crude extract was fractionated by SPE using Amberlite® XAD-16N as absorbent resin and a stepwise gradient from 20% to 100% MeOH in H₂O. Three combined fractions were subsequently purified by SEC using Sephadex™ LH-20 as gel filtration medium and MeOH as eluent. Final purification was achieved by semi-preparative (NUCLEODUR® C18 Gravity-SB, 3 μm, 250 x 10 mm) and analytical (NUCLEODUR® Sphinx RP, 5 μm, 250 x 4.6 mm) HPLC fractionation and adjusted gradients to yield a total of thirteen madurastatin derivatives in sufficient quantity for structure elucidation and further profiling (Scheme 2).

3.4 Structure Elucidation

In accordance with published data, HRMS and NMR analysis confirmed that *Actinomadura* sp. ST100801 indeed produced madurastatin B1 (**50**)^[105] (Table 7) and madurastatin C1 (**48**)^[110] (Table 11) as postulated by dereplication. The two other derivatives detected by activity-guided dereplication were identified as madurastatin D1 (**53**) and D2 (**54**) based on NMR analysis (Fig. 26). These two novel structures containing a 4-imidazolidinone ring had been published by YAN *et al.*^[115] contemporaneously with the present structure elucidation and were therefore not available in any chemical database at the beginning of the isolation campaign.

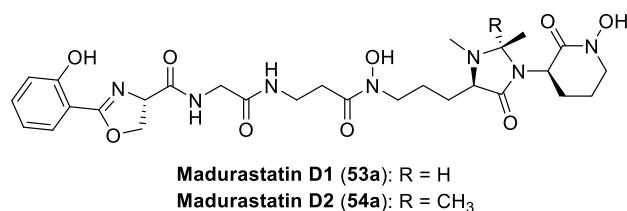
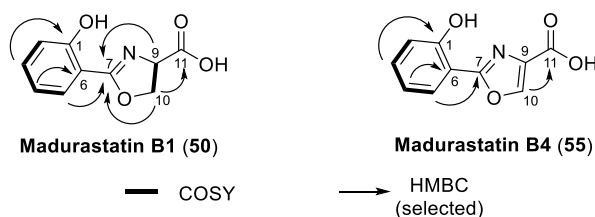


Fig. 26: Chemical structures of madurastatin D1 (**53a**) and D2 (**54a**) including published stereochemistry.

The complete set of NMR and HRMS data available for **48**, **50**, **53** and **54** allowed structure elucidation of the remaining nine isolated madurastatins in a straightforward manner.

Table 7: ¹H and ¹³C data of **55** in comparison to isolated madurastatin B1 (**50**) (¹H: 400 MHz, ¹³C: 101 MHz, DMSO-*d*₆) including COSY and selected HMBC correlations.



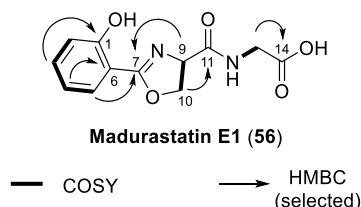
position	50		55	
	δ_H (<i>f</i> in Hz)	δ_C , type	δ_H (<i>f</i> in Hz)	δ_C , type
1	–	159.2	–	156.5
2	7.00, dd (8.2, 0.5)	116.6, CH	7.06, d (8.2)	116.9, CH
3	7.46, ddd (8.4, 7.2, 1.4)	134.2, CH	7.40, ddd (8.2, 7.4, 1.6)	132.3, CH
4	6.94, ddd (7.8, 7.2, 0.8)	119.2, CH	6.99, t (7.5)	119.5, CH
5	7.63, dd (7.8, 1.6)	128.0, CH	7.80, dd (7.8, 1.4)	125.9, CH
6	–	109.9	–	111.0
7	–	166.0	–	159.4
9	4.97, dd (10.1, 7.7)	67.2, CH	–	139.8
10	4.60, dd (16.2, 8.5)	69.6, CH ₂	8.29, s	140.2, CH
11	–	172.0	–	162.4

For compound **55**, the molecular formula C₁₀H₇NO₄ (*m/z* 206.0447 [M+H]⁺, Δppm 0.49) was assigned by positive HRESIMS analysis indicating a high similarity to madurastatin B1 (**50**) with one additional db. NMR data revealed the H-9 proton to be missing. Furthermore, a single H-10 proton (δ_H 8.29 ppm) confirmed the presence of an aromatic oxazole instead of the oxazoline moiety while substitution pattern of the ring was identical (Table 7). It was designated as madurastatin B4, previously unreported.

Compound **56** was assigned the molecular formula C₁₂H₁₂N₂O₅ according to the positive HRMS ion peak at *m/z* 265.0818 ([M+H]⁺, Δppm 0.38). 1D and 2D NMR data indicated a high structural similarity

up to NH-12 in comparison to other isolated madurastatins such as **48**. Two additional methylene protons H-13 (δ_{H} 3.52 ppm / δ_{H} 3.47 ppm) showed COSY correlation to NH-12 and HMBC correlation to the carbonyl carbon C-14 (δ_{C} 170.6 ppm). **56**, designated as madurastatin E1, was identified as dipeptide with glycine being attached to the distinctive oxazoline structure *via* peptide bond (Table 8).

Table 8: ^1H and ^{13}C data of **56** (^1H : 400 MHz, ^{13}C : 101 MHz, $\text{DMSO-}d_6$) including COSY and selected HMBC correlations.

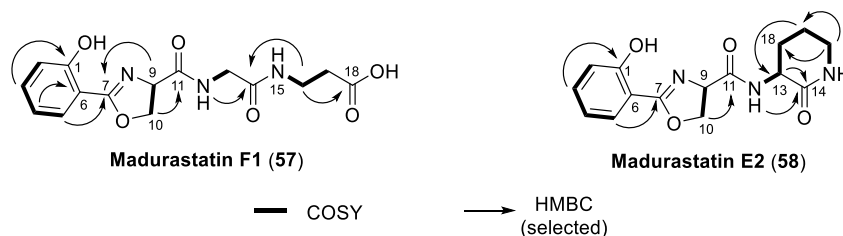


56		
position	δ_{H} (J in Hz)	δ_{C} , type
1	—	159.1
2	7.01, d (8.3)	116.6, CH
3	7.47, ddd (8.3, 7.3, 1.6)	134.1, CH
4	6.95, ddd (7.8, 7.3, 0.8)	119.1, CH
5	7.64, dd (7.8, 1.6)	128.0, CH
6	—	109.9
7	—	165.9
9	5.02, dd (10.4, 7.7)	67.3, CH
10	4.64, dd (10.4, 8.4)	69.6, CH_2
11	4.50, t (8.0)	—
12	—	169.1
13	7.95, t (4.3)	—
13	3.52, dd (16.8, 4.8)	43.1, CH_2
13	3.47, dd (16.6, 4.7)	—
14	—	170.6

For compound **57** and **58**, HRMS analysis suggested the related molecular formulae $\text{C}_{15}\text{H}_{17}\text{N}_3\text{O}_6$ (m/z 336.1190 $[\text{M}+\text{H}]^+$) and $\text{C}_{15}\text{H}_{17}\text{N}_3\text{O}_4$ (m/z 304.1293 $[\text{M}+\text{H}]^+$, Δppm 0.33), respectively. These findings indicated the next amino acids in line, namely β -alanine, being attached to the glycine residue. NMR data confirmed this hypothesis for **57**, named madurastatin F1, identifying it as linear tripeptide (Table 9). Compound **58**, was lacking two oxygen atoms compared to **57**. 1D and 2D NMR data revealed a single H-13 proton (δ_{H} 4.20–4.13 ppm) with similar HMBC correlation to carbonyl carbon C-14 (δ_{C} 169.3 ppm) but showing additional COSY correlations to two methylene protons H-18

(δ_{H} 2.02–1.96 ppm / δ_{H} 1.73–1.65 ppm). The C-terminal amino acid was identified as cyclic ornithine resulting in the dipeptidic structure of **58**, that was therefore named madurastatin E2 (Table 9).

Table 9: ^1H and ^{13}C data of **57** (^1H : 400 MHz, ^{13}C : 101 MHz, $\text{DMSO-}d_6$) and **58** (^1H : 500 MHz, ^{13}C : 126 MHz, $\text{DMSO-}d_6$) including COSY and selected HMBC correlations.

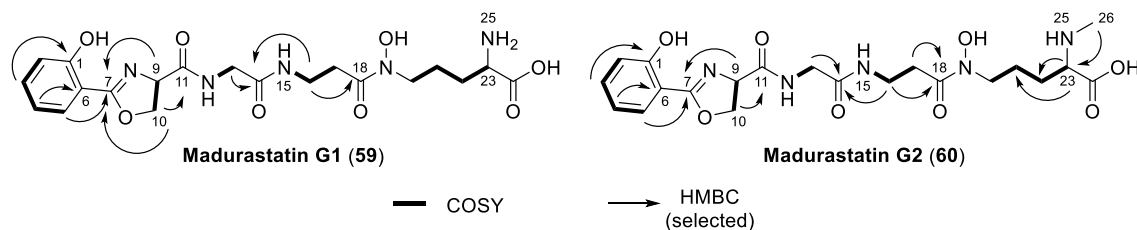


position	57		58	
	δ_{H} (J in Hz)	δ_{C} , type	δ_{H} (J in Hz)	δ_{C} , type
1	–	159.1	–	159.0
2	7.01, dd (8.3, 0.6)	116.6, CH	7.01, dd (8.3, 1.0)	116.5, CH
3	7.47, ddd (8.3, 7.3, 1.6)	134.0, CH	7.47, ddd (8.3, 7.3, 1.7)	134.0, CH
4	6.95, ddd (7.9, 7.2, 0.7)	119.0, CH	6.95, ddd (7.8, 7.3, 1.0)	119.0, CH
5	7.64, dd (7.8, 1.6)	128.1, CH	7.65, dd (7.8, 1.7)	128.0, CH
6	–	109.9	–	109.9
7	–	165.9	–	165.8
9	5.01, dd (10.4, 7.7)	67.4, CH	4.97, dd (10.4, 7.7)	67.4, CH
10	4.64, dd (10.4, 8.5)	69.4, CH ₂	4.65, dd (10.4, 8.4)	69.4, CH ₂
	4.53, t (8.1)		4.50, dd (8.4, 7.7)	
11	–	170.1	–	169.4
12	8.54, t (5.7)	–	8.45, d (8.0)	–
13	3.75, dd (16.5, 6.1)	42.1, CH ₂	4.20–4.13, m	49.1, CH
	3.65, dd (16.5, 5.6)			
14	–	168.2	–	169.3
15	8.01, t (5.4)	–	7.61, br s	–
16	3.23, dd (12.9, 6.6)	35.2, CH ₂	3.15–3.11, m	41.0, CH ₂
17	2.28, t (7.0)	34.8, CH ₂	1.82–1.77, m	21.0, CH ₂
			1.75–1.69, m	
			2.02–1.96, m	
18	–	173.4	1.73–1.65, m	27.4, CH ₂

Based on HRMS analysis, the molecular formulae $\text{C}_{20}\text{H}_{27}\text{N}_5\text{O}_8$ (m/z 466.1933 $[\text{M}+\text{H}]^+$, Δ ppm 0.22) and $\text{C}_{21}\text{H}_{29}\text{N}_5\text{O}_8$ (m/z 480.2089 $[\text{M}+\text{H}]^+$) were assigned for compound **59** and **60**, respectively. 1D and 2D NMR data were in agreement with the published data of madurastatin C1 (**48**) up to C-26. Thus, compound **60**, designated as madurastatin G2, was identified as linear tetrapeptide with $N\alpha$ -methyl

ornithine linked at the N-terminus *via* a hydroxamate moiety. In comparison, compound **59**, titled madurastatin G1, was lacking the *N* α -methyl group at the terminal ornithine residue (Table 10).

Table 10: ^1H and ^{13}C data of **59** and **60** (^1H : 400 MHz, ^{13}C : 101 MHz, $\text{DMSO-}d_6$) including COSY and selected HMBC correlations.



position	59		60	
	δ_{H} (<i>J</i> in Hz)	δ_{C} , type	δ_{H} (<i>J</i> in Hz)	δ_{C} , type
1	–	159.1	–	159.0
2	7.00, d (7.9)	116.7, CH	7.00, d (8.2)	116.6, CH
3	7.47, ddd (8.3, 7.4, 1.5)	134.1, CH	7.47, ddd (8.4, 7.2, 1.4)	134.0, CH
4	6.96, ddd (8.0, 7.0, 1.0)	119.2, CH	6.95, t (7.5)	119.1, CH
5	7.64, dd (7.8, 1.5)	128.1, CH	7.64, dd (7.8, 1.4)	128.1, CH
6	–	110.0	–	109.9
7	–	165.9	–	165.8
9	5.02, dd (10.4, 7.8)	67.5, CH	5.03, dd (10.2, 7.8)	67.4, CH
10	4.64, dd (10.3, 8.6)	69.5, CH ₂	4.65, dd (10.2, 8.6)	69.4, CH ₂
	4.52, t (8.1)		4.52, t (8.1)	
11	–	170.3	–	170.1
12	8.58, t (5.8)	–	8.63, t (5.4)	–
13	3.76, dd (16.4, 5.9)	42.2, CH ₂	3.76, dd (16.5, 5.9)	42.2, CH ₂
	3.67, dd (16.5, 5.5)		3.67, dd (16.6, 5.5)	
14	–	168.5	–	168.4
15	7.98, t (5.4)	–	7.98, t (5.1)	–
16	3.31–3.22, m	34.8, CH ₂	3.31–3.23, m	34.7, CH ₂
17	2.57–2.50, m	32.1, CH ₂	2.57–2.51, m	32.0, CH ₂
18	–	171.0	–	170.9
20	3.67–3.61, m	46.6, CH ₂	3.65–3.57, m	46.7, CH ₂
	3.42–3.36, m		3.46–3.37, m	
21	1.71–1.60, m	28.5, CH ₂	1.71–1.61, m	27.2, CH ₂
22	1.70–1.59, m	22.2, CH ₂	1.67–1.61, m	22.1, CH ₂
23	3.34–3.28, m	53.5, CH	3.16–3.12, m	62.6, CH
24	–	170.9	–	169.7

26

–

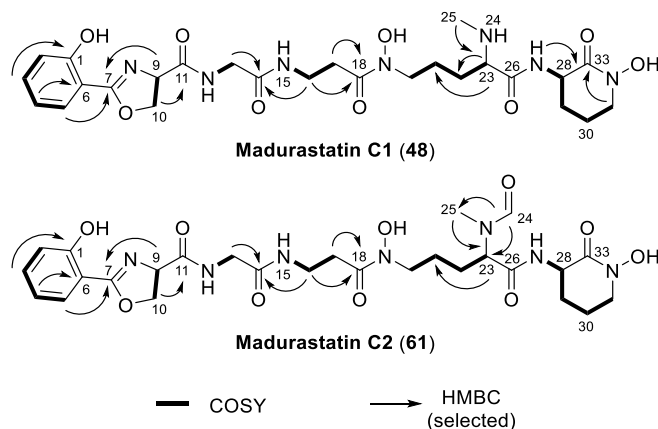
–

2.43, br s

31.6, CH₃

HRMS analysis suggested a molecular formula of C₂₇H₃₇N₇O₁₀ (m/z 620.2667 [M+H]⁺, Δppm 1.29) for compound **61** indicating a high similarity to madurastatin C1 (**48**) with an extra carbonyl group. As NMR data showed additional HMBC correlations to C-23 and C-25 by the aldehyde proton H-24 (δ_{H} 8.08 ppm, δ_{C} 163.3 ppm), **61**, named madurastatin C2, was identified as formamide derivative of **48** (Table 11). A second set of signals was observed for the methyl and formamide substituent at N-24 indicating *cis-trans* isomerization of the amide bond (Fig. S87).^[116] Since **61** was observed in the crude extract and acidic conditions were strictly avoided which excluded the use of formic acid as additive in HPLC solvents, it was most unlikely that the formamide **61** had only been formed during isolation and must therefore be produced biosynthetically.

Table 11: ¹H and ¹³C data of **61** in comparison to madurastatin C1 (**48**) (¹H: 400 MHz, ¹³C: 101 MHz, DMSO-*d*₆) including COSY and selected HMBC correlations.



position	48		61	
	δ_{H} (J in Hz)	δ_{C} , type	δ_{H} (J in Hz)	δ_{C} , type
1	–	159.1	–	159.0
2	6.99, d (8.1)	116.6, CH	7.01, d (8.3)	116.6, CH
3	7.46, t (7.7)	134.0, CH	7.47, ddd (8.1, 7.5, 1.4)	134.0, CH
4	6.93, t (6.5)	119.0, CH	6.95, td (7.5, 1.0)	119.1, CH
5	7.64, dd (7.8, 1.3)	128.1, CH	7.64, dd (7.8, 1.6)	128.1, CH
6	–	110.0	–	109.9
7	–	165.9	–	165.9
9	5.01, dd (10.4, 7.7)	67.4, CH	5.01, dd (10.3, 7.8)	67.4, CH
10	4.64, dd (10.3, 8.7)	69.4, CH ₂	4.65, dd (10.3, 8.5)	69.4, CH ₂
	4.52, t (8.1)		4.52, t (8.1)	
11	–	170.2	–	170.1
12	8.52, t (5.6)	–	8.52, t (5.8)	–

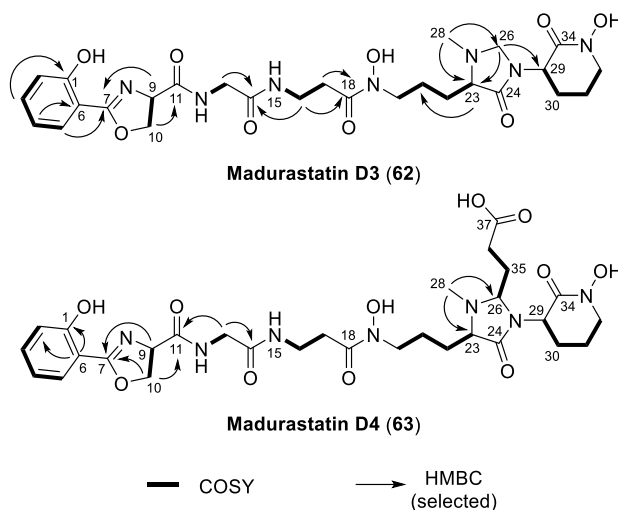
13	3.76, dd (16.5, 6.0) 3.66, dd (16.5, 5.6)	42.2, CH ₂	3.75, dd (16.5, 6.0) 3.66, dd (16.6, 5.8)	42.2, CH ₂
14	–	168.3	–	168.3
15	7.94, br s	–	7.94, br s	–
16	3.26, dd (13.2, 6.9)	34.6, CH ₂	3.26, dd (12.9, 6.7)	34.6, CH ₂
17	2.55–2.51, m	31.9, CH ₂	2.56–2.50, m	31.9, CH ₂
18	–	170.9	–	171.0
20	3.50–3.44, m	47.0, CH ₂	3.54–3.48, m	46.6, CH ₂
21	1.65–1.53, m	22.9, CH ₂	1.47–1.38, m	22.8, CH ₂
22	1.52–1.45, m 1.45–1.35, m	30.3, CH ₂	1.80–1.73, m 1.66–1.59, m	25.2, CH ₂
23	2.84, t (6.5)	63.8, CH	4.13, dd (9.4, 5.7)	59.8, CH
24	–	–	8.08, s	163.3
25	2.20, s	34.3, CH ₃	2.66, s	26.3, CH ₃
26	–	173.7	–	169.3
27	8.07, d (8.2)	–	8.39, d (8.4)	–
28	4.32, ddd (10.1, 8.3, 4.8)	49.3, CH	4.32–4.22, m	49.8, CH
29	1.97–1.87, m 1.67, qd (10.9, 3.4)	27.8, CH ₂	1.90–1.81, m 1.71–1.66, m	27.4, CH ₂
30	1.94–1.83, m	20.3, CH ₂	1.92–1.83, m	20.3, CH ₂
31	3.50–3.44, m	51.2, CH ₂	3.50–3.42, m	51.1, CH ₂
33	–	165.0	–	164.4

In comparison with the published NMR data, compounds **62** and **63** were identified as new derivatives of the madurastatin D series. For **62**, the molecular formula C₂₇H₃₇N₇O₉ (m/z 604.2724 [M+H]⁺, Δppm 0.33) was assigned according to HRMS data. 1D and 2D NMR data revealed only one methyl group to be present in position 28 (δ_{H} 2.32 ppm, δ_{C} 39.5 ppm) in accordance with the published data of madurastatin D1 (**53**) and D2 (**54**). The *N*-methyl protons H-28 showed HMBC correlation with the secondary carbon C-26 (δ_{C} 66.7 ppm). The HSQC correlating methylene protons H-26 (δ_{H} 4.24 / δ_{H} 3.58 ppm) in turn showed HBMC correlation to C-23 (δ_{C} 65.4 ppm) and C-29 (δ_{C} 51.0 ppm). Due to the very similar structure compared to **53** and **54**, **62** was named madurastatin D3 (Table 12).

For compound **63**, HRMS analysis suggested a molecular formulas of C₃₀H₄₁N₇O₁₁ (m/z 676.2937 [M+H]⁺). The NMR spectra proved a high similarity compared to madurastatin D1 (**53**) including the single H-26 proton (δ_{H} 4.04 ppm). COSY correlation to methylene protons H-35 (δ_{H} 1.98–1.92 / δ_{H} 1.87–1.82 ppm) which in turn correlated with methylene protons H-36 (δ_{H} 2.39–2.31 ppm) lead to the hypothesis of **63**, designated as madurastatin D4, being a propionic acid derivative

(Table 12). Limited amount of the isolated sample prevented final confirmation of the structural proposal by according HMBC correlations and chemical shifts of the carbonyl carbons were concluded and assigned based on observations made for the other madurastatins.

Table 12: ^1H and ^{13}C data of **62** and **63** (^1H : 600 MHz, ^{13}C : 151 MHz, $\text{DMSO-}d_6$) including COSY and selected HMBC correlations.



position	62		63	
	δ_{H} (J in Hz)	δ_{C} , type	δ_{H} (J in Hz)	δ_{C} , type
1	—	159.0	—	159.0
2	7.01, d (8.3)	116.6, CH	7.00, dd (8.3, 0.7)	116.6, CH
3	7.47, ddd (8.3, 7.3, 1.5)	134.0, CH	7.47, ddd (8.3, 7.3, 1.6)	134.0, CH
4	6.95, td (7.5, 0.9)	119.0, CH	6.95, ddd (7.9, 7.3, 0.7)	119.0, CH
5	7.65, dd (7.8, 1.8)	128.0, CH	7.64, dd (7.9, 1.6)	128.0, CH
6	—	109.9	—	109.9
7	—	165.8	—	165.8
9	5.01, dd (10.4, 7.8)	67.4, CH	5.02, dd (10.4, 7.7)	67.4, CH
10	4.65, dd (10.4, 8.4) 4.52, t (8.1)	69.4, CH_2	4.64, dd (10.4, 8.5) 4.53, dd (8.5, 7.7)	69.4, CH_2
11	—	170.1	—	170.1
12	8.49, t (5.8)	—	8.57, t (5.9)	—
13	3.75, dd (16.5, 6.1) 3.67, dd (16.5, 5.7)	42.1, CH_2	3.75, dd (16.5, 6.2) 3.67, dd (16.5, 5.7)	42.1, CH_2
14	—	168.3	—	168.3
15	7.91, t (5.1)	—	7.93, t (5.4)	—
16	3.26, dd (13.0, 6.7)	34.6, CH_2	3.26, dd (12.9, 6.7)	34.7, CH_2
17	2.54–2.50, m	31.9, CH_2	2.55–2.51, m	31.8, CH_2
18	—	170.8	—	170.7

3. Oxazoline-containing Madurastatins from *Actinomadura* sp. ST100801

20	3.50–3.44, m	47.2, CH ₂	3.50–3.44, m	47.1, CH ₂
21	1.72–1.66, m	21.9, CH ₂	1.71–1.66, m	21.7, CH ₂
	1.51–1.44, m		1.52–1.48, m	
22	1.90–1.86, m	24.9, CH ₂	1.53–1.48, m	27.2, CH ₂
	1.81–1.77, m			
23	2.86, t (5.4)	65.4, CH	2.86, t (5.2)	64.9, CH
24	–	172.7	–	175.2
26	4.24, d (4.7)	66.7, CH ₂	4.04, br s	77.3, CH
	3.58, dd (4.7, 1.7)			
28	2.32, s	39.5, CH ₃	2.29, s	38.9, CH ₃
29	4.52, t (8.1)	51.0, CH	4.09, br s	51.8, CH
30	1.56–1.50, m	25.8, CH ₂	1.99–1.95, m	24.9, CH ₂
			1.87–1.82, m	
31	1.73–1.67, m	21.9, CH ₂	1.91–1.83, m	20.7, CH ₂
	1.51–1.44, m			
32	3.53–3.47, m	51.1, CH ₂	3.55–3.49, m	50.8, CH ₂
	3.47–3.42, m		3.46–3.40, m	
34	–	162.5	–	162.3
35	–	–	1.98–1.92, m	25.9, CH ₂
			1.87–1.82, m	
36	–	–	2.39–2.31, m	27.1, CH ₂
37	–	–	–	164.9

In conclusion, as postulated by dereplication, structure elucidation by NMR analysis confirmed the biosynthetic production of madurastatin B1 (**50**) and C1 (**48**) by *Actinomadura* sp. ST100801. Furthermore, the other two potentially active derivatives were identified as the very recently published madurastatin D1 (**53**) and D2 (**54**). On top, structure elucidation of nine so far unknown madurastatins was accomplished. The six madurastatins (**48**, **53**, **54** and **61–63**) with a molecular weight above 590 Da were recognized to cluster in the Molecular Network described above proving the concept. Additional three compounds also found in the network were partially purified (Fig. S93–Fig. S95). However, the isolated amount was insufficient for structure elucidation. Yet, the potential of ST100801 to produce a great variety of structurally related madurastatins has still been demonstrated sufficiently.

3.5 Assignment of Absolute Configuration by Marfey's Analysis

With elucidated structures in hand, the absolute configuration of all isolated optically active madurastatins was determined by Advanced Marfey's Analysis using *N* α -(2,4-dinitro-5-fluorophenyl)-L-valinamide (L-FDVA) known as Marfey's reagent.^[117] Enantiopure D-/L-serine, D-/L-ornithine and *N* α -methyl-L-ornithine served as references regarding the retention time of their L-FDVA adducts determined by UPLC-MS for comparison with the hydrolyzed madurastatins featuring unknown stereochemistry (Fig. S96–Fig. S99).

In agreement with published data, the isolated madurastatin B1 (**50**) was identified as (*R*)-**50** based on comparison of the specific rotation value and Marfey's Analysis.^[105] For madurastatin C1 (**48**), two enantiomers had been described in literature.^{[110][115]} According to optical rotation, the isolated **48** was determined as (+)-madurastatin C1 (**48a**) with a configuration of 9*R*, 23*S* and 28*S* which was furthermore confirmed by Marfey's Analysis. In return, its L-FDVA adducts of linear and cyclic *N* δ -hydroxylated L-ornithine including the *N* α -methylated derivative served as further references since the hydroxylamine moieties were relatively stable to acidic digestion and authentic references could not be purchased commercially. The retention times of either single or double derivatized amino acids were considered (Fig. 27).

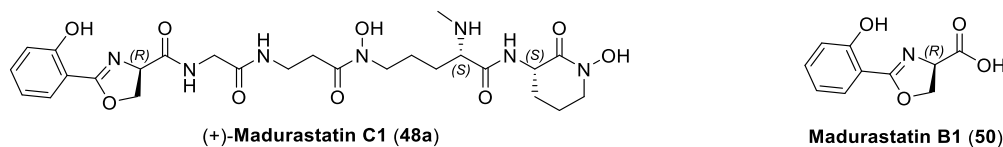


Fig. 27: Absolute configuration of (+)-madurastatin C1 (**48a**) and B1 (**50**).

In alignment with the stereochemistry of **48a** and **50**, the absolute configuration of madurastatin E1 (**56**) and E2 (**58**), F1 (**57**) as well as G1 (**59**) and G2 (**60**) was determined as depicted based on detection of their Marfey adducts (Fig. 28).

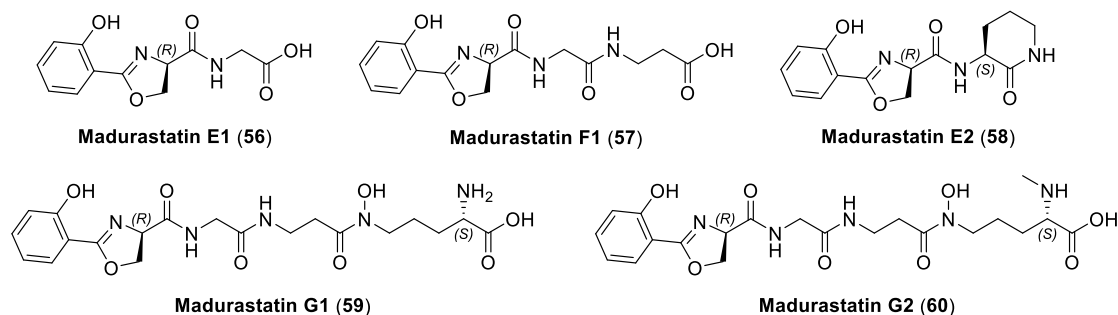


Fig. 28: Absolute configuration of madurastatin E1 (**56**), F1 (**57**), E2 (**58**), G1 (**59**) and G2 (**60**).

In accordance with these findings, the C-9 configuration of madurastatin D1 (**53**) and D2 (**54**) was identified as 9*R* indicating differences to the published data.^[115] In comparison with the Marfey adducts of **48a**, isolated madurastatin D1 (**53**) and D2 (**54**) were postulated to be the total enantiomer

of **53a** and **54a** reported in literature (Fig. 29). However, only for **ent-53a** the optical rotation values⁴ were in good agreement with this hypothesis. Yet, different solvents used for measurement limited the comparability.

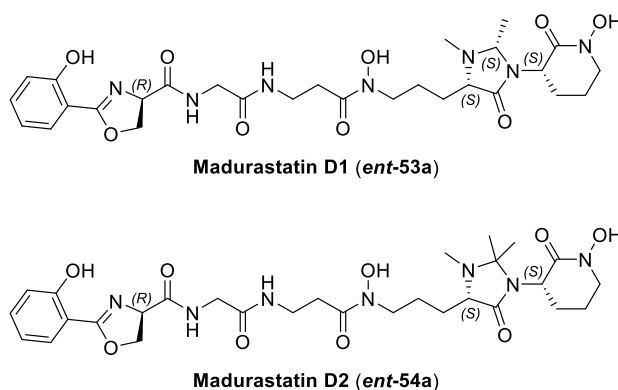


Fig. 29: Absolute configuration of isolated madurastatin D1 (**ent-53a**) and D2 (**ent-54a**).

Consistently, the L-FDVA-derived amino acids of madurastatin C2 (**61**), D3 (**62**) and D4 (**63**) eluted at identical retention times as D-serine and all L-ornithine references. Therefore, their absolute configuration was assigned accordingly. Since in the madurastatin D series, the configuration of residues in position 2 of the 4-imidazolidinone moiety (C-26) is not accessible by Marfey's Analysis, its configuration was postulated according to **ent-53a** (Fig. 30).

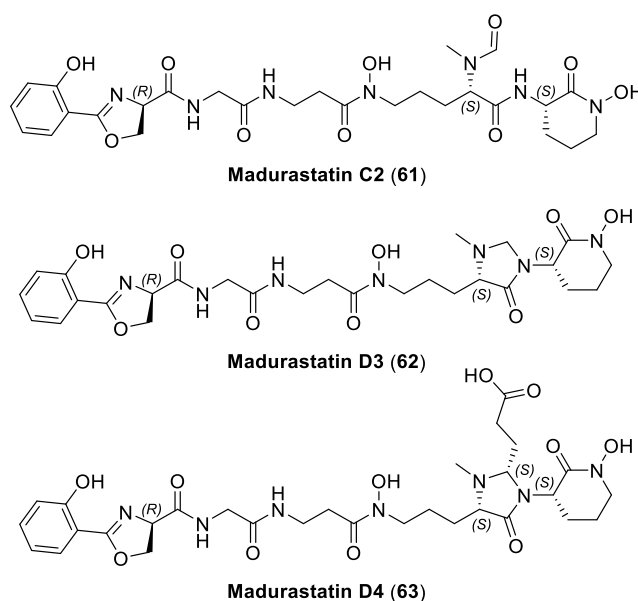


Fig. 30: Absolute configuration of madurastatin C2 (**61**) and D3 (**62**); postulated for madurastatin D4 (**63**).

When present in the molecule, the L-FDVA adducts of glycine and β -alanine were also detected by LC-MS analysis. Overall, Marfey's Analysis was proven appropriate and efficient for assignment of the absolute configuration of all chiral madurastatins.

⁴ Specific rotation: **53a**: $[\alpha]_{436}^{25} +16.6$ (c 0.6, MeOH)^[115], **ent-53a**: $[\alpha]_{\text{D}}^{21} -5.8$ (c 0.2, DMSO); **54a**: $[\alpha]_{436}^{25} -184.3$ (c 1.4, MeOH)^[115], **ent-54a**: $[\alpha]_{\text{D}}^{21} -39.7$ (c 0.15, DMSO).

3.6 Stereoselective Synthesis of Madurastatin B1 and Derivatives

Considering the widely accepted molecular weight cutoff around 600 Da for Gram-negative antibacterials^[118], the much smaller madurastatin B1 (**50**) identified in the crude extract of *Actinomadura* sp. ST100801 were of special interest. Therefore, an extensive literature search regarding potential bioactivity and related natural products was initiated. In fact, a variety of derivatives had been isolated and described. For alcohol **65**, various names were reported for both enantiomers and the outlined activity data of these enantiomers was inconsistent to some extent (Fig. 31).

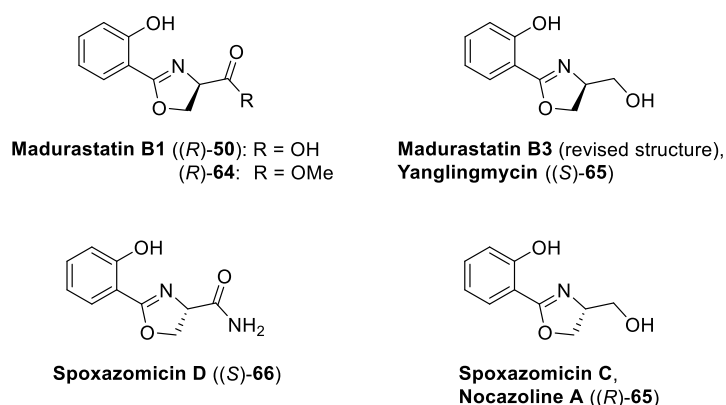
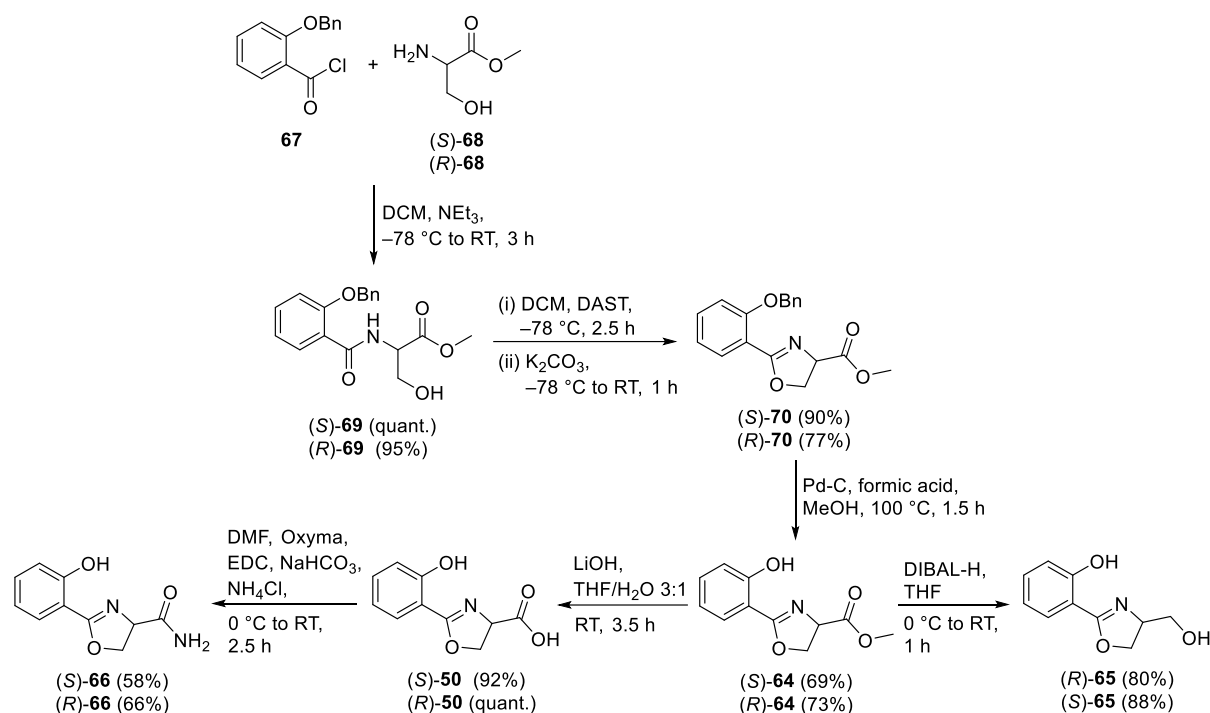


Fig. 31: Overview of madurastatin B1 ((R)-**50**) and B3 ((S)-**65**) and related natural products described in literature. Within the frame of this work, the configuration of **64** was assigned and the structure madurastatin B3 revised from **52** to ((S)-**65**).

In order to comprehensively evaluate the antimicrobial potential of these related small molecules, both enantiomers of methyl ester **64**, carboxylic acid **50**, hydroxyl derivative **65** and carboxamide **66** and were synthesized stereoselectively as part of the bachelor thesis of JANA L. FLÜGEL. Moreover, the originally reported aziridine moiety was revised for madurastatin B1 ((R)-**50**) besides others but has not yet been specifically applied to madurastatin B3 ((S)-**65**).^{[109][110]} Therefore, investigation if the corrected oxazoline structure is also true for **65** was also intended.

Starting from benzoyl chloride **67** and serine methyl esters (S)-**68** resp. (R)-**68**, oxazolines (S)-**70** and (R)-**70** were synthesized in two steps *via* amides (S)-**69** and (R)-**69** according to a literature known procedure.^[110] After benzyl deprotection by transfer hydrogenation, methyl esters (S)-**64** and (R)-**64** were obtained. Subsequently, alcohol derivatives (R)-**65** and (S)-**65** were achieved by reduction with DIBAL-H^[119] while carboxylic acids (S)-**50** and (R)-**50** were synthesized by mild saponification of the ester moieties. Finally, corresponding carboxamides (S)-**66** and (R)-**66** were obtained by EDC-mediated coupling with NH₄Cl (Scheme 3). The target compounds were isolated in good to excellent yields with an enantiomeric excess of above 90% (Fig. S100–Fig. S102) allowing subsequent investigation of their antimicrobial properties.



Scheme 3: Synthesis of carboxylic acid **50**, methyl ester **64**, hydroxyl derivative **65** and caboxamide **66**.

Furthermore, the analytical data of all synthetic references were compared to the natural products described in literature (Table S27). Thereby, the methyl ester **64** isolated by SASAKI *et al.*^[120] was identified as (*R*)-**64**. The published data of madurastatin B1 ((*R*)-**50**)^[105], spoxazomicin D ((*S*)-**66**)^[109], yanglingmycin ((*S*)-**65**)^[121] and its epimer spoxazomicin C^[122] resp. nocazoline A^[123] ((*R*)-**65**) were in full alignment with the synthesized compounds confirming their elucidated structures and configurations. The identical analytical data reported for yanglingmycin and madurastatin B3^[108] clearly indicated that the aziridine structure originally proposed for latter was incorrect. Its structure was revised as it instead features the distinctive oxazoline moiety.

3.7 Antibacterial Activity

The total of 21 compounds, either obtained from isolation or total synthesis, were comprehensively investigated as purified compounds regarding the initially observed antibacterial properties and those reported in literature.

3.7.1 Isolated Madurastatins

The antibacterial activity of all 13 isolated madurastatins was determined by micro broth dilution assay against a selected panel of Gram-negative and Gram-positive bacteria (Table 13).

Table 13: MICs [$\mu\text{g/mL}$] of isolated madurastatins **48a**, **50**, *ent-53a*, *ent-54a* and **55–63**.

	<i>E. coli</i> (MH-II) ATCC 25922	<i>E. coli</i> (MHC) ATCC 25922	<i>M. catarrhalis</i> ATCC 25238	<i>P. aeruginosa</i> ATCC 27853	<i>M. smegmatis</i> ATCC 607	<i>S. aureus</i> ATCC 25923
50	> 128	> 128	> 128	> 128	> 128	> 128
55	> 128	> 128	> 128	> 128	> 128	> 128
56	> 128	> 128	> 128	> 128	> 128	> 128
57	> 128	> 128	> 128	> 128	> 128	> 128
58	> 128	> 128	64–128	> 128	> 128	> 128
59	> 128	128	32	> 128	> 128	> 128
60	> 128	> 128	16–32	> 128	> 128	> 128
48a	> 128	64	4	> 128	> 128	8–16
<i>ent-53a</i>	> 128	64	64	> 128	128	> 128
<i>ent-54a</i>	> 128	128	64	> 128	128	> 128
61	> 128	> 128	8	> 128	> 128	> 128
62	> 128	> 128	8	> 128	> 128	> 128
63	> 128	> 128	16	> 128	> 128	> 128

Activity against Gram-positive *M. luteus* has been consistently reported for the known madurastatin B1 (**50**)^[105], C1 (**48**)^[106], D1 (**53a**) and D2 (**54a**)^[115]. For (+)-madurastatin C1 (**48a**), growth reduction against *B. subtilis*^[110] and *S. aureus*^[106] in disk diffusion assays had also been described, whereas *ent-48a* did not inhibit MRSA (below 100 μM)^[115]. In the present screening, *S. aureus* (MSSA) was the only Gram-positive pathogen included based on its clinical relevance. Growth inhibition was exclusively observed for madurastatin C1 (**48a**) with a MIC value of 8–16 $\mu\text{g/mL}$. Regarding Gram-negative activity, the originally observed growth inhibition towards *E. coli* MHC assigned to madurastatin C1 (**48a**), D1 (*ent-53a*) and D2 (*ent-54a*) by dereplication was reproduced at 64 $\mu\text{g/mL}$ and 128 $\mu\text{g/mL}$, respectively. However, considering these high concentrations, large quantities present in the crude extract and a lower cell density used in 384 well plate screening most likely explain their detection in the first place. No activity was observed for *E. coli* without bicarbonate supplementation and *P. aeruginosa*. Yet, the determined MIC values up to 4 $\mu\text{g/mL}$ against sensitive *M. catarrhalis* allowed evaluation of basic structure-activity relationships. In general, the antibacterial activity of reported madurastatin pentapeptides was described as a result of their siderophore character and related Fe^{3+} uptake inhibition vanishing in ferric iron supplementation experiments.^{[105][106]} This assumption was further supported by the present results indicating a certain length and relevant chelating groups required for growth inhibition. While MIC values of 32 $\mu\text{g/mL}$ were observed for madurastatin G1 (**59**) and G2 (**60**) consisting of four amino

acids, the pentapeptidic madurastatins C1 (**48a**) and C2 (**61**) as well as D1–D4 (**ent-53a**, **ent-54a**, **62**, **63**) were more active on average. However, the rather very low observed antibacterial activity overall discouraged further investigation of the iron dependency by Fe(III) supplementation assay as reported in literature for madurastatin A1 (**47**), C1 (**48a/ent-48a**), D1 (**53a**) and D2 (**54a**).^{[105][106][115]} Instead, iron complex formation was studied by LC-MS analysis (see chapter 3.8).

3.7.2 Synthesized Madurastatin Derivatives

The antibacterial activity of both synthetic enantiomers of **50**, **64**, **65** and **66** was investigated using a similar screening panel. MIC values were analogously determined by micro broth dilution assay. In general, both enantiomers consistently showed identical growth inhibition indicating a stereochemical independent mode of action (Table 14).

Table 14: MICs [$\mu\text{g/mL}$] of the enantiomeric pairs of synthesized compounds **50**, **64**, **65** and **66**.

	(<i>R</i>)- 50	(<i>S</i>)- 50	(<i>R</i>)- 64	(<i>S</i>)- 64	(<i>R</i>)- 65	(<i>S</i>)- 65	(<i>R</i>)- 66	(<i>S</i>)- 66
<i>Escherichia coli</i> ATCC 25922 (MH-II)	> 128	> 128	> 128	> 128	> 128	> 128	> 128	> 128
<i>Escherichia coli</i> ATCC 25922 (MHC)	> 128	> 128	> 128	> 128	64	64	> 128	> 128
<i>Moraxella catarrhalis</i> ATCC 25238	> 128	> 128	16	16	4	4	> 128	> 128
<i>Pseudomonas aeruginosa</i> ATCC 27853	> 128	> 128	> 128	> 128	> 128	> 128	> 128	> 128
<i>Mycobacterium smegmatis</i> ATCC 607	> 128	> 128	> 128	> 128	128	128	> 128	> 128
<i>Bacillus subtilis</i> DSM 10	> 128	> 128	> 128	> 128	> 128	> 128	> 128	> 128
<i>Staphylococcus aureus</i> ATCC 25923	> 128	> 128	> 128	> 128	> 128	> 128	> 128	> 128

For madurastatin B1 ((*R*)-**50**) and its enantiomer (*S*)-**50**, no antibacterial activity was observed against any of the tested strains. This was in alignment with the isolated natural product and literature as mentioned above since *M. luteus* had not been included in the screening.^[105]

Also in agreement with published data, amide **66** showed no growth inhibition up to 128 $\mu\text{g/mL}$. SHAABAN *et al.* had also described a lack antibacterial activity for spoxazomicin D ((*S*)-**66**) against *S. aureus*, *M. luteus*, *E. coli* and *S. enterica* whereas its enantiomer (*R*)-**66** has not been reported so far.^[109]

With a MIC of 16 $\mu\text{g/mL}$, methyl esters **64** showed only weak growth inhibition towards *M. catarrhalis*. Consequently, the activity against *S. aureus*, *B. subtilis* and *E. coli* published for (*R*)-**64** could not be confirmed. The same publication furthermore reported almost complete loss of activity by addition of 50 mM FeCl_3 .^[120]

Regarding antibacterial activity, the hydroxyl derivative **65** was identified as the most potent one. Growth inhibition of *M. smegmatis* (128 µg/mL), *E. coli* MHC (64 µg/mL) and especially *M. catarrhalis* (4 µg/mL) was observed with only the latter being in a relevant range and never having been included in any screening of **65** yet published. In contradiction to the MIC values shown above (Table 14), spoxazomicin C^{[109][122]} and nocazoline A^[123] were described inactive including against *M. smegmatis*. The only activity reported for (*R*)-**65** (found accordingly for (*S*)-**65**) was against *P. syringae* pv. *actinidiae* (7.81 µg/mL) and *R. solanacearum* (15.62 µg/mL).^[124] However, lacking growth inhibition towards *E. coli* (except in MHC), *P. aeruginosa*, *B. subtilis* and *S. aureus* was confirmed by the present results. On the other hand, the antimicrobial activity reported for the enantiomers yanglingmycin^{[121][124]} and madurastatin B3^[108] ((*S*)-**65**) including *E. coli*, *B. subtilis* and *S. aureus* could not be verified.

3.8 Iron Chelating Properties

A feature known especially for the madurastatin pentapeptids is their siderophoric character by comprising one hydroxyphenyloxazoline and two hydroxamate motifs. Iron binding efficiencies comparable to deferoxamine mesylate have been reported for e.g., (–)-madurastatin C1 (**ent-48a**) as well as madurastatin D1 (**53a**) and D2 (**54a**) determined by colorimetric chrome azurol S assay.^[115] Therefore, the iron chelating properties of all madurastatins were investigated by LC-HRESIMS analysis. This approach is also used to identify potential correlations with the observed antibacterial activity.

The traces of ferric iron present in the LC-MS system were sufficient for the corresponding complexes to be formed and detected. The characteristic isotope pattern of iron supported the identification of the resulting $[M-2H+Fe]^+$ adduct ions which were associated with a shift of retention time. Complexation of Fe(III) furthermore caused a characteristic bathochromic shift previously reported (Fig. 32).^{[105][106]} Besides **48a**, **ent-53a** and **ent-54a**, formation of iron complexes was observed for madurastatin C2 (**61**), D3 (**62**) and D4 (**63**) all comprising the three distinctive bidentate ligands (Fig. S103). Furthermore, Fe(III) complexes of madurastatin G1 (**59**) and G2 (**60**) were also detected indicating that the carboxylate moiety represents an appropriate surrogate (Fig. S104). For the smaller madurastatins (**50**, **55–58**) including all synthesized compounds (both enantiomers of **50**, **64–66**) lacking hydroxamate motifs, no Fe(III) chelation occurred. These findings were in alignment with the above-mentioned antibacterial activities supporting the postulated correlation between both features. Yet, for **64** and **65** an iron-independent mode of action needs to be verified by MIC testing with Fe(III) supplementation as formation of complexes involving two or three molecules cannot be precluded, however, are not provable by LC-MS analysis. The madurastatins clearly identified as siderophores

represent a starting point for further investigation including determination of complex formation constants also for trivalent metal ions other than Fe^{3+} . However, these experiments exceed the scope of this work.

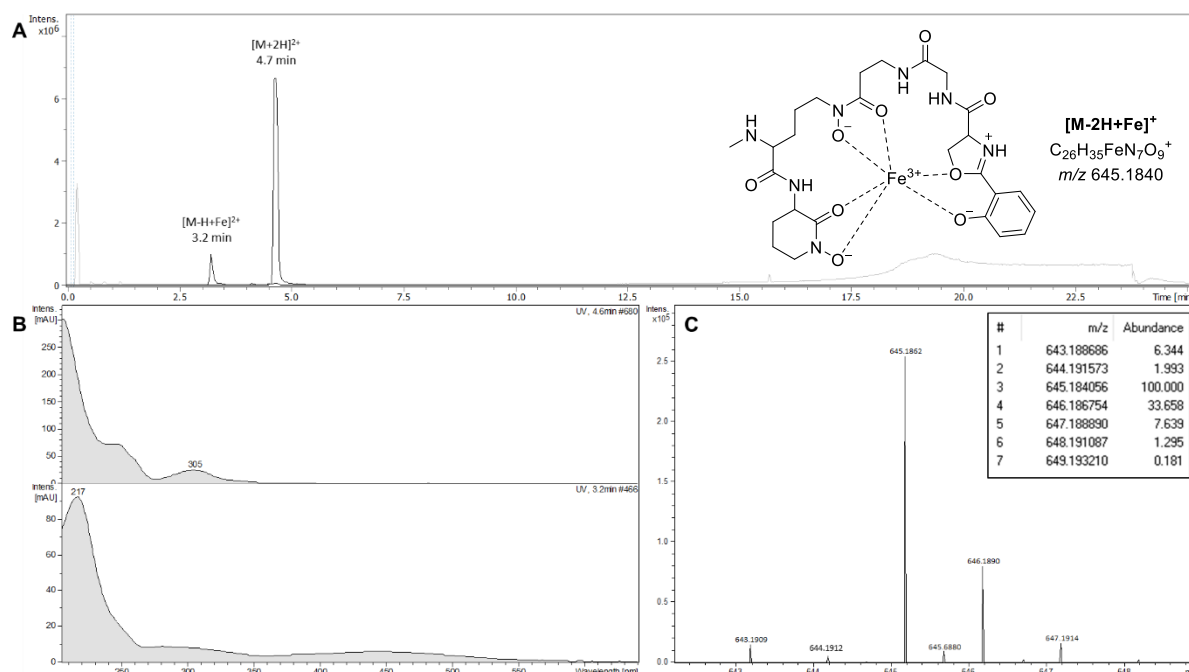


Fig. 32: LC-MS analysis of madurastatin C1 (**48**) and its Fe(III) complex as depicted. A: BPC (grey), EIC (black) of $m/z 323.1058 \pm 0.005$ $[\text{M}-\text{H}+\text{Fe}]^{2+}$ and $m/z 296.6399 \pm 0.005$ $[\text{M}+2\text{H}]^{2+}$; B: UV spectrum of **48** (top) and its Fe(III) complex (bottom); C: Isotope pattern of the $[\text{M}-2\text{H}+\text{Fe}]^+$ adduct ion in alignment with calculated abundance (Compass IsotopePattern, BRUKER).

3.9 Summary and Outlook

The metabolites of *Actinomadura* sp. ST100801 causing the Gram-negative activity against *E. coli* MHC have been investigated. As postulated by dereplication, isolation, structure elucidation and MIC determination of the purified compounds confirmed the known madurastatin C1 (**48a**) and two derivatives as growth inhibiting components. These two analogs were identified as madurastatin D1 (**53**) and D2 (**54**) which had only been published by YAN *et al.* during ongoing isolation.^[115] Assignment of the absolute configuration however revealed the enantiomers of the reported natural products to be produced by ST100801. Thus, **ent-53a** and **ent-54a** are described for the first time.

As the known madurastatin B1 (**50**) was also detected in the crude extract, Molecular Networking was performed and allowed identification of several other potential derivatives produced by ST100801. Detected within the same cluster of **48**, **53** and **54**, three additional compounds (madurastatin C2 (**61**), D3 (**62**) and D4 (**63**)) were isolated and identified now extending the

madurastatin C and D series. Moreover, the structure of six further unpublished madurastatins (B4 (**55**), E1 (**56**) and E2 (**58**), F1 (**57**), G1 (**59**) and G2 (**60**)) breaking the pentapeptidic design was elucidated including assignment of the absolute configuration. For the total of thirteen isolated madurastatins, antibacterial activities and iron chelating properties were determined clearly indicating a correlation between both properties.

Furthermore, based on the correlation between molecular weight and Gram-negative activity, madurastatin B1 (**50**) was of special interest. Therefore, enantioselective total synthesis was performed and extended to the three derivatives **64**, **65** and **66**. The antibacterial potential of all eight compounds was comprehensively studied. Combined analytical and bioactivity data furthermore allowed verification of the results inconsistently reported in literature for the corresponding natural products.

However, taking the determined MIC values into account the pharmaceutical potential of all reported compounds either isolated or synthesized does not meet the requirements for further optimization towards Gram-negative active hit structures. Therefore, evaluation in this direction was stopped. However, other potential applications such as agricultural crop protection targeting e.g., *Septoria tritici* and *Xylella fastidiosa* are suggested to be worth exploring.^{[125][126]}

4. Amino- and Phospholipids from *Olivibacter* sp. FHG000416

4.1 Introduction

Unculturable bacteria or genera consisting of limited known species are most commonly referred to as rare or underexplored.^[127] These microorganisms present both challenges and opportunities at the same time by potentially producing new, antimicrobial active secondary metabolites but requiring innovative cultivation strategies. The phylum Bacteroidetes represents one of the most abundant divisions in the bacterial kingdom. The diverse members of this phylum inhabit almost every ecological niche on the planet including the mammalian microbiome (especially the gastrointestinal tract). A large number of species are known, the majority of which are easy to cultivate.^{[127][128][129]} However, the number of bioactive natural products isolated from Bacteroidetes is very limited. Some of the few antimicrobial active examples are the isopedopeptins (such as isopedopeptin B (**67**))^[130], marinoquinolines (such as marinoquinoline E (**68**))^[131], formadicins^[132], pinensins^[133], TAN-1057 A–D^[134] and elansolid A (**69**)^[135] (Fig. 33).

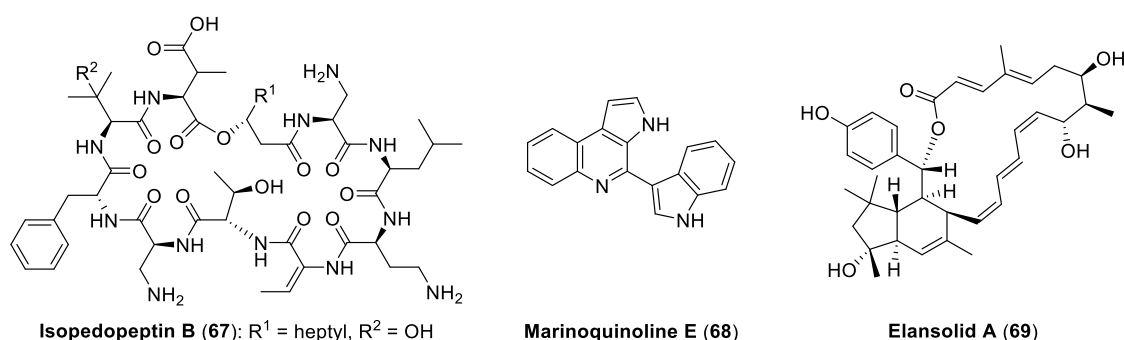


Fig. 33: Antimicrobial active natural products isolated from the phylum Bacteroidetes. Chemical structures of isopedopeptin B (**67**), marinoquinoline E (**68**) and elansolid A (**69**).

These contrary statements indicate not the phylum Bacteroidetes itself but rather its chemical space and biosynthetic potential being underexplored and therefore bearing great potential regarding the discovery of even more new antibiotics of bacterial origin.

4.2 Gram-negative Activity against *E. coli* MHC

Aiming for the discovery of new antimicrobial active secondary metabolites, investigation of the underexplored chemical space of Bacteroidetes was intended. Therefore, a screening project was initiated within the cooperation including all species of the strain collection belonging to this specific

phylum either isolated from environmental samples or purchased commercially. All strains were cultivated in various media, extracted and subjected to primary screening. Among them, the crude extract of FHG000416 was found to inhibit growth of *E. coli* (ATCC 35218) in MHC medium. This strain had previously been isolated from a termite nest provided by the Federal Institute for Materials Research and Testing (BAM) in similar manner as reported.^[70] Based on 16S rRNA gene sequencing, FHG000416 was identified as *Olivibacter* sp. most closely related (94.5%) to type strain *Olivibacter domesticum* (DSM 18733).^{[136][137]}

Based on HRMS/MS-guided UPLC fractionation of the FHG000416 crude extract, activity-based dereplication identified four compounds in two fractions showing growth inhibition (Fig. 34). They were designated as FE003–FE006 (**70–73**).

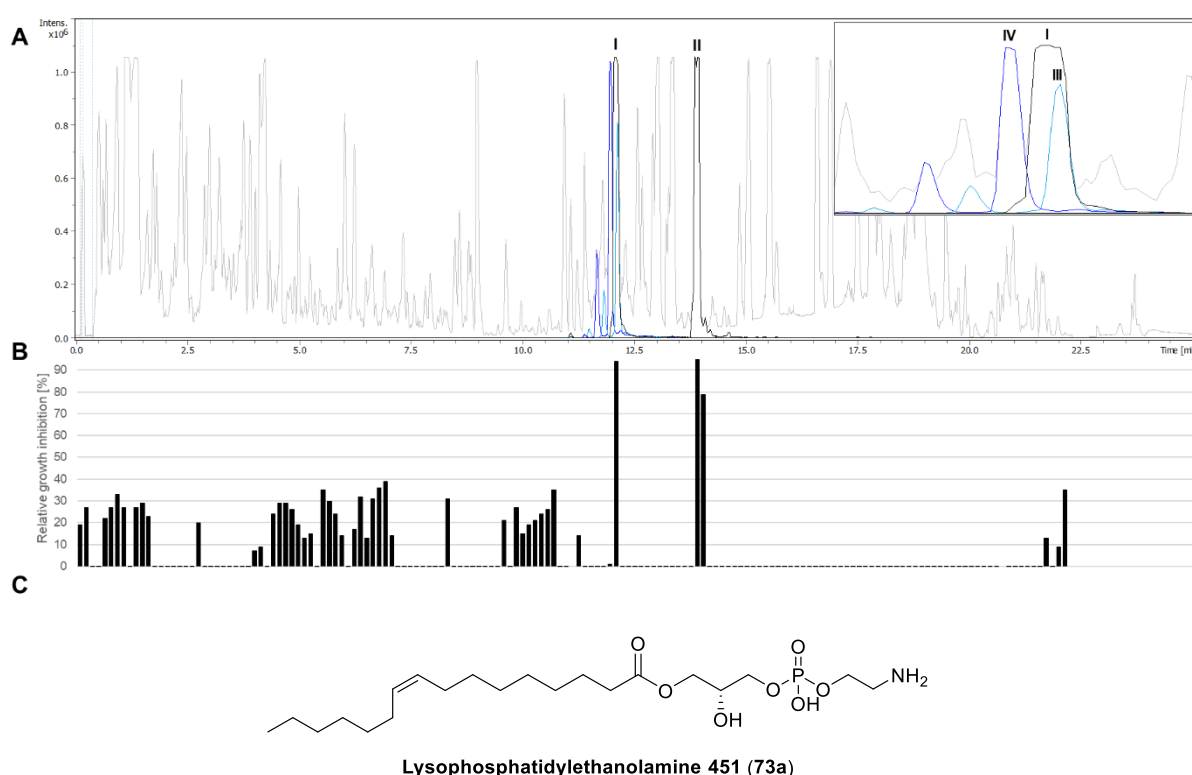


Fig. 34: Crude extract of FHG000416. A: BPC (grey), EIC (black) of I: m/z 376.2694 \pm 0.005, C₁₉H₃₇NO₆ [M+H]⁺ and II: m/z 344.2794 \pm 0.005, C₁₉H₃₇NO₄ [M+H]⁺, EIC (light blue) of III: m/z 440.2770 \pm 0.005, C₂₀H₄₂NO₇P [M+H]⁺ and EIC (dark blue) of IV: m/z 452.2772 \pm 0.005, C₂₁H₄₂NO₇P [M+H]⁺; B: Relative growth inhibition [%] of fractions 1–159 against *E. coli* ATCC 35218 in MHC medium, F-87 and F-100: > 90%; C: Chemical structure of LPE 451 (**73a**) published by WOZNICA *et al.*^[138]

HRMS data suggested the molecular formula C₁₉H₃₇NO₄ (m/z 344.2794, [M+H]⁺, Δ ppm 0.29) for FE003 (**70**) and C₁₉H₃₇NO₆ (m/z 376.2694, [M+H]⁺, Δ ppm 0.33) for FE004 (**71**) indicating derivatives differing in two oxygen atoms. Database search failed to match their analytical features with any known natural product indicating potential novelty. In contrast, for FE006 (**73**) dereplication of the molecular formula C₂₁H₄₂NO₇P (m/z 452.2772, [M+H]⁺) provided LPE 451 (**73a**) (Fig. 34C) as structural hypothesis based on similar MS and MS/MS spectra in accordance with literature (Fig. S105A+B).^[138] This 2-lysophosphatidylethanolamine (C_{16:1}) was isolated from *Algoriphagus*

machipongonensis (*Bacteroidetes* sp.). Based on the molecular formula of $C_{20}H_{42}NO_7P$ according to the positive HRMS ion peak at m/z 440.2770 ($[M+H]^+$, Δ ppm 0.45), FE005 (**72**) was identified as derivative of **73** lacking a single carbon atom. Neutral losses of 141.02 Da corresponding to the phosphatidylethanolamine group followed by 31.00 Da corresponding to the CH_2OH group were equally observed for the MS/MS fragmentation of **72** and **73** indicating the structural variance to be located in the acyl motif (Fig. S105B+C). For structure elucidation and confirmation as well as verification of the antimicrobial potential of FE003–FE006 (**70–73**) produced by *Olivibacter* sp. FHG000416, up-scaled fermentation was performed as starting point for an isolation campaign.

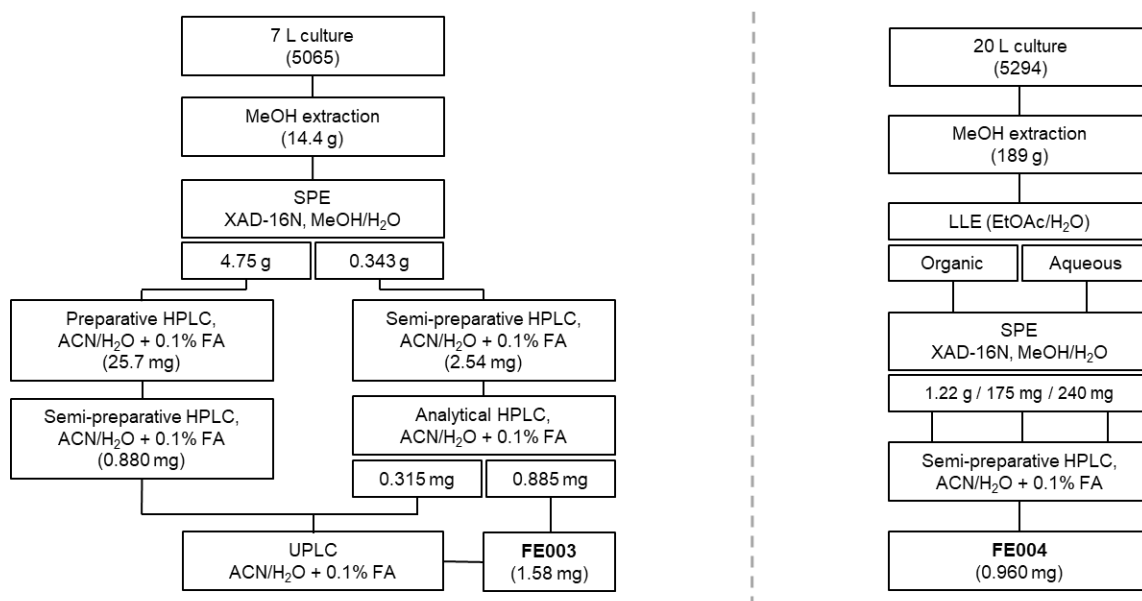
4.3 Isolation

Initial cultivation of all *Bacteroidetes* spp. including FHG000416 was performed under varying conditions including different media. Based on HRMS analysis and relative quantification of all four compounds in the resulting extracts, media for up-scaled fermentation were selected. The highest amount of FE003 (**70**) was observed for cultivation in medium 5065 whereas FE004–FE006 (**71–73**) were produced most sufficiently in medium 5294.

4.3.1 FE003 and FE004

Isolation of FE003 (**70**) started from 7 L fermentation of FHG000416 in medium 5065. The culture was lyophilized and extracted with MeOH followed by SPE fractionation using Amberlite® XAD-16N as absorbent resin and a stepwise increasing gradient of MeOH in H_2O up to 100%. MeOH-soluble components of combined fractions were further fractionated by preparative (Synergi™ Fusion-RP 80 Å, 10 μ m, 250 x 21.2 mm) and/or semi-preparative HPLC (NUCLEODUR® C18 Gravity-SB, 3 μ m, 250 x 10 mm) using gradients of 60–95% and 50–95% ACN in water, respectively. Final purification was achieved by analytical HPLC (Synergi™ Fusion-RP 80 Å, 4 μ m, 250 x 4.6 mm) and UPLC fractionation (ACQUITY UPLC® BEH C18, 1.7 μ m, 100 x 2.1 mm) yielding 1.58 mg FE003 (**70**) (Scheme 4).

Starting point for the isolation of FE004 (**71**) was a fermentation volume of 20 L in medium 5294. Due to the enlarged volume, LLE was performed as additional purification step after MeOH extraction using ethyl acetate and H_2O . Hereafter, the isolation procedure was highly similar to **70**. Semi-preparative HPLC utilizing an adapted gradient of 55–95% ACN in water was appropriate to give 0.960 mg FE004 (**71**) (Scheme 4).



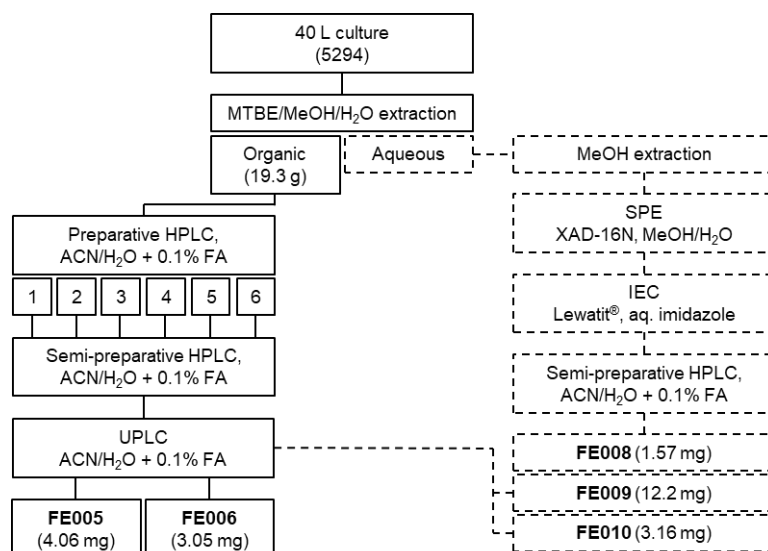
Scheme 4: Isolation scheme of FE003 (**70**) and FE004 (**71**) from liquid culture of FHG000416 in medium 5065 and 5294.

4.3.2 FE005 and FE006

The isolation of FE005 (**72**) and FE006 (**73**) started from another 40 L fermentation of FHG000416 in medium 5294 which was lyophilized and extracted with MTBE/MeOH as reported sufficient for lipid extraction.^[139] Combined organic layers were subsequently fractionated by preparative (Synergi™ Fusion-RP 80 Å, 10 µm, 250 x 21.2 mm) and semi-preparative HPLC (NUCLEODUR® C18 Gravity-SB, 3 µm, 250 x 10 mm) using gradients of 40–95% and 60–95% ACN in water, respectively. Separation of both compounds with very similar elution behavior and final purification was achieved by UPLC fractionation (ACQUITY UPLC® BEH C18, 1.7 µm, 100 x 2.1 mm) yielding 4.06 mg FE005 (**72**) and 3.05 mg FE006 (**73**) (Scheme 5).

4.3.3 Additional compounds

Besides the dereplicated NPs **70–73**, three additional compounds were isolated. The aqueous phase of the initial MTBE extraction (see 4.3.2) was further processed to evaluate the advantage of ion exchange chromatography (IEC) using Lewatit® resin regarding the isolation of remaining phospholipids when FE008–FE010 (**74–76**) were spotted. Semi-preparative HPLC using a C18 column (NUCLEODUR® C18 Gravity-SB, 3 µm, 250 x 10 mm) and gradient elution of 35–85% ACN in water was performed as final isolation step to yield 1.57 mg FE008 (**74**). Combined with purified portions from the organic phase, 12.2 mg FE009 (**75**) and 3.16 mg FE010 (**76**) were obtained (Scheme 5).



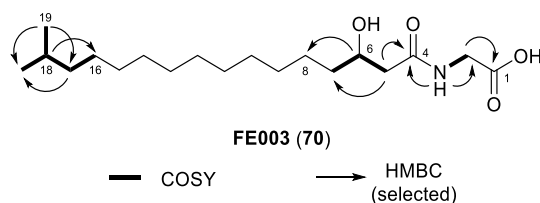
Scheme 5: Isolation scheme of FE005 (72), FE006 (73) (solid outline) and FE008–FE010 (74–76) (dashed outline) from liquid culture of FHG000416 in medium 5294.

All seven metabolites isolated from liquid cultures of *Olivibacter* sp. FHG000416 were obtained in sufficient amount for structure elucidation and further profiling.

4.4 Structure Elucidation

4.4.1 Aminolipids FE003 and FE004

According to dereplication, HRMS analysis suggested the molecular formulas $C_{19}H_{37}NO_4$ (m/z 344.2794, $[M+H]^+$) and $C_{19}H_{37}NO_6$ (m/z 376.2694, $[M+H]^+$) for FE003 (70) and FE004 (71), respectively. In both cases, 1D and 2D NMR spectra revealed an aliphatic acyl group that was identified as *iso*- $C_{17:0}$. The amide protons 3-NH (δ_H 8.01 ppm / 7.76 ppm) showed HMBC correlation to the corresponding carbonyl carbons C-4 (δ_C 171.1 ppm / 171.3 ppm) and additionally COSY correlation to a methylene group (δ_H 3.68 ppm / 3.67 ppm, δ_C 41.0 ppm) showing HMBC correlation to another carbonyl carbon (δ_C 173.8 ppm). Thereby, glycine was identified being connected to the acyl chain *via* peptide bond (Table 15, Table 16). In the case of FE003 (70), the α -methylene protons of the acyl group H-5 (δ_H 2.19 ppm) showed COSY correlation to a single methine proton H-6 (δ_H 3.79–3.74 ppm) suggesting substitution. The chemical shift of the HSQC-correlating carbon atom C-6 (δ_C 67.4 ppm) furthermore supported the hypothesis of a hydroxyl group being attached in β -position. Thus, FE003 (70) was identified as (3-hydroxy-15-methylhexadecanoyl)glycine (Table 15).

Table 15: ^1H and ^{13}C NMR data of FE003 (**70**) (^1H : 600 MHz, ^{13}C : 101 MHz, DMSO- d_6) including COSY and selected HMBC correlations.

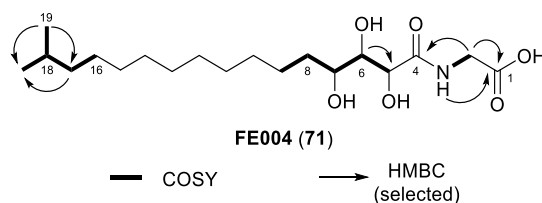
FE003 (70)				
position	structure		δ_{H}	δ_{C}
1	$\text{CH}_2\text{-COOH}$		–	n.d.
2	$\text{NH-CH}_2\text{-COOH}$	3.68, ddd (27.2, 17.4, 5.8 Hz, 2H)		41.0
3	CO-NH-CH_2	8.01, t (5.7 Hz, 1H)		–
4	$\text{CH}_2\text{-CO-NH}$		–	171.1
5	$\text{CH-CH}_2\text{-CO}$	2.19, d (6.4 Hz, 2H)		43.6
6	$\text{CH}_2\text{-CH-CH}_2$	3.79–3.74, m (1H)		67.4
7	$\text{CH}_2\text{-CH}_2\text{-CH}$	1.33–1.27, m (2H)		36.8
8	$\text{CH}_2\text{-CH}_2\text{-CH}$	1.40–1.36, m (2H)		25.1
9–16	aliphatic CH_2	1.26–1.21, m (16H)		29.3, 29.1, 29.1, 29.1, 29.0, 29.0, 29.0, 26.8
17	$\text{CH-CH}_2\text{-CH}_2$	1.15–1.11, m (2H)		38.5
18	$(\text{CH}_3)_2\text{-CH-CH}_2$	1.49, non (6.6 Hz, 1H)		27.4
19	$(\text{CH}_3)_2\text{-CH}$	0.84, d (6.6 Hz, 6H)		22.5

n.d.: Not determined (due to extreme line broadening).

In comparison to **70**, FE004 (**71**) contained two additional oxygen atoms according to its molecular formula. The NMR spectra confirmed the expected similarities except for the methine proton H-6 (δ_{H} 3.44 ppm, δ_{C} 75.4 ppm) showing COSY correlations to methine instead of methylene protons in α - (H-5, δ_{H} 4.19 ppm) and γ -position (H-7, δ_{H} 3.40–3.35 ppm) of the acyl chain. In agreement with the chemical shift of the HSQC-correlating carbon atoms C-5 and C-7 ($\delta_{\text{C-5}}$ 70.9 ppm, $\delta_{\text{C-7}}$ 69.5 ppm) hydroxylation was determined at both sites identifying FE004 (**71**) as (2,3,4-trihydroxy-15-methylhexadecanoyl)glycine (Table 16).

4. Amino- and Phospholipids from *Olivibacter* sp. FHG000416

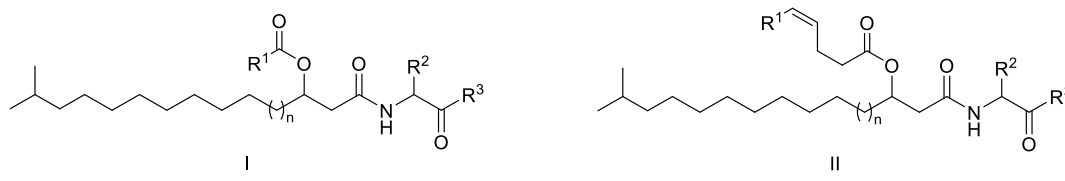
Table 16: ^1H and ^{13}C NMR data of FE004 (71) (^1H : 600 MHz, ^{13}C : 151 MHz, DMSO- d_6) including COSY and selected HMBC correlations.



		FE004 (71)	
position	structure	δ_{H}	δ_{C}
1	$\text{CH}_2\text{-COOH}$	–	173.8
2	$\text{NH-CH}_2\text{-COOH}$	3.67, dd (17.6, 5.3 Hz, 1H) 3.80, dd (17.4, 5.8 Hz, 1H)	41.0
3	CO-NH-CH_2	7.76, t (5.6 Hz, 1H)	–
4	CH-CO-NH	–	171.3
5	CH-CHOH-CO	4.19, s (1H)	70.9
5-OH	CH-CHOH-CO	5.25, br s (1H)	–
6	CH-CHOH-CH	3.44, dd (8.8, 1.1 Hz, 1H)	75.4
6-OH	CH-CHOH-CH	n.o.	–
7	$\text{CH}_2\text{-CHOH-CH}$	3.40–3.35, m (1H) ^a	69.5
7-OH	$\text{CH}_2\text{-CHOH-CH}$	4.43, br s (1H)	–
8	$\text{CH}_2\text{-CH}_2\text{-CHOH}$	1.83–1.79, m (1H), 1.41–1.37, m (1H)	33.4
9	$\text{CH}_2\text{-CH}_2\text{-CHOH}$	1.60–1.55, m (1H), 1.42–1.37, m (1H)	25.1
10–16	aliphatic CH_2	1.35–1.28, m (14H)	29.4, 29.3, 29.2, 29.1, 29.1, 29.1, 26.8
17	$\text{CH-CH}_2\text{-CH}_2$	1.20–1.16, m (2H)	38.5
18	$(\text{CH}_3)_2\text{-CH-CH}_2$	1.49, non (6.6 Hz, 1H)	27.4
19	$(\text{CH}_3)_2\text{-CH}$	0.84, d (6.6 Hz, 6H)	22.5

n.o.: Not observed; ^aAssigned based on HSQC spectrum due to overlapping water signal.

The production of aminolipids by Gram-negative bacteria including *Bacteroidetes* spp. has frequently been reported. In most cases they remain ‘unidentified’ as no isolation efforts are made to allow chemical characterization.^{[140][141][142][143]} However, some exceptions provided the structures of *N*-(β -acyloxyacyl) mono- or dipeptides usually containing glycine, serine or ornithine and unsaturated or monosaturated *iso*-fatty acids varying in length (Table 17). With this compound class, a variety of bioactivities has been associated including macrophage activation^[144], haemagglutination^[145] and antimicrobial properties.^[146]

Table 17: Chemical structures of isolated aminolipids (**77–86**) reported in literature.


	n	R ¹	R ²	R ³	
I	77 ^[146]	3	-(CH ₂) ₁₀ CH(CH ₃) ₂	-H (Gly)	-OH
	78 ^{[147][148][149][150]}	3	-(CH ₂) ₁₁ CH(CH ₃) ₂	-H (Gly)	-OH
	79 ^[145]	3	-(CH ₂) ₁₁ CH(CH ₃) ₂	-CH ₂ OH (Ser)	-OH
	80 ^[145]	3	-(CH ₂) ₁₁ CH(CH ₃) ₂	-(CH ₂) ₂ NH ₂ (Orn)	-OH
	81 ^[151]	2	-(CH ₂) ₁₁ CH(CH ₃) ₂	-H (Gly)	-NH-X-COOH (Ser)
	82 ^{[148][150][151][152]}	3	-(CH ₂) ₁₁ CH(CH ₃) ₂	-H (Gly)	-NH-X-COOH (Ser)
II	83 ^[149]	2	-(CH ₂) ₇ CH(CH ₃) ₂	-H (Gly)	-OH
	84 ^[149]	3	-(CH ₂) ₇ CH(CH ₃) ₂	-H (Gly)	-OH
	85 ^[151]	2	-(CH ₂) ₇ CH(CH ₃) ₂	-H (Gly)	-NH-X-COOH (Ser)
	86 ^[151]	3	-(CH ₂) ₇ CH(CH ₃) ₂	-H (Gly)	-NH-X-COOH (Ser)

X = CHCH₂OH

Furthermore, antibacterial activity has been reported for lipid 430 (**87**), first obtained by enzymatic or chemical hydrolysis of lipid 654 (**82**) (also referred to as flavolipin, topostin D654 and WB-3559 D^[153]) and later isolated from *Algibacter* sp.^{[154][155][156]} Both lipodipeptides feature glycine and L-serine at their C-terminus (Fig. 35).

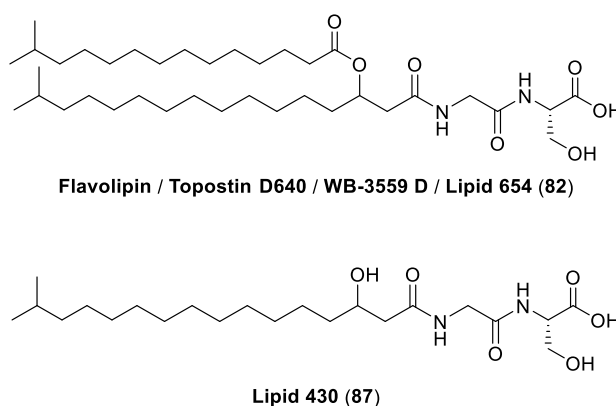


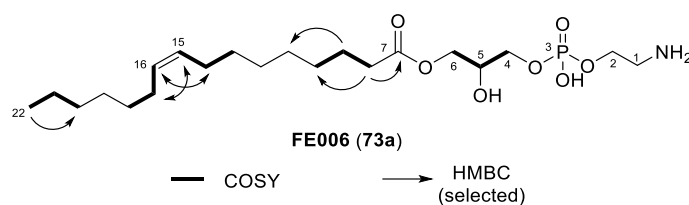
Fig. 35: Chemical structures of lipid 654 (**82**), also referred to as flavolipin, topostin D640 and WB-3559 D, as well as lipid 430 (**87**).

Lipid 654 (**82**) and in particular lipid 430 (**87**) have also been found to activate the Toll-like receptor 2 (TLR2) which plays an important role in pathogen response by activation of the immune system.^[155] The terminal serine residue is the only structural difference of **87** compared to FE003 (**70**).

4.4.2 Lysophospholipids FE005 and FE006

Based on HRMS analysis, the molecular formula $C_{21}H_{42}NO_7P$ (m/z 452.2772, $[M+H]^+$) had been suggested for FE006 (**73**). NMR analysis confirmed the occurrence of lysophosphatidylethanolamine ($C_{16:1}$) as postulated by dereplication (Table 18). According to published data, the double bond (methine protons: δ_H 5.24–5.12 ppm) of the mono-unsaturated palmitoyl motif was assigned to Δ^9 position with (*Z*)-configuration and the acyl chain being attached to the glycerol moiety at *sn*-1 position.^[138] Thus, FE006 (**73a**) was identified as 1-(9*Z*-palmitoyl)-2-hydroxy-*sn*-glycerol-3-phosphoethanol-amine (2-LPE). As the present data did not allow clear differentiation from the constitutional *sn*-2 isomer **73b** with (*E*)-configuration reported by MEYLAERS *et al.*^[157], the structure remains a proposal.

Table 18: 1H and ^{13}C NMR data of FE006 (**73a**) (1H : 600 MHz, ^{13}C : 151 MHz, $CDCl_3/MeOD-d_4$ 2:1) including COSY and selected HMBC correlations.



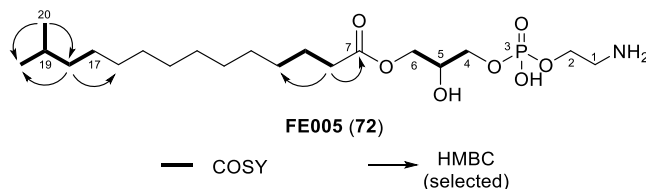
FE006 (73a)				
position	structure	δ_H	δ_C	δ_P
1	CH_2-NH_2	3.01, br s (2H)	40.3	–
2	$P-O-CH_2-CH_2$	3.99–3.92, m (2H) ^a	61.6	–
3	$O-PO_3-CH_2$	–	–	4.42
4	$CH-CH_2-O-P$	3.84–3.70, m (2H) ^a	66.9	–
5	$CH-OH$	3.88–3.82, m (1H) ^a	68.5	–
6	$CO-O-CH_2$	4.01–3.93, m (2H) ^a	64.7	–
7	CH_2-CO-O	–	174.2	–
8	CH_2-CH_2-CO	2.19, t (7.5 Hz, 2H)	33.9	–
9	CH_2-CH_2-CO	1.51–1.43, m (2H)	24.7	–
10–13, 18–20	aliphatic CH_2	1.22–1.10, m (14H)	31.6, 29.6, 29.6, 29.1, 29.0, 29.0, 28.8	–
14+17	$CH_2-CH=CH-CH_2$	1.91–1.83, m (4H)	27.0, 27.0	–
15+16	$CH_2-CH=CH-CH_2$	5.24–5.12, m (2H)	129.9, 129.6	–
21	$CH_3-CH_2-CH_2$	1.18–1.11, m (2H) ^a	22.5	–
22	CH_3-CH_2	0.73, t (6.9 Hz, 3H)	13.8	–

^aAssigned based on HSQC spectrum due to overlapping signals.

In comparison to **73**, HRMS analysis had assigned the molecular formula $C_{20}H_{42}NO_7P$ for FE005 (**72**) according to the positive ESIMS peak at m/z 440.2770 ($[M+H]^+$, Δ ppm 0.45) indicating one carbon

atom and double bond less. 1D and 2D NMR data confirmed the double bond of the acyl chain to be missing with an *iso*-C_{15:0} side chain replacing the unbranched linear alkenyl moiety. Therefore, FE005 (**72**) was identified as 1-isopentadecanoyl-2-hydroxy-*sn*-glycerol-3-phosphoethanolamine (Table 19).

Table 19: ¹H and ¹³C NMR data of FE005 (**72**) (¹H: 600 MHz, ¹³C: 151 MHz, CDCl₃/MeOD-*d*₄ 2:1) including COSY and selected HMBC correlations.



		FE005 (72)		
position	structure	δ_{H}	δ_{C}	δ_{P}
1	$\text{CH}_2\text{-NH}_2$	2.91, br s (2H)	40.3	—
2	$\text{P-O-CH}_2\text{-CH}_2$	3.87–3.83, m (2H) ^a	61.3	—
3	$\text{O-}^-\text{PHO}_3\text{-CH}_2$	—	—	0.75
4	$\text{CH-CH}_2\text{-O-P}$	3.74–3.63, m (2H) ^a	66.7	—
5	CH-OH	3.79–3.74, m (1H) ^a	68.5	—
6	CO-O-CH_2	3.93–3.88, m (2H) ^a	64.6	—
7	$\text{CH}_2\text{-CO-O}$	—	174.1	—
8	$\text{CH}_2\text{-CH}_2\text{-CO}$	2.12, t (7.9 Hz, 2H)	33.8	—
9	$\text{CH}_2\text{-CH}_2\text{-CO}$	1.42–1.36, m (2H)	24.6	—
10–17	aliphatic CH_2	1.11–1.01, m (16H)	29.6, 29.4, 29.3, 29.3, 29.2, 29.0, 28.9, 27.1	—
18	$\text{CH-CH}_2\text{-CH}_2$	0.95–0.90, m (2H)	38.8	—
19	$(\text{CH}_3)_2\text{-CH-CH}_2$	1.29, non (6.7 Hz, 1H)	27.7	—
20	$(\text{CH}_3)_2\text{-CH}$	0.63, d (6.6 Hz, 6H)	22.2	—

^aAssigned based on HSQC spectrum due to overlapping signals.

In general, lysophospholipids result from partial hydrolysis of phospholipids mediated by phospholipase A (PLA). In contrast to their precursors, they are only minor components of cell membranes.^[158] Their biological role however exceeds membrane-associated functions and mediation of extracellular signaling.^[159] Specifically for LPE, induction of neuronal differentiation, stimulation of MAPK cascade as well as antifungal and antibacterial activities have been reported.^[158] With FE005 (**72**), a new member of the LPE class was identified. Evaluation of its antimicrobial potential and TLR2-activating properties was intended to be compared to FE006 (**73a**).

4.4.3 *N*-Acyl Amino Acids FE008, FE009 and FE010

Based on HRESIMS analysis, for FE008 (**74**) the molecular formula $C_{16}H_{23}NO_4$ was assigned according to the positive $[M+H]^+$ peak at m/z 294.1700. MS/MS fragmentation indicated a neutral loss of 112.0886 Da corresponding to $C_7H_{12}O$ which correlates to a saturated acyl group as implied by the carbon to hydrogen ratio and double bond equivalents. The resulting fragment of m/z 182.0814 matched the protonated form of tyrosine ($[M+H]^+$, $C_9H_{11}NO_3$). This hypothesis was further supported by neutral losses of NH_3 and H_2O commonly observed for the fragmentation of amino acids (Fig. 36, Fig. 37A).

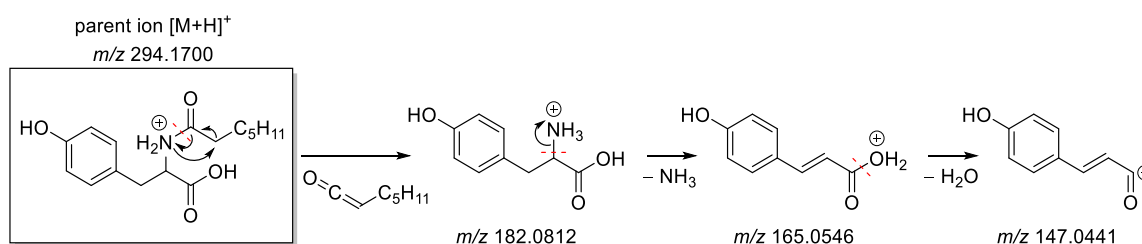


Fig. 36: Postulated MS/MS fragmentation pathway of FE008 (**74**) starting from $[M+H]^+$ parent ion.

The structural hypothesis was confirmed by 1D and 2D NMR. As expected, the AA'BB' pattern of the aromatic protons of tyrosine was observed in the 1H spectrum. Furthermore, an isopropyl group was detected at the end of the acyl moiety identified as *iso*- $C_{7:0}$. This fatty acid side chain was attached to tyrosine *via* peptide bond. Therefore, based on MS and NMR analysis, **74** was identified as *N*-(5-methyl)hexanoyl tyrosine (Table 20).

FE009 (**75**) showed a HRESIMS $[M+H]^+$ ion peak at m/z 322.2013, indicating a molecular formula of $C_{18}H_{27}NO_4$. The MS/MS fragmentation was similar to **74** only the neutral loss of the acyl group differing by 28.0327 Da equivalent to two additional methylene groups (Fig. 37B).

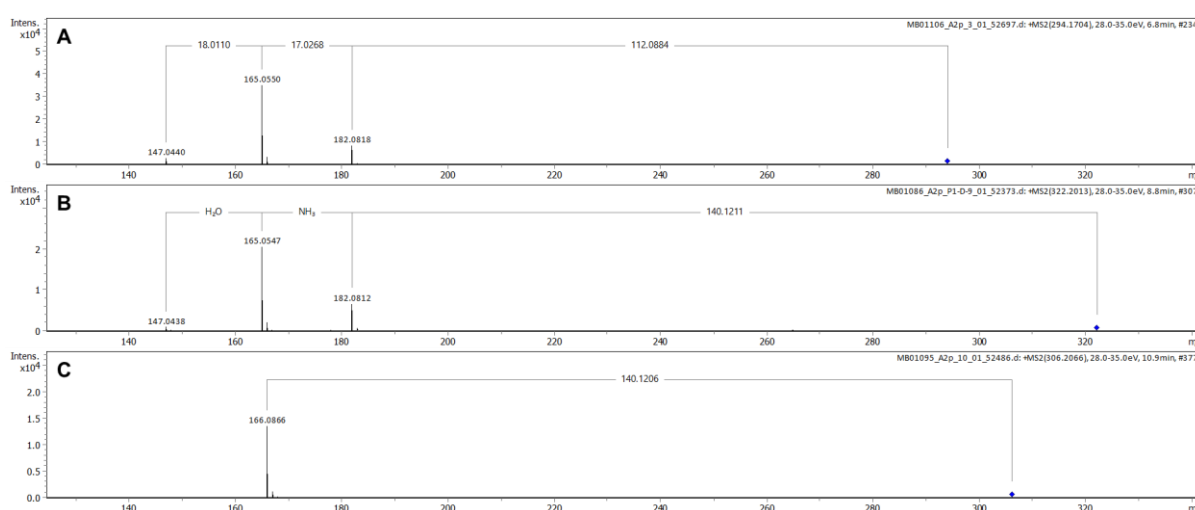
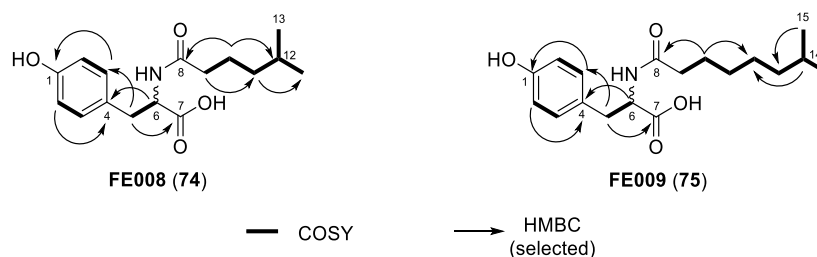


Fig. 37: MS/MS spectra of A: FE008 (**74**), B: FE009 (**75**) and C: FE010 (**76**); neutral losses are annotated.

NMR analysis confirmed the MS fragmentation-based hypothesis and identified **75** as *N*-(7-methyl)octanoyl tyrosine (Table 20).

Table 20: ^1H and ^{13}C -NMR data of the FE008 (**74**) and FE009 (**75**) (^1H : 400 MHz, ^{13}C : 101 MHz, MeOD- d_4) including COSY and selected HMBC correlations.

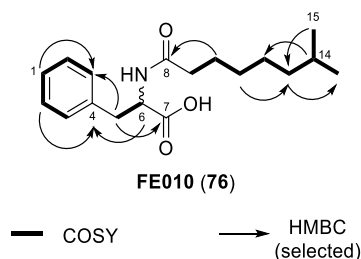
position	FE008 (74)		FE009 (75)	
	δ_{H} (J in Hz)	δ_{C} , type	δ_{H} (J in Hz)	δ_{C} , type
1	–	157.3	–	157.2
2	6.69, dd (6.6, 1.9)	116.1, CH	6.68, dd (6.5, 2.1)	116.1, CH
3	7.04, dd (6.6, 1.9)	131.2, CH	7.03, dd (6.6, 1.5)	131.3, CH
4	–	129.2	–	129.4
5	3.11, dd (14.0, 4.8), 2.83, dd (14.0, 9.3)	37.7, CH ₂	3.11, dd (14.0, 4.9), 2.84, dd (13.9, 8.9)	37.9, CH ₂
6	4.59, dd (9.3, 4.6)	55.3, CH	4.57, dd (8.9, 4.9)	55.7, CH
7	–	175.3	–	175.9
8	–	176.1	–	175.9
9	2.13, t (7.5)	37.1, CH ₂	2.15, t (7.4)	37.0, CH ₂
10	1.55–1.47, m	24.8, CH ₂	1.56–1.48, m	27.0, CH ₂
11	1.14–1.05, m	39.4, CH ₂	1.32–1.24, m	28.2, CH ₂
12	1.52–1.46, m	29.0, CH	1.24–1.18, m	30.4, CH ₂
13	0.86, d (6.6)	22.8/22.9, CH ₃	1.20–1.12, m	40.0, CH ₂
14	–	–	1.57–1.49, m	29.1, CH
15	–	–	0.88, d (6.6)	23.0, CH ₃

For the third compound FE010 (**76**), HRESIMS analysis suggested the molecular formula $\text{C}_{18}\text{H}_{27}\text{NO}_3$ according to the $[\text{M}+\text{H}]^+$ ion peak at m/z 306.2063 (Δppm 0.33). A single neutral loss of 140.1206 Da corresponding to $\text{C}_8\text{H}_{14}\text{O}$ was observed for the MS/MS fragmentation of the parent ion similar to **75**. The resulting fragment with m/z 166.0864 [$\text{C}_9\text{H}_{11}\text{NO}_2^+$] showed one oxygen atom less and was thereby assumed to be phenylalanine instead of tyrosine. However, no further fragmentation was observed (Fig. 37).

1D and 2D NMR data confirmed **76** to consist of the identical terminal single branched acyl chain lacking the aromatic hydroxyl group in *para*-position (Table 21). FE010 (**76**) was identified as *N*-(7-methyl)octanoyl phenylalanine. Moreover, a second set of signals was observed especially for

the aliphatic protons (< 2 ppm) indicating the occurrence of a second isomer at a ratio of 1:3 (Fig. S116). *Cis-trans* isomerization is frequently reported for secondary amides.^[160]

Table 21: ¹H and ¹³C-NMR data of the FE010 (**76**) (¹H: 400 MHz, ¹³C: 101 MHz, MeOD-*d*₄) including COSY and selected HMBC correlations.



FE010 (76)		
position	δ_H (J in Hz)	δ_C , type
1	7.23–7.17, m	127.8, CH
2	7.30–7.22, m	129.4, CH
3	7.26–7.21, m	130.3, CH
4	–	138.7
5	3.22, dd (13.9, 4.8), 2.93, dd (13.9, 9.5)	38.5, CH ₂
6	4.66, dd (9.4, 4.8)	55.1, CH
7	–	175.2
8	–	176.1
9	2.14, t (7.4)	36.9, CH ₂
10	1.55–1.46, m	26.9, CH ₂
11	1.32–1.23, m	28.2, CH ₂
12	1.23–1.14, m	30.4, CH ₂
13	1.22–1.10, m	40.0, CH ₂
14	1.55–1.49, m	29.1, CH
15	0.87, d (6.6)	23.1/23.0, CH ₃

To the best of knowledge, **74–76** have not been described as NPs so far. Yet, BRADY *et al.* reported the isolation of long chain *N*-acyl tyrosines by heterologous expression of environmental DNA (eDNA) from soil samples in *E. coli*. They identified various saturated and mono-unsaturated, however unbranched *N*-acyl substituted *L*-tyrosines with acyl groups ranging from C₈ to C₁₈. The side chain length clearly affected the antibacterial activity against *B. subtilis*.^{[161][162]} Based on the same approach, they furthermore reported the characterization of analogous tryptophans and arginines also exhibiting antibacterial properties.^[163]

Gymnastatin N (**88**) represents another natural product belonging to the class of aliphatic *N*-acyl substituted tyrosines. It was isolated as mixture of two diastereomers from the fungus *Arachniotus punctatus* with reported activity against the anti-cancer target POLO-like kinase 1 (Plk1). Within the frame of the same work, FE010-related *N*-dodecanoyl-L-phenylalanine (**89**) was synthesized (Fig. 38).^[164] However, to the best of knowledge, no aliphatic *N*-acyl substituted phenylalanine has been described as natural products so far.

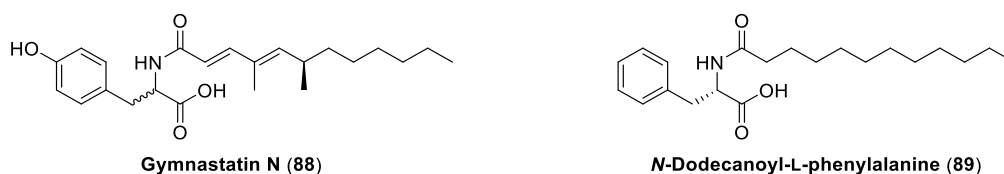


Fig. 38: Chemical structures of gymnastatin N (**88**) and *N*-dodecanoyl-L-phenylalanine (**89**).

4.4.4. Aminolipids Lipid 430 and FE002

Having isolated aminolipid FE003 (**70**) and FE004 (**71**), their structural similarity to TLR2-stimulating lipid 430 (**87**) strongly suggested to include this aspect in the bioactivity profiling. In order to allow conclusive comparison with reported data, the use of **87** as additional positive control in the immunoassays was intended. Since **87** was not produced by FHG000416, the initially cultivated Bacteroidetes set was searched for a producer strain. *Chitinophaga eiseniae* DSM 22224 was identified to sufficiently produce lipid 430 (**87**). This strain was simultaneously exploited in a separate isolation project with regard to other metabolites with antimicrobial potential.⁵ Lipid 430 (**87**) was therefore isolated from provided fractions in a straight-forward manner (see 7.2.3.2). HRMS and NMR data were in agreement with reported data.^[156]

Based on MS/MS analysis, an additional compound produced by DSM 22224 shared the characteristic fragment ion of m/z 326.2693 (corresponding to $C_{19}H_{36}NO_3^+$) that had also been observed for FE003 (**70**) and lipid 430 (**87**) (Fig. S126). This compound with a molecular formula of $C_{27}H_{52}N_4O_7$ according to the positive HRMS peak at m/z 545.3908 was named FE002 (**90**). The MS/MS fragmentation of **90**, revealed neutral losses of H_2O , ornithine and serine resulting in the commonly shared fragment ion. Therefore, FE002 (**90**) was postulated to be the corresponding tripeptidic analog (Fig. 39). It was isolated (see 7.2.3.2) and subjected to NMR analysis. Although sample concentration did not allow recording of an appropriate ^{13}C spectrum, the structure hypothesis could be confirmed based on 1H and 2D data in comparison to lipid 430 (**87**).

⁵ This isolation campaign was performed by STEPHAN BRINKMANN.

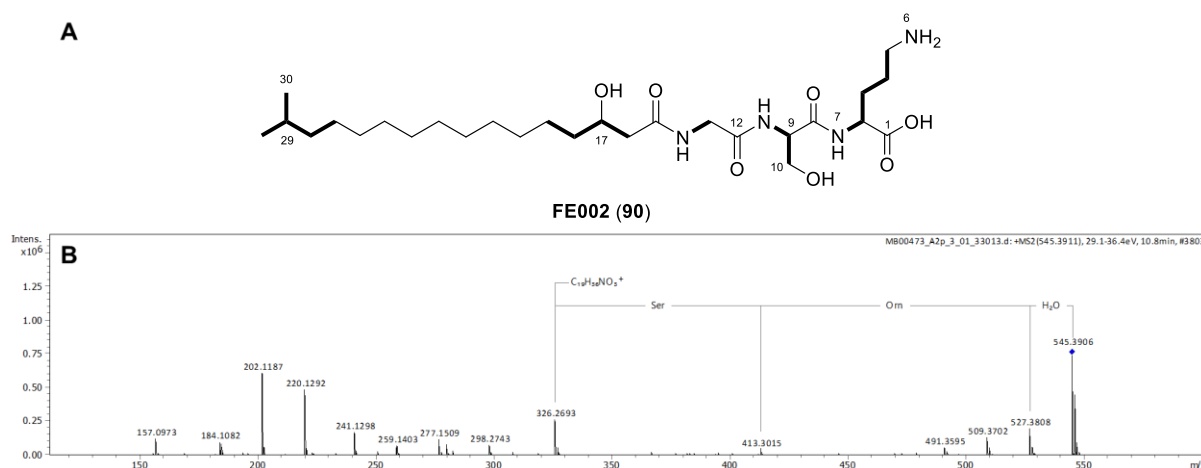


Fig. 39: A: Chemical structure of FE002 (**90**) including observed COSY correlations; B: MS/MS spectrum of **90**, neutral losses leading to fragment of m/z 326.2693 ($C_{19}H_{36}NO_3^+$) are annotated.

4.5 Assignment of Absolute Configuration

The stereochemistry of chiral amino acids incorporated in lipid 430 (**87**) and FE002 (**90**) as well as FE008–FE010 (**74–76**) was determined by Advanced Marfey's Analysis using L-FDVA as Marfey's reagent.^[126] D- and L-enantiomers of serine, ornithine and tyrosine as well as L- and DL-phenylalanine served as retention time references.

In agreement with published data, the serine residue of lipid 430 (**87**) was identified as L-serine (Fig. S127).^[155] This was also true for FE002 (**90**) furthermore containing L-ornithine (Fig. S127, Fig. S128). Regarding the C-3 stereochemistry of the acyl group it was considered reasonable to assume that FE003 (**70**), **87** and **90** share (*R*)-configuration based on: i) the 3*R*-configuration of WB-3559 D (Fig. 35) elucidated by total synthesis^[165] and stereospecific hydrolysis of only (*R*)-lipid 654 (**82a**) by PLA2 yielding lipid 430 (**87**)^[166], ii) the fact that all serine residues share L-configuration further emphasizing a biosynthetic relation of the compounds and iii) the consistently positive optical rotation values (Fig. 40).

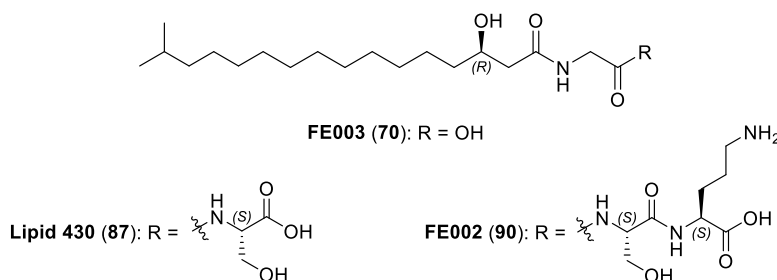


Fig. 40: Absolute configuration of FE003 (**70**), lipid 430 (**87**) and FE002 (**90**) isolated from *Bacteroidetes* spp. FHG000416 and DSM 22224.

A common approach for determination of the absolute configuration of 3-hydroxy fatty acids incorporated *via* amide or ester bond is acidic hydrolysis followed by the derivatization using Mosher's reagent to obtain the corresponding (*S*)-MTPA and (*R*)-MTPA esters that can be analyzed by chiral GC-MS^[167] or NMR^[168]. The demand for larger amounts of compound being sacrificed to hydrolysis, either preparative purification steps or chiral columns as well as preparation of not easily accessible authentic standards represent the disadvantages of this analytical method. An elegant procedure to evade these major drawbacks was developed by MOON *et al.* using Marfey's reagent as CDA instead. The absolute configuration of the resulting *O*-Marfey derivatives can be determined by LC-MS based on their elution order. This adapted method however has only been applied to α -hydroxy fatty acids.^[169] The absolute configuration of FE004 (**71**) will be discussed separately (see chapter 4.7) and was not further investigated for FE005 (**72**) and FE006 (**73a**).

Standard Marfey's Analysis of FE008–FE010 (**74–76**) revealed that all three compound had been isolated as enantiomeric mixtures (Fig. S129–Fig. S131). The D/L-ratio was determined by UV signal integration as 1:16 for **74**, 1:1.7 for **75** (Fig. S130) and 1.6:1 for **76** (Fig. S131). In the case **74** and **75**, the double L-FDVA adducts of tyrosine were considered. Twofold hydrogen-deuterium exchange in benzylic position of tyrosine was observed after hydrolysis in DCl/D₂O.

4.6 Bioactivity Profiling

4.6.1 Antimicrobial Activity

The antimicrobial activity of all nine compounds (**70–76**, **87**, **90**) isolated either from FHG000416 or DSM 22224 was determined by micro broth dilution assay against a total of 13 pathogenic microorganisms up to a test concentration of 64 $\mu\text{g/mL}$ (Table 22, Table S28). Overall, the tested aminolipids **70**, **71**, **87** and **90** as well as the lysophospholipids **72** and **73** showed rather low or no antimicrobial activity. The latter case was true for FE004 (**71**) indicating an adverse effect of additional hydroxylation. FE003 (**70**), FE005 (**72**), FE006 (**73a**) and lipid 430 (**87**) inhibited growth of Gram-negative *M. catarrhalis* and Gram-positive *M. luteus* at test concentrations up to 4 $\mu\text{g/mL}$, however lacked activity against more resilient and clinical relevant test strains. FE002 (**90**) was identified as the most potent compound additionally inhibiting growth of *E. coli* MHC, *M. smegmatis* and *B. subtilis* as well as *C. albicans* with MICs of 64 $\mu\text{g/mL}$ and 8 $\mu\text{g/mL}$, respectively.

For Lipid 430 (**87**), the reported growth inhibition (38% at 50 $\mu\text{g/mL}$ ^[156]) of *S. aureus* could not be reproduced. However, the described lack of activity against *E. coli* and *P. aeruginosa* was in accordance with the present findings. For 2-LPE, selective susceptibility of Gram-positive bacteria including *Staphylococcus* spp. and *B. cereus* was presented by VAN RENSBURG *et al.*^[170] Yet, these results were

not confirmed by MEYLAERS *et al.* as the used micro broth assay was assumed to be less sensitive.^[157] In accordance with that, for the isolated FE006 (**73a**) growth inhibition of Gram-positive bacteria was only detected for *M. luteus* with a MIC of 16 $\mu\text{g/mL}$. The same was true for FE005 (**72**). Both compounds moreover exhibited growth inhibition towards Gram-negative *M. catarrhalis*.

Table 22: MICs [$\mu\text{g/mL}$] of compound **70–73a**, **87** and **90**.

	Lipid 430 (87)	FE002 (90)	FE003 (70)	FE004 (71)	FE005 (72)	FE006 (73a)
<i>Escherichia coli</i> ATCC 35218 (MH-II)	> 64	> 64	> 64	> 64	> 64	> 64
<i>Escherichia coli</i> ATCC 35218 (MHC)	> 64	64	> 64	> 64	> 64	> 64
<i>Escheria coli</i> ATCC 25922 (ΔTolC)	> 64	> 64	> 64	> 64	> 64	> 64
<i>Acinetobacter baumannii</i> ATCC 19606	n.d.	n.d.	> 64	> 64	n.d.	n.d.
<i>Klebsiella pneumoniae</i> ATCC 13883	> 64	> 64	> 64	> 64	> 64	> 64
<i>Moraxella catarrhalis</i> ATCC 25238	16–32	4–8	8	> 64	4–8	16
<i>Pseudomonas aeruginosa</i> ATCC 27853	> 64	> 64	> 64	> 64	> 64	> 64
<i>Mycobacterium smegmatis</i> ATCC 607	> 64	64	> 64	> 64	> 64	> 64
<i>Bacillus subtilis</i> DSM 10	> 64	8	> 64	> 64	> 64	> 64
<i>Staphylococcus aureus</i> ATCC 25923	> 64	> 64	> 64	> 64	> 64	> 64
<i>Micrococcus luteus</i> DSM 20030	32–64	64	> 64	> 64	16	16
<i>Listeria monocytogenes</i> DSM 20600	n.d.	n.d.	> 64	> 64	> 64	n.d.
<i>Candida albicans</i> FH 2173	> 64	64	> 64	> 64	> 64	> 64

n.d.: Not determined.

Considering the metabolites **70–73a** isolated from *Olivibacter* sp. FHG000416, the originally observed activity against *E. coli* MHC could not be reproduced. A reduced cell density used for MIC determination in comparison to the screening of UPLC fractions represents one potential explanation. Furthermore, synergistic activity of two or more components disappearing upon separation has been reported as known complication.^[171] This could be particularly relevant since the amphiphilic character of all compounds suggested an effect on the cell membrane integrity. However, not leading to direct cell lysis, it could instead affect more fragile states of cellular intactness e.g., during cell division as pointed out by SCHNEIDER *et al.*^[156]

The three isolated *N*-acyl amino acids **74–76** did not show antimicrobial activity against the screening panel in a relevant range (Table S28). Growth inhibition towards *M. catarrhalis* and *M. luteus* was only observed for FE008 (**74**) at the highest concentration of 64 $\mu\text{g/mL}$. For the *N*-acylated tyrosines reported in literature, a length of acyl chain between C₁₃ and C₁₆ was described most active against *B. subtilis*. The activity was significantly lower for C₁₁ or C₁₂ *N*-acyl derivatives and disappeared for

even shorter analogs.^[161] Consequently, a lack of activity observed for the enantiomeric mixture of *iso*-C_{7:0} and *iso*-C_{9:0} *N*-acyl tyrosines **74** and **75** isolated from FHG000416 was in alignment with these findings.

4.6.2 TLR2/TLR4 Activity

Based on structural similarity to well-studied diacyl and triacyl lipopeptide TLR2 ligands^[172] as well as correlating activities described in literature, the isolated compounds **70–76**, **87** and **90** were furthermore evaluated regarding their TLR2- and TLR4-stimulating potential in a HEK-Blue™ Detection assay at 10 μM, 1 μM, 0.1 μM and 0.01 μM test concentrations (data only shown for 10 μM and 1 μM). The assays were validated by the selective positive controls PAM2 and LPS for TLR2 and TLR4 cells, respectively. A response was considered valid if reproduced in both individual experiments (Fig. 41, Fig. S132; Fig. 42, Fig. S133).

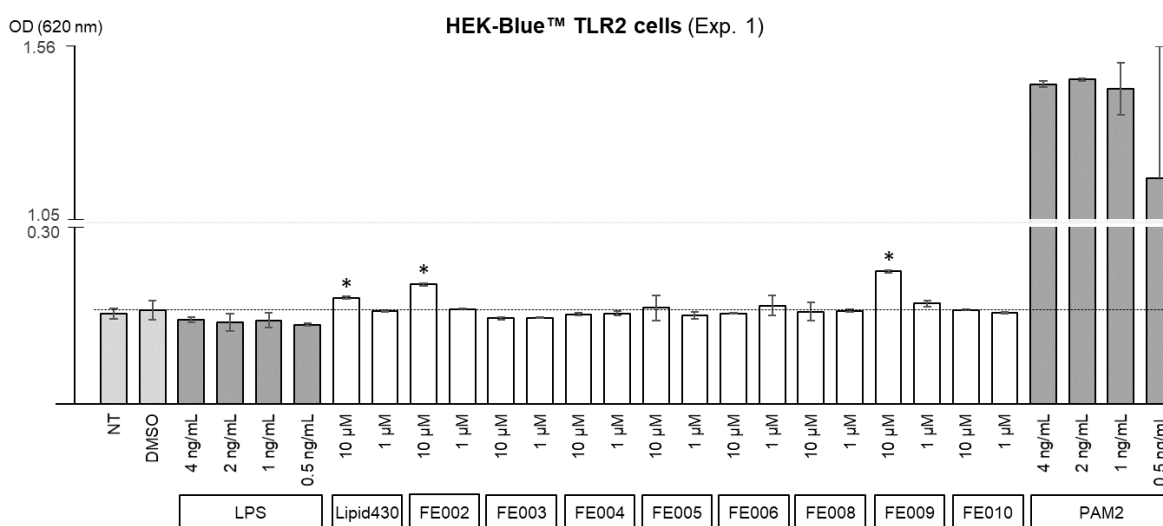


Fig. 41: HEK-Blue™ TLR2 cell activation, experiment 1 (experiment 2: Fig. S132). Cell activation levels are expressed as optical density (OD) at 620 nm. Assays were validated by the specific positive controls (dark grey) PAM2 (TLR2) and LPS (TLR4) as well as untreated (NT) and DMSO-treated (DMSO) negative controls (light grey). Taking standard deviations into account, response levels of compounds (white) elevated over the DMSO negative control in both experiments are marked (*).

Overall, the tested compounds showed rather very low or no effect on TLR2- and TLR4-expressing cells *in vitro*. Conclusive activity was in most cases only observed at the highest test concentration of 10 μM. In the present study, the isolated lipid 430 (**87**) showed an effect on HEK-TLR4 (10 μM and 1 μM) and HEK-TLR2 cells (10 μM). This however did not support the selective TLR2-mediated cell stimulation reported by CLARK *et al.*^[155] Furthermore, the described TLR2 response ratio at 0.69 μg/mL (1.62 μM) was not confirmed even at 6.2-fold increased test concentration (10 μM = 4.31 μg/mL). Not specifying the purity of their tested **87**, minor contaminations with a strong but rather unspecific effect on TLR2 present a potential explanation for the described effect which was not confirmed by the present experiments. The reduced but incompletely blocked response shown after preincubation

of the cells with anti-human TLR2 antibody further supported this hypothesis. Unspecific TLR2 and TLR4 cell activation was also observed for FE002 (**90**) to a lower extent. The even smaller mono-peptide FE003 (**70**) was lacking activity overall. Besides the two aminolipids **87** and **90**, TLR2 cell activation was furthermore detected for FE009 (**75**), however in selective manner as no effect on TLR4 was observed. Apparently, the shorter acyl chain of FE008 (**74**) results in a lack of activity (Fig. 41, Fig. 42).

In contrast to **75**, FE010 (**76**) lacking the phenolic hydroxyl group selectively activated HEK-Blue™ hTLR4 cells. Moreover, FE004 (**71**) and FE006 (**73a**) showed a weak effect on TLR4-expressing cells at 10 μM test concentration (Fig. 42).

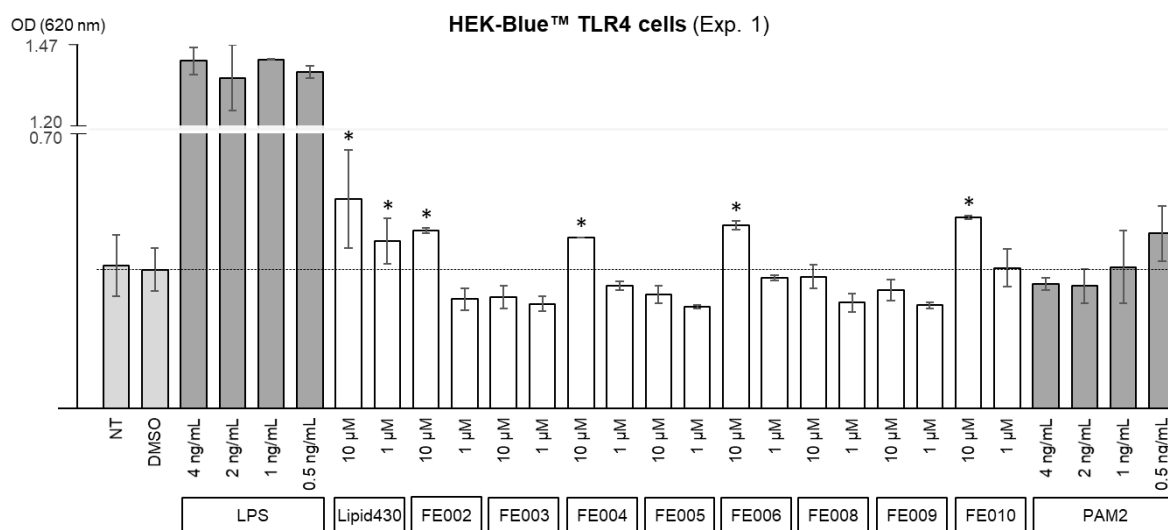


Fig. 42: HEK-Blue™ TLR4 cell activation, experiment 1 (experiment 2: Fig. S133). Cell activation levels are expressed as optical density (OD) at 620 nm. Assays were validated by the specific positive controls (dark grey) LPS (TLR4) and PAM2 (TLR2) as well as untreated (NT) and DMSO-treated (DMSO) negative controls (light grey). Taking standard deviations into account, response levels of compounds (white) elevated over the DMSO negative control in both experiments are marked (*).

Considering both, the presented antibacterial and antifungal activities as well as immune-modulating properties towards TLR2 and TLR4, further efforts regarding hit expansion in either direction were terminated for all metabolites isolated from *Bacteroidetes* spp.

4.7 Stereoselective Total Synthesis of FE004

Since the absolute configuration of the isolated aminolipids had been determined, stereochemical investigation of FE004 (**71**) was also intended and performed in parallel to bioactivity profiling. However, free rotation and flexibility of the molecule **71** did not allow solid prediction of the relative

configuration by NMR analysis based on coupling constants. In general, for 1,2- and 1,3-diols necessary rigidity can be introduced by conversion into more hindered derivatives such as the corresponding acetonides.^[173] This method requires a certain amount of isolated natural product and a defined acetonide to be favored since various regioisomers of five- and six-membered ring acetonides could potentially be formed and NMR analysis is mandatory. Due to the limited quantity of FE004 (**71**) available however, total synthesis was intended.⁶ Considering the three stereocenters of **71**, eight isomers (four pairs of enantiomers) are theoretically possible in total (Fig. 43).

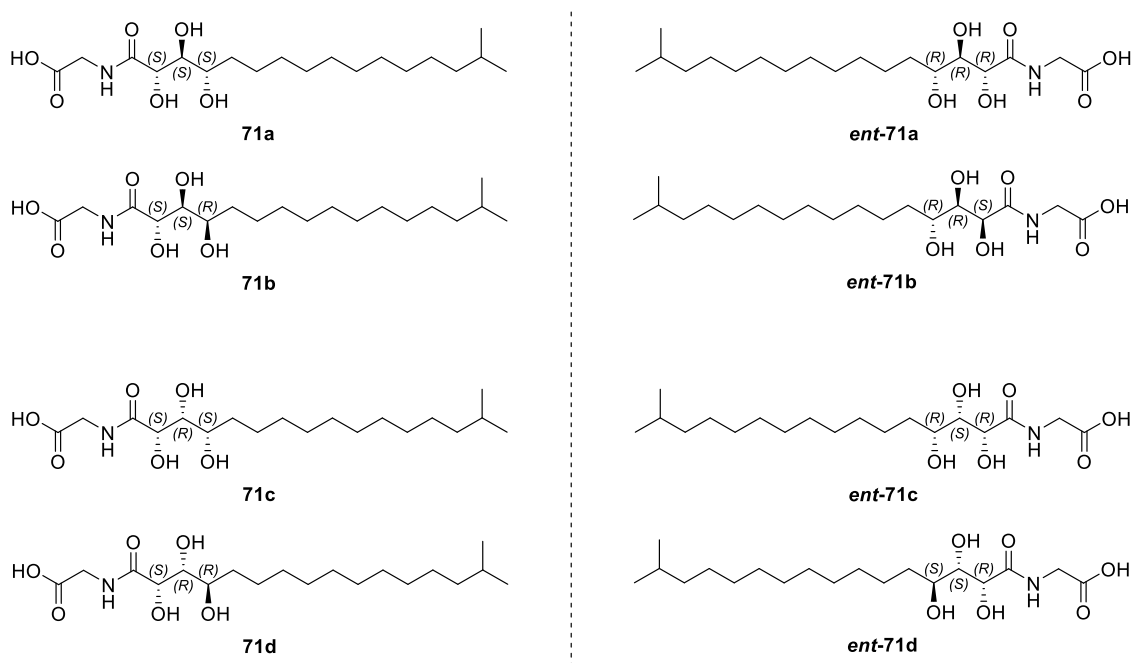


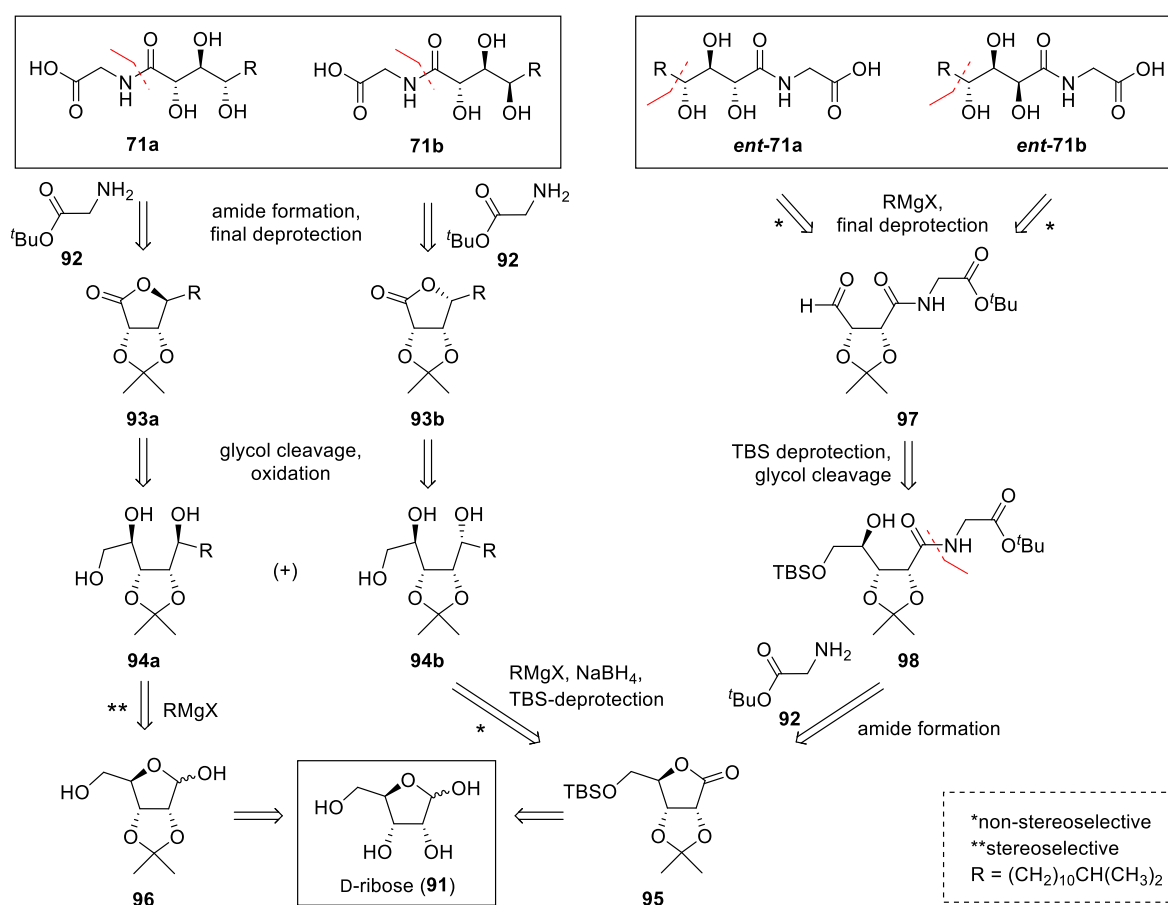
Fig. 43: Overview of the eight configurational isomers of FE004 (**71**).

For assignment of the relative configuration based on matching NMR spectra, one enantiomer in each case is sufficient. The signs of specific rotation values then allow determination of the absolute stereochemistry. However, for such small amounts as isolated FE004 (**71**), the values of specific rotation can be unreliable especially as they are typically lower for open-chain molecules. Therefore, synthesis of both enantiomers subsequently analyzed by chiral HPLC in comparison to FE004 (**71**) represents an alternative and more reliable approach. As **71** is lacking a chromophore however, derivatization of the synthetic references as well as the natural product using e.g., benzoyl chloride is required to allow UV detection.^[174] The sequence of total syntheses was dictated by the synthetic accessibility from chiral building blocks and began with **71a** and **71b** both starting from D-ribose (**91**).

⁶ This project was supported by YOLANDA KLEINER.

4.7.1 Retrosynthetic Analysis: From D-Ribose towards 71a/ent-71a and 71b/ent-71b

The strategy towards total synthesis of **71a** and **71b** as well as *ent-71a* and *ent-71b* was built on commercially available D-ribose (**91**) as template for the configuration of the three adjacent hydroxyl groups (Scheme 6). In the case of **71a** and **71b**, reaction of glycine *tert*-butyl ester (**92**) and **93a** resp. **93b** as well as removal of the protecting groups were planned as final conversion steps. Intermediates **93a** and **93b** were considered accessible *via* glycol cleavage and oxidation of **94a** and **94b**, both obtained by alkylation of **95** using Grignard reagent followed by NaBH₄ reduction and TBS deprotection. As reported by SHING *et al.*, performing the Grignard reaction with **96** provides diastereoselective access to **94a**.^[175] The synthesis of **95** and **96** has been previously described.^{[176][177][178]}



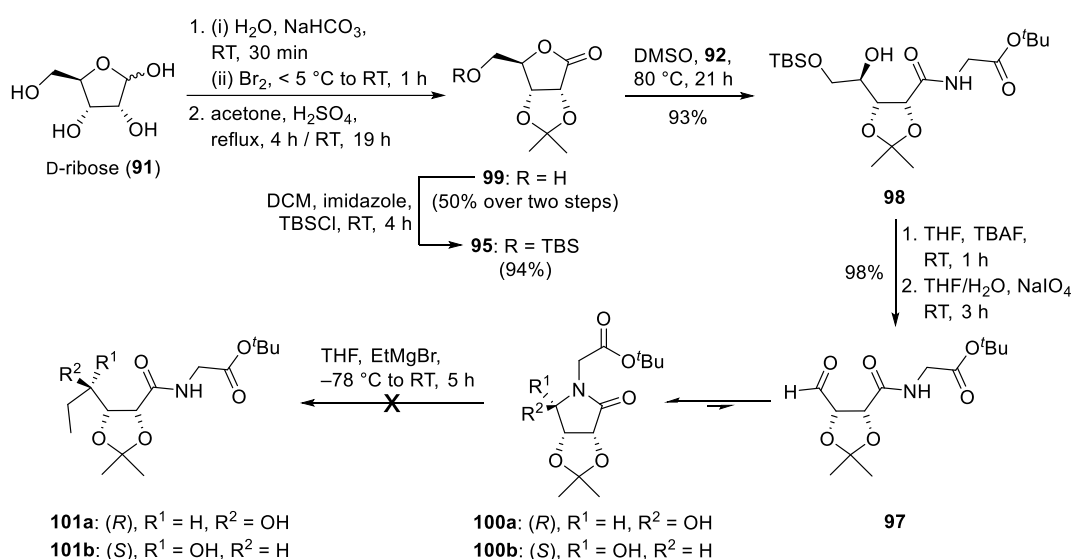
Scheme 6: Retrosynthetic analysis of **71a**, **71b**, *ent-71a* and *ent-71b* starting from D-ribose (**91**).

Starting from **95**, a reversed order of the key conversion steps furthermore provides access to the enantiomers *ent-71a* and *ent-71b* in affordable manner compared to the price of L-ribose (*ent-91*). In this case, introduction of the alkyl chain to **97** by Grignard reaction followed by removal of the protecting groups was intended to represent the final reaction steps. In turn, **97** should be accessible by TBS deprotection and subsequent glycol cleavage of **98** obtained from direct amidation of **95** using glycine *tert*-butyl ester (**92**).

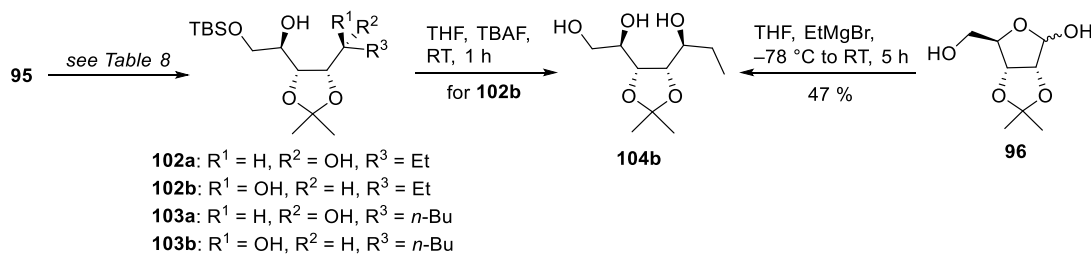
4.7.2 Route Scouting using Ethyl and Butyl Model Systems

The Grignard reagent RMgBr with R = (CH₂)₁₀CH(CH₃)₂ needed to introduce the authentic alkyl moiety had to be synthesized from the corresponding bromide, which in turn required synthesis over three steps starting from commercially available isobutyl bromide and 9-bromo-1-nonanol according to SMITH *et al.*^[179] However, lacking experiences regarding reactivity of the employed systems, this was essential to be evaluated first using commercially available metal-organic reagents present in the lab. Therefore, EtMgBr and *n*-BuLi were chosen. Since the length of the alkyl chain and the terminal isopropyl moiety far off were expected to have very little effect on the coupling constants, the resulting model systems most likely allow solid prediction whether or not they share the same relative configuration as the isolated FE004 (**71**).

The synthesis of **95** was performed over three steps starting from D-ribose (**91**) according to the reaction sequences reported from BATRA *et al.*^[176] and JAYAKANTHAN *et al.*^[177], respectively (Scheme 7). Subsequent, **98** was obtained in excellent yield by direct, catalyst-free amidation of **95** with glycine *tert*-butyl ester (**92**). TBS deprotection of **98** followed by glycol cleavage resulted in complete conversion of the starting material. However, NMR analysis showed not aldehyde **97** but its tautomeric cyclic N,O-hemiacetals **100a** and **100b** were obtained. Formation of the butyrolactam can be explained by: i) the intramolecular distance due to the rigid *cis*-hydroxyl groups and ii) the stability of the resulting five-membered ring. Diastereomers **100a** and **100b** present at a ratio of approx. 6:1 based on NMR and LC-MS analysis were not separated. The attempt to introduce an alkyl group to **100** via Grignard reaction was made using commercially available EtMgBr. However, even with an excess of organomagnesium reagent and extended reaction time at temperatures up to 0 °C, the formation of **101** was not observed by TLC and LC-MS monitoring.

Scheme 7: Synthesis towards **101a** and **101b** starting from **91**.

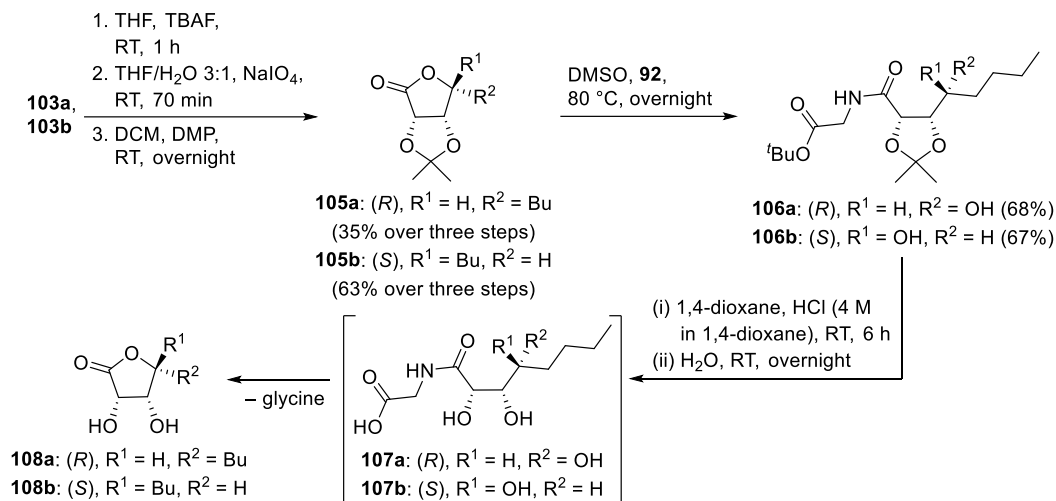
Therefore, route scouting was performed to investigate more efficient ways to gain synthetic access to the configurational isomers of FE004 (**71**) with a focus on the alkylation as key step. Starting from ribonolactone **95**, ethyl or butyl groups were introduced in non-stereoselective manner using either EtMgBr or *n*-BuLi (Scheme 8, Table 23). Due to interconversion of the resulting diastereomeric hemiacetals, separation of the diastereomers was performed after reduction using NaBH₄ giving **102a** and **102b** as well as **103a** and **103b**. The moderate yields over two steps indicated only a minor preference of the (*R*)-isomers **102a** and **103a** (Table 23). For **102b**, TBS deprotection was performed exemplary yielding **104b** which was also obtained by stereoselective Grignard reaction starting from commercially available **96**. The good yield however required a significant excess (12 eq.) of EtMgBr strongly limiting the efficiency of this route. Yet, comparison of NMR data and specific rotation values allowed assignment of the absolute configuration of the analogous butyl derivatives **103a** and **103b**. Overall, all tested conditions were proven to lead to the desired alkylated products.

Scheme 8: Route scouting alkylation experiments starting from **95** and **96**.Table 23: Overview of conditions and yields for the synthesis of **102a**, **102b**, **103a**, and **103b** starting from **95**.

Entry	Conditions	Yields (over two steps)			
		102a: (<i>R</i>)	102b: (<i>S</i>)	103a: (<i>R</i>)	103b: (<i>S</i>)
1	1. THF, EtMgBr, -78 °C to RT, 5 h 2. MeOH, NaBH ₄ , 0 °C to RT, 1 h	23%	14%		
2	1. THF, <i>n</i> -BuLi, -78 °C to RT, 5 min 2. MeOH, NaBH ₄ , 0 °C to RT, 1 h			35%	22%

Starting from **103a** and **103b**, the butyl model system was subsequently used to evaluate the reaction sequence leading to the shortened analogs of **71a** and **71b**, namely **107a** and **107b** (Scheme 9). Therefore, TBS deprotection and glycol cleavage were performed followed by oxidation using Dess-Martin periodinane (DMP). The resulting lactones **105a** and **105b** were obtained in moderate to good yields over three steps. The direct amide formation with glycine *tert*-butyl ester (**92**) also repeatedly demonstrated its efficiency leading to **106a** and **106b**. Final removal of the acetonide and *tert*-butyl protecting groups was achieved by acidic hydrolysis using HCl in 1,4-dioxane. While removal of the *tert*-butyl protecting group was rapidly completed according to LC-MS analysis, hydrolysis of the acetonide required the addition of water. Although **107** was intermediately formed, elimination of glycine resulted in **108**. However, since the reaction mixture had been evaporated to

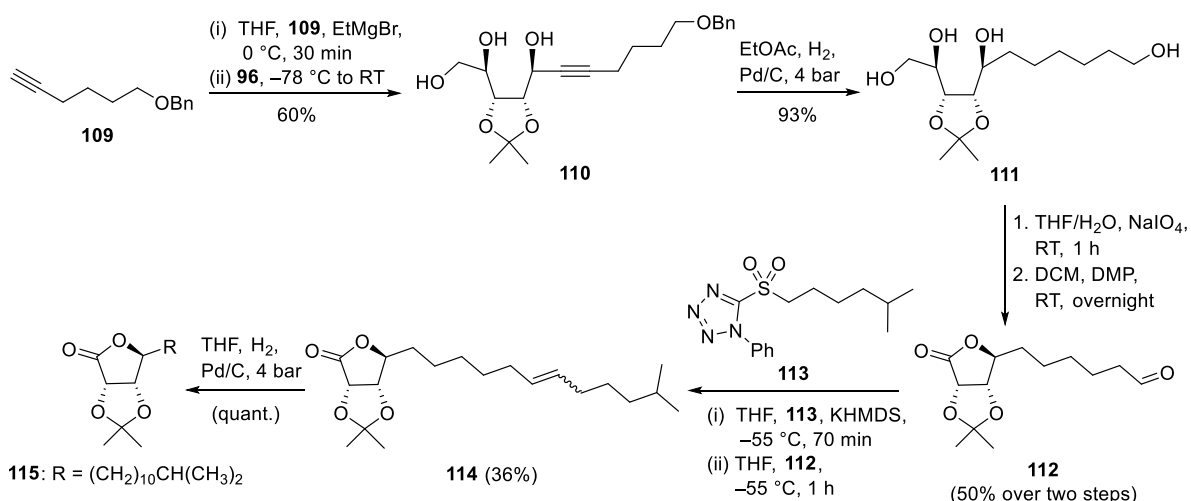
dryness at high vacuum pressure leading to the presence of cleaved glycine in equimolar concentration, the identification of the lactones **108a** and **108b** by NMR analysis was complicated and their formation only suspected later on. Thus, the synthesis towards **71a** and **71b** had been started.



Scheme 9: Synthesis towards **108a** and **108b** starting from **103a** and **103b**.

4.7.3 Synthesis towards **71a** and **71b** from D-Ribose

Stereoselective alkylation of **96** by Grignard reaction had been proven appropriate and was therefore applied to the synthesis of FE004 diastereomers **71a** and **71b**. However, due to large excess of Grignard reagent required, the alkyne **109** was employed instead easily accessible *via* benzyl protection of the commercially available 5-hexyne-1-ol (Scheme 10).^[180]

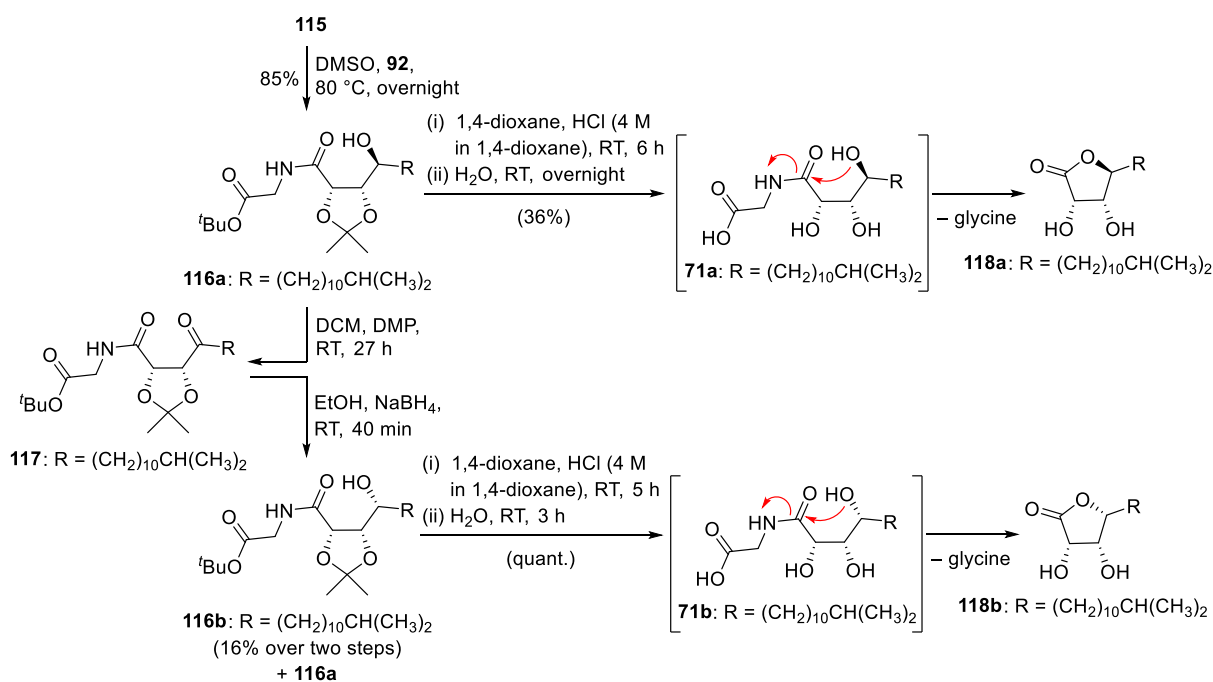


Scheme 10: Synthesis of **115** over six steps starting from **109**.

As Grignard reagents of terminal alkynes are formed by deprotonation, recovery of the starting by simple hydrolysis of the remaining organomagnesium species represented a major advantage of this

approach. After alkylation of **96**, the triple bond as well as the benzyl protecting group of intermediate **110** were removed by hydrogenation over Pd/C catalyst. The resulting alcohol **111** was converted into aldehyde **112** by the established reaction sequence of glycol cleavage and DMP oxidation (Scheme 9). Afterwards, compound **112** allowed the synthesis of the full length alkyl chain *via* Julia-Kocienski olefination. Therefore, sulfone **113** was prepared over two steps starting from commercially available 1-phenyl-1*H*-tetrazole-5-thiol and 5-methyl-1-hexanol as likewise reported by BLANKEMORE *et al.*^[181] With precursor **112** and **113** in hand, the alkene **114** was obtained as mixture of (*E*)- and (*Z*)-isomer (approx. 5:1 based on LC-MS analysis) which was subsequently hydrogenated to yield the alkylated lactone **115** by quantitative conversion.

Identical to **105** (Scheme 9), **115** was glycinated to give **116a** (Scheme 11). By non-stereoselective oxidation and reduction, diastereomer **116b** was partially obtained. For both, deprotection was achieved as previously performed.



Scheme 11: Synthesis towards **118a** and **118b** starting from **115**.

To a very low extent, **71a** and **71b** were detected as [M+H]⁺ parent ion peaks (*m/z* 376.2689, C₁₉H₃₈NO₆⁺, [M+H]⁺, *t_R* = 12.1 min) in LC-MS monitoring after a reaction time of 30 min strongly suggesting *in situ* formation (**71a**: Fig. 44). At the same time, the positive ESIMS peak at *m/z* 323.2689 (C₁₇H₃₂O₄Na⁺, [M+Na]⁺, *t_R* = 14.1 min) was observed at higher intensity. Correlating to the sodium adduct of lactone **118a**, it suggested the favored elimination of glycine and cyclization. As remaining starting material **116a** and incompletely deprotected **119a** were also detected, the reaction was continued. This however led to complete conversion into **118a**. The same was assumed to be true for **107** and **108** respectively, as indicated beforehand. This time, aqueous work up was performed to get

rid of the eliminated glycine. NMR analysis finally confirmed the structure of **118a** (and **118b**) as obtained product.

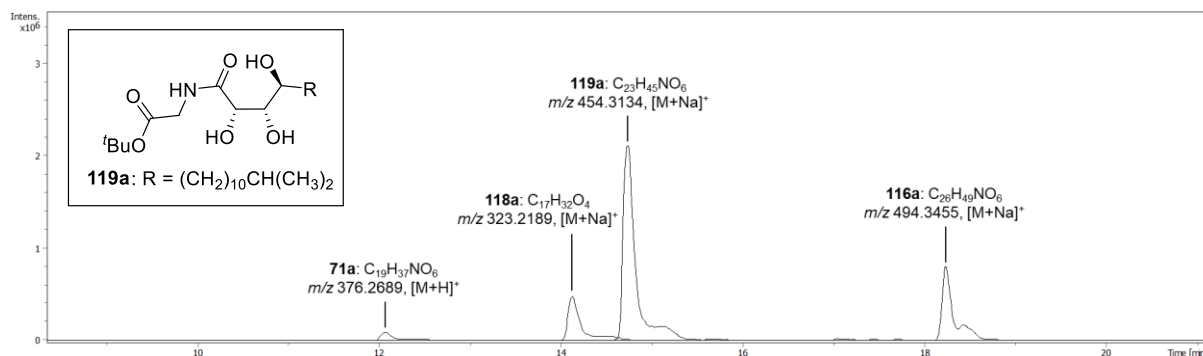


Fig. 44: LC-MS monitoring of the **116a** deprotection reaction.

The chemical behavior of spontaneous lactone formation observed for **71a** and **71b** strongly suggested that these two isomers do not feature the correct configuration of FE004 (**71**) since the natural product had appeared to be stable under acidic conditions during isolation. The specific configuration of the three adjacent hydroxyl groups most likely favors or disfavors the compound's ability to undergo lactone formation as previously postulated for **100** (Scheme 7). Excluding these two stereoisomers as well as their enantiomers *ent*-**71a** and *ent*-**71b** was furthermore supported by comparison of *in situ* formed **71a** and **71b** with the natural product regarding their retention times using non-chiral UPLC-MS (Fig. 45). For this approach, identical ionization was assumed and sample concentrations were adjusted to similar peak intensities of the $[M+H]^+$ ion. The obvious retention time shifts led to the assumption that either **71c/ent-71c** or **71d/ent-71d** feature the absolute configuration of the FE004 natural product.

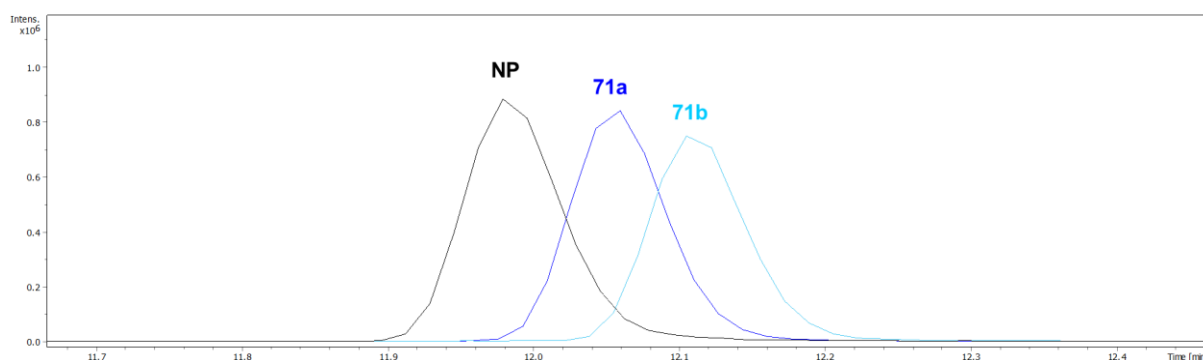
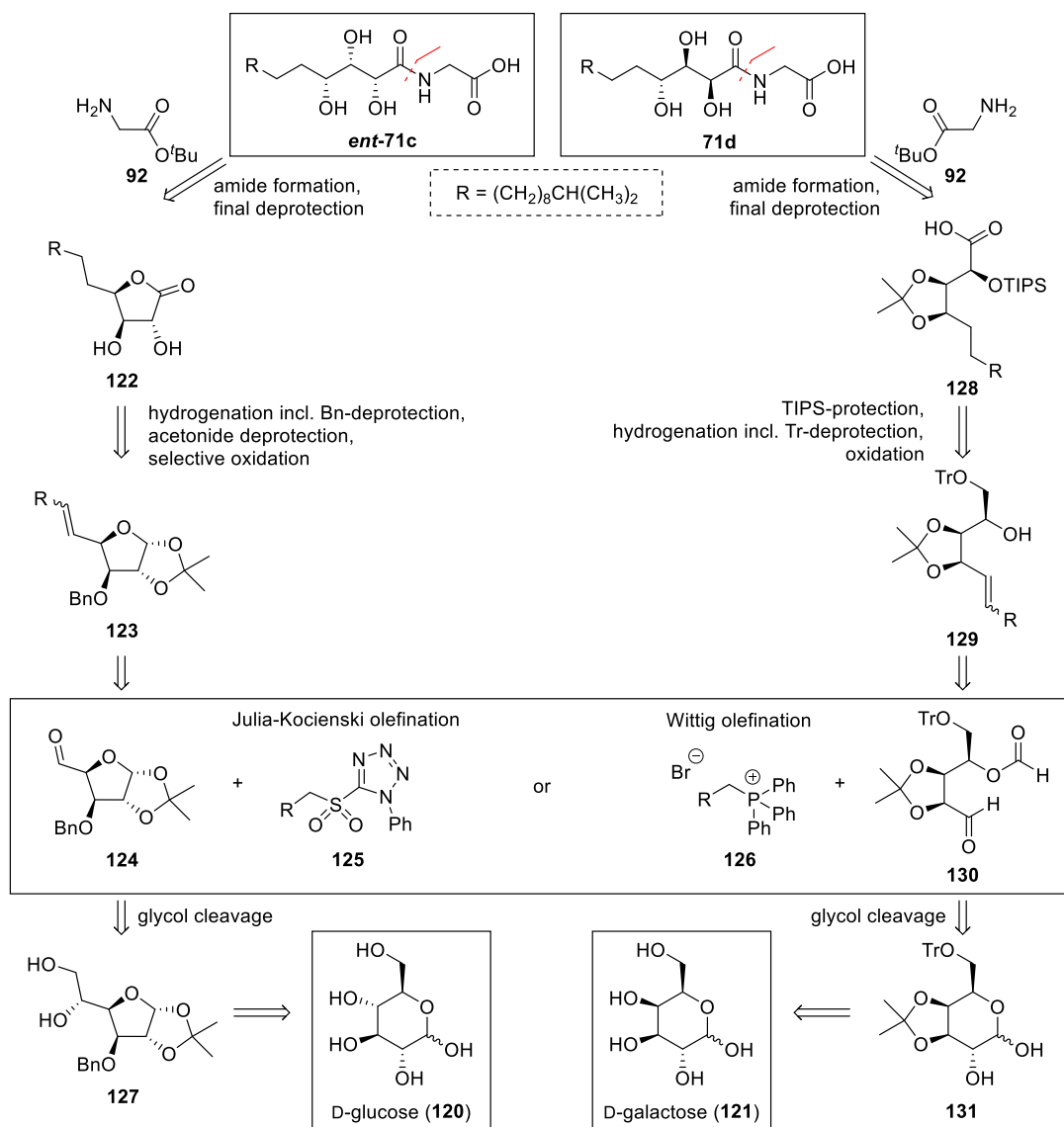


Fig. 45: EICs of m/z 376.2694 \pm 0.005 ($C_{19}H_{37}NO_6$, $[M+H]^+$) for the isolated natural product (black) as well as **71a** (dark blue) and **71b** (light blue) formed *in situ*.

4.7.4 Retrosynthetic Analysis: From D-Glucose and D-Galactose towards *ent*-**71c** and **71d**

Retrosynthetic analysis revealed commercially available D-glucose (**120**) and D-galactose (**121**) as suitable chiral pool compounds towards *ent*-**71c** and **71d**, respectively. Compared to D-ribose (**91**),

these hexoses provide an additional carbon atom therefore requiring an equally shorter alkyl chain to be introduced. In accordance with former synthetic routes, direct amidation of lactone **122** and removal of the *tert*-butyl protecting group were envisaged as final reaction steps towards **ent-71c**. Intermediate **122** was considered accessible by: i) hydrogenation removing the double bond as well as the benzyl protecting group, ii) acetonide deprotection and iii) selective lactol to lactone oxidation^{[182][183]} of **123** which was planned to be obtained by Julia-Kocienski or Wittig olefination of aldehyde **124** using either phenyl-tetrazole sulfone **125** or triphenyl phosphonium ylide **126**. As building block for the key step of the synthesis intermediate **124** was intended to be received from glycol cleavage of **127** which can be synthesized from D-glucose (**120**) over three steps as reported by MITRA *et al.*^[184] (Scheme 12).



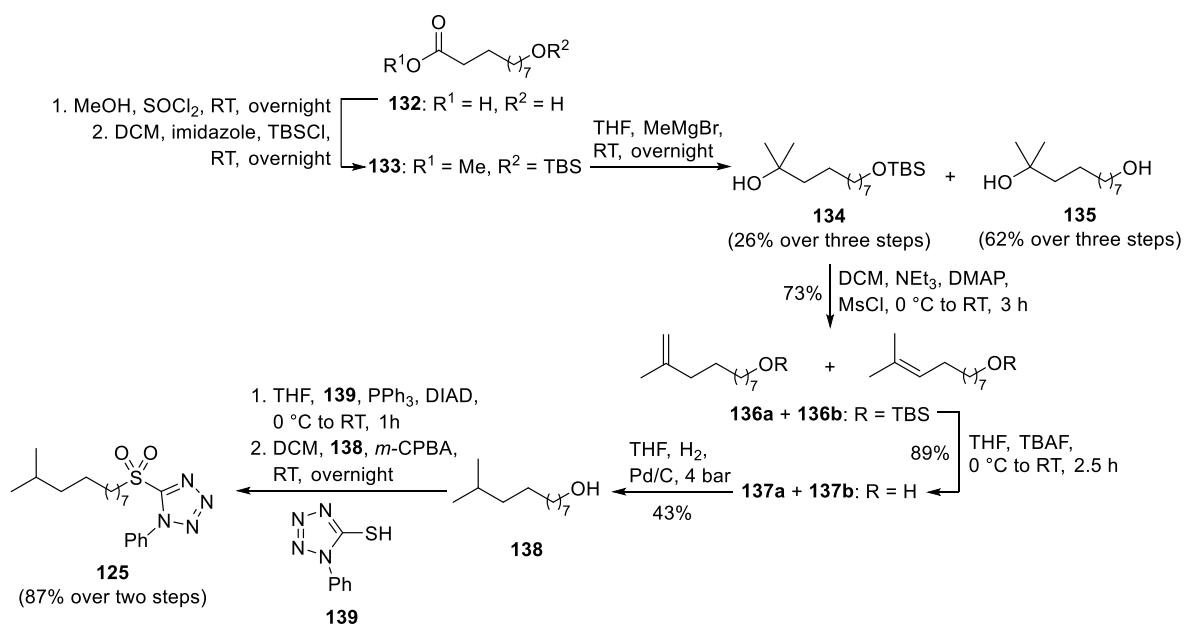
Scheme 12: Retrosynthetic analysis of **ent-71c** and **71d** starting from D-glucose (**120**) and D-galactose (**121**).

Similar to **ent-71c**, amide formation and deprotection were intended to be the final steps towards **71d**. As glycine *tert*-butyl ester (**92**) should be introduced to carboxylic acid **128**, utilizing coupling reagents such as EDC·HCl/Oxyma under mild alkaline conditions.^[185] The subsequent removal of the

TIPS and *tert*-butyl protecting groups was envisaged to be done using TBAF and HCl in dioxane, respectively. **128** was considered accessible from alcohol **129** over three steps including: i) TIPS protection of the hydroxyl group using TIPSOTf and 2,6-lutidine^[186], ii) hydrogenation removing the double bond and the trityl protecting group and iii) TEMPO-catalyzed oxidation of the primary alcohol to the carboxylic acid.^[187] Also similar to the route providing *ent*-**71c**, **129** was envisaged to be synthesized by Julia-Kocienski or Wittig olefination of the aldehyde **130** which can be obtained from D-galactose (**121**) as described by CHENG *et al.*^[188] (Scheme 12).

4.7.5 Synthesis of the Julia-Kocienski Olefination Reagent

Instead of elongating the alkyl moiety, this time Julia-Kocienski olefination was intended to introduce the full length alkyl chain to the aldehyde building blocks **124** resp. **130** and represented the key step of the total synthesis towards *ent*-**71c** and **71d**. Therefore, the according sulfone reagent **125** was synthesized over eight steps starting from 10-hydroxydecanoic acid (**132**). All given yields were not optimized. As the quantity of obtained products was sufficient for small-scale test reactions, re-synthesis was not requiring (Scheme 13).



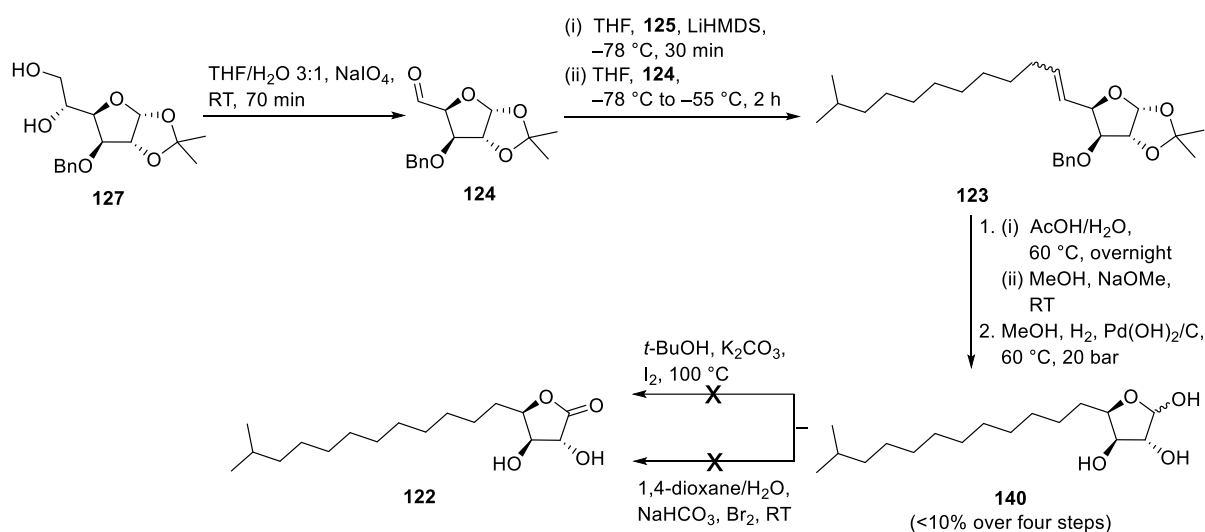
Scheme 13: Synthesis of phenyl-tetrazole sulfone **125** starting from 10-hydroxydecanoic acid (**132**).

The TBS-protected methyl ester **133** was converted into the tertiary alcohol **134** using MeMgBr. The yield (26% over three steps) was most likely restricted due to the formation of thionyl chloride adducts during esterification. In the presence of MeMgBr, these sulfite esters led to the formation of by-product **135** and DMSO being reduced to dimethyl sulfide which was clearly identified based on its characteristic smell. Selective TBS protection favoring less sterically hindered primary alcohols over secondary and tertiary alcohols allows conversion of **135** into **134**.^[189] The tertiary hydroxyl group of **134** was eliminated as mesylate under basic conditions in the next step and yielded the

inseparable mixture of **136a** and **136b** harboring either a terminal vinylidene or 2-methyl-1-propenyl group. After removal of the TBS protecting group, alcohol **138** was obtained from **137a** and **137b** by hydrogenation of the double bond. According to reported procedures, the sulfone **125** was obtained by Mitsunobu reaction and oxidation in good yield over two steps.^[190]

4.7.6 Synthesis towards *ent*-71c from D-Glucose

With sulfone **125** in hand, the synthesis of *ent*-71c started with diol **127** which was synthesized from D-glucose (**120**) over three literature known steps (Scheme 4).^[184] Afterwards, aldehyde **124** was obtained by glycol cleavage as previously performed and directly used without purification in the key step of the route. Julia-Kocienski olefination was performed using the previously synthesized sulfone reagent **125**. Formation of the resulting olefin **123** was confirmed by LC-MS analysis. However, flash chromatography failed to separate **123** from remaining sulfone **125** which had been used in excess. Moreover, the compound was too lipophilic for purification by RP-HPLC. Therefore, the acetonide protecting group was removed by acidic hydrolysis using acetic acid. However, the formation of various acetates was observed and assumed to have occurred during concentration of the reaction mixture under reduced pressure. Aqueous work-up or dilution of the reaction mixture followed by freeze-drying may present appropriate alternatives.



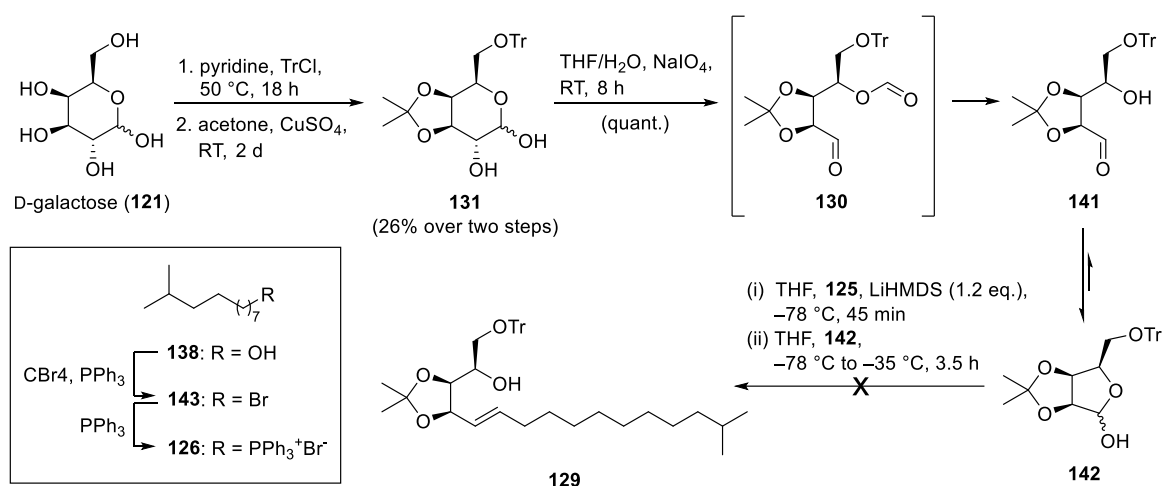
Scheme 14: Synthesis towards **122** starting from **127**.

Separated from **125**, pre-purified fractions were treated with NaOMe in MeOH to remove acetate groups. After aqueous-acidic work-up, the obtained crude product was hydrogenated over Pd(OH)₂/C as Pd/C had proven to be insufficient to remove the benzyl protecting group simultaneously to yield **140**. Even though detected by LC-MS analysis, the strongly limited quantity of **140** moreover lacking purity could explain why neither using I₂^[182] nor Br₂^[183] led to the desired lactone **122** by selective oxidation. Confirmation of the reaction's ineffectiveness however requires up-scaled repetition with

pure **140** accessed by optimized re-synthesis based on deficiencies identified in this first attempt. Furthermore, oxidation using DMP represents an alternative approach. Starting from **123**, this requires acetonide deprotection followed by benzyl protection of the two resulting hydroxyl groups and selective debenzylation by mild acidic hydrolysis of the alcohol group at the anomeric center after hydrogenation.^[191] However, experiments in this direction^[191] were not attempted due to lack of activity observed for FE004 (**71**) in the screenings.

4.7.7 Synthesis towards **71d** from D-Galactose

In parallel to the synthesis of *ent*-**71c**, the preparation of **71d** was started with the conversion of D-galactose (**121**) into **130** over three steps similar to CHENG *et al.*^[188] (Scheme 15). Solvent and reactants lacking anhydrousness in the acetonide protecting step most likely caused the low yield. Subsequent glycol cleavage of **131** was quantitative. However, hydrolysis of formate **130** resulted in hydroxyl aldehyde **141** after work-up. The significantly favored hemiacetal **142** prevented the formation of **129** under the used conditions as at least 2 eq. of base would have been required. Instead, dimerization of **125** was observed in LC-MS monitoring.



Scheme 15: Synthesis towards **129** based Julia-Kocienski olefination plus envisaged synthetic access of Wittig reagent **126** starting from alcohol **138**.

While avoiding reductive work-up of the glycol cleavage reaction could improve the stability of **130** according to CHENG *et al.*, they instead used Wittig olefination to introduce an alkyl moiety in the next step which presented a promising alternative to the Julia-Kocienski reaction for obtaining **129**. Hereby, the formate ester was considered a crucial temporary protecting group preventing the formation of **142** which significantly lowered the yield. Since the formate moiety is also susceptible to Wittig reaction, at least 2 eq. of reagent were needed. Using a 2.5-fold excess of ylide over **130** gave the resulting alkene in good yield.^[188] The ylide **126** required for Wittig reaction is accessible *via* Appel reaction by treating the alcohol **138** with CBr₄ and PPh₃ (Scheme 15).^[192] However, as the

project was terminated due to lack of bioactivity, neither the Wittig reagent was synthesized nor the synthetic strategy leading to **71d** continued (Scheme 12).

4.7.8 Summary and Outlook

In order to assign the absolute configuration of the isolated natural product FE004 (**71**), total synthesis of different isomers of **71** as reference compounds is required since it was not possible to determine the stereochemistry of the hydroxyl groups by NMR spectroscopy. However, stereoselective syntheses of polyhydroxylated compounds are in many cases sophisticated and tedious. A well-established strategy is the use of chiral pool materials such as sugars and other readily available natural products. For structure elucidation of **71**, assignment of the relative configuration was intended first. Therefore, synthetic proposals towards at least one enantiomer for each of the four potential enantiomeric pairs were developed starting from commercially available D-ribose (**91**), D-glucose (**120**) and D-galactose (**121**). In this content, introduction of the alkyl side chain was identified as key step and envisaged to be performed by Grignard reaction. This was comprehensively investigated by route scouting using analogous ethyl and butyl models systems. Total synthesis of **71a** and **71b** was chosen to begin with since all four stereoisomers were accessible starting from D-ribose (**91**). Despite their *in situ* detection, spontaneous lactone formation resulted in glycine elimination. This observed chemical behavior strongly suggested that these two isomers differ from the natural product regarding configuration which was further supported by the comparison of retention times. Therefore, FE004 (**71**) was assumed to match with the enantiomeric pair of either **71c** or **71d**. The total synthesis towards *ent*-**71c** and **71d** started from D-glucose (**120**) and D-galactose (**121**), respectively. Introduction of the alkyl chain to the corresponding aldehydes represented the key step and was approached either by Julia-Kocienski or Wittig olefination. The required sulfone reagent **125** was successfully synthesized over eight steps. Apart from that however, several difficulties along both routes occurred. Optimization of reaction conditions and protecting group strategies as well as evaluation of alternative approaches as discussed represent potential next steps. Completing the synthesis of *ent*-**71c** and **71d** then allows determination of the relative configuration by NMR and LC-MS analysis. Solid assignment of the absolute configuration furthermore requires synthesis of the correlating enantiomer (**71c** or *ent*-**71d**) and their chromophore derivatization prior to chiral HPLC analysis in comparison to the equally modified natural product FE004 (**71**).

4.8 Summary and Outlook

Investigation of rare phyla regarding the production of novel antibiotics was one key aspect of the PPP between Fraunhofer IME and Sanofi resp. Evotec. Therefore, the underexplored chemical space and biosynthetic potential of the phylum Bacteroidetes was evaluated based on metabolites causing the initially observed activity against *E. coli* MHC produced by *Olivibacter* sp. FHG000416. Seven metabolites were successfully isolated including aminolipid FE003 (**70**) and the hydroxylated derivative FE004 (**71**), lysophospholipid FE005 (**72**) and the known analog FE006 (**73a**) as well as *N*-acyl amino acids FE008 (**74**), FE009 (**75**) and FE010 (**76**). In order to compare the bioactivity of the identified aminolipids to the structurally related lipid 430 (**87**) described in literature, **87** was additionally isolated from another in-house Bacteroidetes strain, namely *Chitinophaga eiseniae* DSM 22224. Thereby, tripeptidic derivative FE002 (**90**) was furthermore identified extending the class of isolated aminolipids. Except for **73a** and **87**, all compounds have been reported as natural products for the first time. The absolute configuration of monohydroxylated aminolipid **70**, **87** and **90** as well as *N*-acyl amino acid **74–76** was determined by Marfey's Analysis or postulated in accordance with literature. In order to elucidate polyhydroxylated aminolipid FE004 (**71**), enantioselective total synthesis was performed. Thus, four potential stereoisomers were precluded. Synthetic routes towards the remaining two enantiomeric pairs were presented in detail. Antimicrobial activities as well as TLR2- and TLR4-stimulating effects were comprehensively evaluated for all nine isolated compounds. However, considering the presented MIC values as well as immune-modulating properties, further efforts regarding drug discovery/hit expansion will not be followed up by the industrial partner. Yet, the project represents a starting point for further investigation of compounds influencing the host site during an infection. Overall, proof of concept was provided for the strategic approach that rare phyla will deliver new compounds and starting points for innovative treatment of infectious diseases.

5. Antimycobacterial activity of *Streptomyces* sp. HAG010336

5.1 Introduction

Tuberculosis (TB) represents the world's leading cause of death from an infectious agent with 1.4 million fatalities in 2019. According to the World Health Organization (WHO) about one-quarter of the world's population is estimated to be infected by *Mycobacterium tuberculosis* and 10 million new cases occur every year.^[193]

The recommended treatment for drug-susceptible TB was established over 40 years ago. Standard TB chemotherapy involves a combination of the first-line agents rifampicin (RIF) and isoniazid (INH) for six months, completed with pyrazinamide (PZA) and etambutol (EMB) during the first two months.^[194]

However, antimicrobial resistance is a major contributor to the global TB epidemic.^[195] Worldwide, estimated 465 000 new cases of rifampicin-resistant TB (RR-TB) emerged in 2019, 78% of which were multidrug-resistant TB (MDR-TB). MDR-TB is defined as resistant to at least the two most powerful first-line anti-TB drugs RIF and INH. Therefore, treatment of MDR-TB is much more complex with a significant lower success rate of only 57% (compared to 85% for drug-susceptible TB).^[193] It requires treatment with at least five different drugs furthermore including second-line antibiotics such as aminoglycosides, fluoroquinolones and cycloserine over up to two years. Besides compliance issues, second-line drugs also tend to be more expensive and toxic.^[196] Additional resistance to fluoroquinolones (such as levofloxacin and moxifloxacin) and the second-line injectables (such as amikacin, kanamycin and capreomycin) is called extensively drug-resistant TB (XDR-TB).^[197] Estimated 8.5% of all MDR-TB cases in 2017 were XDR-TB. With currently available drugs the treatment success is only 39% for XDR-TB patients.^[198]

These numbers clearly demonstrate the urgent need for new, more effective, affordable, nontoxic anti-TB drugs with new mechanisms of action significantly shortening the duration of treatment to overcome drug-resistant TB and lower its incidence rate. The urgency becomes even clearer looking at the timeline of anti-TB drug approvals (Fig. 46). Bedaquiline (BDQ), a bactericidal diarylquinoline approved in 2012, was the first new anti-TB drug after 14 years since the approval of rifapentine (RPT) in 1998.^{[199][200]} In addition to that, BDQ targeting the mycobacterial ATP synthase was the first approved drug with a new MoA in nearly 50 years since the discovery of RIF in 1963.^[194] Other recently approved anti-TB compounds for the treatment of MDR-TB are delamanid and pretomanid belonging to the class of nitroimidazoles inhibiting the mycolic acid synthesis.^[201]

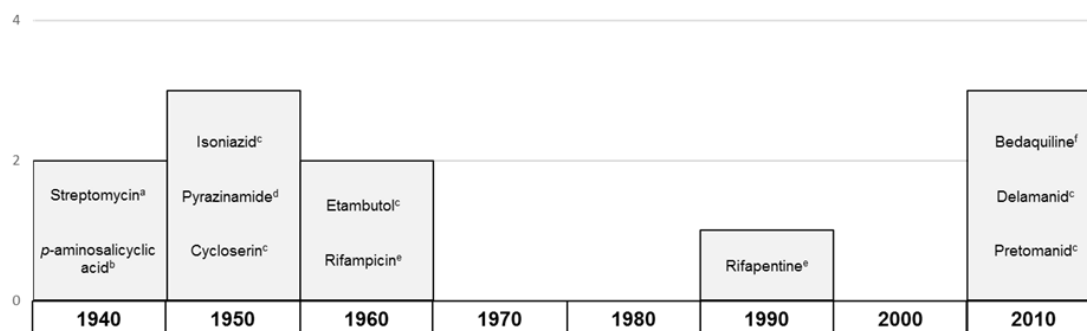


Fig. 46: Approved anti-TB drugs since 1940 sorted by the decade of introduction. Molecular target: ^a30S ribosome, ^bfolic acid metabolism, ^ccell wall synthesis, ^dplasma membrane/energy metabolism, ^eRNA synthesis, ^fATP synthase.

Besides various regimens, repurposed drugs and those who have already received regulatory approval, 13 new compounds are currently in clinical development (status August 2020). Five belong to the known classes of oxazolidinones (TBI-223 (phase I), delpazolid and sutezolid (phase II)), diarylquinolones (TBAJ-876 (phase I)) and riminophenazines like clofazimine (TBI-166 (phase I)).^[193] Derivatization is a well-known strategy in antibiotic development to optimize drugs regarding pharmacodynamic and pharmacokinetic properties.^[202] However, as analogues normally share the same MoA their advantages regarding current resistances are limited.

The other eight compounds (**10** and **143–149**) are NCEs. Compounds **143–146** target the cell wall synthesis by inhibiting DprE1, a novel molecular target (Fig. 47).^[193] In combination with increased activity against *Mtb* and lower toxicity, these candidates could make potential members of new generation anti-TB regimens perhaps shortening the treatment time. However, considering the latent phases of the pathogen, cell wall synthesis inhibitors will most unlikely shorten the treatment period significantly in a monotherapy.

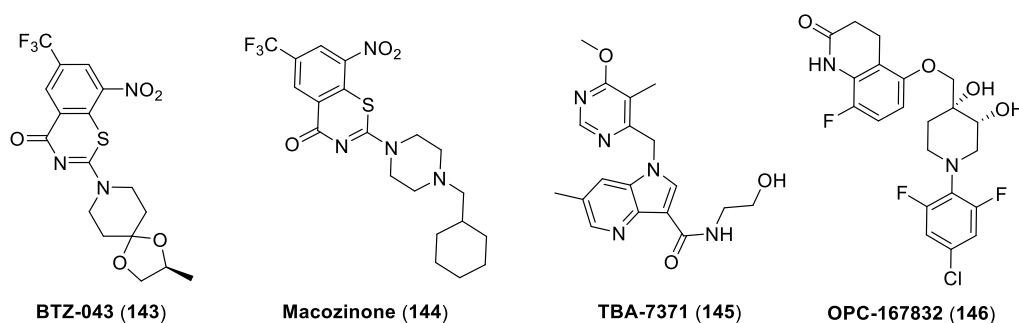


Fig. 47: DprE1 inhibitors as anti-TB drugs in clinical development.

EMB-related SQ109 (**147**), another mycobacterial cell wall synthesis affecting compound currently in phase II, disrupts cell wall assembly by targeting MmpL3 (Fig. 48).^[203] Further new phase II compounds are imidazopyridine amide telacebec (**148**) and oxaborole GSK-3036656 (**149**) depleting ATP synthesis by cytochrome bc1 complex inhibition^[204] and inhibiting protein synthesis by targeting leucyl-tRNA synthetase, respectively.^[205] Similar to fluoroquinolones but with no cross-resistance observed, the benzimidazole SPR720 (**10**), phosphate prodrug of SPR719 (**9**), is a gyrase inhibitor.

Therefore this phase I candidate could be a convenient replacement in second-line regimens especially considering safety concerns.^[206]

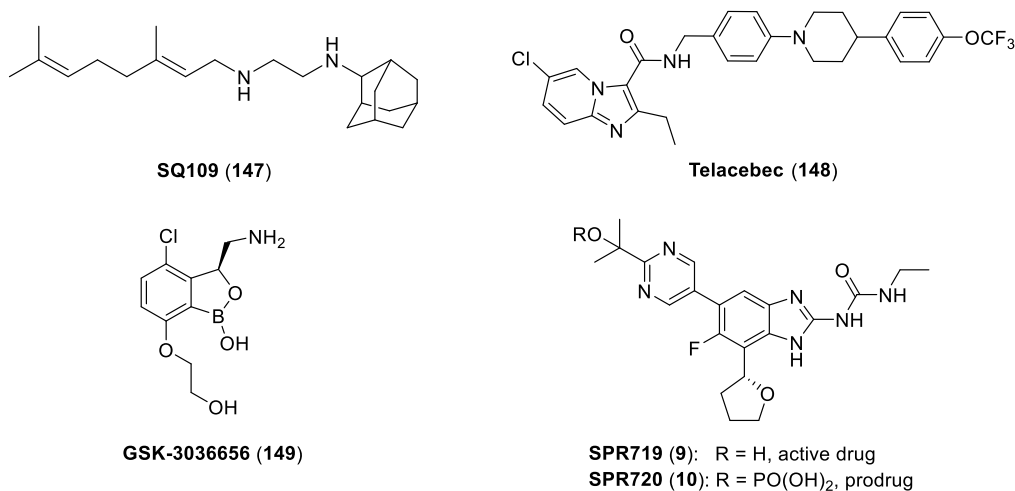


Fig. 48: Further NCEs as anti-TB drugs in clinical development.

The percentage of candidates in clinical development belonging to new antibiotic classes addressing novel targets within the pathways of cell wall synthesis, DNA synthesis, protein synthesis and energy metabolism might raise hope especially for the treatment of drug-resistant TB in the near future. Any improvement regarding shorter treatment, less complex regimens and better tolerability would be advantageous. However, clinical trials have to show if candidates meet the requirement of being sufficiently active in combination and will get approval for the market before facing the even more important question of how long those might be effective towards current resistances. But the ‘magic bullet’ that will ensure reducing the absolute number of TB deaths by 95% (compared to 2015) until 2035 as defined target of the WHO’s End TB Strategy^[193] is most unlikely to be found in clinical development at the present moment.

To end the global TB epidemic, it is of urgent importance to keep finding new anti-TB active compounds. For this reason, TB was added as potential indication for antimicrobial active natural products discovered within the collaboration between Fraunhofer and Sanofi resp. Evotec. However, challenges arise from screening against *M. tuberculosis* due to its slow-growing character and the requirement of biosafety level 3 laboratories. Instead, *M. smegmatis* (ATCC 607) was included in the primary screening panel since its suitability as surrogate has been reported.^[207] The industrial partner provided access to activity assays against the clinical relevant *M. tuberculosis* H37Rv strain which represents a major benefit of the PPP.

5.2 Antibacterial Activity against *M. smegmatis*

Within the standard screening process of the Sanofi-Fraunhofer strain collection, the crude extract originating from *Streptomyces* sp. HAG010336 exhibited antibacterial activity against *M. smegmatis* (ATCC 607). Based on MS/MS-guided fractionation and screening of the extract, the activity was assigned to a compound of m/z 323.1032 ($[M+H]^+$, $C_{18}H_{15}N_2O_4^+$, Δ ppm 1.86). Henceforth, this compound will be referred to as SF009 (**150**). Additionally, the in-house MS/MS database comprising Sanofi legacy database compounds was used as dereplication tool revealing that the compound gave a very similar fragment spectrum as SAR1xxx (**151**). An additional mass of 42.0100 Da which corresponds to a C_2H_2O group suggested a putatively acylated derivative. When screening **151** for antibacterial activity against *M. smegmatis* however, it was found inactive. Furthermore, another active compound was dereplicated as the macrotetralide nonactin (**152**), a known polyketide antibiotic first isolated in 1955 (Fig. 49).^{[208][209]}

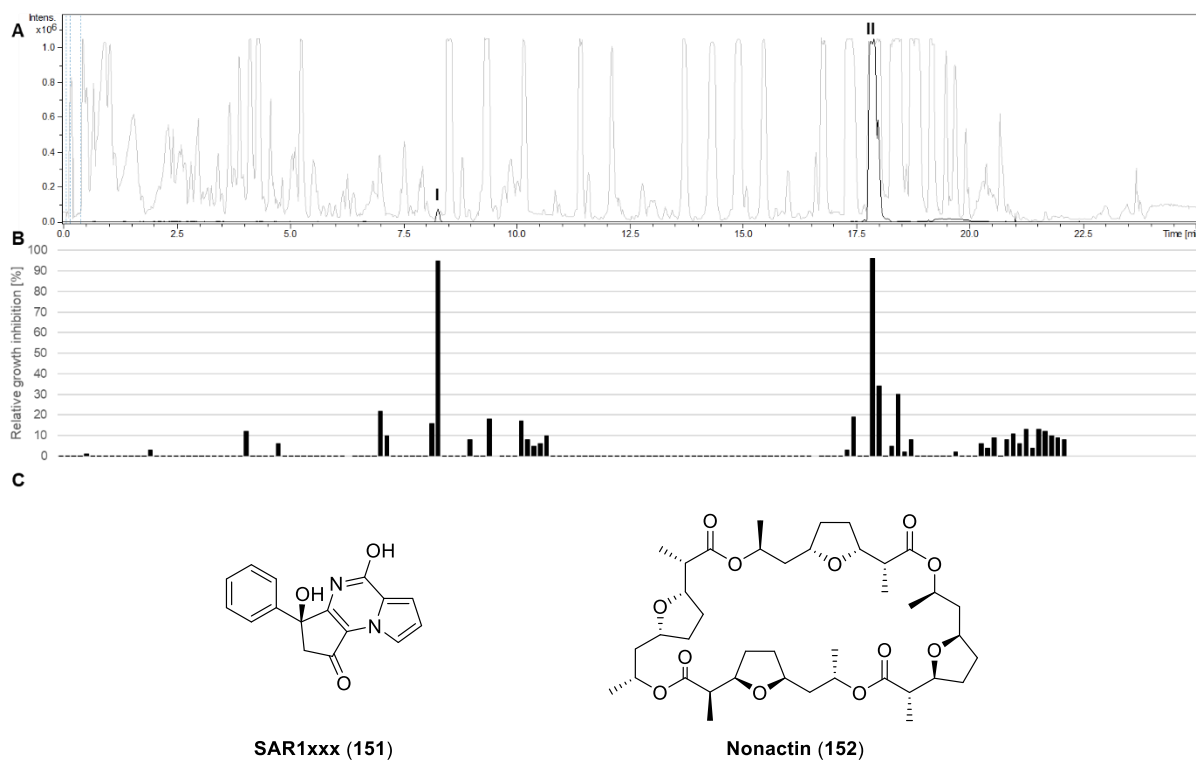


Fig. 49: Crude extract of HAG010336. A: BPC (grey), EICs (black) of I: m/z 323.1026 \pm 0.005, $C_{18}H_{14}N_2O_4$ $[M+H]^+$ and II: m/z 549.4784 \pm 0.005, $C_{42}H_{68}O_{12}$ $[M+H]^+$; B: Relative growth inhibition [%] of fractions 1–159 against *M. smegmatis* ATCC 607; F-60 and F-128: > 90%; C: Chemical structures of SAR1xxx (**151**) and nonactin (**152**).

To verify if the antimycobacterial potential of HAG010336 also includes the target pathogen *M. tuberculosis*, the crude extract was furthermore screened against the H37Rv strain and found active. For identification and characterization of the putatively new antimycobacterial active metabolite SF009 (**150**) from *Streptomyces* sp. HAG010336, an isolation campaign was performed.

5.3 Media Variation

In the standard process, HAG010336 had been cultivated in liquid medium 5265 at 28 °C for 7 days. The first up-scaled fermentation was performed using similar conditions. However, based on LC-MS analysis the relative quantity of SF009 (**150**) produced by the *Streptomyces* sp. was rather limited (Fig. 49A). Therefore, a media variation was performed in parallel. Sixteen different conditions were investigated for their increasing effect on biosynthetic production: various media (5265, 5254, 5065, 5294, 5315, 5367, AMY, SM17, SM25, VPM19), different cultivation temperatures (25 °C and 37 °C), the effect of enhanced oxygen feed using baffled flasks and supplementation of the aromatic amino acids (1 mM tyrosine, 5 mM tryptophan, 5 mM phenylalanine). Samples taken at five different time points (d3, d5, d7, d10, d14) were compared to a medium control. Only one parameter was changed at a time to be able to directly link increased production to a certain condition. The standard process conditions served as reference. Overall six conditions revealed at least one time point with a higher production of **150** in comparison to the original conditions which showed the highest quantity on day 5. The highest production was found for the cultivation of HAG010336 in SM25 medium on day 10 with a 5.6-fold increased yield (Fig. 50). Based on these results, the second 40 L fermentation was performed in the optimized medium SM25.

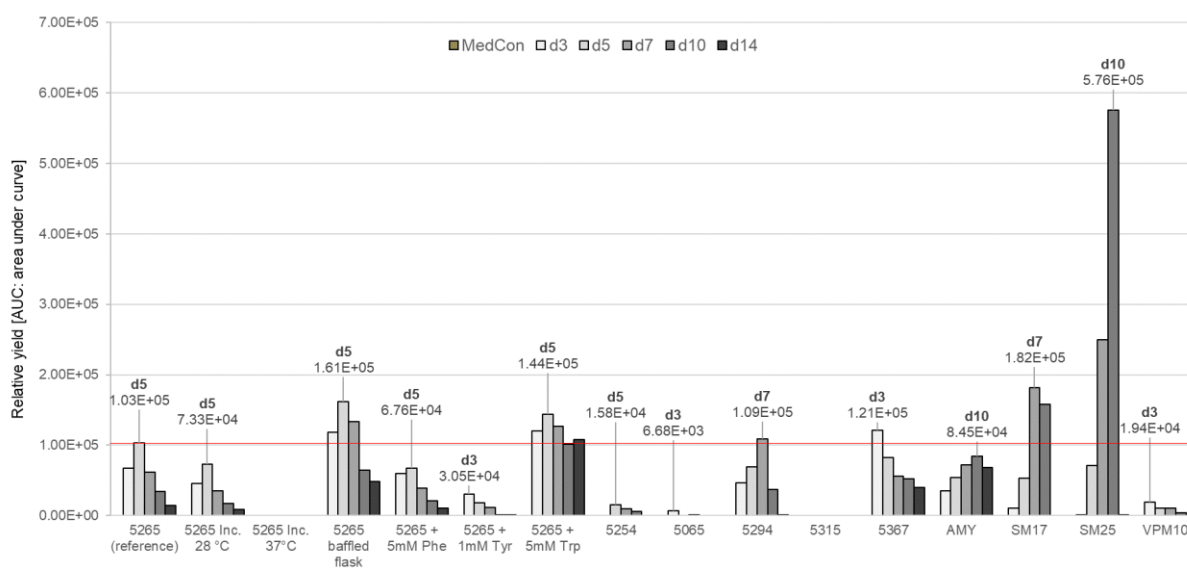


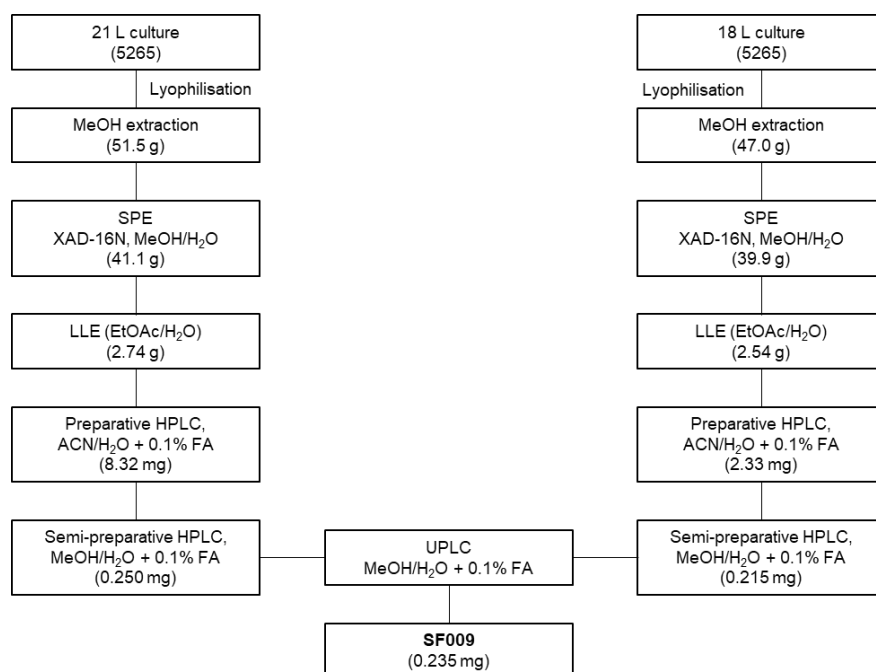
Fig. 50: Results of the media variation. Relative quantity of SF009 (**150**) produced under 16 different conditions at five time points; red line marks highest amount of **150** produced under standard process conditions (d5, reference); highest amount of **150** produced is labelled with time point and relative quantity (area under curve) of EIC C₁₈H₁₄N₂O₄ [M+H, M+Na, M H₂O+H, 2M+H, 2M+Na, 3M+H]⁺.

5.4 Isolation

For the isolation of SF009 (**150**) individual purification strategies were developed depending on the fermentation medium. Due to very limited amounts present, LC-HRMS analysis was performed at each step to detect fractions containing the compound of interest and to determine purity.

5.4.1 Medium 5265

The first round of isolation was performed starting from 39 L liquid culture of HAG010336 in medium 5265. Due to limited fermentation capacity, both batches (21 L and 18 L) were processed successively and only combined for the final purification step (Scheme 16).

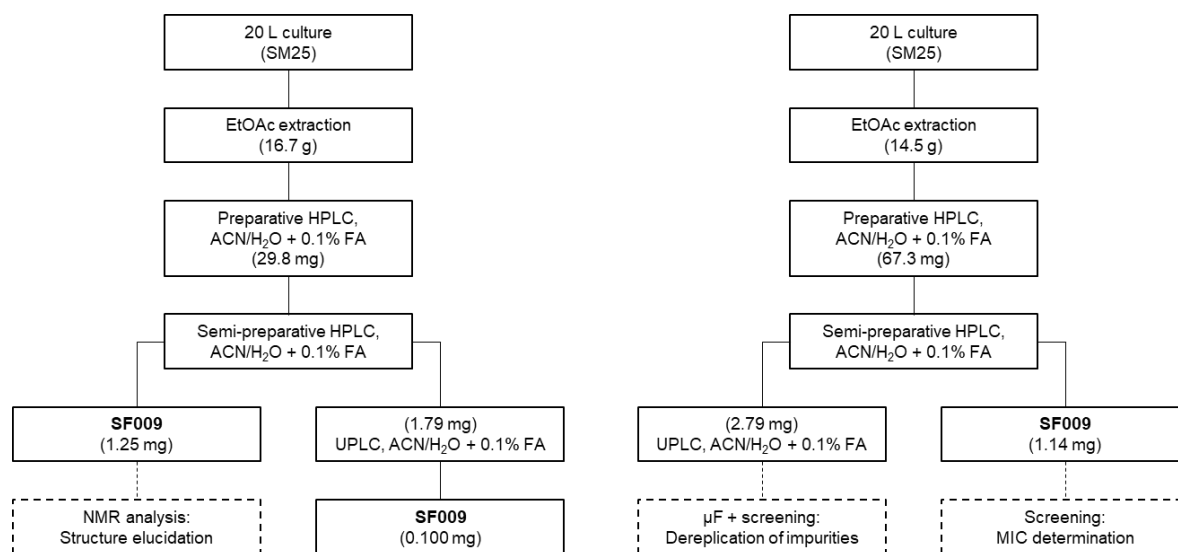


Scheme 16: Isolation scheme of SF009 (**150**) from liquid culture of HAG010336 in medium 5265.

Following fermentation, the liquid culture was lyophilized and extracted with MeOH. SPE was subsequently performed with the crude extract using Amberlite® XAD-16N as solid phase and stepwise increasing percentage of methanol for elution. After evaporating MeOH, the aqueous fractions containing **150** were extracted with ethyl acetate to eliminate highly polar impurities. Further purification was achieved by preparative HPLC using a C18 column (Synergi™ Fusion-RP 80 Å, 250 x 21.2 mm) and a gradient of 5–95% ACN in water followed by semi-preparative HPLC with the same gradient using a NUCLEODUR® C18 Gravity-SB column (250 x 4.6 mm). Final purification of the combined fractions from both batches was achieved by MS-guided UPLC fractionation (ACQUITY UPLC® BEH C18 column, 100 x 2.1 mm) yielding 0.235 mg of pure compound. The amount of SF009 (**150**) isolated over six steps was not sufficient to elucidate its structure by NMR analysis. Therefore, another fermentation was performed based on the outcome of the media variation.

5.4.2 Medium SM25

From cultivation of HAG010336 in medium SM25, different challenges regarding separation and purification arose. Therefore, the isolation protocol had to be adapted (Scheme 17).



Scheme 17: Isolation scheme of SF009 (**150**) from liquid culture of HAG010336 in medium SM25.

The two batches of 20 L liquid culture each were directly extracted with ethyl acetate. The obtained crude extract was fractionated by preparative RP-HPLC as described for the isolation from medium 5265. For both batches, subsequent purification by semi-preparative HPLC (NUCLEODUR® C18 Gravity-SB column, 250 x 4.6 mm) using an adjusted gradient elution of 35–70% ACN in water gave 1.25 mg of SF009 (**150**) as red-purple solid. Impure fractions were united separately and purified by UPLC fractionation. The LC-MS chromatograms illustrate the overall progress (Fig. 51).

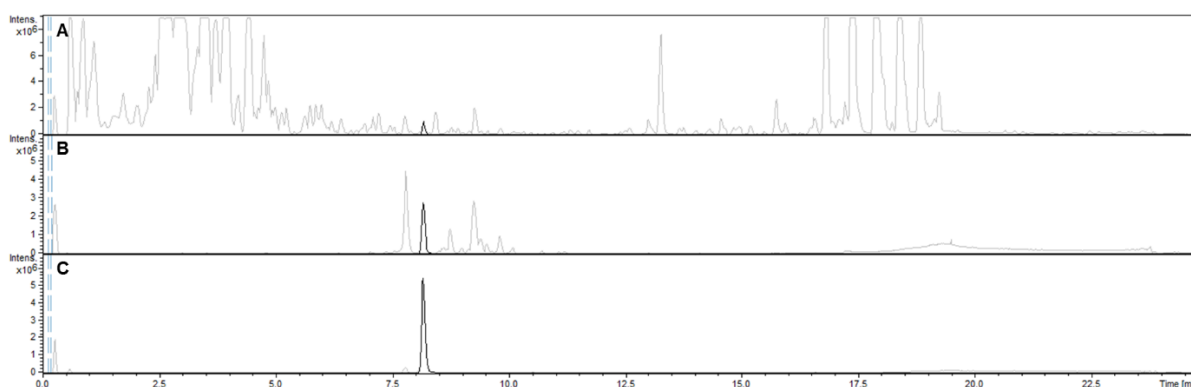
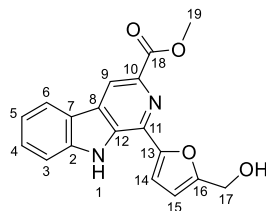


Fig. 51: Isolation of SF009 (**150**) from liquid culture of HAG010336 in medium SM25. BPC (grey) and EIC (black) of **150** (m/z 323.1026 \pm 0.005, $C_{18}H_{14}N_2O_4$ $[M+H]^+$) at different purification steps; A: EtOAc crude extract, B: combined fractions after preparative HPLC, C: combined pure fractions after semi-preparative HPLC.

Both 20 L fermentation yielded sufficient amounts of SF009 (**150**) for structure elucidation by NMR analysis and investigation of the antimicrobial activity.

5.5 Structure Elucidation

Based on the molecular formula $C_{18}H_{14}N_2O_4$ (m/z 323.1027, $[M+H]^+$, Δ ppm 0.31) suggested by positive HRESIMS analysis, NMR data identified the isolated SF009 as flazin methyl ester (**150**) (Table 24).^[210]

Flazin methyl ester (**150**)Table 24: 1H and ^{13}C NMR data of flazin methyl ester (**150**) in comparison to SF009 (*isol-150*) isolated from *Streptomyces* sp. HAG010336 (DMSO- d_6).

position	Flazin methyl ester (literature) ^[211]		SF009 (isolated from HAG010336)	
	δ_H (\mathcal{J} in Hz) (400 MHz)	δ_C (100 MHz)	δ_H (\mathcal{J} in Hz) (500 MHz)	δ_C (126 MHz)
1	11.63, s	–	11.65, s	–
2	–	141.5	–	141.3
3	7.82, d (8.2)	112.9	7.83, d (8.2)	112.9
4	7.66, dd (8.0, 7.9)	129.0	7.65, dd (8.2, 6.8)	128.9
5	7.35, dd (8.2, 8.0)	120.7	7.35, dd (7.9, 6.8)	120.6
6	8.44, d (7.9)	122.1	8.43, d (7.9)	122.0
7	–	121.1	–	120.9
8	–	129.7	–	129.5
9	8.87, s	116.4	8.86, s	116.3
10	–	133.0	–	132.9 ^a
11	–	136.7	–	136.5 ^a
12	–	132.1	–	132.0
13	–	151.2	–	151.0
14	7.29, d (3.4)	111.0	7.29, d (3.2)	110.9
15	6.63, d (3.4)	109.4	6.62, d (3.2)	109.2
16	–	157.4	–	157.3
17	4.68, d (6.1)	56.1	4.68, s	55.9
17-OH	5.50, t (6.1)	–	n.a.	–
18	–	165.9	–	165.8
19	3.94, s	52.2	3.94, s	52.1

^aMight be interchanged (signal at 136.5 ppm did not show any HMBC correlation; signal at 132.9 ppm only showed very weak correlation to H-9); n.a.: Not assigned (due to extreme line broadening). Assignment of signals reported in literature based on own analysis.

Flazin methyl ester (**150**) was first described 1986 semi-synthetically prepared from flazin (**153**), which was isolated from Japanese soy sauce.^[210] Later, methyl ester **150** itself was isolated from

Streptomyces sp. K01-0031.^[212] In this context, a weak activity against brine shrimp *Artemia salina* with a MIC value of 20 $\mu\text{g}/\text{mL}$ was observed. In contrast, for flazin (**153**) quinone reductase induction has been reported with a potential use in cancer chemoprevention.^[213] Furthermore, based on a weak anti-HIV activity found for **153** isolated from fruiting bodies of *Suillus granulatus*, a comprehensive SAR study was performed identifying flazin amide (**154**) as most potent analogue with reduced cytotoxicity.^{[214][215]} However, to the best of knowledge no antimicrobial activity has been reported for flazin (**153**) or any of its derivatives so far.

5.6 Tandem Mass Spectrometric Investigations

Based on its MS/MS fragmentation pattern, SF009 (**150**) was tentatively regarded as derivative of SAR1xxx (**151**). A difference in the monoisotopic mass of 42.0100 Da corresponding to $\text{C}_2\text{H}_2\text{O}$ suggested an additional acetyl group. Having identified SF009 as flazin methyl ester (**150**), a closer look was taken at the MS/MS fragmentation of both compounds in order to explain the high similarity of observed fragments (Fig. 52).

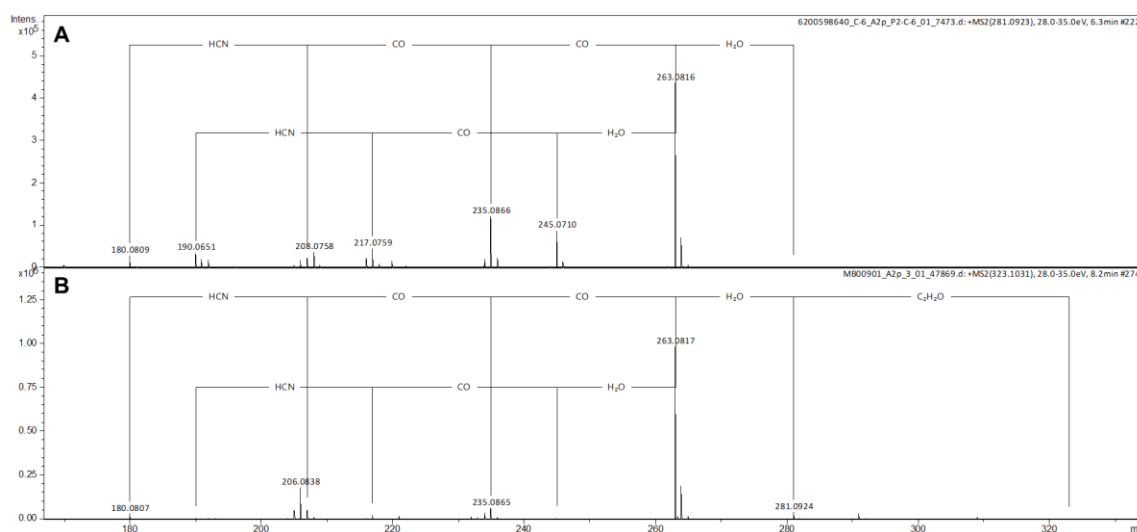


Fig. 52: Collision-induced MS/MS spectra of A: SAR1xxx (**151**) and B: SF009 / flazin methyl ester (**150**). Neutral losses are annotated.

In general, the occurring fragmentation was rather unspecific. Common losses of CO, H_2O and HCN were observed. In both cases, the single, most intensive fragment was found at m/z 263.0817 ($\text{C}_{16}\text{H}_{10}\text{N}_2\text{O}_2^+$). While this occurred after the elimination of H_2O from the $[\text{M}+\text{H}]^+$ parent ion of **151**, for **150** the loss of $\text{C}_2\text{H}_2\text{O}$ at the methyl ester group preceded. Resonance-stabilization explained the high intensity of these fragments. From that, the same two fragmentation routes A and B were observed for both compounds. Neutral losses of CO, H_2O and HCN including various rearrangements

led to the polycyclic, aromatic cations m/z 190.0651 ($C_{14}H_8N^+$) and m/z 180.0809 ($C_{13}H_{10}N^+$) (Fig. 53, Fig. 54).

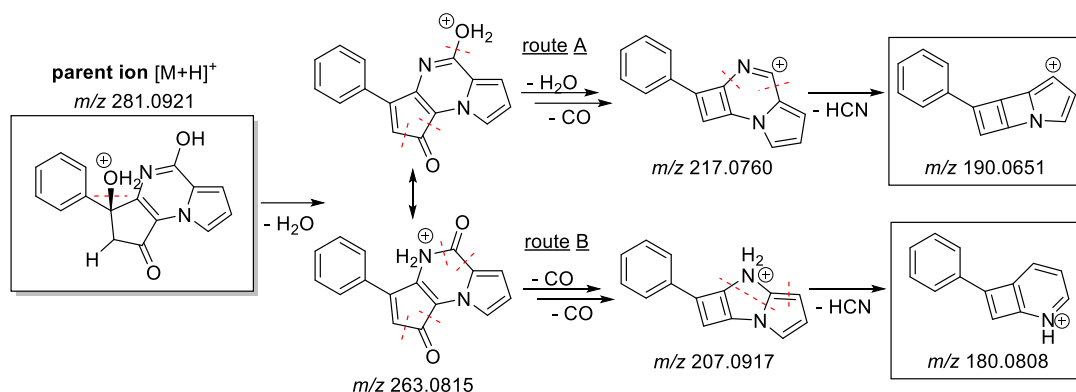


Fig. 53: Postulated fragmentation pathway of SAR1xxx (**151**) starting from $[M+H]^+$ parent ion.

Observed was furthermore the competitive loss of radical $H\dot{C}O$ and non-radical CO from the m/z 235.0865 ($C_{15}H_{11}N_2O^+$) fragment of **150** leading either to the radical cation m/z 206.0838 ($C_{15}H_{11}N_2O^+$) or to the even-electron cationic fragment m/z 207.0912 ($C_{14}H_{11}N_2^+$) (Fig. 54).

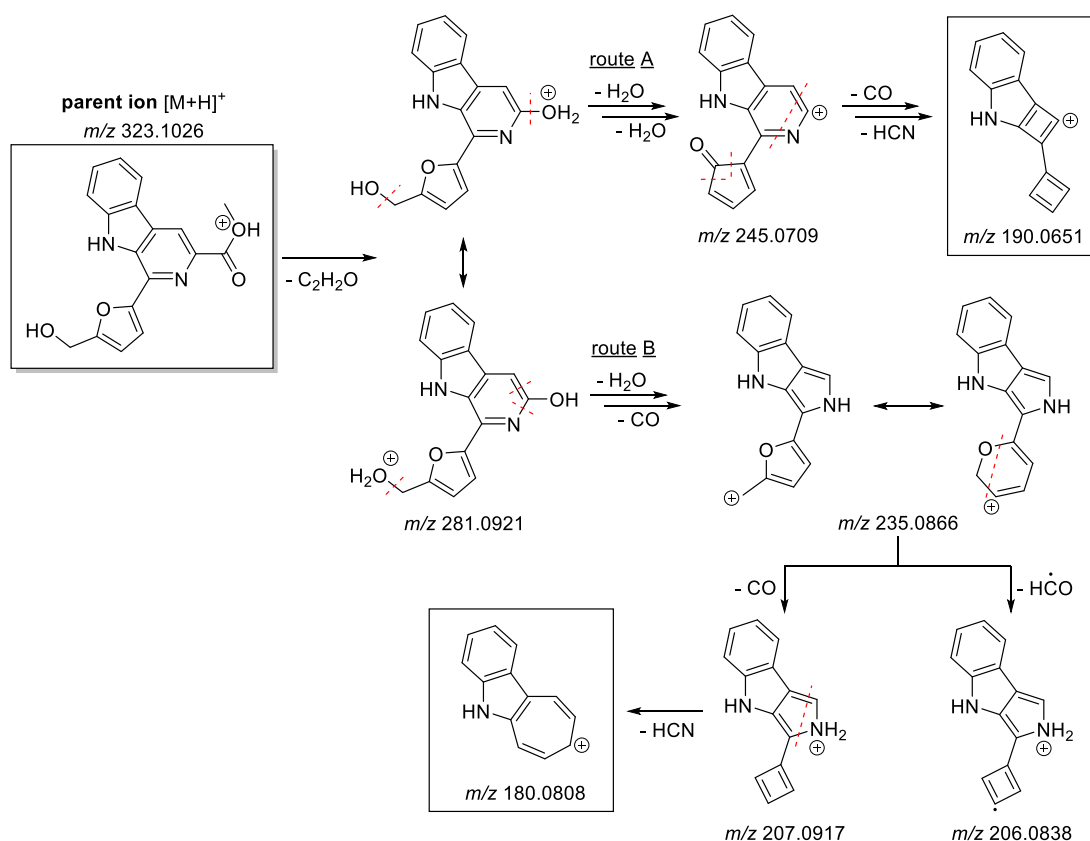


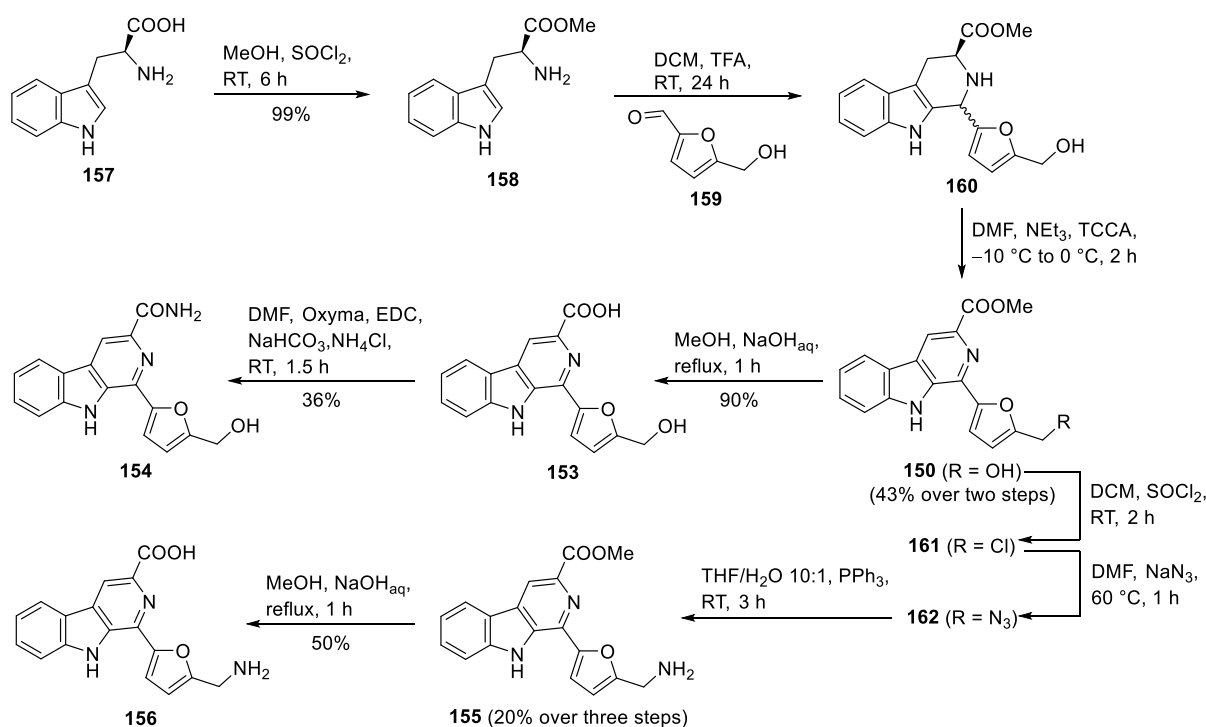
Fig. 54: Postulated fragmentation pathway of flazin methyl ester (**150**) starting from $[M+H]^+$ parent ion.

On one hand, analysis of the MS/MS fragmentation pathway confirmed identification of SF009 as flazin methyl ester (**150**) by NMR structure elucidation. On the other hand, the identical fragmentation pattern of SAR1xxx (**151**) and **150** were explained and therefore justified the original

hypothesis regarding the structure of SF009 as derivative of **151** based on the annotation from the internal MS/MS database.

5.7 Total Synthesis of SF009 and Derivatives

For validation of the findings for the isolated SF009 (*isol-150*) and to get access to a larger amount of pure compound for bioactivity profiling, flazin methyl ester (*synth-150*) was synthesized according to Liu *et al.*^[214] Considering its potential antimycobacterial activity, a minor SAR study was intended. Therefore, flazin (**153**) and the amide derivative **154** were synthesized due to simple accessibility. Since small molecules that are most likely able to penetrate the outer membrane of Gram-negative bacteria contain an amine^[216], the derivatives **155** and **156** were additionally synthesized (Scheme 18).



Scheme 18: Total synthesis of flazin methyl ester (**150**), flazin (**153**), flazin amide (**154**), flazin methyl ester amine (**155**) and flazin amine (**156**).

Starting from L-tryptophan (**157**), the methyl ester **158** was synthesized using thionyl chloride in dry methanol. Without further purification, a Pictet-Spengler reaction was performed with 5-hydroxymethyl-2-furaldehyde (**159**) in the second step to give the diastereomeric mixture of **160**.^[217] NMR analysis revealed a diastereomeric ratio of about 63:37. Without separation of the diastereomeres, the mixture was oxidated using trichloroisocyanuric acid (TCCA) to yield flazin methyl ester (*synth-150*).

Flazin (**153**) was synthesized by saponification of the methyl ester **synth-150** using aqueous NaOH in methanol. From the carboxylic acid **153**, flazin amide (**154**) was obtained using EDC as coupling reagent and Oxyma as additive in the presence of ammonium chloride under mild basic conditions.^[218]

In a second route starting from flazin methyl ester (**synth-150**), the corresponding amine **155** was synthesized in three steps. After chlorination of the primary alcohol using thionyl chloride, the resulting halogenide species **161** was converted into the azide **162** using sodium azide. A Staudinger reaction with triphenylphosphine yielded flazin methyl ester amine (**155**).^[219] However, even under different aqueous acidic conditions tested, a complete hydrolysis of the intermediate formed iminophosphorane into the desired amine **155** was not achieved causing significant decrease of the reaction yield. In an additional step, flazin amine (**156**) was synthesized from **155** via basic saponification as described previously.

All compounds were obtained in sufficient amounts for follow-up investigations and were therefore tested regarding their antimicrobial activity for comparison with the natural product **isol-150** isolated from *Streptomyces* sp. HAG010336.

5.8 Bioactivity Profiling

5.8.1 Antimicrobial Activity

The antimicrobial activity of isolated SF009 (**isol-150**) and synthesized flazin methyl ester (**synth-150**) as well as the four derivatives **153–156** was evaluated in a microbroth dilution assay. The screening panel consisted of four Gram-negative and three Gram-positive bacteria as well as one pathogenic fungal strain (Table 25).

Flazin methyl ester isolated from HAG010336 (SF009, **isol-150**) showed promising antibacterial activity against the tested Gram-positive pathogens. The originally observed growth inhibition of the crude extract towards *M. smegmatis* was replicated. No activity against Gram-negative bacteria (except *M. catarrhalis*) and the opportunistic pathogenic yeast *C. albicans* was found, indicating a certain specificity regarding its antimicrobial activity pattern. These findings however were not supported in comparison to the synthesized flazin methyl ester (**synth-150**) which only showed distinctly lower growth inhibition towards *M. catarrhalis* and *S. aureus*.

While the synthesized flazin amide (**154**) exhibited good antibacterial activity against *M. catarrhalis*, the derivatives flazin (**153**) and flazin amine (**156**) showed insignificant or no effect on this test strain. Furthermore, no activity towards any other screened pathogen was observed for these three compounds (**153**, **154**, **156**). In contrast, flazin methyl ester amine (**155**) inhibited the growth of all bacteria screened appearing to be the most potent derivative. Apparently, conversion of the primary

alcohol group to an amine led to a strong increase of bioactivity. The same could not be observed for flazin amine (**156**) in comparison to flazin (**153**). More consistent however was the finding that the methyl esters **synth-150** and **155** are more effective than their analogous carboxylic acids **153** and **156**. Furthermore, in the series of methylene alcohol being attached to the furan moiety, the amide **154** appears to be even more active against *M. catarrhalis* at least. No antibacterial or antifungal activity has been previously published for the known compounds **150**, **153** and **154**. The compounds **155** and **156** have not yet been described in literature.

Table 25: MICs [$\mu\text{g/mL}$] of flazin methyl ester (**isol-150** and **synth-150**), flazin (**153**), flazin amide (**154**), flazin methyl ester amine (**155**) and flazin amine (**156**).

	isol-150	synth-150	153	154	155	156
<i>Escherichia coli</i> ATCC 35218 (MH-II)	> 128	> 128	> 128	> 128	64	> 128
<i>Escherichia coli</i> ATCC 35218 (MHC)	> 128	> 128	> 128	> 128	64	> 128
<i>Klebsiella pneumoniae</i> DSM 30107	> 128	> 128	> 128	> 128	32–64	> 128
<i>Moraxella catarrhalis</i> ATCC 25238	0.063–0.5	4	64–128	0.125–0.25	0.25–0.5	> 128
<i>Pseudomonas aeruginosa</i> ATCC 27853	> 128	> 128	> 128	> 128	64–128	> 128
<i>Mycobacterium smegmatis</i> ATCC 607	1–2	> 128	> 128	> 128	8	> 128
<i>Bacillus subtilis</i> DSM 10	0.063–0.5	> 128	> 128	> 128	8–16	> 128
<i>Staphylococcus aureus</i> ATCC 25923	0.063–1	64–128	> 128	> 128	64	> 128
<i>Candida albicans</i> FH 2173	> 128	> 128	> 128	> 128	n.d.	> 128

n.d.: Not determined.

With a MIC value of 8 $\mu\text{g/mL}$ towards *M. smegmatis*, flazin methyl ester amine (**155**) was also tested against *M. tuberculosis* H37Rv. The microplate Alamar Blue assay revealed growth inhibition towards the human pathogen with an IC_{80} value of 22.1 μM (Table S29).

5.8.2 Dereplication of Antimycobacterial Active Secondary Metabolites

Due to the significant discrepancy between the antibacterial activity of the isolated (**isol-150**) and synthesized flazin methyl ester (**synth-150**), another look was taken at isolated samples of SF009 as it was assumed that traces of impurities were causing the observed activity. The presence of additional compounds could also explain the difference in color visible in both samples. In general, detection by MS and DAD strongly depends on structural features allowing ionization and UV absorption. Therefore, impurities can only be relatively quantified. Even though considered fairly pure based on MS analysis, the sample used for structure elucidation revealed a significant amount of impurities in NMR analysis underlining the theory.

For confirmation of this hypothesis and determination which metabolites produced by HAG010336 were in fact causing the observed activity, a pre-purified isolation sample of SF009 (*isol-150*) was fractionated quantitatively *via* UPLC. MeOH instead of ACN was used as organic solvent. Changing the mobile phase is a known approach to affect separation and had shown before to be beneficial in terms of resolving co-eluting compounds. Guided by HRMS and bioactivity, three samples A–C were generated separating SF009 (*isol-150*) from other metabolites as far as possible. These samples then were fractionated *via* UPLC using standard conditions and screened against *M. smegmatis* as starting point for dereplication. Based on HRMS/MS data, compounds were identified that could potentially explain the observed activity exceeding mycobacteria.

The activity in sample A was assigned to a compound of m/z 511.0873 ($[M+H]^+$, $C_{25}H_{19}O_{12}^+$, Δ ppm 0.39) (Fig. S138). The molecular formula search gave two hits in the Dictionary of Natural Products, namely griseorhodin B (structure unknown) and griseorhodin G (**163**).^{[220][221]} Griseorhodins belong to the rubromycin group, a large family of extensively modified aromatic polyketides produced by *Actinomyces*.^{[222][223]} Structurally, they are characterized by a naphthoquinone and isocumarin ring linked *via* spiroketal core (Fig. 55).^[224] Antimicrobial^{[225][226]} and cytotoxic^{[221][227]} properties as well as inhibition of reverse transcriptases (HIV-1, M-MLV, human telomerase)^[228] are described for the group of griseorhodins.



Fig. 55: Chemical structure of griseorhodin G (**163**).

In sample B, the activity was assumed to be caused by a metabolite of m/z 415.1385 ($[M+H]^+$, $C_{22}H_{23}O_8^+$, Δ ppm 0.48) partially co-eluting with SF009 (*isol-150*), which was shown to be inactive against *M. smegmatis* by screening of *synth-150*. The molecular formula search yielded 82 hits in the Dictionary of Natural Products indicating a high chance of being a known NP. In this case, the four hits in Antibase were a more straightforward starting point for dereplication. Only two of the four compounds were knowingly produced by *Streptomyces*, namely dihydrofeudomycinone B (**164**) and daidzein G3 (**165**) (Fig. 56). Moreover, in MS fragmentation one major peak (m/z 271.0603, $C_{15}H_{11}O_5^+$) was observed corresponding to a neutral loss of 144.0828 Da which corresponds to a $C_7H_{12}O_3$ moiety (Fig. S139). The same fragment spectrum was recognized for RA037xxx (**166**) ($[M+H]^+$, m/z 403.1024, $C_{20}H_{19}O_9^+$) as hit in the Sanofi legacy MS/MS database which has been published as frangulin B.^[229] The main fragment corresponded to the anthraquinone framework after loss of the glycosyl group.

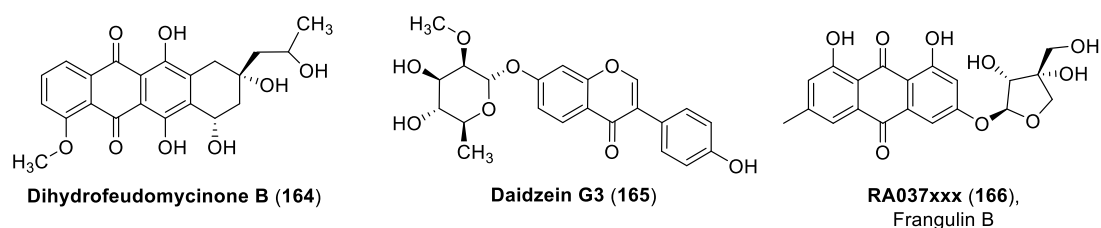


Fig. 56: Chemical structures of dihydrofeudomycinone B (**164**), daidzein G3 (**165**) and RA037xxx (**166**).

These findings strongly suggested that the antimicrobial active compound most likely belongs to the group of either anthraquinones or isoflavones. Antibacterial activity is described for both classes.^{[230][231]}

In the fractionation of sample C, the compounds of m/z 429.0970 ($[M+H]^+$, $C_{25}H_{17}O_7^+$, Δ ppm 0.23) and m/z 408.1557 ($[M+H]^+$, $C_{22}H_{22}N_3O_5^+$, Δ ppm 0.74) were co-eluting in the fraction showing growth inhibition towards *M. smegmatis*. Using again the Dictionary of Natural Products and Antibase, there were no hits for the molecular formula $C_{25}H_{16}O_7$ but two identical hits for $C_{22}H_{21}N_3O_5$: the cytotoxic 7,9-dihydroxy-3-(1*H*-indol-3-ylmethyl)-8-methoxy-2,3,11,11a-tetrahydro-6*H*-pyrazino[1,2-*b*]iso-quinoline-1,4-dione (**167**) isolated from terrestrial *Aspergillus oryzae*^[232] and preoxazinin-7 (**168**) isolated from toxic mussels *Mytilus galloprovincialis*^[233] (Fig. 57).

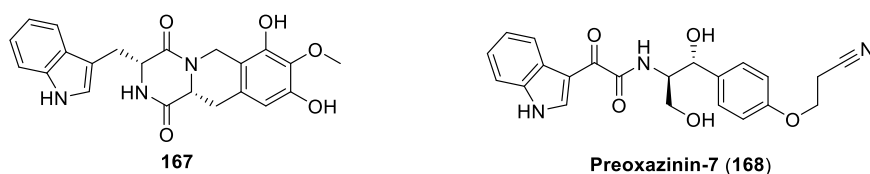


Fig. 57: Chemical structures of **167** and preoxazinin-7 (**168**).

Even though both compounds might explain the bioactivity, their structures do not match the MS/MS fragmentation including the observed loss of a valine residue (Fig. S140). Furthermore, their occurrence in bacteria has not yet been reported making it even more unlikely to be actually produced by HAG010336.

In conclusion, a variety of conceivable secondary metabolites were dereplicated that could have caused the antimicrobial activity initially observed for the flazin methyl ester (**150**) containing fraction as well as for the isolated sample of SF009 (*isol-150*) provided to MIC screening explaining the discrepancy in comparison to *synth-150*. However, the identified compounds either lacked chemical novelty or knowingly exhibited cytotoxic properties and therefore determined one end point of the project without another isolation round being initiated. Overall, this example also demonstrated the great importance, scope and limitations of dereplication as a challenging tool in the natural product drug discovery pipeline.

5.8.3 Cytotoxicity

Of all synthesized compounds, flazin methyl ester amine (**155**) was the most potent derivative regarding antibacterial growth inhibition. Due to its broad but unspecific activity, **155** was furthermore screened for potential cytotoxic properties. IC₅₀ values of 13.4 μM and 13.1 μM were determined for the human acute monocytic leukemia cell line THP-1 and the human hepatoma cell line HepG2, respectively (Fig. S141, Fig. S142).

Taking the MIC value against *Mtb* into account, the synthesized amine derivative **155** of SF009 (*isol-150*) did not show required selectivity regarding its bioactivity. Therefore, further and more detailed investigation of **155** was stopped at this point.

5.9 Summary

The antimycobacterial activity of *Streptomyces* sp. HAG010336 has been investigated. Successfully optimized cultivation conditions led to an increased production of sufficient amount of SF009 (*isol-150*) allowing its isolation and structure elucidation. NMR analysis disproved the initial hypothesis of an unknown SAR1xxx (**151**) derivative and identified SF009 as flazin methyl ester (**150**). However, comparative analysis of postulated MS/MS fragmentation pathways for both compounds explained the original theory. For comparison with the natural product, total synthesis of flazin methyl ester (*synth-150*) was performed unable to confirm the postulated activity against *M. smegmatis*. Instead, a variety of other potential metabolites were identified by dereplication that could explain the originally observed antimycobacterial activity of HAG010336. Additionally, four derivatives of **150** were synthesized allowing investigation of structure-activity relationships regarding their bioactivity. Flazin methyl ester amine (**155**) was identified as the most potent derivative. However, considering the observed cytotoxicity, the compound's pharmaceutical potential is strongly limited and will not be further evaluated by follow up investigations. Yet, it has been demonstrated that *Streptomyces* remain a valuable source for novel TB compounds.

6. Summary and Conclusion

The scientific studies within the Public Private Partnership between Fraunhofer and Sanofi resp. Evotec clearly illustrate the main purpose of this collaboration: the discovery of novel Gram-negative and antimycobacterial active secondary metabolites from microorganisms based on a variety of innovative approaches in terms of producer strains and screening methods. The present study was the first to justify the implemented strategies by demonstrating proof of the following concepts: i) New potential arises from innovative screening conditions even when applied to widely explored Actinobacteria. However, the ability to deliver novel chemistry is left to be proven. ii) Investigating the biosynthetic potential and chemical space of rare and underexplored phyla such as Bacteroidetes provided first evidence towards the discovery of new or even novel compounds. This approach represents by far the most promising to follow up in future projects with potential applications clearly exceeding the use as antibacterial agents. iii) Considering antimycobacterial activity or fungal producer strains, standard high-throughput screening of the diverse Sanofi-Fraunhofer strain collections still allows the identification of new active metabolites. Moreover, the undeniable and continuing relevance of isolation and structure elucidation as key aspects of NP-based drug discovery towards hit identification has also been demonstrated. These efforts resulted in elucidation of 32 natural products within four different projects, out of which 18 compounds have been reported for the first time. Coordinating extensive bioactivity profiling including evaluation of resulting data as well as performing total synthesis of overall 15 NPs or related analogs including SAR studies represent further significant aspects of early-stage discovery pipeline also covered in the present work.

In the first project (chapter 2), investigation of metabolites produced by *Aspergillus terreus* ST000934 displaying Gram-negative activity against *E. coli* led to the new fungal compound SF005-B (**25**) combining a rare oxocane moiety with hemi- and acetal motifs in a unique trioxatricyclic ring system (Fig. 58).

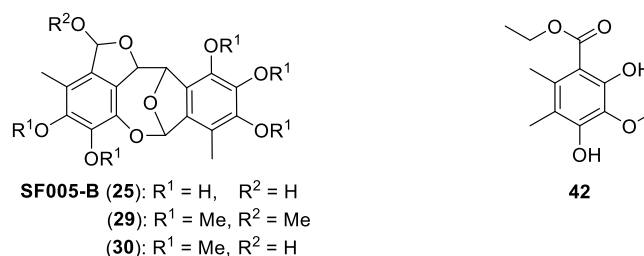


Fig. 58: Chemical structures of new fungal metabolites either isolated from *Aspergillus terreus* ST000934 or obtained by chemical derivatization.

Occurring issues towards structure elucidation were overcome by methylation of the NP and employing extensive NMR as well as ESI-QTOF-MS/MS analysis. As a result, the new related derivatives **29** and **30** were also identified. Additionally, a total of eight fungal metabolites were furthermore isolated with compound **42** being described for the first time. The antibacterial activity of all isolated fungal compounds revealed broad growth inhibition towards Gram-positive and Gram-negative bacteria including MIC values of up to 8–16 $\mu\text{g/mL}$ against *M. catarrhalis*.

In a second project (chapter 3), the advanced combination of innovative screening, HRMS-based dereplication and Molecular Networking led to isolation of 13 madurastatins from *Actinomadura* sp. ST100801 which exhibited Gram-negative activity against *E. coli* MHC. Besides the known madurastatin B1 ((*R*)-**50**) and C1 (**48a**), the new enantiomers of only recently reported imidazolidinone-containing madurastatin D1 (**53**) and D2 (**54**) as well as nine unpublished madurastatins (B4 (**55**), C2 (**61**), D3 (**62**) and D4 (**63**), E1 (**56**) and E2 (**58**), F1 (**57**), G1 (**59**) and G2 (**60**)) were elucidated including absolute stereochemistry based on chiral derivatization. Considering the 600 Da molecular weight cutoff in regards to Gram-negative activity, small madurastatin B1 (**50**) as well as the three derivatives **64–66** were furthermore accessed by enantioselective total synthesis (Fig. 59). These eight synthesized compounds completed the set of 20 madurastatin analogs investigated in a SAR study revealing correlations between structural features, iron chelating properties and antibacterial activity with MIC values of up to 4 $\mu\text{g/mL}$ against Gram-negative *M. catarrhalis*. Agricultural crop protection targeting e.g., *Septoria tritici* and *Xylella fastidiosa* presents further potential applications worth exploring for this NP compound class.

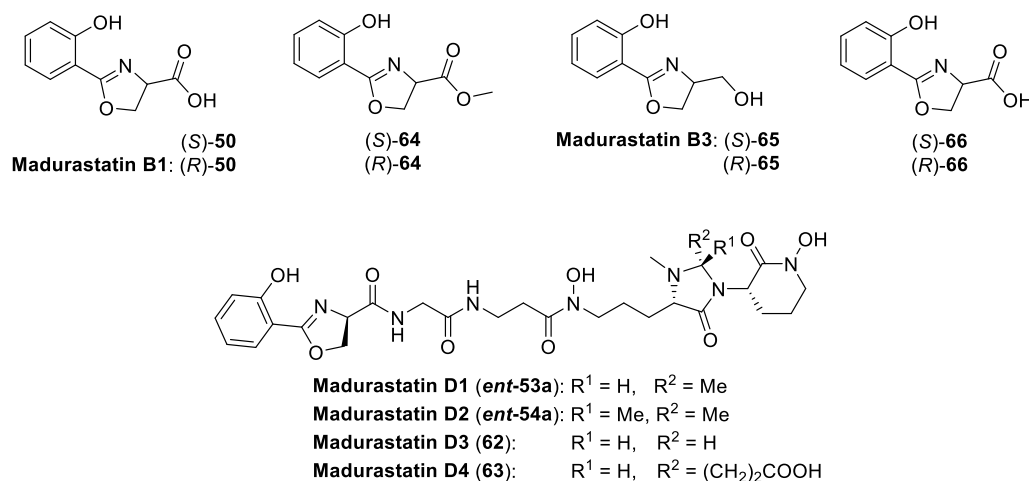


Fig. 59: Chemical structures of small madurastatin analogs **50** and **64–66** accessed by enantioselective total synthesis as well as isolated compounds exemplified by derivatives (**ent-53a**, **ent-54a** and **62**) of the madurastatin D series.

The innovative approach of investigating less-studied phyla such as Bacteroidetes was evaluated based on the initially observed Gram-negative activity of *Olivibacter* sp. FHG000416 against *E. coli* MHC in another project (chapter 4). Seven metabolites belonging to the compound classes of aminolipids (**70** and **71**), lysophospholipids (**72** and **73a**) and *N*-acyl amino acids (**74–76**) were

6. Summary and Conclusion

isolated, six of which were reported for the first time (Fig. 60). Structure elucidation included determination of the absolute configuration addressed by chiral derivatization and complex enantioselective total synthesis of FE004 (**71**). Besides rather weak antimicrobial activities, structural features strongly pointed towards a potential application in the field of immunotherapy. Therefore, TLR2/TLR4-stimulating properties were investigated in comparison to the structurally related and as active reported lipid 430 (**87**) additionally isolated from another in-house Bacteroidetes strain, namely *Chitinophaga eiseniae* DSM 22224, also producing the tripeptidic derivative FE002 (**90**). Although requiring further optimization, the potential of this strategic approach has been clearly demonstrated.

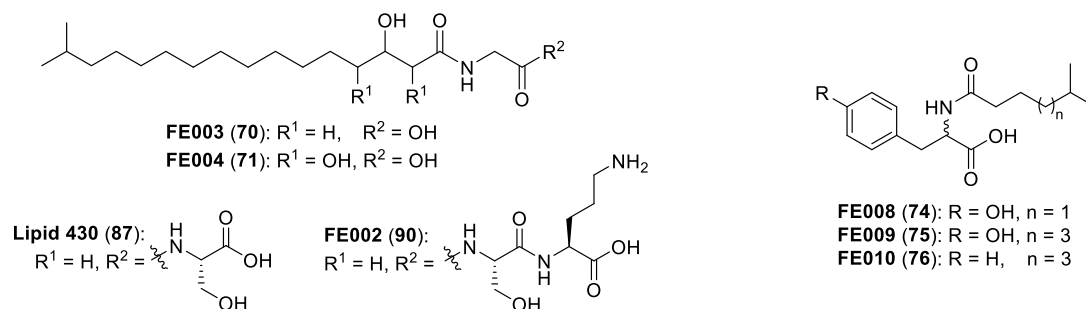


Fig. 60: Chemical structures of **70**, **71** and **74–76** isolated from *Olivibacter* sp. FHG000416 as well as **87** and **90** isolated from *Chitinophaga eiseniae* DSM 22224.

In the final project (chapter 5), the antimycobacterial activity of metabolite SF009 (*isol-150*) produced by *Streptomyces* sp. HAG010336 was investigated. Designing a large media variation led to successfully optimized cultivation conditions which allowed identification of **150** as known flazin methyl ester. Its actual lack of activity against *M. smegmatis* was confirmed by comparison to the synthesized compound but effectively introduced by further synthesis of closely related derivatives **154–156** (Fig. 61). Flazin methyl ester amine (**155**) as most potent analog showed a MIC value of 8 $\mu\text{g/mL}$ against *M. smegmatis* and an IC_{80} value of 22.1 μM against *M. tuberculosis*. However, cytotoxicity assays against THP-1 ($\text{IC}_{50} = 13.4 \mu\text{M}$) and HepG2 ($\text{IC}_{50} = 13.1 \mu\text{M}$) cell lines suggested the need of further optimization in order to achieve desired selectivity.

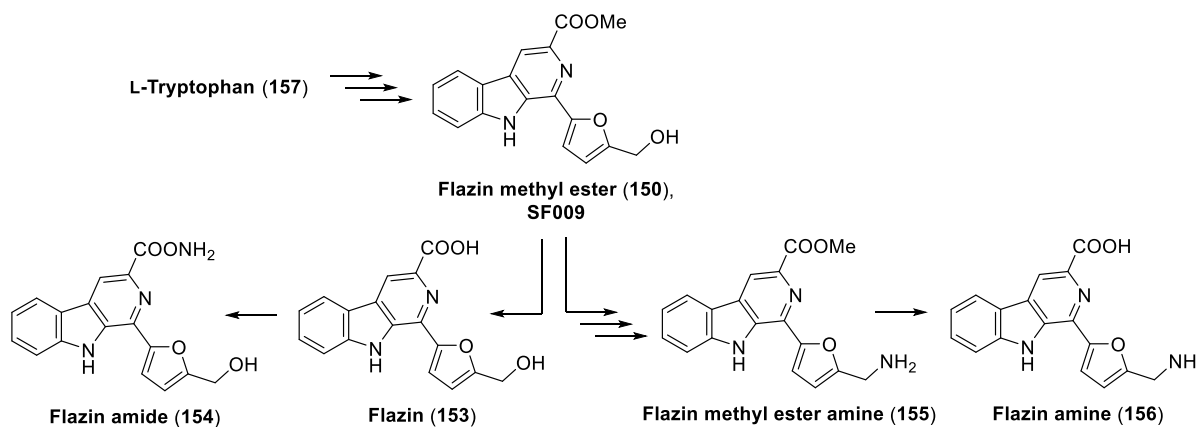


Fig. 61: Chemical structures of flazin methyl ester **150** and derivatives **153–156** accessed by total synthesis.

Overall, various aspects of this work emphasize the following more general conclusion regarding the presence and future of natural product-based antibiotic drug discovery: i) Microorganisms still present a diverse and fertile source of new antimicrobial active compounds. However, in order to avoid re-discovery of known metabolites, dereplication utilizing state-of-the-art analytical technology and internal as well as commercial NP databases remains essential. Moreover, isolation and structure elucidation also benefit from highly sophisticated techniques as they remain crucial but challenging elements of the AE2H phase in NP drug discovery. ii) In order to overcome existing antimicrobial resistances, novel compounds featuring a new mode of action or even addressing new molecular targets are urgently needed. In this regard, exploiting underexplored, rare phyla, using innovative cultivation techniques and augmenting traditional methods by genomic and metabolomics approaches are highly promising advances as also shown by other groups.^[234] The classes of malacidin and humimycin antibiotics as well as pre-clinical candidate teixobactin exemplify proof of concept.^[235] iii) Semi-synthetic modifications and total synthesis have always been and will continue to be of major importance, especially when it comes to structure elucidation and optimization of hit structures towards lead compounds. iv) Recent advancements fuel mankind's battle against antimicrobial resistance. In order to provide promising candidates to the clinical development pipeline which might at some stage fill the therapeutic gap and will ultimately contribute to tackling the current resistance crisis however, focused research efforts and joint forces between academia and industry are essential; most certainly we then will be able to hold frontline on the battlefield of evolution.

7. Experimental

7.1 General Materials and Experimental Procedures

7.1.1 Solvents and Chemicals

For isolation procedures, technical or analytical grade solvents commercially obtained from ALFA AESAR and VWR were used. HPLC systems ran on HPLC grade solvents and deionized water purified by a ultrapure water system (arium® pro, SARTORIUS) while LC-MS was performed with MS grade solvents. In both cases they were purchased from VWR and FISHER SCIENTIFIC.

For synthesis, all starting materials, reagents and solvents were purchased from ABCR, ACROS ORGANICS, FISHER SCIENTIFIC, MERCK, SIGMA ALDRICH and VWR. They were used without further purification.

7.1.2 Synthesis

All reactions were stirred magnetically. Reaction temperatures refer to externally monitored temperatures. Temperatures were adjusted by using heating plates with metal heat-on blocks or ice/water and dry ice/acetone cooling baths. As stated, reactions sensitive to air and/or moisture were carried out under inert gas atmosphere (argon, Schlenk technique). Prior to use, the glassware was dried by storing in a drying oven (Heratherm™, THERMO FISHER SCIENTIFIC) at 80 °C and using a heat gun (630 °C) under high vacuum (E2M28 vacuum pump, EDWARDS) three times (for approx. 5 min each time, flushed with argon in between). All reactions were monitored by TLC or LC-MS analysis (see below). Unless noted otherwise, yields refer to isolated yields.

7.1.3 Chromatography

Thin layer chromatography (TLC). Analytical TLC was performed on silica gel 60 glass plates (10 x 20 cm) coated with fluorescent indicator F254 (MERCK) to monitor reactions, analyze column chromatography fractions and determine R_f values. Used solvent systems are reported. Detection was done by exposure to UV light ($\lambda = 254$ nm; A. KRÜSS OPTRONIC) and/or immersing the plates into staining solutions (KMnO₄ solution: 4.5 g KMnO₄, 30 g K₂CO₃, 4 mL 10% NaOH (w/v), 450 mL H₂O; Cer solution: 10 g Ce(SO₄)₂, 25 g H₃MO₁₂O₄₀P, 10 mL conc. H₂SO₄, 940 mL H₂O) followed by heating with a heat gun.

SPE column chromatography. Large scale SPE was performed using a MCI system consisting of two piston pumps (MCP-CPF Process with pump head, Ismatec®, COLE-PARMER) for sample application (420 rpm, approx. 9 L/h) and elution (80 rpm, approx. 4 L/h), a gradient mixing valve operated by a LKB-LCC 2252 controller (PHARMACIA) and a Labocol FS-3000 fraction collector module (LABOMATIC INSTRUMENTS). The columns (6 x 50 cm / 10 x 35 cm; BioCAT) were packed with the adsorber resin Amberlite® XAD-16N (SIGMA ALDRICH). Prior to use, the solvents (deionized H₂O and technical grade MeOH) were degassed in an ultrasonic bath (10 min).

Silica gel flash chromatography. Isolated extracts or synthetic products were purified by NP flash chromatography using different sized glass columns packed with silica gel 60 M (particle size: 0.063–0.200 mm; MACHEREY-NAGEL) or employing an automated flash column system (SP4™, BIOTAGE) equipped with ISOLUTE® Flash SI II (BIOTAGE) or puriFlash® PF-15SIHC (INTERCHIM) columns of different sizes. In both cases, samples were dissolved in a minimal amount of appropriate solvents (e.g., DCM) and applied onto the pre-conditioned column. Insoluble samples were dried onto silica gel (using e.g., MeOH) and either directly placed inside the column and sealed with a frit or attached after placing and sealing in a separate cartridge. Eluent compositions are reported.

Reversed-phase High Performance Liquid Chromatography (RP-HPLC). Preparative RP-HPLC was performed on a system consisting of two PrepStar SD-1 pumps (VARIAN), an AGILENT 1100 diode array detector (DAD), a manual injection valve with a 5500 µL sample loop and a fraction collector (215 Liquid Handler, GILSON) equipped with a Phenomenex® Synergi™ 4u Fusion-RP 80Å (250 x 21.2 mm) column. The system was run by Chromeleon™ software (THERMO FISHER SCIENTIFIC).

Semi-preparative and analytical HPLC was performed on either AGILENT 1100 systems (G1312A binary pump, G1379A degasser, G1313A autosampler, G1315A DAD) with external column compartment (at room temperature) and fraction collector (215 Liquid Handler, GILSON) computer-controlled by Chromeleon software (THERMO FISHER SCIENTIFIC) or AGILENT 1200 systems (G1312A binary pump, G1379B degasser, G1330B autosampler, G1316B thermostatted column compartment (TCC, at 40 °C), G1315C DAD, G1364C fraction collector) computer-controlled by ChemStation software (AGILENT).

Used solvents, methods (sample concentration, injection volume, flow rate, gradient) and columns are reported in EXPERIMENTAL PROCEDURES (see 7.2).

Reversed-phase Ultra High Performance Liquid Chromatography (RP-UPLC). UPLC was performed on an AGILENT 1290 Infinity system (G4220A binary or G4024A quaternary pump, G4226A autosampler, G1316C TCC, G4212A DAD, G4261B evaporating light scattering detection (ELSD)) or an AGILENT 1290 Infinity II system (G7104A flexible pump, G7167B multisampler, G7116B multicolumn thermostat (MCT), G7117B DAD, G7102A ELSD) computer-controlled by HyStar

software (BRUKER). Both UPLC systems were equipped with an ACQUITY UPLC® BEH C18 1.7 μm (100 x 2.1 mm) column (WATERS) plus ACQUITY UPLC® BEH C18 1.7 μm VanGuard™ (5 x 2.1 mm) pre-column (WATERS) and an external fraction collector (ZINSSER ANALYTIC) run by Zinnser Method Runner software. UPLC systems were combined with high resolution mass spectrometers (micrOTOF or maXis II, BRUKER; see below). Unless noted otherwise, the following parameters were used as standard method on the UPLC system combined with maXis II: mobile phase A: H₂O (0.1% FA), mobile phase B: ACN (0.1% FA), gravimetrically prepared; flow rate: 0.6 mL/min; gradient: 5.00% B (0.00–0.30 min), 5.00–95.25% B (0.30–18.00 min), 95.25–100.00% B (18.00–18.10 min), 100.00% B (18.10–22.50 min), 100.00–5.00% B (22.50–22.60 min), 5.00% B (22.60–25.00 min); column oven temperature: 45 °C; injection volume: up to 5 μL ; UV detection range: 205–640 nm.

7.1.4 Mass Spectrometry (HR-ESI-QTOF-MS)

Ultra high resolution (UHR) electrospray ionization (ESI) quadrupole time-of-flight (QTOF) mass spectrometry was performed using a maXis II (BRUKER). For MS analysis, the following parameters were applied: positive polarity, 50–2000 m/z mass range, 1.00 Hz spectra rate, ESI at 4500 V (capillary; end plate offset: 500 V), 1.6 bar N₂ nebulizer gas and 7.5 L/min N₂ heated dry gas ($T = 250$ °C). During MS/MS experiments, spectra were recorded at a rate of 6.00 Hz using collision induced fragmentation (6.0 eV collision energy).

High resolution (HR) electrospray ionization (ESI) time-of-flight (TOF) mass spectra were recorded on a micrOTOF (BRUKER). The following MS method was used: positive polarity, 50–2500 m/z mass range, 1.00 Hz spectra rate, ESI at 4500 V (capillary; end plate offset: 500 V), 1.3 bar N₂ nebulizer gas and 7.5 L/min N₂ heated dry gas ($T = 250$ °C).

10 mM sodium formate (SIGMA ALDRICH) solution in 1:1 isopropanol/H₂O was used for calibration (flow rate: 0.18 mL/min) and as internal calibration standard during analysis (flow rate: 0.05 mL/min) in positive mode (maXis II: 25% (v/v) in 1:1 isopropanol/H₂O; micrOTOF: 100% (v/v)). NMR spectra analysis was performed using DataAnalysis (BRUKER).

7.1.5 NMR Spectroscopy

NMR spectra were recorded either on a BRUKER AVANCE II WB spectrometer (400 MHz), an AVANCE III HD spectrometer (400 MHz) and an AVANCE III HD spectrometer (600 MHz) at $T = 298$ K (JLU Gießen, Germany) or a BRUKER AVANCE III HD (500 MHz) equipped with a 10 mm MNP cryoprobe (at $T = 303$ K) resp. 5 mm TCI cryoprobe (at $T = 300$ K) (Sanofi, Germany; Evotec, France). Chemical shifts (δ) are given in parts per million (ppm) and referenced to the undeuterated solvent signals (δ ¹H / ¹³C [ppm]: CDCl₃ 7.26 / 77.2, MeOD-*d*₄ 3.31 / 49.0, DMSO-*d*₆ 2.50 / 39.5). In case

a solvent mixture was used, the ratio is stated with the reference solvent underlined. Spectral data is provided from downfield to upfield in the following order: chemical shift in ppm (multiplicity, coupling constant J in Hz, signal integration, assignment in molecule). The following abbreviations for multiplicity and combination thereof are used: (s) singlet, (d) doublet, (t) triplet, (q) quartet, (quin) quintet, (sept) septet, (non) nonet, (br) broad signal. NMR spectra analysis was performed using TopSpin (BRUKER).

7.1.6 Optical Rotation

Optical rotation values were measured on a P3000 polarimeter (A. KRÜSS OPTRONIC) using light of the standard wavelength $\lambda = 589$ nm (sodium D line, D). The specific rotation values $[\alpha]_D^T$ are given in units of $^{\circ}\cdot\mu\text{L}\cdot\text{mg}^{-1}\cdot\text{dm}^{-1}$. Furthermore, the temperature T , the concentration c in $\text{g}\cdot 100\text{ mL}^{-1}$ and the used solvent are reported.

7.1.7 Advanced Marfey's Analysis

Advanced Marfey's Analysis was performed adopted from BHUSHAN *et al.*^[117] For the reference amino acids (L-/D-serine, L-/D-ornithine monohydrochloride, N α -methyl-L-ornithine monohydrochloride; SIGMA ALDRICH), a 5 mM stock solution in H₂O was prepared. To 50 μL stock solution, 20 μL 1 M NaHCO₃ and 50 μL 7 mM L-FDVA (SIGMA ALDRICH) in acetone was added. The solution was stirred at 40 $^{\circ}\text{C}$ for 3 h and then quenched by adding 20 μL 1 M HCl. After evaporation to dryness, the residue was dissolved in 40 μL DMSO and analyzed by UPLC-HRMS (maXis II). Of all peptidic samples to be analyzed, 0.1 μmol was dissolved in 200 μL 6 M DCl in D₂O and stirred at 160 $^{\circ}\text{C}$ for 7 h. After concentrating the solution under reduced pressure, the residue was dissolved in 200 μL H₂O. 100 μL 1 M NaHCO₃ and 200 μL 7 mM L-FDVA in acetone was added. After stirring for 3 h at 40 $^{\circ}\text{C}$, the solution was quenched by adding 100 μL 1 M HCl. After evaporation to dryness, the residue was dissolved in 50 μL DMSO and analyzed by UPLC-HRMS (maXis II).

7.1.8 Microbiological Materials and Procedures

All microbiological procedures were performed under sterile conditions.

Growth media. All growth media components used were purchased from the companies CARL ROTH, SIGMA ALDRICH and OXOID. The growth media were prepared with purified water, the pH was adjusted as specified using 1 M HCl and 1 M NaOH and subsequently sterilized in an autoclave for 20 min at 121 $^{\circ}\text{C}$.

5065: 15 g/L soluble starch, 10 g/L glucose, 10 g/L soy flour, 3 g/L NaCl, 1 g/L yeast extract, 1 g/L K₂HPO₄; pH 7.4

5189: 20 g/L malt extract, 10 g/L glucose, 2 g/L yeast extract, 0.5 g/L (NH₄)₂HPO₄; pH 6.00

5254: 15 g/L glucose, 15 g/L soy flour, 5 g/L corn steep, 5 g/L NaCl, 2 g/L CaCO₃; pH 7.00

5265: 10 g/L malt extract, 4 g/L yeast extract, 4 g/L glucose; pH 7.00

5294: 10 g/L soluble starch, 10 g/L glucose, 10 g/L glycerol, 5 g/L peptone, 3 g/L CaCO₃, 2.5 g/L liquid corn steep, 2 g/L yeast extract, 1 g/L NaCl; pH 7.20

5315: 20 g/L oatmeal, 2.5 mL/L trace element solution 5314 (3 g/L CaCl₂ · 2 H₂O, 1 g/L Fe(III) citrate, 0.2 g/L MnSO₄, 0.2 g/L Na₂B₄O₇, 0.1 g/L ZnCl₂, 0.02 g/L CuSO₄ · 5 H₂O, 0.01 g/L Na₂MoO₄); pH 7.20

5367: 24 g/L potato dextrose broth

AMY: 20 g/L glucose, 20 g/L galactose, 10 g/L soytone, 2 g/L (NH₄)₂SO₄, 2 g/L CaCO₃; pH 7.40

R2A: 0.5 g/L yeast extract, 0.5 g/L proteose peptone, 0.5 g/L casamino acids, 0.5 g/L glucose, 0.5 g/L soluble starch, 0.5 g/L sodium pyruvate, 0.3 g/L K₂HPO₄, 0.05 g/L MgSO₄ · 7 H₂O; pH 6.5

SM17: 40 g/L glycerol, 5 g/L soy flour, 5 g/L peptone, 5 g/L yeast extract, 5 g/L NaCl, 2 g/L glucose, 2 g/L soluble starch, 2 g/L CaCO₃

SM25: 40 g/L glycerol, 21 g/L malt extract, 10 g/L peptone

VPM10: 30 g/L mannose, 5 g/L yeast extract, 1.5 g/L asparagine, 0.5 g/L MgSO₄ · 7 H₂O, 0.1 g/L NaCl, 0.1 g/L CaCl₂ · 2 H₂O; pH 7.00

7.1.9 Antimicrobial Activity Screening

The growth inhibitory activity of crude extracts, UPLC-fractionated extracts or pre-purified samples as well as isolated and synthesized compounds was determined in-house by microbroth dilution assays in different setups. The pathogenic test strains included *Escherichia coli* ATCC 35218 and ATCC 25922 (Δ TolC), *Acinetobacter baumannii* ATCC 19606, *Klebsiella pneumoniae* ATCC 13883, *Moraxella catarrhalis* ATCC 25238, *Pseudomonas aeruginosa* ATCC 27853, *Mycobacterium smegmatis* ATCC 607, *Bacillus subtilis* DSM 10, *Staphylococcus aureus* ATCC 25923 (MSSA), *Candida albicans* FH 2173, *Micrococcus luteus* DSM 20030 and *Listeria monocytogenes* DSM 20600.

For most bacteria, cultures were grown in cation-adjusted Mueller-Hinton II broth (BECTON DICKINSON) overnight at 37 °C. Pre-cultures of *C. albicans* were incubated for 48 h at 28 °C. *M. smegmatis* pre-cultures were also grown for 48 h but in Brain Heat Infusion broth (BECTON DICKINSON) supplemented with 1% Tween 80 (SIGMA ALDRICH) and at 37 °C (Table 26).

Following incubation, the density of all pre-cultures was adjusted to McFarland 1 and further diluted using Mueller-Hinton II broth. Supplementation of 3.7 g/L sodium bicarbonate resulted in Mueller-Hinton bicarbonate (MHC) screening medium partially used for *E. coli* ATCC 35218. The final cell density was adjusted depending on assay type and test strain (see below).

Table 26: Cultivation conditions for individual test strains.

Test strain	Liquid medium	Incubation	Temperature	
General procedure	Mueller-Hinton II	overnight	37 °C	180 rpm
<i>C. albicans</i>	Mueller-Hinton II	48 h	28 °C	180 rpm
<i>M. smegmatis</i>	Brain Heart Infusion (+ 1% Tween 80)	48 h	37 °C	180 rpm

After incubation (37 °C, 180 rpm, 85% rH) for 18 h or 48 h (*C. albicans* and *M. smegmatis*), cell viability was evaluated by turbidity measurement at 590 nm (LUMIstar® Optima, BMG LABTECH) or BacTiter-Glo™ assay (PROMEGA) according to manufacturer instructions and luminescence read-out (LUMIstar® Optima, BMG LABTECH). The latter case was primarily used for *C. albicans* and *M. smegmatis*.

For validation of the assay, gentamycin served as control antibiotic except for *C. albicans* (nystatin) and *M. smegmatis* (isoniazid). Untreated cell suspension served as negative control (high count) while pure medium was used as positive control (low count). Both were taken into account to calculate the percent growth inhibition from absorption (AU) or luminescence units (LU):

$$\text{Growth inhibition [\%]} = 100 \cdot \left[1 - \frac{\text{AU}_{\text{sample}} - \text{AU}_{\text{low}}}{\text{AU}_{\text{high}} - \text{AU}_{\text{low}}} \right]$$

Varying parameters of the different assay setups are described in the following.

Extract screening. Primary screening of the 100-fold concentrated methanolic crude extract was carried out by placing 0.5 µL, 0.25 µL and 0.125 µL (in duplicate) aliquots in a 384 well microtiter assay plate. The final cell suspension density was diluted to 2×10^4 cells/mL except for *C. albicans* and *M. smegmatis* (1×10^5 cells/mL). 50 µL of seeding cell suspension was added to each well.

UPLC fractionation screening. For the purpose of bioassay-guided dereplication, active crude extracts (or other samples) were fractionated using the maXis II™ UPLC-MS/MS system at standard conditions (see 7.1.3 and 7.1.4). Over a period of 22 min, 159 fractions (~ 8 sec, approx. 90 µL) were collected in a 384-well plate using the attached fraction collector. In most cases, extracts were screened at two different concentrations (injection volumes: 2 µL and 5 µL / 5 µL and 10 µL (2x 5 µL)). An equal volume of the extract was pipetted into F-160 (H-05 / P-05) as positive control. After evaporation of the solvent, the screening was conducted similar to the above-mentioned extract screening using 20 µL of seeding cell suspension per well.

MIC determination. For determination of the minimum inhibitory concentration (MIC), isolated and synthesized test compounds were provided as stock solutions of 6.4 mg/mL, 12.8 mg/mL or 25.6 mg/mL in DMSO. In 96-well assay plates equipped with 100 μ L cell suspension (5×10^5 cells/mL and 1×10^6 cells/mL (*C. albicans* and *M. smegmatis*), respectively), dilution series were prepared using 2 μ L stock solution. The assays were validated using a DMSO negative control as well as three different antibiotic positive controls (64–0.03 μ g/mL). This included rifamycin and tetracycline or tebuconazole and amphotericin B (*C. albicans*) besides the ones previously mentioned. The assays were performed in either duplicates or triplicates (n = 2, 3).

7.1.10 Other Equipment

During isolation and synthesis, large volumes of solvent were removed under reduced pressure using BÜCHI rotary evaporators at 40 °C waterbath temperature equipped with recirculating coolers (Unichiller, HUBER) and employing diaphragm pumps (MD 4C, VACUUBRAND).

An evaporator system (HT-12, GENEVAC) with condenser (VC3000D) and dry scroll pump (nXDS6i, EDWARDS) was used to remove smaller volumes of solvent from plates, vials and tubes.

Frozen cultures and samples were lyophilized using a Beta 2-8 LSCplus or a Delta 2-24 LSCplus (CHRIST) were employed.

7.2 Experimental Procedures

7.2.1 Gram-negative active metabolites from *Aspergillus terreus* ST000934

7.2.1.1 Cultivation and Extraction

The strain *Aspergillus terreus* ST000934 was stored grown on a piece of agar (approx. 0.5 x 0.5 cm) in 1.5 mL 50% glycerine at $-196\text{ }^{\circ}\text{C}$. After defrosting, the content of the cryogenic vial was transferred into a 100 mL Erlenmeyer flask containing 30 mL medium 5189 and incubated on a rotary shaker at 180 rpm and $25\text{ }^{\circ}\text{C}$ for 7 days. The pre-culture was turraxed and homogenized before using 5 mL (1% inoculum) for inoculation of each of the ten 2 L Erlenmeyer flasks with 500 mL medium 5189. After 7 days of incubation on a rotary shaker at 180 rpm and $25\text{ }^{\circ}\text{C}$ the cultivation was stopped by freezing the flasks at $-50\text{ }^{\circ}\text{C}$ and subsequent lyophilization.

The freeze-dried main culture was extracted twice using 80vol% MeOH. Combined MeOH extracts were evaporated to dryness under reduced pressure to give 13.9 g crude extract.

7.2.1.2 Isolation and Purification

Compound 25, 35–37, 39, 41 and 42: The crude extract was dissolved in 300 mL H_2O and 1 M NaOH (20 mL) was added to adjust to pH 9. The aqueous phase was then extracted with ethyl acetate (3 x 300 mL) and combined organic phases were dried under reduced pressure to yield 2.97 g extract. The same extraction after acidifying the aqueous phase (pH 2–3) using 2 M HCl (18 mL) resulted in 3.65 g extract.

The ethyl acetate extract obtained under alkaline conditions was dissolved in MeOH ($c \approx 120\text{ mg/mL}$) and fractionated by preparative RP-HPLC (Synergi™ Fusion-RP 80 Å, 4 μm , 250 x 21.2 mm) using linear gradient elution of 5–55% ACN/ H_2O + 0.1% FA (15 mL/min) over 19 min. Various fractions were separately combined to give the following four samples that were further purified: F-07–F-23 (sample 1, 98.1 mg), F-61–F-64 (sample 2, 34.0 mg), F-76+F-77 (sample 3, 28.3 mg) and F-80–F-84 (sample 4, 44.1 mg).

Final purification was achieved *via* semi-preparative HPLC using a C18 column (NUCLEODUR® Gravity-SB, 3 μm , 250 x 4.6 mm) as stationary phase. Samples were dissolved in MeOH at approx. 50 mg/mL (injection volume: 50 μL). The following gradients were used:

- METHOD A: 5–30% ACN/ H_2O + 0.1% FA over 14 min, 2 mL/min
- METHOD B: 35–65% ACN/ H_2O + 0.1% FA over 15 min, 2 mL/min
- METHOD C: 35–60% ACN/ H_2O + 0.1% FA over 15 min, 2 mL/min

If necessary, an additional step of UPLC fractionation (ACQUITY UPLC® BEH C18, 1.7 μm , 100 x 2.1 mm) was performed with samples dissolved in MeOH or DMSO at approx. 25 mg/mL (injection volume: 5 μL) using one of the following elution methods:

7. Experimental

- METHOD D: 5–95.25% ACN/H₂O + 0.1% FA over 17.45 min, 0.6 mL/min
- METHOD E: 40–95% ACN/H₂O + 0.1% FA over 17.3 min, 0.6 mL/min
- METHOD F: 43–70% ACN/H₂O + 0.1% FA over 17 min, 0.6 mL/min

While sample 1 was fractionated using METHOD A and METHOD D to yield **25** (0.895 mg), sample 2 was fractionated using Method B to afford **39** (2.46 mg) and **37** (8.34 mg). **41** (10.8 mg) was obtained from sample 3 using Method C and sample 4 was further processed using METHOD B to yield **35** (8.85 mg) followed by METHOD E and METHOD F to yield **36** (1.94 mg) and **42** (1.76 mg), respectively.

Compound 38 and 40: Another 2 L culture of ST000934 was fermented identically as described above. The fungal fruit bodies were separated from the rest of the liquid culture by filtration. Both portions were then separately lyophilized and extracted with MeOH as previously described. Dried crude extracts of 1.63 g and 5.21 g were obtained from cells and culture filtrate, respectively. Only latter was further processed.

One aliquot of the methanolic extract (approx. 700 mg) was fractionated by silica column chromatography twice using step elution with 10:1, 5:1, 2:1, 1:1, 1:2, 1:5, 1:10 DCM/MeOH + 0.1% AcOH. After the second round, the combined fractions were dried (25.8 mg) and dissolved in 210 μ L MeOH. Precipitation occurred. The supernatant was removed, the precipitate washed with ice-cold MeOH and dried under reduced pressure. Compound **40** (2.57 mg) was obtained.

A second aliquot of approx. 1.40 g crude extract was dissolved in MeOH and fractionated *via* preparative RP-HPLC (Synergi™ Fusion-RP 80 Å, 4 μ m, 250 x 21.2 mm) using linear gradient elution of 5–95% ACN/H₂O + 0.1% FA (15 mL/min) over 25 min. Combined fractions were subsequently purified by silica column chromatography as described before. Final purification was achieved using METHOD D to yield **38** (0.905 mg).

SF005-B (25): yellow solid; LC-UV (ACN/H₂O) λ_{\max} 208, 273 nm; ¹H and ¹³C-NMR data: n.d.⁷; ESI-MS (positive ions): *m/z* 359.0761 [M–H₂O+H]⁺, *m/z* 377.0867 [M+H]⁺, *m/z* 399.0791 [M+Na]⁺; HRMS (ESI-TOF, +): *m/z* calcd. for C₁₈H₁₇O₉ [M+H]⁺ 377.0867, found 377.0864.

Butyrolactone I (35): colorless solid; LC-UV (ACN/H₂O) λ_{\max} 229, 306 nm; ¹H-NMR (400 MHz, CDCl₃): δ = 7.62 (d, *J* = 8.8 Hz, 2H), 6.91 (d, *J* = 8.9 Hz, 2H), 6.60 (dd, *J* = 8.2, 2.1 Hz, 1H), 6.54 (d, *J* = 8.2 Hz, 1H), 6.52 (d, *J* = 2.0 Hz, 1H), 5.11 (t, *J* = 7.2 Hz, 1H), 3.78 (s, 3H), 3.55 (d, *J* = 14.5 Hz, 1H), 3.49 (d, *J* = 14.5 Hz, 1H), 3.15 (d, *J* = 7.2 Hz, 2H), 1.71 (s, 3H), 1.67 (s, 3H); ¹³C-NMR (101 MHz, CDCl₃): δ = 169.8, 169.1, 156.5, 153.3, 137.2, 134.6, 131.9, 129.6, 129.3, 127.7, 126.4, 124.7, 122.3, 121.5, 116.0, 115.2, 86.0, 53.6, 38.6, 29.3, 25.7, 17.8; ESI-MS (positive ions): *m/z* 425.1593 [M+H]⁺, *m/z* 447.1413 [M+Na]⁺, *m/z* 849.3111 [2M+H]⁺, *m/z* 871.2928 [2M+Na]⁺; HRMS (ESI-TOF, +): *m/z* calcd. for C₂₄H₂₅O₇ [M+H]⁺ 425.1595, found 425.1593.

⁷ Not determined due to inhomogeneity of the NMR sample (as described above).

Butyrolactone VII (36): colorless solid; $[\alpha]_{\text{D}}^{23.9} +37.8$ (c 0.11, MeOH); LC-UV (ACN/H₂O) λ_{max} 223, 308 nm; ¹H-NMR (400 MHz, DMSO-*d*₆): δ = 10.49 (s, 1H), 9.92 (s, 1H), 9.13 (s, 1H), 7.51 (d, J = 9.1 Hz, 2H), 6.87 (d, J = 8.8 Hz, 2H), 6.53 (d, J = 8.2 Hz, 1H), 6.47 (dd, J = 8.2, 2.1 Hz, 1H), 6.38 (d, J = 1.8 Hz, 1H), 5.01 (tt, J = 7.3, 1.3 Hz, 1H), 4.21 (q, J = 7.1 Hz, 2H), 3.38 (d, J = 15.4 Hz, 2H), 2.99 (d, br, J = 7.2 Hz, 2H), 1.62 (s, 3H), 1.53 (s, 3H), 1.14 (t, J = 7.1 Hz, 3H); ¹³C-NMR (101 MHz, DMSO-*d*₆): δ = 169.2, 167.9, 157.8, 153.7, 138.0, 131.1, 130.0, 128.8, 128.4, 127.5, 126.4, 123.2, 122.3, 121.0, 115.6, 114.1, 84.8, 62.3, 38.1, 27.5, 25.5, 17.5, 13.8; ESI-MS (positive ions): m/z 439.1751 [M+H]⁺, m/z 461.1571 [M+Na]⁺, m/z 877.3430 [2M+H]⁺, m/z 899.3250 [2M+Na]⁺; HRMS (ESI-TOF, +): m/z calcd. for C₂₅H₂₇O₇ [M+H]⁺ 439.1751, found 439.1751.

Butyrolactone II (37): colorless solid; $[\alpha]_{\text{D}}^{23.8} +73.2$ (c 0.12, MeOH); LC-UV (ACN/H₂O) λ_{max} 223, 309 nm; ¹H-NMR (400 MHz, DMSO-*d*₆): δ = 10.58 (s, 1H), 9.95 (s, 1H), 9.23 (s, 1H), 7.52 (d, J = 8.8 Hz, 2H), 6.88 (d, J = 8.8 Hz, 2H), 6.59 (d, J = 8.6 Hz, 2H), 6.50 (d, J = 8.6 Hz, 2H), 3.74 (s, 3H), 3.40 (dd, J = 18.8, 14.7 Hz, 2H); ¹³C-NMR (101 MHz, DMSO-*d*₆): δ = 169.7, 167.9, 157.9, 156.3, 138.1, 131.1, 128.8, 127.4, 123.1, 121.0, 115.8, 114.6, 84.7, 53.6, 38.0; ESI-MS (positive ions): m/z 357.0970 [M+H]⁺, m/z 379.0790 [M+Na]⁺, m/z 713.1871 [2M+H]⁺, m/z 735.1685 [2M+Na]⁺; HRMS (ESI-TOF, +): m/z calcd. for C₁₉H₁₇O₇ [M+H]⁺ 357.0969, found 357.0970.

Flavipin (38): yellow solid; LC-UV (ACN/H₂O) λ_{max} 227, 263, 334 nm; ¹H-NMR (400 MHz, DMSO-*d*₆): δ = 10.36 (s, 1H), 10.25 (s, 1H), 2.30 (s, 3H); ¹³C-NMR (101 MHz, DMSO-*d*₆): δ = 194.6, 193.3, 150.3, 150.2, 136.1, 128.1, 122.2, 113.0, 10.5; ESI-MS (positive ions): m/z 197.0445 [M+H]⁺, m/z 179.0339 [M-H₂O+H]⁺; HRMS (ESI-TOF, +): m/z calcd. for C₉H₉O₅ [M+H]⁺ 197.0445, found 197.0445.

Epicoccolide B (39): yellow solid; LC-UV (ACN/H₂O) λ_{max} 243, 308, 364 nm; ¹H-NMR (400 MHz, DMSO-*d*₆): δ = 10.49 (s, 1H), 9.47 (s, 1H), 7.47 (s, 1H), 2.57 (s, 3H), 2.01 (s, 3H); ¹³C-NMR (101 MHz, DMSO-*d*₆): δ = 194.8, 190.2, 151.7, 151.6, 150.2, 142.4, 141.0, 136.7, 132.7, 127.5, 124.9, 122.9, 118.8, 117.1, 112.6, 109.0, 12.7, 11.1; ESI-MS (positive ions): m/z 359.0763 [M+H]⁺, m/z 381.0583 [M+Na]⁺, m/z 341.6580 [M-H₂O+H]⁺; HRMS (ESI-TOF, +): m/z calcd. for C₁₈H₁₅O₈ [M+H]⁺ 359.0761, found 359.0763.

Dibefurin (40): colorless solid; LC-UV (ACN/H₂O) λ_{max} 217, 273 nm; ¹H-NMR (500 MHz, DMSO-*d*₆): δ = 7.20 (s, 2H), 4.63 (d, J = 15.6 Hz, 2H), 4.57 (d, J = 15.6 Hz, 2H), 4.35 (d, J = 9.4 Hz, 2H), 4.23 (d, J = 9.4 Hz, 2H), 1.62 (s, 6H); ¹³C-NMR (126 MHz, DMSO-*d*₆): δ = 195.9, 192.3, 158.0, 128.0, 88.7, 69.9, 65.9, 64.3, 12.3; ESI-MS (positive ions): m/z 361.0919 [M+H]⁺, m/z 382.0740 [M+Na]⁺, m/z 743.1588 [2M+Na]⁺; HRMS (ESI-TOF, +): m/z calcd. for C₁₈H₁₇O₈ [M+H]⁺ 361.0918, found 361.0919.

Ethyl 2,4-dihydroxy-5,6-dimethyl benzoate (41): colorless solid; LC-UV (ACN/H₂O) λ_{max} 231, 262, 304 nm; ¹H-NMR (600 MHz, DMSO-*d*₆): δ = 9.64 (s, 1H), 9.56 (s, 1H), 6.26 (s, 1H), 4.22 (q, J = 7.1 Hz, 2H), 2.10 (s, 3H), 1.94 (s, 3H), 1.26 (t, J = 7.1 Hz, 3H); ¹³C-NMR (151 MHz, DMSO-*d*₆): δ = 169.1, 157.2, 154.4, 135.9, 113.8, 112.2, 99.9, 60.2, 17.1, 14.1, 11.0; ESI-MS (positive ions): m/z 211.0964 [M+H]⁺,

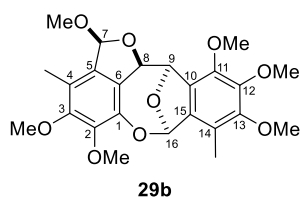
m/z 183.0650 $[M-C_2H_4+H]^+$, m/z 165.0544 $[M-C_2H_4-H_2O+H]^+$; HRMS (ESI-TOF, +): m/z calcd. for $C_{11}H_{15}O_4$ $[M+H]^+$ 211.0965, found 211.0964.

Ethyl 2,4-dihydroxy-3-methoxy-5,6-dimethyl benzoate (42): colorless solid; LC-UV (ACN/H₂O) λ_{max} 217, 268, 306 nm; ¹H and ¹³C-NMR data: Table 5; ESI-MS (positive ions): m/z 241.1072 $[M+H]^+$, m/z 263.0892 $[M+Na]^+$, m/z 503.1893 $[2M+Na]^+$, m/z 195.0653 $[M-C_2H_4-H_2O+H]^+$; HRMS (ESI-TOF, +): m/z calcd. for $C_{12}H_{17}O_5$ $[M+H]^+$ 241.1071, found 241.1072.

7.2.1.3 Methylation of SF005-B

Preparative HPLC was performed as previously reported. Combined fractions were then used for methylation. Therefore, the pre-purified sample of **25** (0.991 g) was dissolved in anhydrous DMF (20 mL). An excess amount of K₂CO₃ (2.99 g) and CH₃I (5.50 mL) was added. After stirring at room temperature for 24 h, saturated aqueous NH₄Cl (15 mL) was added. The mixture was extracted with ethyl acetate (3 x 100 mL) and the combined organic layers were washed with saturated aqueous NaCl (40 mL), dried over MgSO₄, filtered and concentrated under reduced pressure to give 1.02 g crude product. Pre-purification was performed by silica flash column chromatography using a 25 g column (puriFlash® 15 μ m, INTERCHIM) pre-conditioned with *n*-heptane + 1% TEA. The crude product was dissolved in 6 mL DCM and split into two portions that were successively fractionated using gradient elution of 0–100% ethyl acetate in *n*-heptane over 40 min. Fractions were dried under reduced pressure and further purified by analytical HPLC (AGILENT 1200 system) over a C18 column (Synergi™ Fusion-RP 80 Å, 4 μ m, 250 x 21.2 mm) with a linear gradient of 40–80% ACN/H₂O + 5% NH₄HCO₃ buffer (pH 8) over 24 min and a flow rate of 1 mL/min to yield **29a** (0.405 mg) and **29b** (0.555 mg).

2,4,5,9,10,11-hexamethoxy-3,8-dimethyl-2,7,12,12a-tetrahydro-7,12-epoxybenzo[6,7]oxocino[4,3,2-cd]iso-



benzofuran (29b): yellow solid; LC-UV (ACN/H₂O) λ_{max} 218, 277 nm;

¹H-NMR (500 MHz, DMSO-*d*₆): δ = 6.81 (s, 1H, H-16), 6.61 (d, J = 1.5 Hz, 1H, H-7), 5.77 (d, J = 4.0 Hz, 1H, H-9), 5.32 (dd, J = 4.0, 1.5 Hz, 1H, H-8), 3.90 (s, 3H, 11-OCH₃), 3.73 (s, 3H, 2-OCH₃), 3.65 (s, 3H, 3-OCH₃), 3.63 (s, 3H, 13-OCH₃), 3.62 (s, 3H, 12-OCH₃), 3.10 (s, 3H, 7-OCH₃), 2.11 (s, 3H, 14-CH₃), 1.95 (s, 3H, 4-CH₃); ¹³C-NMR⁸ (126 MHz, DMSO-*d*₆): δ = 151.7 (C-13), 151.4 (C-3), 146.2 (C-11), 145.1 (C-12), 143.9 (C-2), 139.8 (C-1), 131.5 (C-15), 130.7 (C-5), 125.6 (C-10), 124.4 (C-6), 120.4 (C-4), 120.1 (C-14), 107.3 (C-7), 102.8 (C-16), 85.3 (C-8), 78.8 (C-9), 60.8 (2-OCH₃), 60.2 (3-OCH₃), 60.2 (12-OCH₃), 60.2 (13-OCH₃), 59.2 (11-OCH₃), 52.2 (7-OCH₃), 11.2 (14-CH₃), 10.4 (4-CH₃); ESI-MS (positive ions): m/z 461.1809 $[M+H]^+$, m/z 483.1628 $[M+Na]^+$, m/z 429.1547 $[M-CH_4O+H]^+$; HRMS (ESI-TOF, +): m/z calcd. for $C_{24}H_{29}O_9$ $[M+H]^+$ 461.1806, found 461.1809.

⁸ The ¹³C chemical shifts were determined based on HSQC and HMBC spectra.

7.2.1.4 MIC Determination

The determination of MIC values was performed in duplicates ($n = 2$) according to GENERAL MATERIALS AND EXPERIMENTAL PROCEDURES (see 7.1.9). All compounds were provided as stock solutions of 25.6 mg/mL in DMSO.

7.2.2 Oxazoline-containing Madurastatins from *Actinomadura* sp. ST100801

7.2.2.1 Cultivation and Extraction

For fermentation, the strain *Actinomadura* sp. ST100801 was re-activated from a piece of agar stored in 1.5 mL 50% glycerine at $-196\text{ }^{\circ}\text{C}$ in a 100 mL Erlenmeyer flask with 30 mL liquid medium 5254. After incubation for 9 days on a rotary shaker at 180 rpm and $28\text{ }^{\circ}\text{C}$, the pre-culture was used to inoculate two 300 mL Erlenmeyer flasks containing 100 mL medium 5254 (5% inoculum). Incubation took place at 180 rpm and $28\text{ }^{\circ}\text{C}$ for 5 days. The pre-culture was then further multiplied by inoculation and incubation of 13 x 300 mL Erlenmeyer flasks with 100 mL medium in the same manner and then used to inoculate (5% inoculum) 40 x 2 L Erlenmeyer flasks containing 500 mL medium 5265. After 5 days at $28\text{ }^{\circ}\text{C}$ and 180 rpm, the cultivation was stopped by cooling to $-50\text{ }^{\circ}\text{C}$ and subsequent lyophilization. The second 20 L batch was fermented equally.

The freeze-dried culture was extracted with 80vol% MeOH. The combined methanolic extracts were concentrated under reduced pressure to yield 196 g crude extract.

7.2.2.2 Isolation and Purification

The crude extract was dissolved in 10 L 10% MeOH to perform SPE a 3 L column (10 x 35 cm) of Amberlite® XAD-16N (MCI system) and step gradient elution of 10%, 20%, 40%, 60%, 80% and 100% MeOH in H₂O. Based on LC-MS analysis, various fractions were combined and evaporated to dryness to give 1.55 g, 1.22 g and 0.623 g.

In the next step, these samples were fractionated successively by SEC using a Sephadex™ LH-20 (SIGMA ALDRICH) column (3 x 80 cm) and methanol as eluent at a flow rate of approx. 0.5 mL/min. Fractions (15 min/fraction) were collected by a SuperFrac fraction collector (PHARMACIA BIOTECH). Compound **6** (1.18 g) was obtained.

Further separately combined Sephadex fractions were purified by semi-preparative HPLC (AGILENT 1100 system) using a C18 column (NUCLEODUR® Gravity-SB, 3 μm , 250 x 10 mm). Samples were dissolved in MeOH at approx. 45 mg/mL (injection volume: 20 μL). A gradient of 5–50% ACN/H₂O + 5% NH₄HCO₃ buffer (pH 8) over 43 min was used at a flow rate of 2 mL/min to yield compound **50** (14.4 mg), **53** (2.15 mg), **54** (1.39 mg), **58** (0.840 mg), **59** (3.91 mg), **60** (8.49 mg), **61** (5.66 mg), **62** (5.19 mg) and **63** (2.27 mg).

An additional purification step was performed using analytical HPLC (AGILENT 1100 system) over a bifunctional RP column (NUCLEODUR® Sphinx RP, 3 μm , 250 x 4.6 mm) with a gradient of 5–25% ACN/H₂O + 5% NH₄HCO₃ buffer (pH 8) over 19 min and a flow rate of 1 mL/min to yield compound **56** (3.65 mg) and **57** (2.76 mg). Alternatively, a C18 column (NUCLEODUR® Gravity-SB, 3 μm , 250 x 4.6 mm) was used under the same conditions to give compound **55** (1.31 mg).

(+)-*Madurastatin C1 (48a)*: light yellow oil; $[\alpha]_{\text{D}}^{21.7} +7.0$ (*c* 1.73, MeOH); LC-UV (ACN/H₂O) λ_{max} 206, 248, 305 nm; ¹H and ¹³C-NMR: Table 11; ESI-MS (positive ions): *m/z* 296.6406 [M+2H]²⁺, *m/z* 592.2729 [M+H]⁺; HRMS (ESI-TOF, +): *m/z* calcd. for C₂₆H₃₈N₇O₉ [M+H]⁺ 592.2726, found 592.2729.

Madurastatin B1 (50): light yellow oil; $[\alpha]_{\text{D}}^{21.2} -19.5$ (*c* 0.15, DMSO); LC-UV (ACN/H₂O) λ_{max} 210, 255, 323 nm; ¹H and ¹³C-NMR: Table 7; ESI-MS (positive ions): *m/z* 208.0604 [M+H]⁺; HRMS (ESI-TOF, +): *m/z* calcd. for C₁₀H₁₀NO₄ [M+H]⁺ 208.0604, found 208.0604.

Madurastatin D1 (ent-53a): light yellow oil; $[\alpha]_{\text{D}}^{20.9} -5.8$ (*c* 0.17, DMSO); LC-UV (ACN/H₂O) λ_{max} 208, 249, 305 nm; ¹H-NMR (500 MHz, DMSO-*d*₆) δ = 8.50 (dd, *J* = 6.2, 5.7, 1H), 7.93 (t, *J* = 5.3, 1H), 7.64 (dd, *J* = 7.9, 1.6, 1H), 7.47 (ddd, *J* = 8.3, 7.3, 1.6, 1H), 7.01 (br d, *J* = 8.3, 1H), 6.95 (ddd, *J* = 7.9, 7.3, 0.7, 1H), 5.02 (dd, *J* = 10.4, 7.7, 1H), 4.65 (dd, *J* = 10.4, 8.5, 1H), 4.52 (dd, *J* = 8.5, 7.7, 1H), 4.29–4.25 (m, 1H), 4.01 (q, *J* = 5.6, 1H), 3.75 (dd, *J* = 16.5, 6.2, 1H), 3.66 (dd, *J* = 16.5, 5.7, 1H), 3.57–3.51 (m, 1H), 3.48–3.44 (m, 2H), 3.47–3.41 (m, 1H), 3.27–3.23 (m, 2H), 2.89–2.86 (m, 1H), 2.55–2.49 (m, 2H), 2.30 (s, 3H), 2.00–1.95 (m, 2H), 1.91–1.85 (m, 2H), 1.72–1.67 (m, 1H), 1.54–1.47 (m, 2H), 1.46–1.41 (m, 1H), 1.21 (d, *J* = 5.6, 3H); ¹³C-NMR (126 MHz, DMSO-*d*₆) δ = 171.6, 170.7, 170.1, 168.3, 165.8, 162.4, 159.0, 134.0, 128.0, 119.1, 116.6, 109.9, 74.6, 69.4, 67.4, 64.8, 51.7, 51.0, 47.3, 42.1, 37.8, 34.6, 31.9, 26.6, 26.6, 21.6, 20.8, 19.6; ESI-MS (positive ions): *m/z* 309.6482 [M+2H]²⁺, *m/z* 618.2884 [M+H]⁺; HRMS (ESI-TOF, +): *m/z* calcd. for C₂₈H₄₀N₇O₉ [M+H]⁺ 618.2882, found 618.2884.

Madurastatin D2 (ent-54a): light yellow oil; $[\alpha]_{\text{D}}^{20.9} -39.7$ (*c* 0.15, DMSO); LC-UV (ACN/H₂O) λ_{max} 209, 249, 305 nm; ¹H-NMR (600 MHz, DMSO-*d*₆) δ = 8.49 (t, *J* = 5.7, 1H), 7.91 (t, *J* = 5.4, 1H), 7.65 (dd, *J* = 7.7, 1.7, 1H), 7.47 (ddd, *J* = 8.2, 7.4, 1.8, 1H), 7.00 (dd, *J* = 8.5, 0.9, 1H), 6.95 (ddd, *J* = 7.9, 7.3, 1.0, 1H), 5.01 (dd, *J* = 10.4, 7.7, 1H), 4.65 (dd, *J* = 10.4, 8.4, 1H), 4.52 (t, *J* = 8.1, 1H), 3.90 (q, *J* = 5.8, 1H), 3.75 (dd, *J* = 16.5, 6.1, 1H), 3.67 (dd, *J* = 16.5, 5.7, 1H), 3.54–3.41 (m, 4H), 3.26 (dd, *J* = 12.9, 6.8, 2H), 2.96 (t, *J* = 2.8, 1H), 2.55–2.51 (m, 2H), 2.43–2.35 (m, 1H), 2.24 (s, 3H), 2.00–1.87 (m, 3H), 1.75–1.67 (m, 2H), 1.47–1.36 (m, 2H), 1.29 (s, 3H), 1.12 (s, 3H); ¹³C-NMR (151 MHz, DMSO-*d*₆) δ = 170.1, 169.9, 168.3, 165.8, 163.2, 159.0, 134.0, 128.0, 119.0, 116.6, 109.9, 77.8, 69.4, 67.4, 61.9, 51.8, 51.0, 47.5, 42.1, 34.6, 32.4, 31.9, 25.7, 25.5, 25.0, 21.3, 20.9, 19.8; ESI-MS (positive ions): *m/z* 316.6558 [M+2H]²⁺, *m/z* 632.3037 [M+H]⁺; HRMS (ESI-TOF, +): *m/z* calcd. for C₂₉H₄₂N₇O₉ [M+H]⁺ 632.3039, found 632.3037.

Madurastatin B4 (55): colorless solid; LC-UV (ACN/H₂O) λ_{max} 210, 261, 307 nm; ¹H and ¹³C-NMR: Table 7; ESI-MS (positive ions): *m/z* 206.0448 [M+H]⁺; HRMS (ESI-TOF, +): *m/z* calcd. for C₁₀H₈NO₄ [M+H]⁺ 206.0448, found 206.0448.

Madurastatin E1 (56): light yellow oil; $[\alpha]_{\text{D}}^{23.6} -20.7$ (*c* 0.19, MeOH); LC-UV (ACN/H₂O) λ_{max} 207, 250, 306 nm; ¹H and ¹³C-NMR, see Table 8; ESI-MS (positive ions): *m/z* 265.0818 [M+H]⁺; HRMS (ESI-TOF, +): *m/z* calcd. for C₁₂H₁₃N₂O₅ [M+H]⁺ 265.0819, found 265.0818.

Madurastatin F1 (57): light yellow oil; $[\alpha]_{\text{D}}^{23.6} -82.1$ (c 0.12, MeOH); LC-UV (ACN/H₂O) λ_{max} 206, 250, 306 nm; ¹H and ¹³C-NMR: Table 9; ESI-MS (positive ions): m/z 336.1190 [M+H]⁺, m/z 671.2304 [2M+H]⁺, m/z 693.2123 [2M+Na]⁺; HRMS (ESI-TOF, +): m/z calcd. for C₁₅H₁₈N₃O₆ [M+H]⁺ 336.1190, found 336.1190.

Madurastatin E2 (58): light yellow oil; $[\alpha]_{\text{D}}^{23.8} -129.0$ (c 0.02, MeOH); LC-UV (ACN/H₂O) λ_{max} 209, 250, 307 nm; ¹H and ¹³C-NMR: Table 9; ESI-MS (positive ions): m/z 304.2884 [M+H]⁺, m/z 629.2329 [2M+Na]⁺; HRMS (ESI-TOF, +): m/z calcd. for C₁₅H₁₈N₃O₄ [M+H]⁺ 304.1292, found 304.1292.

Madurastatin G1 (59): light yellow oil; $[\alpha]_{\text{D}}^{23.5} -8.7$ (c 0.23, MeOH); LC-UV (ACN/H₂O) λ_{max} 206, 250, 306 nm; ¹H and ¹³C-NMR: Table 10; ESI-MS (positive ions): m/z 233.6005 [M+2H]²⁺, m/z 466.1932 [M+H]⁺; HRMS (ESI-TOF, +): m/z calcd. for C₂₀H₂₈N₅O₈ [M+H]⁺ 466.1932, found 466.1932.

Madurastatin G2 (60): light yellow oil; $[\alpha]_{\text{D}}^{23.9} -18.7$ (c 0.11, MeOH); LC-UV (ACN/H₂O) λ_{max} 206, 250, 307 nm; ¹H and ¹³C-NMR: Table 10; ESI-MS (positive ions): m/z 240.6083 [M+2H]²⁺, m/z 480.2089 [M+H]⁺; HRMS (ESI-TOF, +): m/z calcd. for C₂₁H₃₀N₅O₈ [M+H]⁺ 480.2089, found 480.2089.

Madurastatin C2 (61): light yellow oil; $[\alpha]_{\text{D}}^{23.8} -27.4$ (c 0.29, MeOH); LC-UV (ACN/H₂O) λ_{max} 205, 249, 306 nm; ¹H and ¹³C-NMR: Table 11; ESI-MS (positive ions): m/z 310.6373 [M+2H]²⁺, m/z 620.2667 [M+H]⁺; HRMS (ESI-TOF, +): m/z calcd. for C₂₇H₃₈N₇O₁₀ [M+H]⁺ 620.2675, found 620.2667.

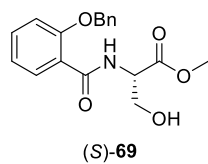
Madurastatin D3 (62): light yellow oil; $[\alpha]_{\text{D}}^{26.5} +21.5$ (c 0.47, MeOH); LC-UV (ACN/H₂O) λ_{max} 206, 249, 305 nm; ¹H and ¹³C-NMR: Table 12; ESI-MS (positive ions): m/z 302.6402 [M+2H]²⁺, m/z 604.2724 [M+H]⁺; HRMS (ESI-TOF, +): m/z calcd. for C₂₇H₃₈N₇O₉ [M+H]⁺ 604.2726, found 604.2724.

Madurastatin D4 (63): light yellow oil; $[\alpha]_{\text{D}}^{23.8} -47.1$ (c 0.11, MeOH); LC-UV (ACN/H₂O) λ_{max} 206, 247, 306 nm; ¹H and ¹³C-NMR: Table 12; ESI-MS (positive ions): m/z 338.6509 [M+2H]²⁺, m/z 676.2937 [M+H]⁺; HRMS (ESI-TOF, +): m/z calcd. for C₃₀H₄₂N₇O₁₁ [M+H]⁺ 676.2937, found 676.2937.

7.2.2.3 Advanced Marfey's Analysis

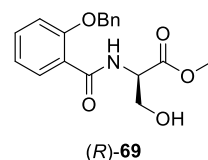
Advanced Marfey's Analysis was performed according to GENERAL MATERIALS AND EXPERIMENTAL PROCEDURES (see 7.1.7). Commercially purchased enantiopure L- and D-serine, L- and D-ornithine monohydrochloride as well as N α -methyl-L-ornithine monohydrochloride (SIGMA ALDRICH) served as references.

7.2.2.4 Stereoselective Synthesis of Madurastatin B1 and Derivatives

Methyl (2*S*)-2-[(2-benzyloxybenzoyl)amino]-3-hydroxy-propanoate ((*S*)-69)

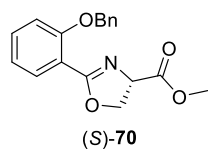
The synthesis of (*S*)-69 was performed according to a literature known procedure.^[110] L-Serine methyl ester hydrochloride ((*S*)-68) (0.505 g, 3.24 mmol, 1.00 eq.) was suspended in anhydrous DCM (5 mL). NEt₃ (1.10 mL, 8.11 mmol, 2.50 eq.) was added and the mixture was allowed to stir at room temperature for 5 min. The resulting mixture was added to a stirring solution of 2-(benzyloxy) benzoyl chloride (67) (0.923 g, 3.73 mmol, 1.15 eq.) in anhydrous DCM (5 mL) at -78 °C. The reaction solution was stirred for 3 h without cooling and then quenched with aqueous 1 M HCl (30 mL). The mixture was extracted with ethyl acetate (100 mL) and the organic layer was washed with saturated aqueous NaHCO₃ (30 mL) and saturated aqueous NaCl (30 mL), dried over MgSO₄, filtered and concentrated under reduced pressure to yield (*S*)-69 (1.07 g, 3.24 mmol, quant.) as slightly yellow solid which was used in the next stage without further purification.

R_f (*n*-heptane/ethyl acetate 4:1): 0.20; **¹H-NMR** (400 MHz, CDCl₃): δ = 8.76 (d, *J* = 7.1 Hz, 1H), 8.20 (dd, *J* = 7.8, 1.8 Hz, 1H), 7.53–7.34 (m, 6H), 7.14–7.04 (m, 2H), 5.26 (d, *J* = 11.1 Hz, 1H), 5.22 (d, *J* = 11.1 Hz, 1H), 4.85 (dt, *J* = 7.2, 3.9 Hz, 2H), 3.95–3.85 (m, 2H), 3.70 (s, 3H), 1.76 (s, br, 1H); **¹³C-NMR** (101 MHz, CDCl₃): δ = 171.0, 165.7, 157.2, 135.7, 133.4, 132.6, 129.0, 128.8, 128.3, 121.7, 121.4, 113.0, 71.6, 63.9, 55.4, 52.7; **HRMS** (ESI-TOF, +) *m/z* calcd. for C₁₈H₂₀NO₅ [M+H]⁺ 330.1336, found 330.1336.

Methyl (2*R*)-2-[(2-benzyloxybenzoyl)amino]-3-hydroxy-propanoate ((*R*)-69)

(*R*)-69 (2.03 g, 6.15 mmol, 95%) was synthesized in analogous manner starting from D-serine methyl ester hydrochloride ((*R*)-68) (1.00 g, 6.44 mmol). The NMR data are identical to the ones reported for (*S*)-69.

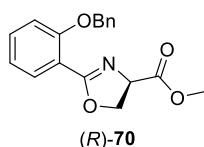
R_f (*n*-heptane/ethyl acetate 1:1): 0.20; **HRMS** (ESI-TOF, +) *m/z* calcd. for C₁₈H₂₀NO₅ [M+H]⁺ 330.1336, found 330.1338.

Methyl (4*S*)-2-(2-benzyloxyphenyl)-4,5-dihydrooxazole-4-carboxylate ((*S*)-70)

The synthesis of (*S*)-70 was performed according to a literature known procedure.^[110] The reaction was carried out under argon atmosphere. To a solution of alcohol (*S*)-69 (0.577 g, 1.75 mmol, 1.00 eq.) in anhydrous DCM (14 mL), DAST (0.301 mL, 2.28 mmol, 1.30 eq.) was added at -78 °C. After stirring for 2.5 h at -78 °C, K₂CO₃ (0.605 g, 4.38 mmol, 2.50 eq.) was added and the reaction mixture was allowed to stir for 1 h without cooling. Saturated aqueous NaHCO₃ (30 mL) was added. The mixture was extracted with ethyl acetate (2 x 100 mL) and the combined organic layers were washed with saturated aqueous NaCl (50 mL), dried over MgSO₄, filtered and concentrated under reduced pressure. The crude product was purified by flash column chromatography (0–70% ethyl acetate in *n*-heptane) to give (*S*)-70 (0.490 g, 1.57 mmol, 90%) as a colorless solid.

R_f (*n*-heptane/ethyl acetate 1:1): 0.35; $[\alpha]_{\text{D}}^{24.8} +50.4$ (*c* 0.81, CHCl₃); **¹H-NMR** (400 MHz, CDCl₃): $\delta = 7.81$ (dd, *J* = 7.7, 1.8 Hz, 1H), 7.53–7.47 (m, 2H), 7.44–7.34 (m, 3H), 7.33–7.27 (m, 1H), 7.03–6.95 (m, 2H), 5.19 (s, 2H), 4.98 (dd, *J* = 10.7, 8.1 Hz, 1H), 4.67 (t, *J* = 8.4 Hz, 1H), 4.58 (dd, *J* = 10.7, 8.7 Hz, 1H), 3.81 (s, 3H); **¹³C-NMR** (101 MHz, CDCl₃): $\delta = 171.9, 165.8, 157.8, 137.0, 132.8, 131.8, 128.6, 127.8, 126.9, 120.9, 117.4, 113.9, 70.8, 69.4, 68.8, 52.8$; **HRMS** (ESI-TOF, +) *m/z* calcd. for C₁₈H₁₈NO₄ [M+H]⁺ 312.1230, found 312.1230.

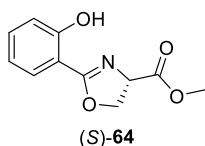
Methyl (4*R*)-2-(2-benzyloxyphenyl)-4,5-dihydrooxazole-4-carboxylate ((*R*)-70)



(*R*)-70 (1.78 g, 5.72 mmol, 77%) was synthesized in analogous manner starting from (*R*)-69 (2.44 g, 7.41 mmol). The NMR data are identical to the ones reported for (*S*)-70.

R_f (*n*-heptane/ethyl acetate 1:1): 0.35; $[\alpha]_{\text{D}}^{24.8} -50.1$ (*c* 0.73, CHCl₃); **HRMS** (ESI-TOF, +) *m/z* calcd. for C₁₈H₁₈NO₄ [M+H]⁺ 312.1230, found 312.1228.

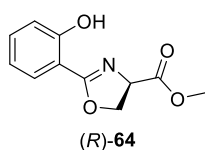
Methyl (4*S*)-2-(2-hydroxyphenyl)-4,5-dihydrooxazole-4-carboxylate ((*S*)-64)



Cleavage of the benzyl ether was carried out under argon atmosphere. To a solution of (*S*)-70 (0.207 g, 0.665 mmol, 1.00 eq.) in MeOH (8 mL) was added Pd-C (10%, 0.0410 mg, 0.04 mmol, 0.06 eq.) and formic acid (0.250 mL, 6.63 mmol, 10.00 eq.). The resulting mixture was stirred at 100 °C for 1.5 h⁹ and the conversion was monitored by TLC. After filtration over a frit with Celite® (4 x 6 cm), which was flushed with ethanol (500 mL), the solvent was removed *in vacuo*. The crude product was purified by flash column chromatography (0–70% ethyl acetate in *n*-heptane) to give alcohol (*S*)-64 (0.101 g, 0.467 mmol, 69%) as colorless oil.

R_f (*n*-heptane/ethyl acetate 1:1): 0.57; $[\alpha]_{\text{D}}^{24.8} +27.9$ (*c* 0.44, CHCl₃); **¹H-NMR** (400 MHz, CDCl₃): $\delta = 11.67$ (s, br, 1H), 7.66 (dd, *J* = 7.9, 1.7 Hz, 1H), 7.40 (ddd, *J* = 8.4, 7.3, 1.7 Hz, 1H), 7.02 (dd, *J* = 8.4, 0.8 Hz, 1H), 6.88 (ddd, *J* = 7.9, 7.3, 1.0 Hz, 1H), 4.99 (dd, *J* = 10.5, 7.5 Hz, 1H), 4.69 (dd, *J* = 8.8, 7.5 Hz, 1H), 4.59 (dd, *J* = 10.5, 8.8 Hz, 1H), 3.81 (s, 3H); **¹³C-NMR** (101 MHz, CDCl₃): $\delta = 171.1, 167.7, 160.1, 134.2, 128.5, 119.0, 117.1, 110.2, 69.1, 67.4, 53.0$; **HRMS** (ESI-TOF, +) *m/z* calcd. for C₁₁H₁₂NO₄ [M+H]⁺ 222.0761, found 222.0760; **chiral HPLC** (Chiralpak IA; hexane:isopropyl alcohol 96:4): (*S*)-64 (*t_R* = 7.8 min) : (*R*)-64 (*t_R* = 7.0 min) 98.9 : 1.1 (98% *ee*).

Methyl (4*R*)-2-(2-hydroxyphenyl)-4,5-dihydrooxazole-4-carboxylate ((*R*)-64)

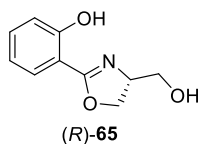


(*R*)-64 (0.916 g, 4.14 mmol, 73%) was synthesized in analogous manner starting from (*R*)-70 (1.76 g, 5.64 mmol). The NMR data are identical to the ones reported for (*S*)-64.

⁹ Longer reaction time at lower temperature (e.g. 60 °C for 10 h) lead to ring opening of the oxazoline.

R_f (*n*-heptane/ethyl acetate 1:1): 0.57; $[\alpha]_{\text{D}}^{24.8} -38.8$ (*c* 0.46, CHCl₃); **HRMS** (ESI-TOF, +) *m/z* calcd. for C₁₁H₁₂NO₄ [M+H]⁺, 222.0761, found: 222.0760 (M+H)⁺; **chiral HPLC** (Chiralpak IA; hexane:isopropyl alcohol 96:4): (*R*)-**64** (*t_R* = 7.0 min) : (*S*)-**64** (*t_R* = 7.8 min) 97.7 : 2.3 (95% *ee*).

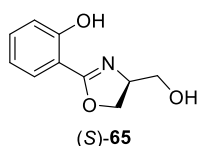
2-[(4*R*)-4-(hydroxymethyl)-4,5-dihydrooxazol-2-yl]phenol ((*R*)-**65**)



The synthesis of (*R*)-**65** was performed according to a literature known procedure in a slightly modified manner.^[236] Under inert atmosphere, DIBAL-H in toluene (1.20 M, 1.70 mL, 2.02 mmol, 3.00 eq.) was added slowly to ester (*S*)-**64** (0.149 g, 0.674 mmol, 1.00 eq.) in anhydrous THF (5 mL) at 0 °C, and the resulting mixture was allowed to warm to room temperature. After 1 h reaction time, the solution was cooled to 0 °C and ethyl acetate (10 mL) followed by saturated aqueous Rochelle's salt solution (15 mL) were added carefully. The resulting suspension was left to warm to room temperature and stirred vigorously overnight. The organic layer was separated and the aqueous layer was extracted with ethyl acetate (3 x 50 mL). The combined organic layers were washed with saturated aqueous NaCl (50 mL), dried over MgSO₄, filtered and concentrated under reduced pressure. The crude product was purified by flash column chromatography (0–100% ethyl acetate in *n*-heptane) to give alcohol (*R*)-**65** (0.104 g, 0.538 mmol, 80%) as colorless solid.

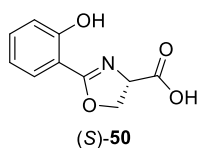
R_f (*n*-heptane/ethyl acetate 1:3): 0.52; $[\alpha]_{\text{D}}^{24.8} +24.3$ (*c* 0.53, CHCl₃); **¹H-NMR** (400 MHz, CDCl₃): δ = 11.88 (s, br, 1H), 7.66 (dd, *J* = 7.8, 1.7 Hz, 1H), 7.39 (ddd, *J* = 8.4, 7.3, 1.7 Hz, 1H), 7.01 (dd, *J* = 8.4, 0.8 Hz, 1H), 6.88 (ddd, *J* = 7.8, 7.3, 1.0 Hz, 1H), 4.57–4.45 (m, 2H), 4.42–4.30 (m, 1H), 3.90 (m, 1H), 3.71 (m, 1H), 1.74 (s, br, 1H); **¹³C-NMR** (101 MHz, CDCl₃): δ = 167.1, 160.0, 133.8, 128.4, 118.9, 116.9, 110.5, 68.7, 67.0, 64.1; **HRMS** (ESI-TOF, +) *m/z* calcd. for C₁₀H₁₂NO₃ [M+H]⁺ 194.0812, found 194.0812; **chiral HPLC** (Chiralpak IA; hexane:isopropyl alcohol 90:10): (*R*)-**65** (*t_R* = 13.4 min) : (*S*)-**65** (*t_R* = 10.1 min) 99.1 : 0.9 (98% *ee*).

2-[(4*S*)-4-(hydroxymethyl)-4,5-dihydrooxazol-2-yl]phenol ((*S*)-**65**)



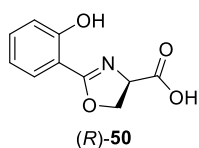
(*S*)-**65** (0.117 g, 0.606 mmol, 88%) was synthesized in analogous manner starting from (*R*)-**64** (0.151 g, 0.683 mmol). The NMR data are identical to the ones reported for (*R*)-**65**.

R_f (*n*-heptane/ethyl acetate 1:3): 0.52; $[\alpha]_{\text{D}}^{24.8} -23.7$ (*c* 0.45, CHCl₃); **HRMS** (ESI-TOF, +) *m/z* calcd. for C₁₀H₁₂NO₃ [M+H]⁺ 194.0812, found 194.0812; **chiral HPLC** (Chiralpak IA; hexane:isopropyl alcohol 90:10): (*S*)-**65** (*t_R* = 10.0 min) : (*R*)-**65** (*t_R* = 14.5 min) 98.6 : 1.4 (97% *ee*).

(4S)-2-(2-hydroxyphenyl)-4,5-dihydrooxazole-4-carboxylic acid ((S)-50)

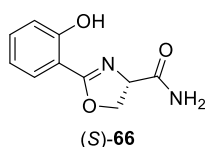
To a solution of (S)-64 (0.401 g, 1.81 mmol, 1.00 eq.) in THF/H₂O (3:1, 21 mL/7 mL) was added LiOH · H₂O (0.381 g, 9.07 mmol, 5.00 eq.). After stirring at room temperature for 3.5 h, TLC and LC-MS showed a full conversion of the starting material. The reaction mixture was acidified with aqueous 1 M HCl (pH 3, 10 mL) and extracted with ethyl acetate (3 x 50 mL). The combined organic layers were washed with saturated aqueous NaCl/saturated aqueous NaHCO₃ (40 mL/5 mL), dried over MgSO₄, filtered and concentrated under reduced pressure to yield (S)-50 (0.346 g, 1.67 mmol, 92%) as colorless solid which was sufficiently pure to be used in the next step without further purification. For analytical purposes, a small amount was purified by flash column chromatography (0–100% ethyl acetate in *n*-heptane).¹⁰

$[\alpha]_{\text{D}}^{23.0} +72.8$ (*c* 0.09, DMSO); ¹H-NMR (400 MHz, DMSO-*d*₆): δ = 13.12 (s, br, 1H), 11.98 (s, br, 1H), 7.64 (dd, *J* = 7.8, 1.7 Hz, 1H), 7.47 (ddd, *J* = 8.4, 7.3, 1.7 Hz, 1H), 7.01 (dd, *J* = 8.4, 0.7 Hz, 1H), 6.95 (td, *J* = 7.7, 0.9 Hz, 1H), 5.03 (dd, *J* = 10.2, 7.5 Hz, 1H), 4.71–4.58 (m, 2H); ¹³C-NMR (101 MHz, DMSO-*d*₆): δ = 171.7, 166.2, 159.1, 134.2, 128.0, 119.1, 116.6, 109.7, 69.3, 66.7; HRMS (ESI-TOF, +) *m/z* calcd. for C₁₀H₁₀NO₄ [M+H]⁺ 208.0604, found 208.0606; chiral HPLC *ee* ≥ 95%¹¹.

(4R)-2-(2-hydroxyphenyl)-4,5-dihydrooxazole-4-carboxylic acid ((R)-50)

(R)-50 (0.265 g, 1.28 mmol, quant.) was synthesized in analogous manner starting from (R)-64 (0.283 g, 1.28 mmol). For analytical purposes, a small amount was purified by flash column chromatography (0–100% ethyl acetate in *n*-heptane).¹⁰ The NMR data are identical to the ones reported for (S)-50.

$[\alpha]_{\text{D}}^{24.8} -48.0$ (*c* 0.40, DMSO); HRMS (ESI-TOF, +) *m/z* calcd. for C₁₀H₁₀NO₄ [M+H]⁺ 208.0604, found 208.0605; chiral HPLC *ee* ≥ 92%¹¹.

(4S)-2-(2-hydroxyphenyl)-4,5-dihydrooxazole-4-carboxamide ((S)-66)

To a solution of acid (S)-50 (0.122 g, 0.589 mmol, 1.00 eq.) in DMF (2.2 mL), Oxyma (0.126 g, 0.887 mmol, 1.50 eq.), EDC · HCl (0.170 g, 0.887 mmol, 1.50 eq.), NaHCO₃ (0.496 g, 5.90 mmol, 10.00 eq.) and NH₄Cl (0.315 g, 5.90 mmol, 10.00 eq.) were added at 0 °C. The reaction mixture was allowed to warm to room temperature and stirred for 2.5 h. The conversion was monitored by LC-MS. Saturated aqueous NaHCO₃ (30 mL) and ethyl acetate (100 mL) were added as well as water (40 mL). After separation of the layers, the aqueous layer was extracted with a second portion of ethyl acetate (50 mL). The combined organic layers were washed with aqueous citric acid (10%, 50 mL) and saturated aqueous NaCl (50 mL), dried

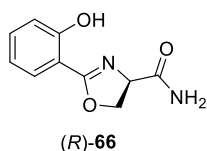
¹⁰ Purification by flash column chromatography was associated with high loss of material and is therefore not recommended to be applied to preparative scale; instead conditions used for isolation are suggested.

¹¹ The *ee*-determination of acid (S)-50 and (R)-50 was not possible due to broad signals during analytical chiral chromatography. The *ee* was determined for the corresponding amides (S)-66 and (R)-66 and led to an *ee* estimation of their educts (S)-50 and (R)-50.

over MgSO_4 , filtered and concentrated under reduced pressure. The crude product was purified by flash column chromatography (0–100% ethyl acetate in *n*-heptane) to give amide (*S*)-**66** (70.5 mg, 0.342 mmol, 58%) as colorless solid.

$[\alpha]_{\text{D}}^{24.8} -73.7$ (*c* 0.95, CHCl_3), $[\alpha]_{\text{D}}^{24.8} +34.4$ (*c* 1.08, MeOH/DMSO 85:15); **$^1\text{H-NMR}$** (400 MHz, CDCl_3): $\delta = 11.40$ (s, br, 1H, 7.69 (dd, $J = 7.9, 1.6$ Hz, 1H), 7.43 (ddd, $J = 8.4, 7.3, 1.7$ Hz, 1H), 7.02 (dd, $J = 8.4, 0.7$ Hz, 1H), 6.91 (td, $J = 7.6, 0.9$ Hz, 1H), 6.38 (s, br, 1H), 5.80 (s, br, 1H), 4.94 (dd, $J = 10.0, 8.9$ Hz, 1H), 4.69 (s, 1H), 4.67 (d, $J = 0.8$ Hz, 2H); **$^{13}\text{C-NMR}$** (101 MHz, CDCl_3): $\delta = 173.3, 168.1, 159.8, 134.5, 128.7, 119.4, 117.1, 110.1, 69.7, 67.9$; **HRMS** (ESI-TOF, +) *m/z* calcd. for $\text{C}_{10}\text{H}_{11}\text{N}_2\text{O}_3$ $[\text{M}+\text{H}]^+$ 207.0764, found 207.0764; **chiral HPLC** (Chiralpak IA; hexane:isopropyl alcohol 85:15): (*S*)-**66** ($t_{\text{R}} = 13.0$ min) : (*R*)-**66** ($t_{\text{R}} = 8.7$ min) 97.3 : 2.7 (95% *ee*).

(4*R*)-2-(2-hydroxyphenyl)-4,5-dihydrooxazole-4-carboxamide ((*R*)-**66**)



(*R*)-**66** (66.7 mg, 0.324 mmol, 66%) was synthesized in analogous manner starting from (*R*)-**50** (0.101 g, 0.488 mmol). The NMR data are identical to the ones reported for (*S*)-**66**.

$[\alpha]_{\text{D}}^{24.8} +60.7$ (*c* 1.10, CHCl_3), $[\alpha]_{\text{D}}^{24.8} -28.5$ (*c* 1.09, MeOH/DMSO 85:15); **HRMS** (ESI-TOF, +) *m/z* calcd. for $\text{C}_{10}\text{H}_{11}\text{N}_2\text{O}_3$ $[\text{M}+\text{H}]^+$ 207.0764, found 207.0763; **chiral HPLC** (Chiralpak IA; hexane:isopropyl alcohol 85:15): (*R*)-**66** ($t_{\text{R}} = 8.7$ min) : (*S*)-**66** ($t_{\text{R}} = 13.3$ min) 96.0 : 4.0 (92% *ee*).

7.2.2.5 MIC Determination

The determination of MIC values was performed in triplicates ($n = 3$) according to GENERAL MATERIALS AND EXPERIMENTAL PROCEDURES (see 7.1.9). All compounds were provided as stock solutions of 12.8 mg/mL in DMSO.

7.2.3 Amino- and Phospholipids from *Olivibacter* sp. FHG000416

7.2.3.1 Cultivation and Extraction

All fermentations of FHG000416 started by inoculation of 30 mL pre-culture medium R2A in a 100 mL Erlenmeyer flask from an agar plate which was then in turn used for scaling up the pre-culture volume by inoculation of 100 mL pre-culture medium in 300 mL Erlenmeyer flasks using 5% inoculum. In both cases incubation was done on a rotary shaker at 180 rpm and 28 °C for 5 days. All main cultures were fermented in 2 L Erlenmeyer flask filled with 500 mL medium (5065 or 5294) inoculated with 5% pre-culture and incubated at 180 rpm and 28 °C for 7 days. Cultivation was stopped by freezing to -50 °C followed by lyophilization.

The freeze-dried cultures were extracted using either 80 vol% MeOH or MTBE/H₂O/MeOH 5.5:2.5:1. The crude extracts were obtained by concentrating the combined organic layers under reduced pressure.

7.2.3.2 Isolation and Purification

Compound 70: The 7 L fermentation of FHG000416 in medium 5065 yielded 14.4 g methanolic crude extract which was dissolved in 1 L 10% MeOH to be fractionated by SPE using a glass column filled with 500 mL (4 x 40 cm) Amberlite® XAD-16N and step gradient elution of 10%, 30%, 50%, 80% and 100% MeOH in H₂O. Based on HRMS analysis, fractions which eluted at 10% and 30% MeOH as well as 80% and 100% MeOH were combined and evaporated to dryness to give 4.75 g and 0.343 g, respectively.

In the first case, fractionation by preparative HPLC (Synergi™ Fusion-RP 80 Å, 4 µm, 250 x 21.2 mm) was performed using linear gradient elution of 60–95% ACN/H₂O + 0.1% FA (15 mL/min) over 20 min to yield 25.71 mg. Further purification was achieved by semi-preparative HPLC (AGILENT 1100 system) using a C18 column (NUCLEODUR® Gravity-SB, 3 µm, 250 x 10 mm) and a linear gradient of 50–95% ACN/H₂O + 0.1% FA over 22 min at a flow rate of 2 mL/min to yield 0.880 mg. This was equally performed for the other combined XAD fractions and gave 2.54 mg.

Final purification included fractionation *via* analytical HPLC (AGILENT 1200 system, method A) and/or UPLC (micrOTOF, method B) under the following conditions and yielded 1.58 mg FE003 (**70**) overall.

- METHOD A: c ≈ 10 mg/mL in MeOH, 10 µL injection volume; Synergi™ Fusion-RP 80 Å, 4 µm, 250 x 21.2 mm; 60–95% ACN/H₂O + 0.1% FA over 25 min, 1 mL/min
- METHOD B: c ≈ 10 mg/mL in MeOH, 5 µL injection volume; ACQUITY UPLC® BEH C18, 1.7 µm, 100 x 2.1 mm; 60% ACN/H₂O + 0.1% FA over 18.30 min, 0.6 mL/min

Compound 71: The 20 L fermentation of FHG000416 in medium 5294 gave 189 g methanolic crude extract. Dissolved in 4 L H₂O it was in portions extracted with ethyl acetate (2 x 100 vol%). Both

phases were fractionated using Amberlite® XAD-16N as absorbent resin. Therefore, the combined aqueous layers were diluted to 5 L 10% MeOH and applied onto a 1.5 L column (6 x 50 cm, MCI system) and eluted using a step gradient (10%, 50%, 100%) of MeOH in H₂O. Fractions obtained at 50% and 100% MeOH were combined separately and gave 172 mg and 240 mg, respectively. The combined organic layers (5.32 g) were instead dissolved in 1 L 10% MeOH and fractionated manually using a 500 mL column (4 x 40 cm). Combined fractions were concentrated under vacuum to give 1.22 g.

All three samples obtained from SPE were further purified by semi-preparative HPLC (AGILENT 1100 system). Dissolved in MeOH at approx. 100 mg/mL (injection volume: 50 µL), a C18 column (NUCLEODUR® Gravity-SB, 3 µm, 250 x 10 mm) and gradient elution of 55–95% ACN/H₂O + 0.1% FA (2 mL/min) over 30 min were used to yield 0.960 mg FE004 (**71**).

Compound 72 and 73a: The 40 L fermentation of FHG000416 in medium 5294 yielded 19.2 g crude extract representing the combined organic layers of MTBE/MeOH extraction. It was dissolved in MeOH (*c* ≈ 200 mg/mL, injection volume: 2 mL) and fractionated *via* preparative HPLC (Synergi™ Fusion-RP 80 Å, 4 µm, 250 x 21.2 mm) using linear gradient elution of 40–95% ACN/H₂O + 0.1% FA (15 mL/min) over 20 min. Various combined fractions (V1: 34.9 mg, V2: 47.7 mg, V3: 55.6 mg, V4: 154 mg, V5: 140 mg, V6: 171 mg) were further processed by semi-preparative HPLC (AGILENT 1100 system) using C18 column (NUCLEODUR® Gravity-SB, 3 µm, 250 x 10 mm) and linear gradients of 35–95%, 45–95% or 60–95% ACN/H₂O + 0.1% FA (2 mL/min) over 30 min (*c* ≈ 50 mg/mL in MeOH, injection volume: 50 µL). Separation of both compounds and final purification was achieved by UPLC fractionation (microTOF). Therefore, the samples (*c* ≈ 35 mg/mL in MeOH, injection volume: 5 µL) were injected onto a C18 column (ACQUITY UPLC® BEH C18, 1.7 µm, 100 x 2.1 mm) and eluted with an isocratic gradient of 48% ACN/H₂O + 0.1% FA (0.6 mL/min) over 16.50 min. 4.06 mg FE005 (**72**) and 3.05 mg FE006 (**73a**) were obtained.

Compound 74–76: The remaining aqueous phase of the MTBE/MeOH extraction was freeze-dried and extracted with MeOH. This extract was dissolved in 1 L 10% MeOH and fractionated manually by SPE using a 500 mL column (4 x 40 cm) of Amberlite® XAD-16N and a step gradient (10%, 50%, 100%) of MeOH in H₂O. Based on HRMS analysis, relevant fractions were combined and concentrated under reduced pressure to yield 97.4 g. Subsequently, it was dissolved in 40 mL 75% MeOH and fractionated by ion exchange chromatography using a 500 mL column of Lewatit® (5 x 25 cm) previously equilibrated with 5% FeCl₃. For elution, aqueous imidazole (200 mM) was used. Obtained fractions were further purified by semi-preparative HPLC (AGILENT 1100 system) using a C18 column (NUCLEODUR® Gravity-SB, 3 µm, 250 x 10 mm) and a linear gradient of 30–85% ACN/H₂O + 0.1% FA over 18.50 min at a flow rate of 2 mL/min. Combined with pure substance obtained during processing the organic MTBE/MeOH extraction phase, 1.57 mg FE008 (**74**), 12.2 mg FE009 (**75**) and 3.16 mg FE010 (**76**) were obtained.

Compound 87 and 90: Isolation of lipid430 (**87**) and FE002 (**90**) started from samples that were generated within the frame of another isolation project by MeOH extraction of 40 L lyophilized culture of DSM 22224 in medium 3018 followed by SPE using Amberlite® XAD-16N (1.5 L, 6 x 50 cm, MCI system) and stepwise increasing percentage of MeOH in H₂O. The provided fraction (6.10 g) was dissolved in MeOH (*c* ≈ 200 mg/mL, injection volume: 2 mL) and fractionated *via* preparative HPLC (Synergi™ Fusion-RP 80 Å, 4 μm, 250 x 21.2 mm) using linear gradient elution of 5–95% ACN/H₂O + 0.1% FA (15 mL/min) over 32 min. Combined fractions were subsequently purified by semi-preparative HPLC (AGILENT 1100 system). Dissolved in MeOH at approx. 100 mg/mL (injection volume: 50 μL), a C18 column (NUCLEODUR® Gravity-SB, 3 μm, 250 x 10 mm) and gradient elution of 50–100% ACN/H₂O + 0.1% FA (3 mL/min) over 22 min were used to yield 3.69 mg lipid 430 (**87**) and 1.90 mg FE002 (**90**).

FE003 (70): colorless solid; $[\alpha]_D^{21.7} +66.7$ (*c* 0.02, MeOH); LC-UV (ACN/H₂O) λ_{\max} 224 nm; ¹H and ¹³C-NMR: Table 15; ESI-MS (positive ions): *m/z* 344.2805 [M+H]⁺, *m/z* 366.2624 [M+Na]⁺, *m/z* 709.5350 [2M+Na]⁺; HRMS (ESI-TOF, +): *m/z* calcd. for C₁₉H₃₈NO₄ [M+H]⁺ 344.2795, found 344.2804.

FE004 (71): colorless solid; $[\alpha]_D^{21.7} -76.9$ (*c* 0.03, MeOH); LC-UV (ACN/H₂O) λ_{\max} 224 nm; ¹H and ¹³C-NMR: Table 16; ESI-MS (positive ions): *m/z* 376.2697 [M+H]⁺, *m/z* 358.2591 [M–H₂O+H]⁺, *m/z* 398.2516 [M+Na]⁺, *m/z* 773.5135 [2M+Na]⁺; HRMS (ESI-TOF, +): *m/z* calcd. for C₁₉H₃₈NO₆ [M+H]⁺ 376.2694, found 376.2697.

FE005 (72): colorless solid; LC-UV (ACN/H₂O) λ_{\max} 224 nm; ¹H and ¹³C-NMR: Table 19; ESI-MS (positive ions): *m/z* 440.2781 [M+H]⁺, *m/z* 879.5480 [2M+H]⁺; HRMS (ESI-TOF, +): *m/z* calcd. for C₂₀H₄₃NO₇P [M+H]⁺ 440.2772, found 440.2775.

FE006 (73a): colorless solid; LC-UV (ACN/H₂O) λ_{\max} 223 nm; ¹H and ¹³C-NMR: Table 18; ESI-MS (positive ions): *m/z* 452.2767 [M+H]⁺, *m/z* 903.5456 [2M+H]⁺, *m/z* 1354.8139 [3M+H]⁺; HRMS (ESI-TOF, +): *m/z* calcd. for C₂₁H₄₃NO₇P [M+H]⁺ 452.2850, found 452.2777.

FE008 (74): yellowish solid; LC-UV (ACN/H₂O) λ_{\max} 224, 277 nm; ¹H and ¹³C-NMR: Table 20; ESI-MS (positive ions): *m/z* 294.1700 [M+H]⁺, *m/z* 316.1518 [M+Na]⁺, *m/z* 587.3324 [2M+H]⁺; HRMS (ESI-TOF, +): *m/z* calcd. for C₁₆H₂₄NO₄ [M+H]⁺ 294.1700, found 294.1700.

FE009 (75): yellowish solid; LC-UV (ACN/H₂O) λ_{\max} 225, 277 nm; ¹H and ¹³C-NMR: Table 20; ESI-MS (positive ions): *m/z* 322.2016 [M+H]⁺, *m/z* 643.3952 [2M+H]⁺; HRMS (ESI-TOF, +): *m/z* calcd. for C₁₈H₂₈NO₄ [M+H]⁺ 322.2013, found 322.2013.

FE010 (76): off-white solid; LC-UV (ACN/H₂O) λ_{\max} 217 nm; ¹H and ¹³C-NMR: Table 21; ESI-MS (positive ions): *m/z* 306.2063 [M+H]⁺, *m/z* 328.1882 [M+Na]⁺, *m/z* 611.4053 [2M+H]⁺; HRMS (ESI-TOF, +): *m/z* calcd. for C₁₈H₂₈NO₃ [M+H]⁺ 306.2064, found 306.2064.

Lipid430 (87): colorless solid; $[\alpha]_{\text{D}}^{25.9} +16.3$ (*c* 0.37, MeOH); LC-UV (ACN/H₂O) λ_{max} 220 nm; ¹H-NMR (400 MHz, MeOD-*d*₄): δ = 4.50 (t, *J* = 4.3 Hz, 1H), 4.02–3.94 (m, 2H), 3.91 (dd, *J* = 11.5, 4.5 Hz, 1H), 3.90 (d, *J* = 16.7 Hz, 1H), 3.83 (dd, *J* = 11.3, 3.8 Hz, 1H), 2.41 (dd, *J* = 14.0, 4.3 Hz, 1H), 2.34 (dd, *J* = 14.0, 8.6 Hz, 1H), 1.56–1.48 (m, 1H), 1.53–1.46 (m, 2H), 1.50–1.43 (m, 1H), 1.36–1.25 (m, 17H), 1.17 (q, *J* = 6.7 Hz, 2H), 0.88 (d, *J* = 6.7 Hz, 6H); ¹³C-NMR (101 MHz, MeOD-*d*₄): δ = 175.0, 173.4, 171.6, 70.0, 63.0, 56.2, 44.8, 43.5, 40.2, 38.4, 31.0, 30.8, 30.7, 29.2, 28.5, 26.7, 23.0; ESI-MS (positive ions): *m/z* 431.3113 [M+H]⁺, *m/z* 413.3008 [M–H₂O+H]⁺, *m/z* 453.2933 [M+Na]⁺, *m/z* 883.5955 [2M+Na]⁺; HRMS (ESI-TOF, +): *m/z* calcd. for C₂₂H₄₃N₂O₆ [M+H]⁺ 431.3116, found 431.3116.

FE002 (90): colorless solid; $[\alpha]_{\text{D}}^{20.6} +21.1$ (*c* 0.19, MeOH); LC-UV (ACN/H₂O) λ_{max} 223 nm; ¹H-NMR (500 MHz, DMSO-*d*₆): δ = 8.10–8.04 (m, 1H, NH-14), 7.91–7.81 (m, 1H, NH-11), 7.66–7.59 (m, 1H, NH-7), 4.25 (dd, *J* = 12.6, 6.2 Hz, 1H, H-9), 3.82–3.75 (m, 2H, H-2, H-17), 3.73 (d, *J* = 4.6 Hz, 2H, H-13), 3.55 (dd, *J* = 9.1, 5.3 Hz, 1H, H-10), 3.50 (dd, *J* = 9.5, 4.3 Hz, 1H, H-10), 2.80–2.73 (m, 2H, H-5), 2.20 (dd, *J* = 16.4, 10.5 Hz, 2H, H-16), 1.80–1.68 (m, 2H, H-3), 1.66–1.56 (m, 2H, H-4), 1.50 (sept, *J* = 6.6 Hz, 1H, H-29), 1.39–1.31 (m, 2H, H-18), 1.26–1.21 (m, 18H, H-19–H-27), 1.16–1.11 (m, 2H, H-28), 0.85 (d, *J* = 6.6 Hz, 6H, H-30); ESI-MS (positive ions): *m/z* 545.3909 [M+H]⁺; HRMS (ESI-TOF, +): *m/z* calcd. for C₂₇H₅₃N₄O₇ [M+H]⁺ 545.3909, found 545.3909.

7.2.3.3 Advanced Marfey's Analysis

Advanced Marfey's Analysis was performed according to GENERAL MATERIALS AND EXPERIMENTAL PROCEDURES (see 7.1.7). Commercially purchased D- and L-enantiomers of serine, ornithine monohydrochloride and tyrosine as well as L- and DL-phenylalanine (SIGMA ALDRICH) served as references.

7.2.3.4 MIC Determination

The determination of MIC values was performed in triplicates (*n* = 3) according to GENERAL MATERIALS AND EXPERIMENTAL PROCEDURES (see 7.1.9). All compounds were provided as stock solutions of 6.4 mg/mL in DMSO.

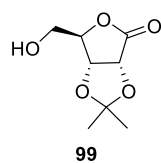
7.2.3.5 TLR2/TLR4 Assay

A HEK-Blue™ Detection assay was performed by an industrial partner (Evotec, Lyon, France) to analyze TLR2 and TLR4 stimulation induced by **70–76**, **87** and **90** provided as 10 mM stock solutions in DMSO. Therefore, HEK-Blue™ hTLR2 and hTLR4 cells were resuspended in HEK-Blue™ Detection cell culture medium and distributed into 96 well plates. The cells were treated with the provided compounds at final doses of 0.01 μM, 0.1 μM, 1 μM and 10 μM followed by incubation for 24 h at 37 °C. Afterwards, readout was done using a spectrophotometer at 620 nm. The assays were performed in duplicates (*n* = 2) and in two independent experiments for TLR2 and TLR4, respectively. PAM2 and

LPS (4 ng/mL, 2 ng/mL, 1 ng/mL and 0.5 ng/mL) were used as positive controls. Untreated (NT) and DMSO-treated cells served as negative control.

7.2.3.6 Stereoselective Total Synthesis of FE004

(3aR,6R,6aR)-6-(hydroxymethyl)-2,2-dimethyldihydrofuro[3,4-d][1,3]dioxol-4(3aH)-one (99)

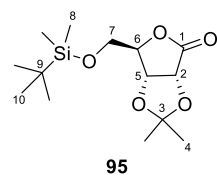


The synthesis of **99** was performed according to literature known procedures.^{[237][238]} D-Ribose (**91**) (9.40 g, 62.6 mmol, 1.00 eq.) and NaHCO₃ (10.5 g, 125 mmol, 2.00 eq.) were dissolved in water (60 mL) and stirred at room temperature for 30 min. The suspension was then cooled to <5 °C using an ice-water bath. At this temperature and during vigorous stirring, Br₂ (3.80 mL, 11.9 g, 74.2 mmol, 1.20 eq.) was added slowly using a pressure-equalizing dropping funnel. After the addition was completed, the reaction mixture was stirred at room temperature for 1 h before NaHSO₃ (0.656 g, 6.34 mmol, 0.10 eq.) was added. The aqueous solution was evaporated using a rotary evaporator at 50 °C bath temperature and water aspirator pressure. The resulting slurry was taken up in a mixture of abs. EtOH (40 mL) and toluene (10 mL) and evaporated again. The crude product was obtained as colourless solid and further used without purification.

The solution of the crude product in acetone (190 mL) and conc. H₂SO₄ (0.340 mL, 6.26 mmol, 0.10 eq.) was heated at reflux temperature (65 °C) for 4 h and then stirred at room temperature for additional 19 h. The reaction mixture was then filtered, the residue washed with acetone and the filtrate concentrated *in vacuo*. The crude product was purified by silica gel column chromatography using gradient elution from 10:1 to 1:2 PE/EE to afford 5.62 g (31.1 mmol, 50% over two steps) **99** as colorless solid.

R_f (*n*-heptane/ethyl acetate 1:1): 0.29; **¹H-NMR** (400 MHz, CDCl₃): δ = 4.84 (d, *J* = 5.6 Hz, 1H), 4.78 (d, *J* = 5.7 Hz, 1H), 4.63 (t, *J* = 2.0 Hz, 1H), 4.00 (dd, *J* = 12.2, 2.3 Hz, 1H), 3.82 (dd, *J* = 12.2, 1.6 Hz, 1H), 1.48 (s, 3H), 1.39 (s, 3H); **¹³C-NMR** (101 MHz, CDCl₃): δ = 174.9, 113.3, 82.7, 78.4, 75.8, 62.2, 26.9, 25.6; **HRMS** (ESI-TOF, +): *m/z* calcd. for C₈H₁₂O₅Na [M+Na]⁺ 211.0577, found 211.0577.

(3aR,6R,6aR)-6-(((*tert*-butyldimethylsilyl)oxy)methyl)-2,2-dimethyldihydrofuro[3,4-d][1,3]dioxol-4(3aH)-one (95)

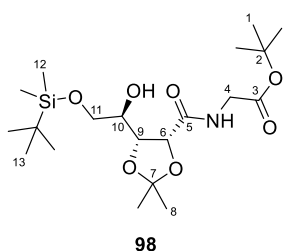


To a solution of **99** (5.86 g, 31.1 mmol, 1.00 eq.) in 80 mL anhydrous DCM (80 mL), imidazole (2.55 g, 37.5 mmol, 1.20 eq.) and subsequent TBSCl (5.64 g, 37.4 mmol, 1.20 eq.) was added under argon atmosphere. After stirring for 4 h at room temperature, MeOH (20 mL) was added. Extraction was performed using Et₂O (150 mL) and 1 M HCl (60 mL). The organic phase was washed with saturated aqueous NH₄Cl (60 mL) and saturated aqueous NaCl (50 mL), dried over MgSO₄, filtered and evaporated to dryness. The crude

product was applied onto silica gel and purified by column chromatography using gradient elution up to PE/EA 8:1 to yield **95** (8.85 g, 29.3 mmol, 94 %) as colorless solid.

R_f (petroleum ether/ethyl acetate 8:1): 0.38; [α]_D^{21.7} -45.0 (*c* 1.04, CHCl₃); **¹H-NMR** (400 MHz, CDCl₃): δ = 4.73 (d, *J* = 5.6 Hz, 1H, H-2), 4.70 (d, *J* = 5.6 Hz, 1H, H-5), 4.60 (t, *J* = 1.6 Hz, 1H, H-6), 3.89 (dd, *J* = 11.4, 2.1 Hz, 1H, H-7), 3.80 (dd, *J* = 11.3, 1.3 Hz, 1H, H-7), 1.47 (s, 3H, H-4), 1.39 (s, 3H, H-4), 0.87 (s, 9H, H-10), 0.07 (s, 3H, H-8), 0.05 (s, 3H, H-8); **¹³C-NMR** (101 MHz, CDCl₃): δ = 174.3 (C-1), 113.1 (C-3), 82.4 (C-6), 78.6 (C-5), 75.9 (C-2), 63.1 (C-7), 26.9 (C-4), 25.9 (C-10), 25.7 (C-4), -5.5/-5.6 (C-8); **HRMS** (ESI-TOF, +): *m/z* calcd. for C₁₄H₂₆O₅SiNa [M+Na]⁺ 325.1442, found 325.1443.

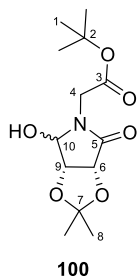
tert-butyl ((4*R*,5*R*)-5-((*R*)-2-((*tert*-butyldimethylsilyl)oxy)-1-hydroxyethyl)-2,2-dimethyl-1,3-dioxolane-4-carbonyl)glycinate (98**)**



Glycine *tert*-butyl ester hydrochloride (6.84 g, 40.8 mmol, 3.00 eq.) was dissolved in saturated aqueous NaHCO₃ (50 mL) and extracted with Et₂O (150 mL). The organic phase was washed with saturated aqueous NaCl (50 mL), dried (MgSO₄), filtered and carefully evaporated under reduced pressure to yield glycine *tert*-butylester (**92**) as a yellow oil.

95 (4.11 g, 13.6 mmol, 1.00 eq.) dissolved in DCM was added to the extracted **92** and the solvent was carefully removed under reduced pressure up to 500 mbar. DMSO (3 mL) was added and the reaction mixture was stirred at 80 °C. Until LC-MS confirmed complete conversion of the starting material, further glycine *tert*-butyl ester (**92**) identically extracted was added over a period of 21 h in total. After cooling to room temperature, saturated aqueous NH₄Cl (30 mL) was added to the mixture which was then extracted with ethyl acetate (100 ml). The organic layer was washed with saturated aqueous NaCl (30 mL), dried over MgSO₄, filtered and concentrated under reduced pressure. The crude product was purified by SiO₂ column chromatography using gradient elution from PE/EA 15:1 to 1:1. **98** (5.48 g, 12.65 mmol, 93%) was obtained as colorless solid.

R_f (petroleum ether/ethyl acetate 6:1): 0.32; [α]_D^{21.1} +8.4 (*c* 1.01, CHCl₃); **¹H-NMR** (400 MHz, CDCl₃): δ = 7.30 (t, *J* = 4.7 Hz, 1H, 4-NH), 4.64 (d, *J* = 7.2 Hz, 1H, H-6), 4.58 (d, *J* = 3.7 Hz, 1H, 10-OH), 4.49 (dd, *J* = 9.4, 7.2 Hz, 1H, H-9), 4.04 (dd, *J* = 18.4, 5.7 Hz, 1H, H-4), 3.89 (dd, *J* = 18.4, 4.8 Hz, 1H, H-4), 3.87 (dd, *J* = 10.7, 2.3 Hz, 1H, H-11), 3.77 (dd, *J* = 10.7, 4.4 Hz, 1H, H-11), 3.61-3.55 (m, 1H, H-10), 1.60 (s, 3H, H-8), 1.48 (s, 9H, H-1), 1.38 (s, 3H, H-8), 0.90 (s, 9H, H-14), 0.08 (s, 3H, H-12), 0.08 (s, 3H, H-12); **¹³C-NMR** (101 MHz, CDCl₃): δ = 171.8 (C-5), 168.3 (C-3), 110.6 (C-7), 82.9 (C-2), 77.4 (C-9), 77.2 (C-6), 71.1 (C-10), 64.7 (C-11), 41.9 (C-4), 28.2 (C-1), 27.3 (C-8), 26.1 (C-14), 24.9 (C-8), 18.7 (C-13), -5.1 (C-12), -5.2 (C-12); **HRMS** (ESI-TOF, +): *m/z* calcd. for C₂₀H₄₀NO₇Si [M+H]⁺ 434.2569, found 434.2570.

***tert*-butyl 2-((3*aS*,6*aR*)-4-hydroxy-2,2-dimethyl-6-oxotetrahydro-5*H*-[1,3]dioxolo[4,5-*c*]pyrrol-5-yl)acetate (**100**)**

In a round-bottom flask made of teflon, **98** (1.20 g, 2.77 mmol, 1.00 eq.) was dissolved in THF (50 mL). 1 M TBAF in THF (3.33 mL, 3.33 mmol, 1.20 eq.) was added slowly and the resulting reaction mixture was stirred at room temperature for 1 h.

THF (10 mL) and H₂O (20 mL) were then added as well as NaIO₄ (1.79 g, 8.37 mmol, 3.02 eq.). The reaction mixture was stirred at room temperature. After 2 h, an additional equivalent (595 mg, 2.78 mmol, 1.00 eq.) of NaIO₄ was added. 1 h later, TLC and LC-MS

showed full conversion of the starting material. The reaction mixture was quenched by adding saturated aqueous Na₂SO₃ (20 mL) and extracted with ethyl acetate (3 x 200 mL). The combined organic layers were washed with saturated aqueous NaCl (200 mL), dried (MgSO₄), filtered and concentrated under reduced pressure. The resulting yellowish oil was applied onto silica gel and purified by flash chromatography (50% ethyl acetate in *n*-heptane). **100** (782 mg, 2.72 mmol, 98 %) was obtained as a colorless oil and an inseparable mixture of both diastereomers **100a** and **100b**.

R_f (petroleum ether/ethyl acetate 1:2): 0.52; **¹H-NMR** (400 MHz, CDCl₃): δ = 5.11 (d, *J* = 3.6 Hz, 1H, H-10), 4.85 (d, *J* = 5.5 Hz, 1H, H-6), 4.78 (d, *J* = 3.6 Hz, 1H, 10-OH), 4.59 (d, *J* = 18.0 Hz, 1H, H-4), 4.55 (d, *J* = 5.7 Hz, 1H, H-9), 3.74 (d, *J* = 17.8 Hz, 1H, H-4), 1.48 (s, 9H, H-1), 1.41 (s, 3H, H-8), 1.38 (s, 3H, H-8); **¹³C-NMR** (101 MHz, CDCl₃): δ = 172.4 (C-5), 170.4 (C-3), 113.5 (C-7), 86.1 (C-10), 84.1 (C-2), 79.4 (C-9), 76.2 (C-6), 45.3 (C-4), 28.1 (C-1), 27.2 (C-8), 26.0 (C-8); **HRMS** (ESI-TOF, +): *m/z* calcd. for C₁₃H₂₁NO₆Na [M+Na]⁺ 310.1261, found 310.1265.

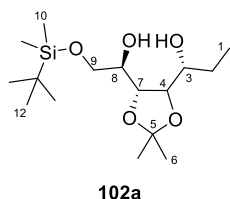
(*R*)-1-((4*S*,5*R*)-5-((*R*)-2-((*tert*-butyldimethylsilyl)oxy)-1-hydroxyethyl)-2,2-dimethyl-1,3-dioxolan-4-yl)propan-1-ol (102a**) and (*S*)-1-((4*S*,5*R*)-5-((*R*)-2-((*tert*-butyldimethylsilyl)oxy)-1-hydroxyethyl)-2,2-dimethyl-1,3-dioxolan-4-yl)propan-1-ol (**102b**)**

The reaction was carried out in moisture-free glassware under inert atmosphere. To a suspension of **95** (499 mg, 1.65 mmol, 1.00 eq.) in anhydrous THF (10 mL), EtMgBr in THF (0.9 M, 3.67 mL, 3.30 mmol, 2.00 eq.) was added dropwise at -78 °C. The suspension was stirred at -78 °C for 30 min and overnight at room temperature. Because the TLC showed remaining starting material the next day, additional EtMgBr in THF (2.00 eq.) was added at -78 °C. After stirring for 5 h at room temperature, the TLC showed almost complete conversion of the starting material. The reaction mixture was quenched with saturated aqueous NH₄Cl (30 mL). The mixture was extracted with ethyl acetate (2 x 75 mL) and the combined organic layers were washed with saturated aqueous NaCl (50 mL), dried over MgSO₄, filtered, and concentrated under reduced pressure to yield a diastereomeric mixture (509 mg, 1.53 mmol, 93%) as slightly yellow oil which was used in the next stage without further purification.

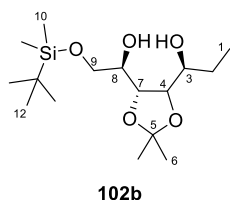
Dissolved in anhydrous MeOH (10 mL), NaBH₄ (116 mg, 3.06 mmol, 2.00 eq.) was added at 0 °C. After stirring at 0 °C for 30 min, the TLC showed remaining starting material. Additional NaBH₄ (1.00 eq.)

7. Experimental

was added. The mixture was stirred at room temperature for 1 h. Saturated aqueous NH_4Cl (30 mL) was added and the mixture extracted with ethyl acetate (2 x 75 mL). Combined organic layers were washed with saturated aqueous NaCl (50 mL), dried over MgSO_4 , filtered, and concentrated under reduced pressure. The crude product was pre-purified by flash column chromatography (0–40% ethyl acetate in *n*-heptane) and finally purified by flash column chromatography (0–35% ethyl acetate in *n*-heptane) to give **102a** (128 mg, 0.383 mmol, 23% over two steps) and **102b** (78.3 mg, 0.234 mmol, 14% over two steps) as colorless oils.



R_f (*n*-heptane/ethyl acetate 2:1): 0.43; **¹H-NMR** (400 MHz, CDCl_3): δ = 4.05–4.00 (m, 2H, H-4, H-7), 3.88 (dd, J = 10.0, 3.2 Hz, 1H, H-9), 3.83–3.75 (m, 1H, H-8), 3.68–3.60 (m, 1H, H-9), 3.66–3.61 (m, 1H, H-3), 1.83 (dtd, J = 21.5, 7.6, 2.8 Hz, 1H, H-2), 1.54–1.44 (m, 1H, H-2), 1.37 (s, 3H, H-6), 1.32 (s, 3H, H-6), 1.03 (t, J = 7.4 Hz, 3H, H-1), 0.91 (s, 9H, H-12), 0.10 (s, 6H, H-10); **¹³C-NMR** (101 MHz, CDCl_3): δ = 108.6 (C-5), 80.9 (C-7), 77.5 (C-4), 70.1 (C-3), 69.5 (C-8), 64.5 (C-9), 28.2 (C-6), 27.0 (C-2), 26.0 (C-12), 25.6 (C-6), 18.5 (C-11), 9.6 (C-1), –5.2/–5.3 (C-10); **HRMS** (ESI-TOF, +): m/z calcd. for $\text{C}_{16}\text{H}_{34}\text{O}_5\text{SiNa}$ $[\text{M}+\text{Na}]^+$ 357.2068, found 357.2069.



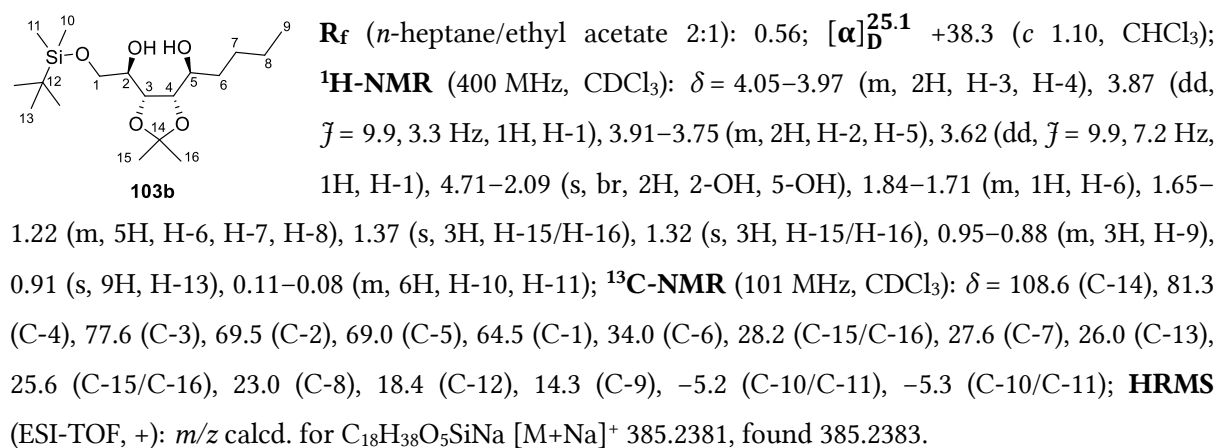
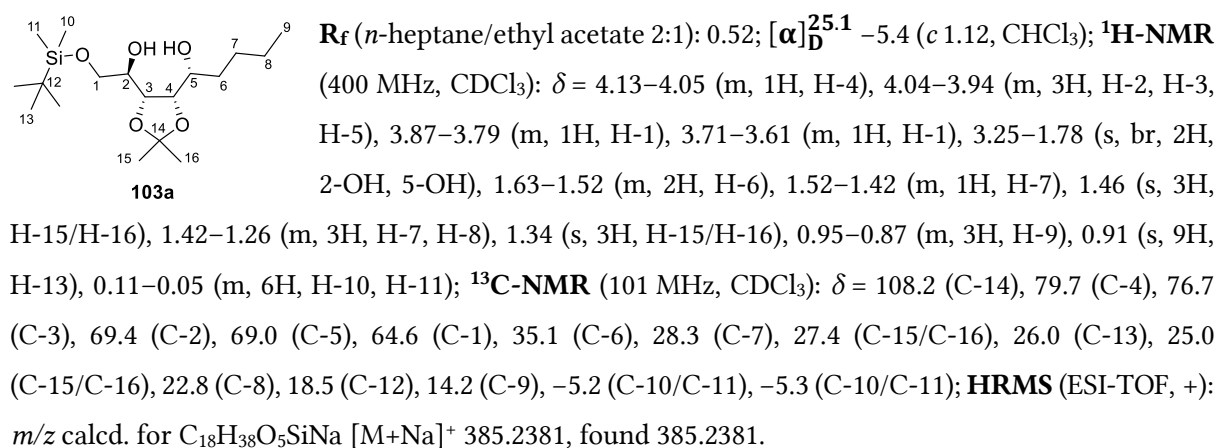
R_f (*n*-heptane/ethyl acetate 2:1): 0.52; **¹H-NMR** (400 MHz, CDCl_3): δ = 4.11–4.08 (m, 1H, H-7), 4.03–3.99 (m, 2H, H-4, H-8), 3.93–3.88 (m, 1H, H-3), 3.85–3.81 (m, 1H, H-9), 3.69–3.64 (m, 1H, H-9), 1.64–1.54 (m, 2H, H-2), 1.46 (s, 3H, H-6), 1.34 (s, 3H, H-6), 1.01 (dd, J = 7.3, 2.7 Hz, 3H, H-1), 0.91 (s, 9H, H-12), 0.09 (s, 6H, H-10); **¹³C-NMR** (101 MHz, CDCl_3): δ = 108.2 (C-5), 79.3 (C-7), 76.7 (C-4), 70.4 (C-3), 69.4 (C-8), 64.6 (C-9), 28.2 (C-2), 27.4 (C-6), 26.0 (C-12), 25.0 (C-6), 18.5 (C-11), 9.4 (C-1), –5.2/–5.3 (C-10); **HRMS** (ESI-TOF, +): m/z calcd. for $\text{C}_{16}\text{H}_{34}\text{O}_5\text{SiNa}$ $[\text{M}+\text{Na}]^+$ 357.2068, found 357.2066.

(R)-1-((4S,5R)-5-((R)-2-((tert-butyl)dimethylsilyloxy)-1-hydroxyethyl)-2,2-dimethyl-1,3-dioxolan-4-yl)pentan-1-ol (103a) and (S)-1-((4S,5R)-5-((R)-2-((tert-butyl)dimethylsilyloxy)-1-hydroxyethyl)-2,2-dimethyl-1,3-dioxolan-4-yl)pentan-1-ol (103b)

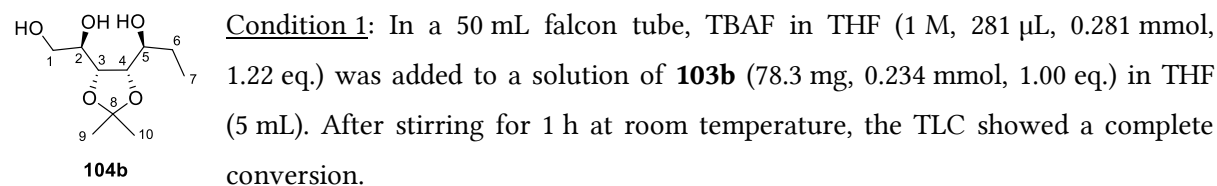
The reaction was carried out in moisture-free glassware under inert atmosphere. To a suspension of **95** (506 mg, 1.67 mmol, 1.00 eq.) in anhydrous THF (10 mL), *n*-BuLi in *n*-hexane (2.5 M, 736 μL , 1.84 mmol, 1.10 eq.) was added dropwise at -78 °C. The suspension was stirred at -78 °C for 30 min. The TLC showed almost complete conversion of the starting material. The reaction mixture was stirred at room temperature for 5 min and then quenched with saturated aqueous NH_4Cl (30 mL). The mixture was extracted with ethyl acetate (2 x 75 mL) and the combined organic layers were washed with saturated aqueous NaCl (50 mL), dried over MgSO_4 , filtered, and concentrated under reduced pressure to yield a diastereomeric mixture (555 mg, 1.54 mmol, 92%) which was used in the next stage without further purification.

7. Experimental

Dissolved in anhydrous MeOH (10 mL), NaBH₄ (0.116 g, 3.08 mmol, 2.00 eq.) was added at 0 °C. After stirring at 0 °C for 30 min, the TLC showed remaining starting material. Additional NaBH₄ (1.00 eq.) was added. The mixture was stirred at room temperature for 1 h. Saturated aqueous NH₄Cl (30 mL) was then added. The mixture was extracted with ethyl acetate (2 x 75 mL) and the combined organic layers were washed with saturated aqueous NaCl (50 mL), dried over MgSO₄, filtered, and concentrated under reduced pressure. The crude product was pre-purified by flash column chromatography (0–40% ethyl acetate in *n*-heptane) and finally purified by flash column chromatography (0–35% ethyl acetate in *n*-heptane) to give **103a** (212 mg, 0.585 mmol, 35% over two steps) and **103b** (134 mg, 0.370 mmol, 22% over two steps) as colorless oils.



(*R*)-1-((4*R*,5*S*)-5-((*S*)-1-hydroxypropyl)-2,2-dimethyl-1,3-dioxolan-4-yl)ethane-1,2-diol (**104b**)

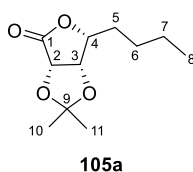


Condition 2: The reaction was carried out in moisture-free glassware under inert atmosphere. To a suspension of commercially available 2,3-*O*-(1-methylethylidene)-*D*-ribo-furanose (**96**) (1.00 g,

5.26 mmol, 1.00 eq.) in anhydrous THF (15 mL), EtMgBr in THF (0.9 M, 35.1 mL, 31.6 mmol, 6.00 eq.) was added dropwise at $-78\text{ }^{\circ}\text{C}$. The mixture was stirred at $-78\text{ }^{\circ}\text{C}$ for 20 min and overnight at room temperature. Because the TLC showed remaining starting material, EtMgBr in THF (6.00 eq.) was added a second time at $-78\text{ }^{\circ}\text{C}$. After stirring for 2 h at room temperature, the TLC showed sufficient conversion. The reaction mixture was carefully quenched with saturated aqueous NH_4Cl (90 mL). The mixture was extracted with ethyl acetate (100 mL and 150 mL) and the combined organic layers were washed with saturated aqueous NaCl (75 mL), dried over MgSO_4 , filtered, and concentrated under reduced pressure. The crude product was purified by flash column chromatography (0–100% ethyl acetate in *n*-heptane) to give **104b** (548 mg, 2.49 mmol, 47%) as colorless oil.

R_f (*n*-heptane/ethyl acetate 1:2): 0.24; $[\alpha]_D^{23.2} +22.3$ (c 1.08, CHCl_3); $^1\text{H-NMR}$ (400 MHz, CDCl_3): δ = 4.10 (dd, J = 9.2, 5.4 Hz, 1H, H-3), 4.02 (dd, J = 9.2, 5.4 Hz, 1H, H-4), 3.91–3.82 (m, 2H, H-1, H-2), 3.78 (td, J = 8.7, 3.0 Hz, 1H, H-5), 3.71 (dd, J = 12.1, 6.8 Hz, 1H, H-1), 3.50 (s, br, 3H, 1-OH, 2-OH, 5-OH), 1.91–1.78 (m, 1H, H6), 1.58–1.44 (m, 1H, H6), 1.37 (s, 3H, H-9/H-10), 1.33 (s, 3H, H-9/H-10), 1.02 (t, J = 7.4 Hz, 3H, H-7); $^{13}\text{C-NMR}$ (101 MHz, CDCl_3): δ = 108.8 (C-8), 80.1 (C-4), 77.8 (C-3), 70.8 (C-5), 69.6 (C-2), 64.5 (C-1), 28.1 (C-9/C-10), 27.0 (C-6), 25.6 (C-9/C-10), 9.3 (C-7); **HRMS** (ESI-TOF, +): m/z calcd. for $\text{C}_{10}\text{H}_{20}\text{O}_5\text{Na}$ $[\text{M}+\text{Na}]^+$ 243.1203, found 243.1203.

(3aS,6R,6aS)-6-butyl-2,2-dimethyldihydrofuro[3,4-*d*][1,3]dioxol-4(3a*H*)-one (105a)



In a 50 mL falcon tube, to a solution of **103a** (212 mg, 0.585 mmol, 1.00 eq.) in THF (10 mL) TBAF in THF (1 M, 703 μL , 0.703 mmol, 1.20 eq.) was added. After stirring for 1 h at room temperature, the TLC showed a complete conversion. The reaction mixture was diluted by adding 8 mL THF and 6 mL H_2O (THF/ H_2O 3:1).

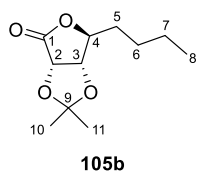
To this solution, NaIO_4 (376 mg, 1.76 mmol, 3.00 eq.) was added. After stirring for 70 min at room temperature, the TLC showed complete conversion of the starting material. The mixture was quenched with saturated aqueous Na_2SO_3 (20 mL) and extracted with ethyl acetate (2 x 40 mL). The combined organic layers were washed with saturated aqueous NaCl (30 mL), dried over MgSO_4 , filtered and concentrated under reduced pressure.

The obtained crude product was dissolved in DCM (6 mL) and Dess-Martin periodinane (DMP, 15% in DCM, 2.43 mL, 1.17 mmol, 1.98 eq.) was added. After stirring for 1 h and 4 h at room temperature, additional DMP (2.00 eq. and 1.00 eq.) was added because LC-MS showed incomplete conversion of the starting material. After stirring overnight, complete conversion was observed. The reaction solution was filtered through a short silica column (100% DCM, 10 g silica) and purified by flash column chromatography (0–30% ethyl acetate in *n*-heptane) to give **105a** (43.3 mg, 0.202 mmol, 35% over three steps) as colorless solid.

R_f = 0.32 (*n*-heptane/ethyl acetate 2:1); $[\alpha]_D^{24.6} +74.2$ (c 0.82, CHCl_3); $^1\text{H-NMR}$ (400 MHz, CDCl_3): δ = 4.79 (d, J = 5.4 Hz, 1H, H-2), 4.72 (dd, J = 5.4, 3.4 Hz, 1H, H-3), 4.42 (ddd, J = 7.9, 6.2, 3.5 Hz, 1H,

H-4), 1.97–1.71 (m, 2H, H-5), 1.56–1.32 (m, 4H, H-6, H-7), 1.46 (s, 3H, H-10/H-11), 1.39 (s, 3H, H-10/H-11), 0.98–0.86 (m, 3H, H-8); $^{13}\text{C-NMR}$ (101 MHz, CDCl_3): δ = 174.2 (C-1), 114.0 (C-9), 80.0 (C-4), 77.1 (C-3), 76.5 (C-2), 28.9 (C-5), 27.5 (C-6), 26.9 (C-10/C-11), 26.1 (C-10/C-11), 22.6 (C-7), 14.0 (C-8); **HRMS** (ESI-TOF, +): m/z calcd. for $\text{C}_{11}\text{H}_{18}\text{O}_4\text{Na}$ $[\text{M}+\text{Na}]^+$ 237.1097, found 237.1097.

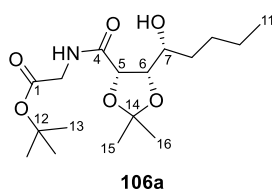
(3a*S*,6*S*,6a*S*)-6-butyl-2,2-dimethyldihydrofuro[3,4-*d*][1,3]dioxol-4(3a*H*)-one (105b)



Lactone **105b** (50.1 mg, 0.234 mmol, 63% over three steps) was synthesized in analogous manner to **105a** starting from **103b** (134 mg, 0.369 mmol, 1.00 eq.). It was obtained as slightly yellow oil.

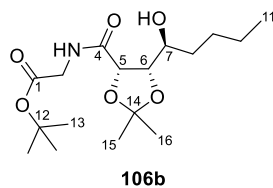
R_f (*n*-heptane/ethyl acetate 2:1): 0.43; $[\alpha]_D^{24.5} +39.4$ (*c* 0.99, CHCl_3); $^1\text{H-NMR}$ (400 MHz, CDCl_3): δ = 4.74 (d, J = 5.7 Hz, 1H, H-2), 4.55 (dd, J = 7.5, 6.2 Hz, 1H, H-4), 4.53 (d, J = 5.7 Hz, 1H, H-3), 1.72–1.53 (m, 2H, H-5), 1.48 (s, 3H, H-10/H-11), 1.46–1.30 (m, 4H, H-6, H-7), 1.38 (s, 3H, H-10/H-11), 0.96–0.87 (m, 3H, H-8); $^{13}\text{C-NMR}$ (101 MHz, CDCl_3): δ = 174.0 (C-1), 114.0 (C-9), 83.0 (C-4), 79.6 (C-3), 75.0 (C-2), 33.6 (C-5), 26.9 (C-10/C-11), 26.9 (C-6), 25.8 (C-10/C-11), 22.4 (C-7), 13.9 (C-8); **HRMS** (ESI-TOF, +): m/z calcd. for $\text{C}_{11}\text{H}_{18}\text{O}_4\text{Na}$ $[\text{M}+\text{Na}]^+$ 237.1097, found 237.1098.

***tert*-butyl ((4*S*,5*S*)-5-((*R*)-1-hydroxypentyl)-2,2-dimethyl-1,3-dioxolane-4-carbonyl)glycinate (106a)**



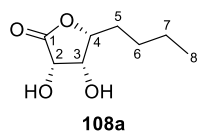
106a was synthesized similar to **100**. Previously extracted (using 100 mL DCM) glycine *tert*-butyl ester (**92**) (133 mg, 1.01 mmol, 5.02 eq.) was added to lactone **105a** (43.3 mg, 0.202 mmol, 1.00 eq.) in DMSO (0.5 mL). The crude product was purified *via* flash column chromatography (0–40% ethyl acetate in *n*-heptane) to give **106a** (47.1 mg, 0.136 mmol, 68%) as colorless oil.

R_f (*n*-heptane/ethyl acetate 2:1): 0.25; $[\alpha]_D^{23.9} -20.8$ (*c* 1.80, CHCl_3); $^1\text{H-NMR}$ (400 MHz, CDCl_3): δ = 7.08 (t, J = 5.2 Hz, 1H, H-3), 4.28 (d, J = 8.0 Hz, 1H, H-5), 4.33 (dd, J = 8.1, 2.1 Hz, 1H, H-6), 4.05 (dd, J = 18.2, 5.9 Hz, 1H, H-2), 3.84 (dd, J = 18.1, 5.1 Hz, 1H, H-2), 3.89–3.76 (m, 1H, H-7), 2.70 (d, J = 8.1 Hz, 1H, 7-OH), 1.62 (s, 3H, H-15/H-16), 1.60–1.43 (m, 2H, H-8), 1.47 (s, 9H, H-13), 1.39 (s, 3H, H-15/H-16), 1.38–1.23 (m, 4H, H-9, H-10), 0.89 (t, J = 7.2 Hz, 3H, H-11); $^{13}\text{C-NMR}$ (101 MHz, CDCl_3): δ = 170.5 (C-4), 169.2 (C-1), 109.9 (C-14), 80.8 (C-12), 80.4 (C-6), 76.3 (C-5), 68.6 (C-7), 41.7 (C-2), 34.3 (C-8), 28.7 (C-13), 28.3 (C-9), 26.7 (C-15/C-16), 24.8 (C-15/C-16), 22.7 (C-10), 14.2 (C-11); **HRMS** (ESI-TOF, +): m/z calcd. for $\text{C}_{17}\text{H}_{31}\text{NO}_6\text{Na}$ $[\text{M}+\text{Na}]^+$ 368.2044, found 368.2048.

tert-butyl ((4*S*,5*S*)-5-((*S*)-1-hydroxypentyl)-2,2-dimethyl-1,3-dioxolane-4-carbonyl)glycinate (106b**)**

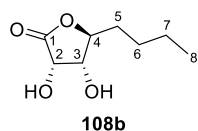
In analogous manner to **106a**, **106b** (54.0 mg, 0.156 mmol, 67%) was synthesized in starting from **39b** (50.1 mg, 0.234 mmol). It was obtained as colorless oil.

R_f (*n*-heptane/ethyl acetate 2:1): 0.35; [α]_D^{23.9} +3.3 (*c* 0.92, CHCl₃); **¹H-NMR** (400 MHz, CDCl₃): δ = 7.34 (t, *J* = 5.0 Hz, 1H, H-3), 4.65 (s, br, 1H, 7-OH), 4.63 (d, *J* = 7.2 Hz, 1H, H-5), 4.19 (dd, *J* = 9.3, 7.2 Hz, 1H, H-6), 4.04 (dd, *J* = 18.3, 5.6 Hz, 1H, H-2), 3.90 (dd, *J* = 18.4, 4.7 Hz, 1H, H-2), 3.50 (td, *J* = 9.2, 2.6 Hz, 1H, H-7), 1.76–1.22 (m, 6H, H-8, H-9, H-10), 1.60 (s, 3H, H-15/H-16), 1.48 (s, 9H, H-13), 1.39 (s, 3H, H-15/H-16), 0.90 (t, *J* = 6.9 Hz, 3H, H-11); **¹³C-NMR** (101 MHz, CDCl₃) δ [ppm] = 172.1 (C-4), 168.2 (C-1), 110.5 (C-14), 82.9 (C-12), 81.7 (C-6), 77.4 (C-5), 70.3 (C-7), 41.9 (C-2), 33.8 (C-8), 28.2 (C-13), 27.4 (C-9), 27.2 (C-15/C-16), 24.8 (C-15/C-16), 23.0 (C-10), 14.2 (C-11); **HRMS** (ESI-TOF, +): *m/z* calcd. for C₁₇H₃₂NO₆ [M+H]⁺ 346.2224, found 346.2223.

(3*S*,4*R*,5*R*)-5-butyl-3,4-dihydroxydihydrofuran-2(3*H*)-one (108a**)**

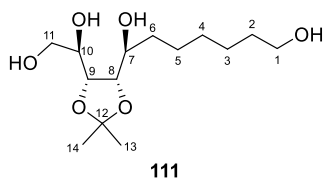
106a (20.5 mg, 59.3 μ mol, 1.00 eq.) was dissolved in anhydrous 1,4-dioxane (2 mL) and HCl in dioxane (4 M, 400 μ L, 1.60 mmol, 27.0 eq.) was added. After stirring at room temperature for 6 h, two drops of water were added. The mixture was stirred at room temperature overnight and then evaporated to dryness. After lyophilization, **108a** (14.8 mg, 59.3 μ mol, quant.) was obtained as colorless solid.

R_f (*n*-heptane/ethyl acetate 1:4): 0.39; **¹H-NMR** (400 MHz, CDCl₃): δ = 5.75 (s, br, 1H, 3-OH), 5.31 (s, br, 1H, 2-OH), 4.41 (d, *J* = 4.4 Hz, 1H, H-2), 4.25 (td, *J* = 7.0, 2.4 Hz, 1H, H-4), 4.15–4.05 (m, 1H, H-3), 1.71–1.54 (m, 2H, H-5), 1.39–1.20 (m, 4H, H-6, H-7), 0.88 (t, *J* = 6.9 Hz, 3H, H-8); **¹³C-NMR** (101 MHz, CDCl₃): δ = 176.2 (C-1), 79.6 (C-4), 70.8 (C-3), 69.8 (C-2), 27.8 (C-5), 26.6 (C-6), 22.0 (C-7), 13.8 (C-8); **HRMS** (ESI-TOF, +): *m/z* calcd. for C₈H₁₄O₄Na [M+Na]⁺ 197.0784, found 197.0783.

(3*S*,4*R*,5*S*)-5-butyl-3,4-dihydroxydihydrofuran-2(3*H*)-one (108b**)**

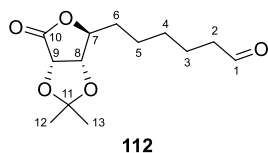
108b (13.6 mg, 54.5 μ mol, quant.) was synthesized in analogous manner to **108a** starting from **106b** (18.9 mg, 54.7 μ mol). It was obtained as colorless solid.

R_f (*n*-heptane/ethyl acetate 1:4): 0.44; **¹H-NMR** (400 MHz, CDCl₃): δ = 5.75 (s, br, 1H, 3-OH), 5.43 (s, br, 1H, 2-OH), 4.40 (d, *J* = 5.3 Hz, 1H, H-2), 4.17 (dd, *J* = 8.5, 6.3 Hz, 1H, H-4), 3.96 (d, *J* = 4.9 Hz, 1H, H-3), 1.65–1.48 (m, 2H, H-5), 1.38–1.25 (m, 4H, H-6, H-7), 0.87 (t, *J* = 6.9 Hz, 3H, H-8); **¹³C-NMR** (101 MHz, CDCl₃): δ = 175.9 (C-1), 84.7 (C-4), 71.0 (C-3), 68.2 (C-2), 31.3 (C-5), 27.4 (C-6), 21.8 (C-7), 13.8 (C-8); **HRMS** (ESI-TOF, +): *m/z* calcd. for C₈H₁₄O₄Na [M+Na]⁺ 197.0784, found 197.0783.

(S)-1-((4S,5R)-5-((R)-1,2-dimethyl-1,3-dioxolan-4-yl)heptane-1,7-diol (111)

The starting material **45** was synthesized over three steps starting from 5-hexyne-1-ol by a cooperation partner and provided as colorless oil.

R_f (ethyl acetate): 0.20; $[\alpha]_D^{23.9} = +6.8$ (c 0.89, CHCl_3); $^1\text{H-NMR}$ (400 MHz, $\text{DMSO-}d_6$): $\delta = 5.43$ (d, $J = 3.9$ Hz, 1H, 10-OH), 5.04 (d, $J = 4.0$ Hz, 1H, 7-OH), 4.48 (t, $J = 5.7$ Hz, 1H, 11-OH), 4.32 (t, $J = 5.1$ Hz, 1H, 1-OH), 3.97 (dd, $J = 9.3$, 5.6 Hz, 1H, H-9), 3.86 (dd, $J = 9.1$, 5.5 Hz, 1H, H-8), 3.70–3.56 (m, 3H, H-7, H-10, H-11), 3.44–3.34 (m, 3H, H-1, H-11), 1.69–1.54 (m, 1H, H-6), 1.54–1.37 (m, 3H, H-2, H-3), 1.36–1.21 (m, 6H, H-3, H-4, H-5, H-6), 1.28 (s, 3H, H-13/H-14), 1.24 (s, 3H, H-13/H-14); $^{13}\text{C-NMR}$ (101 MHz, $\text{DMSO-}d_6$): $\delta = 107.4$ (C-12), 80.1 (C-8), 76.9 (C-9), 69.7 (C-10), 68.1 (C-7), 63.1 (C-11), 60.7 (C-1), 33.7 (C-6), 32.5 (C-2), 29.1 (C-4), 27.8 (C-13/C-14), 25.5 (C-5), 25.5 (C-13/C-14), 24.5 (C-3); **HRMS** (ESI-TOF, +): m/z calcd. for $\text{C}_{14}\text{H}_{28}\text{O}_6\text{Na}$ $[\text{M}+\text{Na}]^+$ 315.1778, found 315.1776.

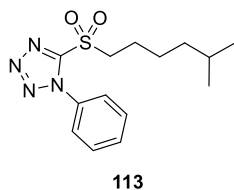
6-((3aS,4S,6aS)-2,2-dimethyl-6-oxotetrahydrofuro[3,4-d][1,3]dioxol-4-yl)hexanal (112)

111 (889 mg, 3.04 mmol, 1.00 eq.) was dissolved in THF (45 mL). NaIO_4 (1.95 g, 9.12 mmol, 3.00 eq.) in H_2O (15 mL) was added. After stirring for 1 h at room temperature, the TLC and LC-MS showed complete conversion of the starting material. The mixture was quenched with saturated aqueous Na_2SO_3 (50 mL) and extracted with ethyl acetate (100 mL and 150 mL). The combined organic layers were washed with saturated aqueous NaCl (100 mL), dried over MgSO_4 , filtered and concentrated under reduced pressure.

The obtained crude product was dissolved in DCM (15 mL) and DMP (15% in DCM, 22.2 mL, 10.7 mmol, 4.00 eq.) was added. After stirring overnight at room temperature, additional DMP (1.00 eq.) was added because TLC and LC-MS showed incomplete conversion of the starting material. After stirring for 1 h, almost complete conversion was observed. The reaction solution was filtered through a short silica column (100% DCM, 10 g silica) and purified by flash column chromatography (0–100% ethyl acetate in *n*-heptane) to give **112** (392 mg, 1.53 mmol, 50% over two steps) as colorless solid.

The obtained crude product was dissolved in DCM (15 mL) and DMP (15% in DCM, 22.2 mL, 10.7 mmol, 4.00 eq.) was added. After stirring overnight at room temperature, additional DMP (1.00 eq.) was added because TLC and LC-MS showed incomplete conversion of the starting material. After stirring for 1 h, almost complete conversion was observed. The reaction solution was filtered through a short silica column (100% DCM, 10 g silica) and purified by flash column chromatography (0–100% ethyl acetate in *n*-heptane) to give **112** (392 mg, 1.53 mmol, 50% over two steps) as colorless solid.

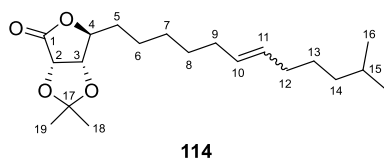
R_f (*n*-heptane/ethyl acetate 1:1): 0.39; $[\alpha]_D^{23.1} = +31.9$ (c 1.16, CHCl_3); $^1\text{H-NMR}$ (400 MHz, CDCl_3): $\delta = 9.75$ (s, 1H, H-1), 4.73 (d, $J = 5.7$ Hz, 1H, H-8), 4.56–4.48 (m, 2H, H-7, H-9), 2.44 (td, $J = 7.2$, 1.5 Hz, 2H, H-2), 1.71–1.52 (m, 4H, H-3, H-4), 1.52–1.29 (m, 4H, H-5, H-6), 1.46 (s, 3H, H-12/H-13), 1.36 (s, 3H, H-12/H-13); $^{13}\text{C-NMR}$ (101 MHz, CDCl_3): $\delta = 202.3$ (C-1), 173.8 (C-10), 114.0 (C-11), 82.8 (C-9), 79.5 (C-7), 74.9 (C-9), 43.7 (C-2), 33.7 (C-6), 28.7 (C-4), 26.9 (C-12/C-13), 25.7 (C-12/C-13), 24.7 (C-3), 21.8 (C-5); **HRMS** (ESI-TOF, +): m/z calcd. for $\text{C}_{13}\text{H}_{20}\text{O}_5\text{Na}$ $[\text{M}+\text{Na}]^+$ 279.1203, found 279.1201.

5-(5-Methylhexylsulfonyl)-1-phenyl-1H-tetrazole (113)

The synthesis of **113** was performed according to a literature known procedure.^[181] Commercially available 5-methyl-1-hexanol (500 mg, 4.30 mmol, 1.00 eq.) and PPh₃ (2.26 g, 8.61 mmol, 2.00 eq.) were added to a solution of 1-phenyltetrazole-5-thiol (**139**) (1.53 g, 8.61 mmol, 2.00 eq.) in anhydrous THF (30 mL). DIAD (1.69 mL, 8.61 mmol, 2.00 eq.) was added at 0 °C. The reaction mixture was stirred at room temperature for 2 h. TLC showed complete conversion of the starting material. The crude product was purified *via* flash column chromatography (0-30% ethyl acetate in *n*-heptane).

The obtained sulfide was dissolved in DCM (30 mL). At 0 °C, *m*-CPBA (70%, 3.00 g, 12.2 mmol, 3.00 eq.) was added slowly. After stirring overnight at room temperature, LC-MS showed complete conversion of the starting material. The mixture was quenched by adding saturated aqueous Na₂SO₃ (50 mL) and extracted with diethyl ether (2 x 150 mL). The combined organic layers were washed with 1 M NaOH (2 x 80 mL) and saturated aqueous NaCl (100 mL), dried over MgSO₄, filtered and concentrated under reduced pressure. Purification was achieved by flash column chromatography (0-30% ethyl acetate in *n*-heptane) to give **113** (1.20 g, 3.91 mmol, 96% over two steps) as colorless oil. NMR data was in good agreement with literature.^[239]

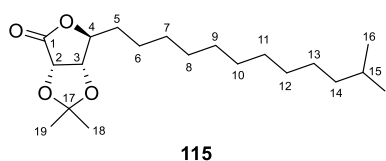
R_f (*n*-heptane/ethyl acetate 4:1): 0.37; **¹H-NMR** (400 MHz, CDCl₃): δ = 7.73–7.66 (m, 2H), 7.66–7.56 (m, 3H), 3.78–3.70 (m, 2H), 2.00–1.88 (m, 2H), 1.63–1.44 (m, 3H), 1.28–1.19 (m, 2H), 0.89 (s, 3H), 0.87 (s, 3H); **¹³C-NMR** (101 MHz, CDCl₃): δ = 153.7, 133.2, 131.6, 129.9, 125.2, 56.2, 38.2, 27.8, 26.1, 22.6, 22.6, 22.3; **HRMS** (ESI-TOF, +): *m/z* calcd. for C₁₄H₂₁N₄O₂S [M+H]⁺ 309.1380, found 309.1378.

(3a*S*,6*S*,6a*S*)-2,2-dimethyl-6-(11-methyldodec-6-en-1-yl)dihydrofuro[3,4-*d*][1,3]dioxol-4(3a*H*)-one (114)

The reaction was carried out in moisture-free glassware under inert atmosphere. To a suspension of **113** (524 mg, 1.70 mmol, 1.20 eq.) in anhydrous THF (10 mL), KHDMS (0.7 M in toluene, 2.43 mL, 1.70 mmol, 1.20 eq.) was added at -55 °C. After stirring at -55 °C for 70 min, **112** (364 mg, 1.42 mmol, 1.00 eq.) in anhydrous THF (1 mL) was added. After stirring at -55 °C for 1 h, TLC and LC-MS indicated complete conversion of the starting material. The mixture was quenched with saturated aqueous NH₄Cl (15 mL) and extracted with ethyl acetate (2 x 100 mL). The combined organic layers were washed with saturated aqueous NaCl (50 mL), dried (MgSO₄), filtered and concentrated under reduced pressure. The crude product was applied onto silica gel and pre-purified by flash column chromatography (0-30% ethyl acetate in *n*-heptane). Final purification was achieved *via* flash column chromatography (0-30% ethyl acetate in *n*-heptane) and yielded **114** (171 mg, 0.505 mmol, 36%) as colorless oil.

R_f (*n*-heptane/ethyl acetate 4:1): 0.30; **¹H-NMR** (400 MHz, CDCl₃): δ = 5.45–5.28 (m, 2H, H-10, H-11), 4.73 (d, *J* = 5.7 Hz, 1H, H-2), 4.54 (dd, *J* = 7.4, 6.2 Hz, 1H, H-4), 4.52 (d, *J* = 5.4 Hz, 1H, H-3), 2.07–1.89 (m, 4H, H-9, H-12), 1.72–1.47 (m, 3H, H-5, H-15), 1.48 (s, 3H, H-18), 1.48–1.24 (m, 8H, H-6, H-7, H-8, H-13), 1.38 (s, 3H, H-18), 1.23–1.10 (m, 2H, H-14), 0.87 (s, 3H, H-16), 0.85 (s, 3H, H-16); **¹³C-NMR** (101 MHz, CDCl₃): δ = 173.9 (C-1), 131.0 (C-10/C-11), 129.9 (C-10/-11), 114.0 (C-17), 83.0 (C-4), 79.6 (C-3), 75.0 (C-2), 38.7 (C-14), 33.9 (C-5), 33.0/32.5 (C-9, C-12), 29.4 (CH₂), 28.7 (CH₂), 28.0 (C-15), 27.6 (CH₂), 26.9 (C-18/C-19), 25.8 (C-18/C-19), 24.7 (CH₂), 22.8 (C-16); **HRMS** (ESI-TOF, +): *m/z* calcd. for C₂₀H₃₅O₄ [M+H]⁺ 339.2530, found 339.2526.

(3a*S*,6*S*,6a*S*)-2,2-dimethyl-6-(11-methyldodecyl)dihydrofuro[3,4-*d*][1,3]dioxol-4(3a*H*)-one (115)



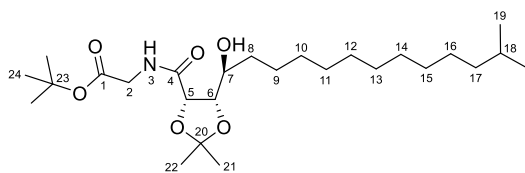
115

The synthesis of **115** was performed by a cooperation partner. Under argon atmosphere, Pd/C was added to **114** (171 mg, 0.505 mmol, 1.00 eq.) in THF (20 mL). The mixture was hydrogenated overnight at 4 bar using an autoclave and then

filtered through Celite®. The solvent was evaporated *in vacuo* to give **115** (178 mg, 0.523 mmol, quant.) as colorless, crystalline solid.

R_f (*n*-heptane/ethyl acetate 4:1): 0.34; [α]_D^{23.7} +24.4 (*c* 1.35, CHCl₃); **¹H-NMR** (400 MHz, CDCl₃): δ = 4.74 (d, *J* = 5.7 Hz, 1H, H-2), 4.54 (dd, *J* = 7.5, 6.2 Hz, 1H, H-4), 4.52 (d, *J* = 5.6 Hz, 1H, H-3), 1.69–1.56 (m, 2H, H-5), 1.57–1.49 (m, 1H, H-15), 1.48 (s, 3H, H-18), 1.45–1.20 (m, 16H, H-6–H-13), 1.38 (s, 3H, H-18), 1.19–1.09 (m, 2H, H-14), 0.87 (s, 3H, H-16), 0.85 (s, 3H, H-16); **¹³C-NMR** (101 MHz, CDCl₃): δ = 194.0 (C-1), 114.0 (C-17), 83.0 (C-4), 79.6 (C-3), 75.0 (C-2), 39.2 (C-14), 33.9 (C-5), 30.1 (CH₂), 29.8 (CH₂), 29.7 (CH₂), 29.6 (CH₂), 29.5 (CH₂), 29.3 (CH₂), 28.1 (C-15), 27.5 (CH₂), 26.9 (C-18/C-19), 25.8 (C-18/C-19), 24.8 (CH₂), 22.8 (C-16); **HRMS** (ESI-TOF, +): *m/z* calcd. for C₂₀H₃₇O₄ [M+H]⁺ 341.2686, found 341.2684.

***tert*-butyl ((4*S*,5*S*)-5-((*S*)-1-hydroxy-12-methyltridecyl)-2,2-dimethyl-1,3-dioxolane-4-carbonyl)glycinate (116a)**



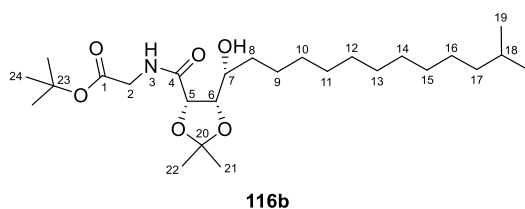
116a

116a was synthesized identical to **106a** starting from **115** (178 mg, 0.523 mmol). The crude product was purified by flash column chromatography (0–60% ethyl acetate in *n*-heptane) to yield **116a** (205 mg, 0.435 mmol, 85%) as colorless oil.

R_f (*n*-heptane/ethyl acetate 2:1): 0.41; [α]_D^{24.1} +1.3 (*c* 0.79, CHCl₃); **¹H-NMR** (400 MHz, CDCl₃): δ = 7.34 (t, *J* = 5.3 Hz, 1H, 3-NH), 4.65 (s, br, 1H, 7-OH), 4.62 (d, *J* = 7.2 Hz, 1H, H-5), 4.19 (dd, *J* = 9.3, 7.2 Hz, 1H, H-6), 4.04 (dd, *J* = 18.4, 5.7 Hz, 1H, H-2), 3.90 (dd, *J* = 18.4, 4.7 Hz, 1H, H-2), 3.50 (td, *J* = 9.0, 2.4 Hz, 1H, H-7), 1.81–1.18 (m, 19H, H-8–H-16, H-18), 1.61 (s, 3H, H-21/H-22), 1.48 (s, 9H, H-24), 1.39

(s, 3H, H-21/H-22), 1.19–1.10 (m, 2H, H-17), 0.86 (s, 3H, H-19), 0.85 (s, 3H, H-19); $^{13}\text{C-NMR}$ (101 MHz, CDCl_3): δ = 172.1 (C-4), 168.2 (C-1), 110.5 (C-20), 82.9 (C-23), 81.7 (C-6), 77.4 (C-5), 70.4 (C-7), 41.9 (C-2), 39.2 (C-17), 34.1 (C-8), 30.9 (CH_2), 29.9 (CH_2), 29.9 (CH_2), 29.8 (CH_2), 29.8 (CH_2), 29.8 (CH_2), 28.2 (C-24), 28.1 (C-18), 27.6 (CH_2), 27.2 (C-21/C-22), 25.2 (CH_2), 24.8 (C-21/C-22), 22.8 (C-19); **HRMS** (ESI-TOF, +): m/z calcd. for $\text{C}_{26}\text{H}_{50}\text{NO}_6$ $[\text{M}+\text{H}]^+$ 472.3633, found 472.3635.

***tert*-butyl ((4*S*,5*S*)-5-((*R*)-1-hydroxy-12-methyltridecyl)-2,2-dimethyl-1,3-dioxolane-4-carbonyl)glycinate (**116b**)**

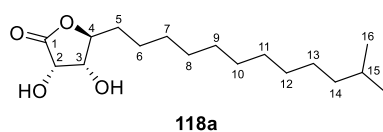


To a suspension of **116a** (97.1 mg, 0.206 mmol, 1.00 eq.) in DCM (5 mL), DMP (15% in DCM, 0.855 mL, 0.424 mmol, 2.06 eq.) was added. The reaction mixture was stirred at room temperature for 2 h. As TLC showed incomplete conversion of the starting material,

DMP (2 x 2.00 eq.) was added. After stirring overnight, almost complete conversion was observed by TLC. The reaction solution was filtered through a short silica column (100% DCM, 10 g silica) and concentrated under reduced pressure.

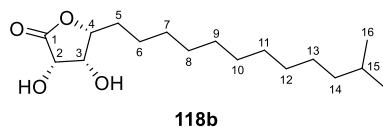
The obtained crude product was dissolved in abs. ethanol (5 mL) and NaBH_4 (14.4 mg, 0.381 mmol, 1.85 eq.) was added. After stirring at room temperature for 30 min, saturated aqueous NH_4Cl (15 mL) was added. The mixture which was extracted with ethyl acetate (2 x 50 mL). The organic layer was washed with saturated aqueous NaCl (30 mL), dried over MgSO_4 , filtered and concentrated under reduced pressure. The crude product was pre-purified by flash column chromatography (0–50% ethyl acetate in *n*-heptane) and finally purified by flash column chromatography (0–35% ethyl acetate in *n*-heptane) to give **116b** (16.0 mg, 33.9 μmol , 14% over two steps) as colorless oil.

R_f (*n*-heptane/ethyl acetate 2:1): 0.34; $[\alpha]_{\text{D}}^{21.1}$ –2.0 (*c* 0.50, CHCl_3); $^1\text{H-NMR}$ (400 MHz, CDCl_3): δ = 7.09 (t, J = 5.6 Hz, 1H, 3-NH), 4.58 (d, J = 8.0 Hz, 1H, H-5), 4.33 (dd, J = 8.0, 2.0 Hz, 1H, H-6), 4.05 (dd, J = 18.2, 5.9 Hz, 1H, H-2), 3.84 (dd, J = 18.2, 5.3 Hz, 1H, H-2), 3.89–3.79 (m, 1H, H-7), 2.70 (d, J = 7.6 Hz, 1H, 7-OH), 1.62 (s, 3H, H-21/H-22), 1.58–1.42 (m, 4H, H-8, H-16, H-18), 1.47 (s, 9H, H-24), 1.39 (s, 3H, H-21/H-22), 1.37–1.18 (m, 15H, H-9–H-16), 1.18–1.08 (m, 2H, H-17), 0.86 (s, 3H, H-19), 0.84 (s, 3H, H-19); $^{13}\text{C-NMR}$ (101 MHz, CDCl_3): δ = 170.5 (C-4), 169.2 (C-1), 109.9 (C-20), 82.8 (C-23), 80.4 (C-6), 76.3 (C-5), 68.6 (C-7), 41.7 (C-2), 39.2 (C-17), 34.6 (C-8), 30.1 (CH_2), 29.9 (CH_2), 29.8 (CH_2), 29.8 (CH_2), 29.8 (CH_2), 29.7 (CH_2), 28.2 (C-24), 28.1 (C-18), 27.6 (CH_2), 26.7 (C-21/C-22), 26.1 (CH_2), 24.8 (C-21/C-22), 22.8 (C-19); **HRMS** (ESI-TOF, +): m/z calcd. for $\text{C}_{26}\text{H}_{50}\text{NO}_6$ $[\text{M}+\text{H}]^+$ 472.3633, found 472.3635.

(3*S*,4*R*,5*S*)-3,4-dihydroxy-5-(11-methyldodecyl)dihydrofuran-2(3*H*)-one (118a)

118a was synthesized in analogous manner to **108a** starting from **116a** (51.4 mg, 0.109 mmol, 1.00 eq.). The crude product was dissolved in H₂O (15 mL) and extracted with diethyl ether (3 x 30 mL). The combined organic layers were washed with saturated aqueous NaCl (20 mL), dried over MgSO₄, filtered, and concentrated under reduced pressure to give **118a** (12.8 mg, 42.6 μmol, 39%) as colorless solid.

R_f (*n*-heptane/ethyl acetate 1:2): 0.42; $[\alpha]_{\text{D}}^{20.5} +10.7$ (*c* 0.28, MeOH); **¹H-NMR** (400 MHz, DMSO-*d*₆): δ = 5.74 (d, *J* = 7.4 Hz, 1H, 3-OH), 5.38 (d, *J* = 4.0 Hz, 1H, 2-OH), 4.40 (dd, *J* = 7.3, 5.1 Hz, 1H, H-2), 4.17 (dd, *J* = 8.0, 6.5 Hz, 1H, H-4), 3.95 (ddd, *J* = 5.0, 4.0, 1.0 Hz, 1H, H-3), 1.64–1.50 (m, 2H, H-5), 1.49 (sept, *J* = 6.4 Hz, 1H, H-15), 1.34–1.25 (m, 2H, H-6), 1.29–1.18 (m, 14H, H-7–H-13), 1.17–1.08 (m, 2H, H-14), 0.84 (d, *J* = 6.6 Hz, 6H, H-16); **¹³C-NMR** (101 MHz, DMSO-*d*₆): δ = 175.9 (C-1), 84.8 (C-4), 71.0 (C-3), 68.2 (C-2), 38.5 (C-14), 31.6 (C-5), 29.3 (CH₂), 29.1 (CH₂), 29.0 (CH₂), 29.0 (CH₂), 28.9 (CH₂), 28.6 (CH₂), 27.4 (C-15), 26.8 (CH₂), 25.2 (C-6), 22.5 (C-16); **HRMS** (ESI-TOF, +): *m/z* calcd. for C₁₇H₃₃O₄ [M+H]⁺ 301.2373, found 301.2374.

(3*S*,4*R*,5*R*)-3,4-dihydroxy-5-(11-methyldodecyl)dihydrofuran-2(3*H*)-one (118b)

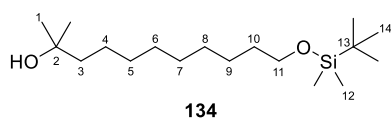
In analogous manner to **118a**, **118b** (8.26 mg, 27.5 μmol, quant.) was synthesized starting from **116b** (12.8 mg, 27.1 μmol).

R_f (*n*-heptane/ethyl acetate 1:2): 0.37; $[\alpha]_{\text{D}}^{20.5} +29.1$ (*c* 0.38, MeOH); **¹H-NMR** (400 MHz, DMSO-*d*₆): δ = 5.73 (d, *J* = 7.5 Hz, 1H, 3-OH), 5.26 (d, *J* = 4.1 Hz, 1H, 2-OH), 4.41 (dd, *J* = 7.5, 4.6 Hz, 1H, H-2), 4.28 (td, *J* = 7.0, 2.5 Hz, 1H, H-4), 4.08 (dd, *J* = 7.2, 4.4 Hz, 1H, H-3), 1.61 (non, *J* = 6.9 Hz, 2H, H-5), 1.49 (sept, *J* = 6.7 Hz, 1H, H-15), 1.34–1.26 (m, 2H, H-6), 1.28–1.18 (m, 14H, H-7–H-13), 1.17–1.09 (m, 2H, H-14), 0.84 (d, *J* = 6.6 Hz, 6H, H-16); **¹³C-NMR** (101 MHz, DMSO-*d*₆): δ = 176.2 (C-1), 79.7 (C-4), 70.8 (C-3), 69.8 (C-2), 38.5 (C-14), 29.3 (CH₂), 29.1 (CH₂), 29.0 (CH₂), 29.0 (CH₂), 28.9 (CH₂), 28.9 (CH₂), 28.1 (C-5), 27.4 (C-15), 26.8 (CH₂), 24.5 (C-6), 22.5 (C-16); **HRMS** (ESI-TOF, +): *m/z* calcd. for C₁₇H₃₃O₄ [M+H]⁺ 301.2373, found 301.2375.

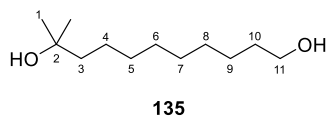
11-((*tert*-butyldimethylsilyloxy)-2-methylundecan-2-ol (134) and 10-methylundecane-1,10-diol (135)

The synthesis of **134** was performed by a cooperation partner starting from commercially available 10-hydroxydecanoic acid (**132**) (10.0 g, 53.1 mmol, 1.00 eq.) over three steps. The received crude product was purified *via* flash column chromatography (0–100% ethyl acetate in *n*-heptane) to give **134** (4.42 g, 14.0 mmol, 26% over three steps) and **135** (6.65 g, 32.9 mmol, 62% over three steps) as colorless oils.

7. Experimental

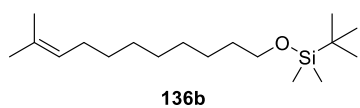
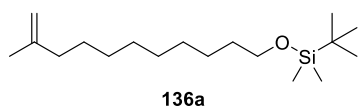


R_f (*n*-heptane/ethyl acetate 4:1): 0.28; **¹H-NMR** (400 MHz, CDCl₃): δ = 3.59 (t, *J* = 6.7 Hz, 2H, H-11), 1.55–1.48 (m, 2H, H-10), 1.51–1.41 (m, 2H, H-9), 1.38–1.31 (m, 2H, H-3), 1.36–1.29 (m, 2H, H-8), 1.33–1.26 (m, 8H, H-4–H-7), 1.20 (s, 6H, H-1), 0.89 (s, 9H, H-14), 0.05 (s, 6H, H-12); **¹³C-NMR** (101 MHz, CDCl₃): δ = 71.2 (C-2), 63.5 (C-11), 44.2 (C-9), 33.0 (C-10), 30.3 (CH₂), 29.7 (CH₂), 29.7 (CH₂), 29.6 (CH₂), 29.4 (C-1), 26.1 (C-14), 25.9 (C-8), 24.5 (C-3), 18.5 (C-13), –5.1 (C-12); **HRMS** (ESI-TOF, +): *m/z* calcd. for C₁₈H₃₉OSi [M–H₂O+H]⁺ 299.2765, found 299.2764.



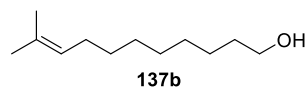
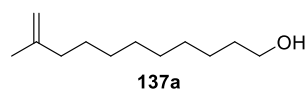
R_f (*n*-heptane/ethyl acetate 1:1): 0.21; **¹H-NMR** (400 MHz, CDCl₃): δ = 3.63 (t, *J* = 6.6 Hz, 2H, H-11), 1.56 (quin, *J* = 6.8 Hz, 2H, H-10), 1.49–1.40 (m, 2H, H-9), 1.43–1.36 (m, 2H, H-3), 1.37–1.24 (m, 10H, H-4–H-8), 1.20 (s, 6H, H-1); **¹³C-NMR** (101 MHz, CDCl₃): δ = 71.2 (C-2), 63.2 (C-11), 44.1 (C-9), 32.9 (C-10), 30.3 (CH₂), 29.7 (CH₂), 29.7 (CH₂), 29.5 (CH₂), 29.3 (C-1), 25.9 (CH₂), 24.5 (C-3); **HRMS** (ESI-TOF, +): *m/z* calcd. for C₁₂H₂₅O [M–H₂O+H]⁺ 185.1900, found 185.1898.

***tert*-butyldimethyl((10-methylundec-10-en-1-yl)oxy)silane (136a) and *tert*-butyldimethyl((10-methylundec-9-en-1-yl)oxy)silane (136b)**



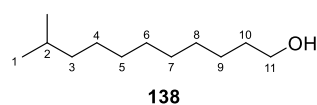
To a suspension of **134** (3.79 g, 12.0 mmol, 1.00 eq.) in anhydrous DCM (60 mL), NEt₃ (4.97 mL, 35.9 mmol, 3.00 eq.) and 4-dimethylaminopyridine (DMAP, 58.1 mg, 0.476 mmol, 0.04 eq.) were added. At 0 °C, mesyl chloride (MsCl, 1.39 mL, 18.0 mmol, 1.50 eq.) was then added. Since incomplete conversion of the starting material was observed after stirring for 1.5 h at room temperature, additional MsCl (1.00 eq.) was added at 0 °C. After stirring for 1.5 h at room temperature, complete conversion of the starting material was observed by TLC. The reaction mixture was quenched by adding H₂O (14 mL) and stirring for 10 min. Aqueous citric acid (10% (w/v), 75 mL) and extracted with diethyl ether (200 mL). The organic layer was washed with saturated aqueous NaHCO₃ (75 mL), saturated aqueous NaCl (75 mL), dried (MgSO₄), filtered and concentrated under reduced pressure. Of the obtained crude product (3.53 g), only a small portion (51.5 mg) was purified by flash column chromatography (0–4% ethyl acetate in *n*-heptane) to give an inseparable mixture of **136a** and **136b** (37.9 mg; 8.70 mmol, 73%) as colorless oil.

R_f (*n*-heptane/ethyl acetate 60:1): 0.19 / 0.26; **HRMS** (ESI-TOF, +): *m/z* calcd. for C₁₈H₃₉OSi [M+H]⁺ 299.2765, found 299.2766.

10-methylundec-10-en-1-ol (137a) and 10-methylundec-9-en-1-ol (137b)

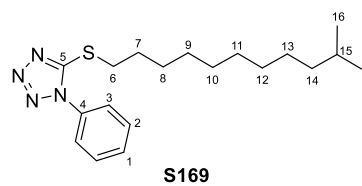
137a and **137b** were synthesized identical to **105b** (condition 1) starting from the mixture of **135a** and **135b** (3.48 g, 11.7 mmol). The crude product was purified by flash column chromatography (0–50% ethyl acetate in *n*-heptane) to yield the inseparable mixture of **137a** and **137b** (1.91 g, 10.4 mmol, 89%) as colorless oil.

R_f (*n*-heptane/ethyl acetate 2:1): 0.41 / 0.45; **HRMS** (ESI-TOF, +): *m/z* calcd. for C₁₂H₂₅O [M+H]⁺ 185.1900, found 185.1899.

10-Methylundecan-1-ol (138)

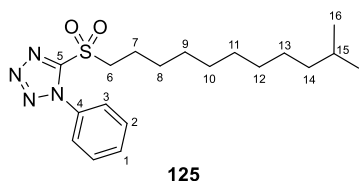
The synthesis of **138** was performed by a cooperation partner. Under argon atmosphere, Pd/C was added to **137a/137b** (2.15 g, 11.7 mmol, 1.00 eq.) in THF (200 mL). The mixture was hydrogenated overnight at 4 bar using an autoclave and then filtered through Celite®. The filtrate was concentrated under reduced pressure. The crude product was purified by flash column chromatography (0–40% ethyl acetate in *n*-heptane) to give **138** (1.16 g, 6.23 mmol, 53%) and as colorless oil.

R_f (*n*-heptane/ethyl acetate 4:1): 0.29; **¹H-NMR** (400 MHz, CDCl₃): δ = 3.64 (t, *J* = 6.7 Hz, 2H, H-11), 1.61–1.52 (m, 2H, H-10), 1.51 (sept, 1H, H-2), 1.39–1.29 (m, 2H, H-9), 1.34–1.22 (m, 10H, H-4–H-8), 1.34–1.22 (m, 2H, H-3), 0.86 (d, *J* = 6.6 Hz, 6H, H-1); **¹³C-NMR** (101 MHz, CDCl₃): δ = 63.3 (C-11), 39.2 (C-3), 33.0 (C-10), 30.0 (CH₂), 29.8 (CH₂), 29.6 (CH₂), 28.1 (C-2), 27.6 (CH₂), 25.9 (C-9), 22.8 (C-1); **HRMS** (ESI-TOF, +): *m/z* calcd. for C₁₂H₂₅ [M–H₂O+H]⁺ 169.1951, found 169.1951.

5-((10-Methylundecyl)thio)-1-phenyl-1H-tetrazole (S169)

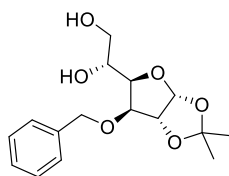
The sulfide **S169** was synthesized as previously described for the first reaction in the synthesis towards **113** starting from **139** (1.02 g, 5.46 mmol, 1.00 eq.). The crude product was purified by flash chromatography (0–30% ethyl acetate in *n*-heptane) to give **S169** (1.72 g, 4.96 mmol, 91%) and as colorless oil.

R_f (*n*-heptane/ethyl acetate 4:1): 0.45; **¹H-NMR** (400 MHz, CDCl₃): δ = 7.62–7.50 (m, 5H, H-1, H-2, H-3), 3.39 (t, *J* = 7.3 Hz, 2H, H-6), 1.81 (quin, *J* = 7.5 Hz, 2H, H-7), 1.51 (sept, 1H, H-15), 1.48–1.39 (m, 2H, H-8), 1.36–1.20 (m, 10H, H-9–H-13), 1.19–1.10 (m, 2H, H-14), 0.86 (d, *J* = 6.6 Hz, 6H, H-16); **¹³C-NMR** (101 MHz, CDCl₃): δ = 154.7 (C-5), 133.9 (C-4), 130.2 (C-1), 129.9 (C-2), 124.0 (C-3), 39.2 (C-14), 33.5, (C-6), 30.0 (CH₂), 29.7 (CH₂), 29.6 (CH₂), 29.2 (CH₂), 29.2 (C-7), 28.8 (C-8), 28.1 (C-15), 27.5 (CH₂), 22.8 (C-16); **HRMS** (ESI-TOF, +): *m/z* calcd. for C₁₉H₃₁N₄S [M+H]⁺ 347.2264, found 347.2265.

5-((10-Methylundecyl)sulfonyl)-1-phenyl-1H-tetrazole (**125**)**125**

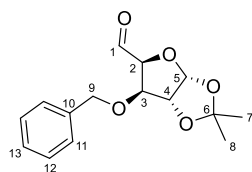
The sulfone **125** was synthesized as previously described for the second step in the synthesis towards **113** starting from **S169** (1.71 g, 4.93 mmol, 1.00 eq.). The crude product was purified by flash chromatography (0–25% ethyl acetate in *n*-heptane) to obtain **125** (1.79 g, 4.73 mmol, 96%) and as colorless oil.

R_f (*n*-heptane/ethyl acetate 4:1): 0.43; **¹H-NMR** (400 MHz, CDCl₃): δ = 7.72–7.67 (m, 2H, H-3), 7.64–7.55 (m, 3H, H-1, H-2), 3.73 (t, J = 8.0 Hz, 2H, H-6), 1.95 (quin, J = 7.8 Hz, 2H, H-7), 1.56–1.44 (m, 3H, H-8, H-15), 1.39–1.21 (m, 10H, H-9–H-13), 1.19–1.11 (m, 2H, H-14), 0.86 (d, J = 6.6 Hz, 6H, H-16); **¹³C-NMR** (101 MHz, CDCl₃): δ = 153.7 (C-5), 133.2 (C-4), 131.6 (C-1), 129.9 (C-2), 125.2 (C-3), 56.2 (C-6), 39.2 (C-14), 30.0 (CH₂), 29.6 (CH₂), 29.3 (CH₂), 29.1 (CH₂), 28.3 (C-8), 28.1 (C-15), 27.5 (CH₂), 22.8 (C-16), 22.1 (C-7); **HRMS** (ESI-TOF, +): *m/z* calcd. for C₁₉H₃₁N₄O₂S [M+H]⁺ 379.2162, found 379.2162.

(R)-1-((3aR,5R,6S,6aR)-6-(benzyloxy)-2,2-dimethyltetrahydrofuro[2,3-d][1,3]dioxol-5-yl)ethane-1,2-diol (127**)****127**

The synthesis of **127** was performed by a cooperation partner according to literature known procedure starting from D-glucose (**120**) over three steps. The analytical data were in accordance to the reported data in literature.^[185]

R_f (*n*-heptane/ethyl acetate 1:2): 0.38; [α]_D^{26.4} –12.6 (*c* 0.88, MeOH); **¹H-NMR** (400 MHz, CDCl₃): δ = 7.41–7.30 (m, 5H), 5.94 (d, J = 3.8 Hz, 1H), 4.74 (d, J = 11.8 Hz, 1H), 4.63 (d, J = 3.8 Hz, 1H), 4.55 (d, J = 11.6 Hz, 1H), 4.15–4.08 (m, 2H), 4.03 (ddd, J = 7.9, 5.2, 3.2 Hz, 1H), 3.81 (dd, J = 11.4, 3.5 Hz, 1H), 3.69 (dd, J = 11.5, 5.5 Hz, 1H), 2.16 (s, br, 2H), 1.49 (s, 3H), 1.32 (s, 3H); **¹³C-NMR** (101 MHz, CDCl₃): δ = 137.3, 128.9, 128.4, 128.1, 112.0, 105.3, 82.2, 82.2, 80.1, 72.3, 69.5, 64.6, 26.9, 26.4; **HRMS** (ESI-TOF, +): *m/z* calcd. for C₁₆H₂₂O₆Na [M+Na]⁺ 333.1309, found 333.1309.

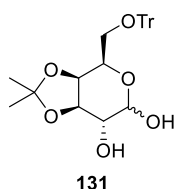
(3aR,5S,6S,6aR)-6-(benzyloxy)-2,2-dimethyltetrahydrofuro[2,3-d][1,3]dioxole-5-carbaldehyde (124**)****124**

In analogous manner to **112**, **124** (1.71 g, 6.14 mmol, quant.) was synthesized starting from **127** (1.86 g, 5.98 mmol) and obtained as yellowish oil without further purification.

R_f (*n*-heptane/ethyl acetate 1:2): 0.60; **¹H-NMR** (400 MHz, CDCl₃): δ = 9.68 (d, J = 1.5 Hz, 1H, H-1), 7.39–7.28 (m, 3H, H-12, H-13), 7.27–7.22 (m, 2H, H-11), 6.13 (d, J = 3.4 Hz, 1H, H-5), 4.65 (d, J = 3.5 Hz, 1H, H-2), 4.61 (d, J = 11.9 Hz, 1H, H-9), 4.57 (dd, J = 3.7, 1.5 Hz, 1H, H-4), 4.49 (d, J = 11.7 Hz, 1H, H-9), 4.34 (d, J = 3.8 Hz, 1H, H-3), 1.47 (s, 3H, H-7/H-8), 1.34 (s, 3H, H-7/H-8); **¹³C-NMR** (101 MHz, CDCl₃): δ = 200.1 (C-1), 136.8 (C-10), 128.7 (C-12), 128.4 (C-13), 127.9 (C-11), 112.8

(C-6), 106.4 (C-5), 84.8 (C-4), 83.9 (C-3), 82.4 (C-2), 72.6 (C-9), 27.1 (C-7/C-8), 26.5 (C-7/C-8); **HRMS** (ESI-TOF, +): m/z calcd. for $C_{15}H_{20}O_6Na$ $[M+H_2O+Na]^+$ 319.1152, found 319.1154.

(3a*S*,4*R*,7*R*,7a*R*)-2,2-dimethyl-4-((trityloxy)methyl)tetrahydro-4*H*-[1,3]dioxolo[4,5-*c*]pyran-6,7-diol (131)



The synthesis of **131** was performed over two steps according to literature known procedure.^[188] To a solution of D-galactose (**121**) (4.06 g, 22.5 mmol, 1.00 eq.) in anhydrous pyridine (60 mL), trityl chloride (TrCl, 6.59 g, 23.6 mmol, 1.05 eq.) was added. After stirring at 50 °C for 18 h, the reaction mixture was concentrated in vacuo. The obtained slurry crude product was dissolved in DCM and purified by chromatography through short silica column. The tritylated galactose was eluted with ethyl acetate and concentrated under reduced pressure.

The obtained crude product was dissolved in anhydrous acetone (150 mL) and CuSO₄ (20.0 g, 125 mmol, 5.56 eq.) was added. After stirring for 35 h at room temperature, the reaction mixture was filtered through Celite® and concentrated under reduced pressure. The crude product was pre-purified by flash chromatography (4.5 x 24 cm) using gradient elution (4:1, 2:1, 1:1, 1:2 *n*-heptane/ethyl acetate) to afford anomeric **131** (2.71 g, 5.86 mmol, 26% over two steps) as colorless oil.

R_f (*n*-heptane/ethyl acetate 1:1): 0.17 / 0.25; **HRMS** (ESI-TOF, +): m/z calcd. for $C_{28}H_{30}O_6Na$ $[M+Na]^+$ 485.1935, found 485.1933.

7.2.4 Antimycobacterial activity of *Streptomyces* sp. HAG010336

7.2.4.1 Media variation

A piece of agar plate (0.5 x 0.5 cm) *Streptomyces* sp. HAG010336 had grown on was used to inoculate 30 mL pre-culture medium 5254 in a 100 mL Erlenmeyer flask. After incubation on a rotary shaker at 180 rpm and 28 °C for 7 days, the pre-culture was multiplied by inoculation of 3 x 100 mL pre-culture medium in 300 mL Erlenmeyer flasks with 5 mL (5% inoculum) of the previous pre-culture. Incubation took place under the same conditions as before.

Of all media used, 100 mL was prepared in 300 mL Erlenmeyer flasks (of which one was baffled), inoculated with 5 mL (5% inoculum) pre culture and incubated on a rotary shaker at 180 rpm and 28 °C in most cases. Two flasks containing 5265 medium were shaken in an incubator at 240 rpm and 28 °C or at 180 rpm and 37 °C. At each time point (day 3, day 5, day 7, day 10 and day 14) a sample (4 mL) was transferred into a 24 well plate. This was also done for the non-inoculated media controls on day 14.

The 24-well plates were then freeze dried. Extraction was performed by adding 100vol% MeOH (4 mL) to each well. After shaking for 3 h and centrifugation, 2 x 1.25 mL MeOH extract was transferred subsequently into a 96 well MASTERBLOCK® which was dried in-between (GeneVac). The total MeOH extract volume of 2.50 mL per well was then re dissolved in 200 µL MeOH per well of which a 50 µL sample was analyzed by UPLC-MS (5 µL injection volume, maXis II).

Relative quantification was performed using the Compass QuantAnalysis (Version 4.4) software (BRUKER).

7.2.4.2 Cultivation and Extraction

Medium 5265: Precultures of *Streptomyces* sp. HAG010336 were prepared by inoculation of 30 mL pre-culture medium 5254 in a 100 mL Erlenmeyer flask with a 0.5 x 0.5 cm piece of agar plate the strain was previously grown on. Pre-cultures were multiplied by inoculation of 100 mL pre-culture medium in a 300 mL Erlenmeyer flask with 5 mL (5% inoculum) of a previous pre culture. Incubation took place on a rotary shaker at 180 rpm and 28 °C for 7 days. For both main culture batches (21 L and 18 L), 25 mL (5% inoculum) pre-culture was then used to inoculate each one of the 2 L Erlenmeyer flasks (42 x and 36 x) containing 0.5 L of the main-culture medium 5265. After incubation for 7 days on a rotary shaker at 180 rpm and 28 °C, the main culture was frozen and freeze dried.

The lyophilized culture was extracted with 80vol% MeOH and the combined MeOH extracts were dried under reduced to yield 51.5 g and 47.0 g respectively.

Medium SM25: Fermentation of both 20 L batches in SM25 medium was performed identically as described above except for incubation for 10 days instead.

After cultivation, 2 L portions of the culture were transferred into 5 L wide neck Schott Duran® glass bottles. 2 L ethyl acetate was added and after stirring for 30 min, the organic layer was vacuumed off and evaporated to dryness to yield 16.7 g and 14.5 g of crude extract.

7.2.4.3 Isolation and Purification

Medium 5265: Solid phase extraction was performed with the crude extracts (MCI system). Therefore, they were dissolved in 10% MeOH (5 L and 4 L) and applied onto a 1 L (6 cm x 50 cm) column packed with Amberlite® XAD-16N. Elution was done using a step gradient (10%, 40%, 60%, 80%, 100%) of MeOH in H₂O. Fractions containing the compound were combined and MeOH was removed under reduced pressure.

The aqueous phases were extracted two times with 100vol% ethyl acetate. The combined organic layers were concentrated under reduced pressure to give 2.74 g and 2.54 g, respectively.

Dissolved in MeOH ($c \approx 50$ mg/mL), the ethyl acetate extracts were fractionated *via* preparative RP-HPLC (Synergi™ Fusion RP 80 Å, 4 µm, 250 x 21.2 mm) using linear gradient elution of 5–95% ACN/H₂O + 0.1% FA (15 mL/min) over 25 min to yield 8.32 mg and 2.33 mg.

Further purification was achieved by semi-preparative HPLC (NUCLEODUR® C18 Gravity-SB, 3 µm, 250 x 4.6 mm) and linear gradient elution of 5–95% MeOH/H₂O + 0.1% FA (2 mL/min) over 40 min. Fractions containing the compound were combined.

Final purification was achieved by MS-guided UPLC fractionation (ACQUITY UPLC® BEH C18, 1.7 µm, 100 x 2.1 mm) using an adjusted linear gradient of 35–50% MeOH/H₂O + 0.1% FA (0.6 mL/min) over 17.45 min to yield 0.235 mg of SF009 (**isol-150**).

Medium SM25: The crude extract was dissolved in MeOH at a concentration of approx. 150 mg/mL to be fractionated by preparative RP-HPLC in analogous manner as described before to yield 29.8 mg and 67.3 mg respectively.

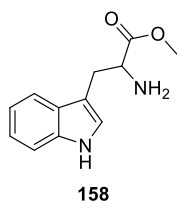
Further purification was achieved by semi-preparative HPLC (NUCLEODUR® C18 Gravity-SB, 3 µm, 250 x 4.6 mm) and an adjusted gradient of 35–70% ACN/H₂O + 0.1% FA (2 mL/min) over 15.5 min. Pure fractions were combined to yield 1.25 mg and 1.14 mg of SF009 (**isol-150**).

Separately combined impure fractions were purified in an additional step of MS-guided UPLC fractionation (ACQUITY UPLC® BEH C18, 1.7 µm, 100 x 2.1 mm) using linear gradient elution of 30–95% ACN/H₂O + 0.1% FA (0.6 mL/min) over 17 min. Additional 0.100 mg pure compound **isol-150** was obtained.

SF009 (isol-150): red-purple solid; LC-UV (ACN/H₂O) λ_{\max} 221, 274, 300, 377 nm; ¹H and ¹³C-NMR data: see Table 24; ESI-MS (positive ions): m/z 323.1025 [M+H]⁺, m/z 345.0845 [M+Na]⁺, m/z 667.1798 [2M+Na]⁺; HRMS (ESI-TOF, +): m/z calcd. for C₁₈H₁₅N₂O₅ [M+H]⁺ 323.1026, found 323.1025.

7.2.4.4 Total Synthesis of SF009 and Derivatives

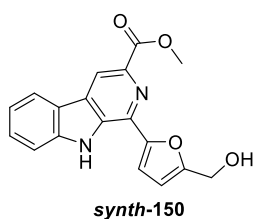
L-Tryptophan methyl ester (**158**)



The synthesis of **158** was performed according to a literature known procedure.^[214] L-tryptophan (**157**) (2.26 g, 11.1 mmol, 1.00 eq.) was dissolved in anhydrous MeOH (50 mL). Under ice-cooling, SOCl₂ (2.20 mL, 11.3 mmol, 1.02 eq.) was added dropwise. The mixture was stirred at room temperature for 5 h. After the reaction was completed, MeOH was removed under reduced pressure. The obtained residue was dissolved in saturated aqueous NaHCO₃ (25 mL) and the pH was adjusted to 9–10 using aqueous 1 M NaOH. The aqueous phase was extracted with ethyl acetate (3 x 80 mL) and the combined organic layers were washed with saturated aqueous NaCl (80 mL), dried over MgSO₄, filtered and concentrated under reduced pressure to yield **158** (2.39 g, 11.0 mmol, 99%) as colorless solid which was subsequently used without further purification.

LC-UV (ACN/H₂O): λ_{max} 218, 278 nm; **¹H-NMR** (400 MHz, CDCl₃): δ = 8.18 (s, br, 1H), 7.62 (d, J = 7.8 Hz, 1H), 7.36 (d, J = 8.0 Hz, 1H), 7.20 (t, J = 7.4 Hz, 1H), 7.13 (t, J = 7.4 Hz, 1H), 7.06 (s, br, 1H), 3.84 (dd, J = 7.7, 4.8 Hz, 1H), 3.72 (s, 3H), 3.29 (dd, J = 14.4, 4.8 Hz, 1H), 3.06 (dd, J = 14.4, 7.7 Hz, 1H); **¹³C-NMR** (101 MHz, CDCl₃): δ = 175.9, 136.4, 127.6, 123.0, 122.3, 119.7, 118.9, 111.4, 111.3, 55.1, 52.1, 30.9; **ESI-MS** (positive ions): m/z 202.0861 [M+NH₃]⁺, m/z 219.1126 [M+H]⁺, m/z 241.0945 [M+Na]⁺; **HRMS** (ESI-TOF, +) m/z calcd. for C₁₂H₁₅N₂O₂ [M+H]⁺ 219.1128, found 219.1126.

1-[5-(Hydroxymethyl)furan-2-yl]-3-carbomethoxy-9H-pyrido[3,4-b]indole (**150**)

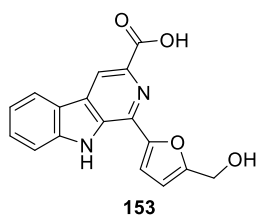


The synthesis of **150** was performed according to a literature known procedure.^[214] In the presence of 4 Å molecular sieves, **158** (2.18 g, 9.99 mmol, 1.00 eq.) was dissolved in anhydrous DCM (100 mL). TFA (0.20 mL, 2.60 mmol, 0.26 eq.) and 5-(hydroxymethyl)furfural (**159**) (1.00 mL, 10.2 mmol, 1.02 eq.) was added. After stirring for 24 h at room temperature, the solution was filtered through a frit packed with Celite[®] and washed with ethyl acetate. The solvent was evaporated under reduced pressure to give the crude diastereomeric mixture of **160** (3.52 g, 10.8 mmol, quant.) as deep red solid.

Without further purification **160** (2.01 g, 6.16 mmol, 1.00 eq.) was dissolved in DMF (15 mL). Et₃N (3.30 mL 23.8 mmol, 3.87 eq.) was added. The reaction mixture was cooled to -10 °C before trichlorocyanuric acid (TCCA, 2.02 g, 8.69 mmol, 1.41 eq.) in DMF (6 mL) was added slowly. After stirring for 1 h at 0 °C, H₂O (30 mL) was added and the aqueous phase was extracted with ethyl acetate (3 x 100 mL). The combined organic layers were washed with saturated aqueous NaCl (90 mL), dried over MgSO₄, filtered and concentrated under reduced pressure. The crude product was purified by silica gel column chromatography using gradient elution from 1:0 to 1:3 DCM/ethyl acetate to afford **150** (0.854 g, 2.65 mmol, 43% over two steps) as yellow amorphous powder.

R_f (ethyl acetate): 0.64; **LC-UV** (ACN/H₂O): λ_{\max} 219, 273, 299, 376 nm; **¹H-NMR** (400 MHz, CDCl₃): δ = 9.98 (s, 1H), 8.48 (s, 1H), 7.99 (d, J = 7.7 Hz, 1H), 7.51 (t, J = 7.4 Hz, 1H), 7.47 (t, J = 7.5 Hz, 1H), 7.29 (d, J = 7.5 Hz, 1H), 7.21 (d, J = 3.4 Hz, 1H), 6.34 (d, J = 3.3 Hz, 1H), 4.76 (s, 2H), 4.02 (s, 3H); **¹³C-NMR** (101 MHz, CDCl₃): δ = 166.7, 154.9, 153.2, 141.0, 137.0, 133.1, 132.6, 130.1, 129.0, 121.7, 121.4, 121.0, 116.4, 112.3, 110.8, 110.6, 57.6, 52.7; **ESI-MS** (positive ions): m/z 323.1026 [M+H]⁺, m/z 345.0844 [M+Na]⁺, m/z 667.1796 [2M+Na]⁺; **HR-MS** (ESI-TOF, +): m/z calcd. for C₁₈H₁₅N₂O₄ [M+H]⁺ 323.1026, found 323.1026.

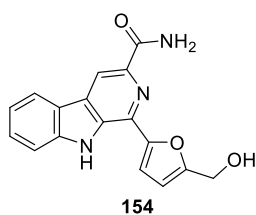
1-[5-(Hydroxymethyl)furan-2-yl]-9H-pyrido[3,4-b]indolo-3-carboxylic acid (**153**)



To a solution of **150** (0.194 g, 0.602 mmol, 1.00 eq.) in MeOH (15 mL), 2 M NaOH (1.5 mL) was added. After heating to reflux for 1 h, the mixture was allowed to cool to room temperature, acidified to pH 5–6 by adding 2 M HCl (approx. 1.5 mL), diluted with H₂O (20 mL) and extracted with ethyl acetate (3 x 120 mL). The combined organic layers were washed with saturated aqueous NaCl (100 mL), dried over MgSO₄, filtered and concentrated under reduced pressure to give **153** (0.168 g, 0.545 mmol, 90%) as yellow solid.

LC-UV (ACN/H₂O): λ_{\max} 219, 289, 353, 380, 412 nm; **¹H-NMR** (400 MHz, DMSO-*d*₆): δ = 12.69 (s, br, 1H), 11.58 (s, 1H), 8.85 (s, 1H), 8.42 (d, J = 7.8 Hz, 1H), 7.82 (d, J = 8.3 Hz, 1H), 7.65 (t, J = 7.3 Hz, 1H), 7.43 (d, J = 3.2 Hz, 1H), 7.35 (t, J = 7.4 Hz, 1H), 6.63 (d, J = 3.3 Hz, 1H), 5.49 (s, br, 1H), 4.69 (s, 2H); **¹³C-NMR** (101 MHz, DMSO-*d*₆): δ = 166.4, 157.3, 151.2, 141.4, 137.0, 132.5, 131.9, 129.8, 129.0, 122.0, 121.0, 120.6, 115.7, 112.8, 111.1, 109.2, 56.0; **ESI-MS** (positive ions): m/z 309.0869 [M+H]⁺; **HR-MS** (ESI-TOF, +): m/z calcd. for C₁₇H₁₃N₂O₄ [M+H]⁺ 309.0870, found 309.0869.

1-[5-(Hydroxymethyl)furan-2-yl]-9H-pyrido[3,4-b]indolo-3-carboxamide (**154**)

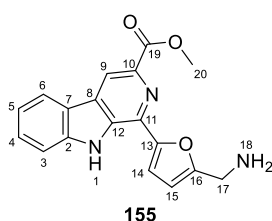


To a solution of **153** (0.101 g, 0.328 mmol, 1.00 eq.) in DMF (2 mL), Oxyma (70.5 mg, 0.568 mmol, 1.70 eq.), EDC · HCl (0.124 g, 0.647 mmol, 1.97 eq.), NaHCO₃ (0.272 g, 3.24 mmol, 9.82 eq.) and NH₄Cl (0.173 g, 3.23 mmol, 9.78 eq.) were added successively at 0 °C. After stirring for 1.5 h at room temperature, saturated aqueous NaHCO₃ (30 mL) was added and the aqueous phase extracted with ethyl acetate (2 x 100 mL). The combined organic layers were washed with 10% aqueous citric acid (40 mL) and saturated aqueous NaCl (40 mL), dried over MgSO₄, filtered and evaporated to yield 95.4 mg crude product. For analytical purposes and bioactivity screening, a small amount was purified by semi-preparative RP-HPLC using a C18 column (NUCLEODUR® C18 Gravity-SB, 3 μ m, 250 x 4.6 mm) and linear gradient elution of 5–95% ACN/H₂O + 0.1% FA (2 mL/min) over 19 min. Pure fractions were combined to yield **154** as yellow solid.

R_f (DCM/MeOH 9:1): 0.49; **LC-UV** (ACN/H₂O): λ_{\max} 217, 274, 298, 379 nm; **¹H-NMR** (400 MHz, DMSO-*d*₆): δ = 11.47 (s, 1H), 8.76 (s, 1H), 8.40 (d, J = 7.8 Hz, 1H), 8.24 (d, J = 2.4 Hz, 1H), 7.81 (d,

δ = 8.2 Hz, 1H), 7.64 (t, J = 7.4 Hz, 1H), 7.60 (d, J = 3.4 Hz, 1H), 7.56 (d, J = 2.4 Hz, 1H), 7.33 (t, J = 7.4 Hz, 1H), 6.62 (d, J = 3.3 Hz, 1H), 5.47 (t, J = 5.9 Hz, 1H), 4.69 (d, J = 5.0 Hz, 2H); $^{13}\text{C-NMR}$ (101 MHz, DMSO- d_6): δ = 166.6, 157.2, 151.6, 141.4, 139.7, 131.5, 131.4, 130.2, 128.8, 122.0, 121.1, 120.3, 112.7, 112.5, 111.0, 109.1, 56.0; **ESI-MS** (positive ions): m/z 308.1030 $[\text{M}+\text{H}]^+$; m/z 330.0850 $[\text{M}+\text{Na}]^+$; **HR-MS** (ESI-TOF, +): m/z calcd. for $\text{C}_{17}\text{H}_{14}\text{N}_3\text{O}_3$ $[\text{M}+\text{H}]^+$ 308.1030, found 308.1030.

1-[5-(Aminomethyl)furan-2-yl]-3-carbomethoxy-9H-pyrido[3,4-b]indole (**155**)

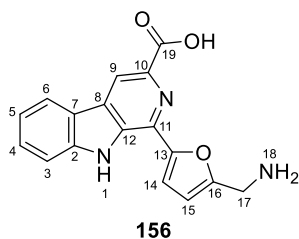


To a solution of **150** (0.854 g, 2.65 mmol, 1.00 eq.) in anhydrous DCM (30 mL) was cooled to 0 °C before SOCl_2 (0.58 mL, 7.99 mmol, 3.02 eq.) was added slowly. The reaction mixture was stirred for 2 h at room temperature before the solvent was removed under reduced pressure to yield chloride **161** of the as a brown solid.

Without purification, **161** was dissolved in DMF (4 mL). After adding NaN_3 (0.258 g, 3.97 mmol, 1.50 eq.) the solution was stirred at 60 °C for 1 h. At room temperature, saturated aqueous NaHCO_3 (50 mL) was added and the aqueous phase extracted with ethyl acetate (2 x 150 mL). The combined organic layers were washed with saturated aqueous NaCl (50 mL), dried over MgSO_4 , filtered and evaporated to dryness to yield **162** as a brown oil.

To a solution of **162** in THF/ H_2O 10:1 (11 mL), PPh_3 (0.771 g, 2.94 mmol, 1.11 eq.) was added. After stirring at room temperature for 3 h, LC-MS showed a full conversion of the starting material. However, a significant amount of intermediate formed imine was observed. 2 M HCl (3 mL) was added to the mixture to promote acidic hydrolysis. After stirring at room temperature for 2 h, very little effect was observed by LC-MS analysis. Therefore, the reaction mixture was then stirred in acetic acid (20 mL) at 40 °C for 3 h before being concentrated under reduced pressure. The crude product was purified by preparative HPLC (SynergiTM 4 μm Fusion-RP 80 Å, 50 x 21.1 mm) using linear gradient elution of 5–95% $\text{ACN}/\text{H}_2\text{O}$ + 0.1% FA (15 mL/min) over 24 min. Pure fractions were combined to give **155** (0.169 g, 0.526 mmol, 20% over three steps) as yellow solid.

R_f (DCM/MeOH 9:1): 0.13; **LC-UV** (ACN/ H_2O): λ_{max} 218, 274, 297, 375 nm; **$^1\text{H-NMR}$** (400 MHz, DMSO- d_6): δ = 12.19 (s, br, 1H, H-1), 8.87 (s, 1H, H-9), 8.43 (d, J = 7.8 Hz, 1H, H-6), 7.91 (d, J = 8.3 Hz, 1H, H-3), 7.65 (t, J = 7.3 Hz, 1H, H-4), 7.35 (t, J = 7.4 Hz, 1H), 7.27 (d, J = 3.4 Hz, 1H, H-14), 6.72 (d, J = 3.4 Hz, 1H, H-15), 4.18 (s, 2H, H-17), 3.94 (s, 3H, H-20); **$^{13}\text{C-NMR}$** (101 MHz, DMSO- d_6): δ = 165.7 (C-19), 153.4 (C-13), 141.6 (C-2), 136.5 (C-12), 132.5 (C-11), 131.9 (C-10), 129.7 (C-8), 128.9 (C-4), 122.0 (C-6), 120.8 (C-7), 120.6 (C-5), 116.4 (C-9), 112.9 (C-3), 110.7 (C-15), 110.5 (C-14), 52.1 (C-20), 36.6 (C-17); **ESI-MS** (positive ions): m/z 322.1187 $[\text{M}+\text{H}]^+$; m/z 305.0921 $[\text{M}-\text{NH}_4+\text{H}]^+$; m/z 344.1007 $[\text{M}+\text{Na}]^+$; m/z 665.2121 $[\text{2M}+\text{Na}]^+$; **HR-MS** (ESI-TOF, +): m/z calcd. for $\text{C}_{18}\text{H}_{16}\text{N}_3\text{O}_3$ $[\text{M}+\text{H}]^+$ 322.1186, found 322.1185.

1-[5-(Aminomethyl)furan-2-yl]-9H-pyrido[3,4-b]indolo-3-carboxylic acid (156)

155 (18.5 mg, 57.6 μmol , 1.00 eq.) was dissolved in MeOH (3 mL). After adding 1 M NaOH (1 mL), the reaction solution was heated to reflux for 1 h. The mixture was neutralized by adding 2 M HCl (0.5 mL) and subsequently evaporated to dryness. The crude product was taken purified by semi-preparative RP-HPLC using a C18 column (NUCLEODUR[®] C18 Gravity-SB, 3 μm , 250 x 4.6 mm) and linear gradient elution of 5–95% ACN/H₂O + 0.1% FA (2 mL/min) over 19 min. Pure fractions were combined to yield **56** (8.95 mg, 29.1 μmol , 50%) as yellow solid.

LC-UV (ACN/H₂O) λ_{max} 215, 289, 349, 378, 408 nm; **¹H-NMR** (400 MHz, DMSO-*d*₆): δ = 12.16 (s, br, 1H, H-1), 8.86 (s, 1H, H-9), 8.39 (d, J = 7.8 Hz, 1H, H-6), 8.04 (d, J = 8.6 Hz, 1H, H-3), 7.60 (t, J = 7.6 Hz, 1H, H-4), 7.44 (d, J = 3.4 Hz, 1H, H-14), 7.32 (t, J = 7.5 Hz, 1H, H-5), 6.82 (d, J = 3.2 Hz, 1H, H-15), 4.32 (s, 2H, H-17); **¹³C-NMR** (101 MHz, DMSO-*d*₆): δ = 166.7 (C-19), 153.1 (C-13), 149.8 (C-16), 141.7 (C-2), 137.7 (C-12), 131.7 (C-11), 131.7 (C-10), 130.0 (C-8), 128.8 (C-4), 121.9 (C-8), 120.8 (C-7), 120.5 (C-5), 116.0 (C-9), 113.3 (C-3), 112.6 (C-15), 110.6 (C-14), 35.5 (C-17); **ESI-MS** (positive ions): m/z 308.1030 [M+H]⁺; m/z 291.0765 [M-NH₄+H]⁺; **HR-MS** (ESI-TOF, +): m/z calcd. for C₁₇H₁₄N₃O₃ [M+H]⁺ 308.1030, found 308.1030.

7.2.4.4 MIC Determination

The in-house determination of MIC values was performed in triplicates ($n = 3$) according to GENERAL MATERIALS AND EXPERIMENTAL PROCEDURES (see 7.1.9). Isolated and synthesized compounds were provided as stock solutions of 12.8 mg/mL in DMSO. In the first screening of isolated SF009 (*isol-11*), growth inhibition was observed down to the last dilution for *S. aureus* MSSA, *B. subtilis* and *M. catarrhalis*. For these test strains, a second screening was performed with a stock solution concentration of 0.8 mg/mL. However, the sample appeared less active. Both runs were still taken into account to determine the MIC range noted (Table 25).

7.2.4.5 IC₈₀ Determination: *M. tuberculosis* H37Rv

Determination of the *in vitro* antibacterial activity against the virulent *M. tuberculosis* strain H37Rv (ATCC 27294) was performed by EVOTEC (Lyon, France). IC₈₀ values against *M. tuberculosis* H37Rv ATCC 27294 were determined *via* the Microplate Almar Blue Assay (MABA) as reported in literature, using the detection reagent provided with the CellTiter-Blue assay kit (PROMEGA).^[240] An EnVision fluorescence microplate reader (PERKINELMER USA) was used for readout.

7.2.4.6 Dereplication of Antimycobacterial Active Secondary Metabolites

Combining impure HPLC fractions yielded a pre-purified sample of SF009 ($m = 2.79$ mg) (Scheme 17). Dissolved in 210 μL MeOH, 2 μL and 5 μL were fractionated using the micrOTOF UPLC-MS system and the following method: mobile phase A: H_2O (+0.1% FA), mobile phase B: ACN (+0.1% FA), flow rate: 0.6 mL/min, gradient: 5.00% B (0.00–0.85 min), 5.00–95.25% B (0.85–18.30 min), 95.25–100.00% B (18.30–18.80 min), 100.00% B (18.80–23.30 min), 100.00–5.00% B (23.30–23.40 min), 5.00% B (23.40–25.00 min). Over a period of 19.2 min, 159 fractions (6 sec) were collected in a 384 well microtiter assay plate and screened against *M. smegmatis* according to GENERAL MATERIALS AND EXPERIMENTAL PROCEDURES (see 7.1.9). Furthermore, the same method was used to partition 10 x 5 μL of the sample into 79 fractions (6 sec) collected in a 96-well MASTERBLOCK[®] (GREINER). The following fractions were combined: F-57–F-62 (sample A), F-65+F-66 (sample B) and F-71+F-72 (sample C). After evaporation of the solvent, each fraction was dissolved in 50 μL MeOH and subjected to μF and screening under standard conditions (see 7.1.9).

7.2.4.7 Cytotoxicity Assay

Cytotoxicity assays were performed by EVOTEC (Toulouse, France). After 4 hours of HepG2 cell line (provided by ATCC) plating at 2.500 cells/well in 384-well plates, compounds were added to the cells. After an incubation at 37 °C for 40 hours, the CellTiter-Glo[®] assay (provided by PROMEGA) was performed. Luminescence measurement is related to the cell viability. Compound activity is determined by using the control wells with no treatment as control (100% of growth). The identical protocol was also used for the THP1 cell line.

8. Appendix

8.1 Gram-negative active metabolites from *Aspergillus terreus* ST000934

8.1.1 MS/MS Fragmentation

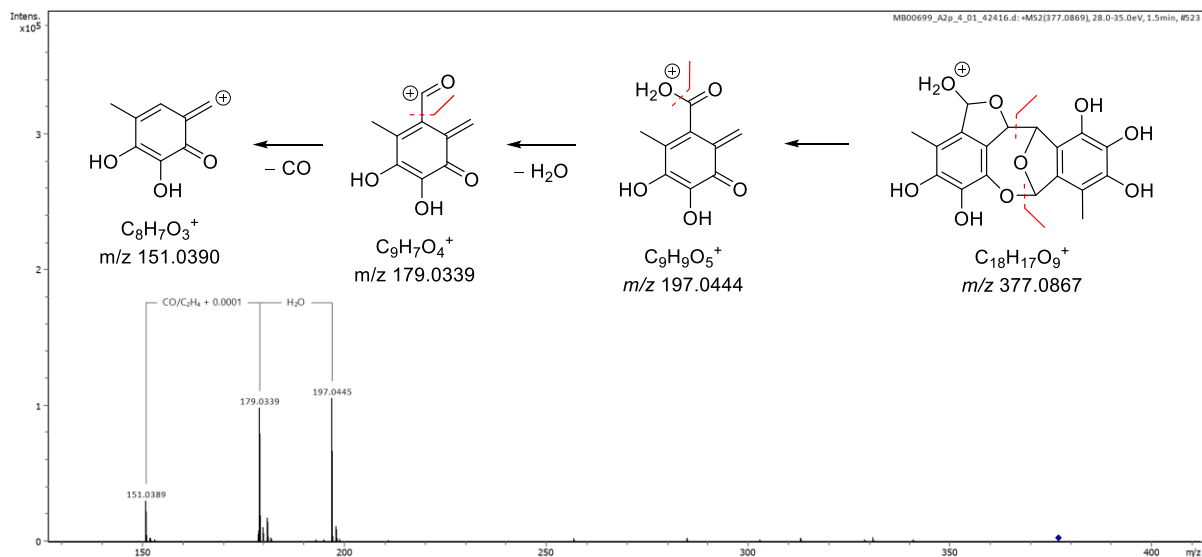


Fig. S62: MS/MS spectrum of SF005-B (25) including the postulated fragmentation pathway.

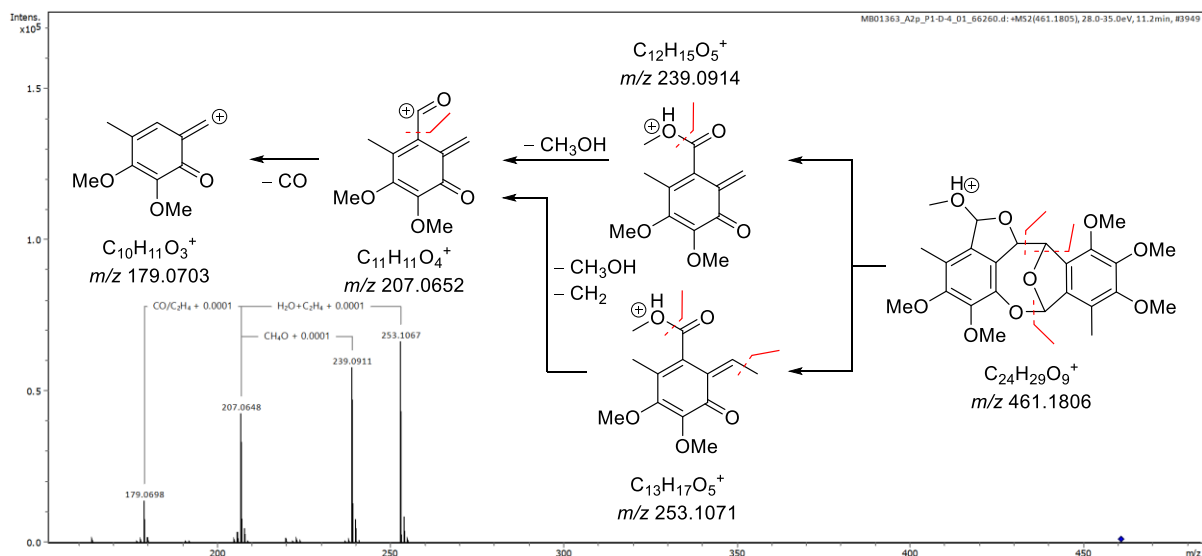


Fig. S63: MS/MS spectrum of 29b including the postulated fragmentation pathway.

8. Appendix

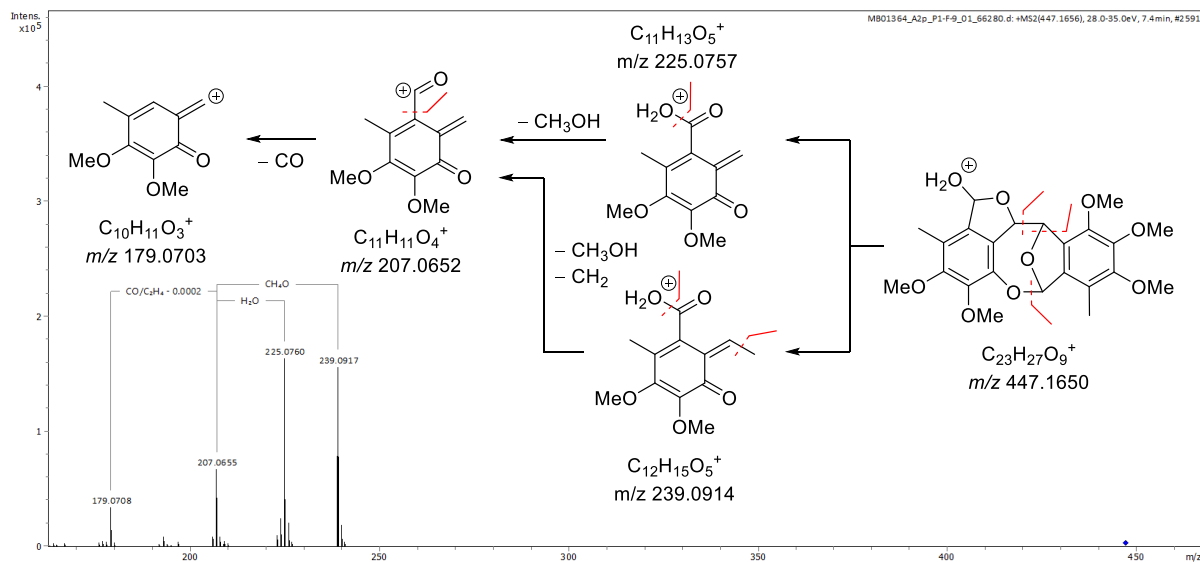


Fig. S64: MS/MS spectrum of **30** including the postulated fragmentation pathway.

8.1.2 NMR spectra

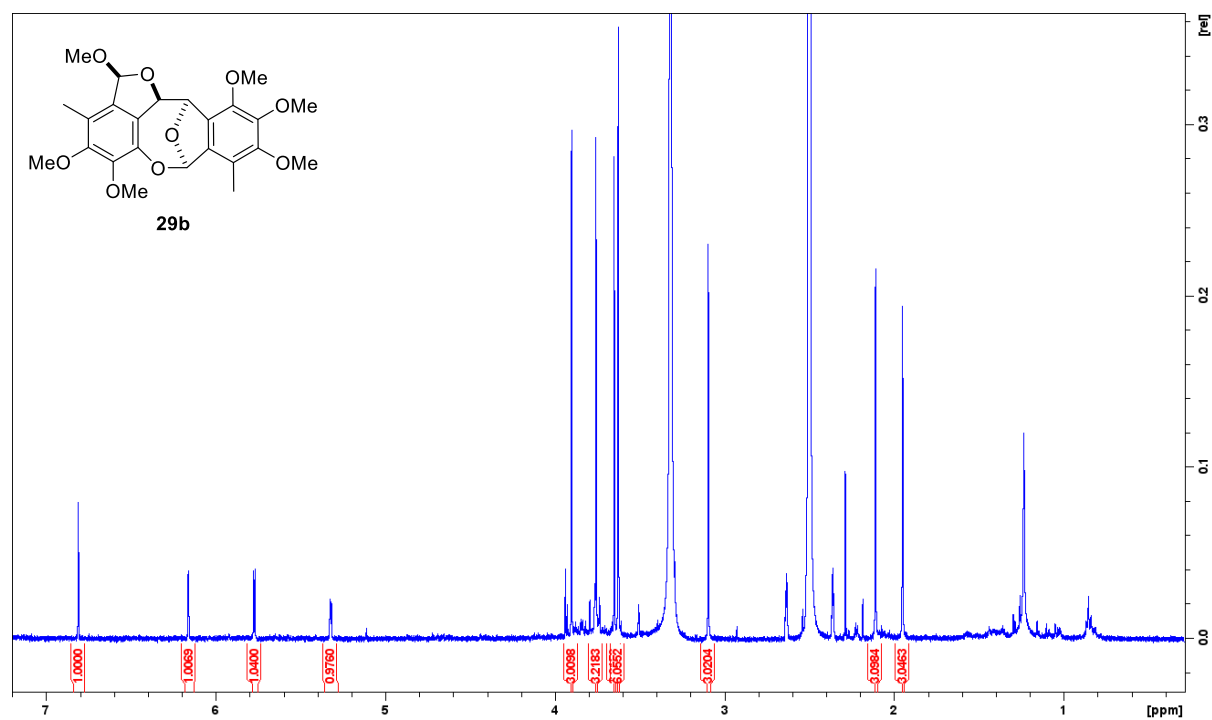
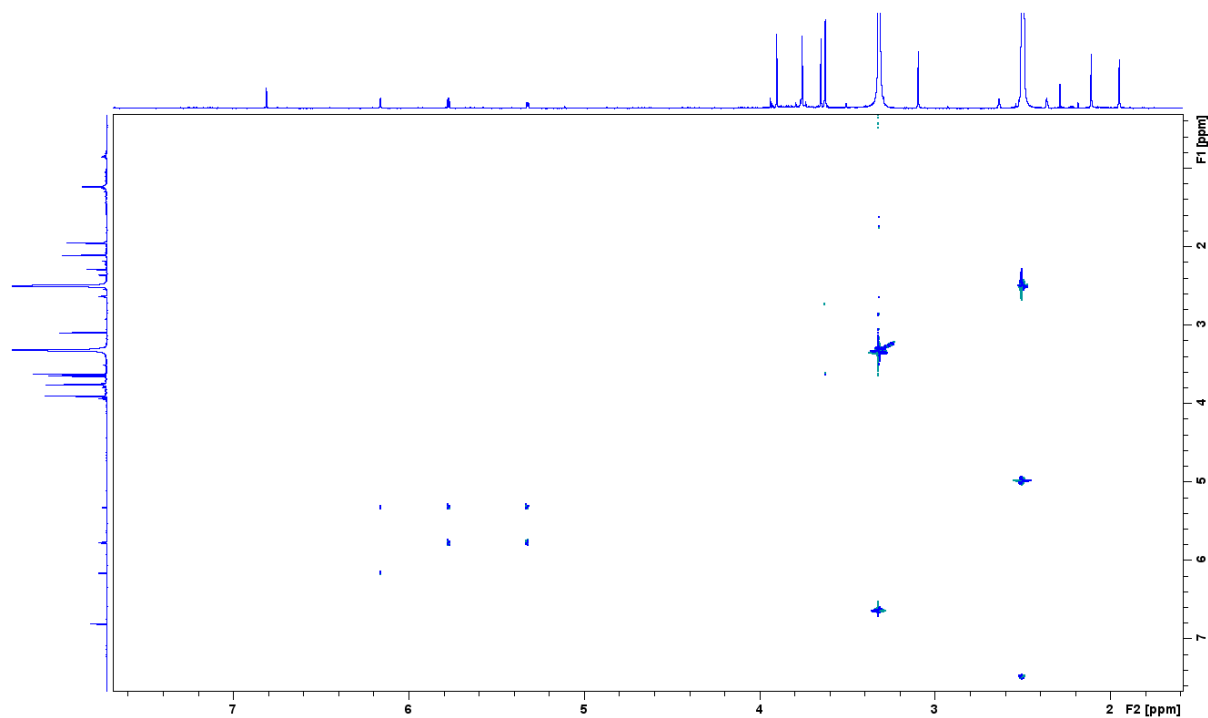
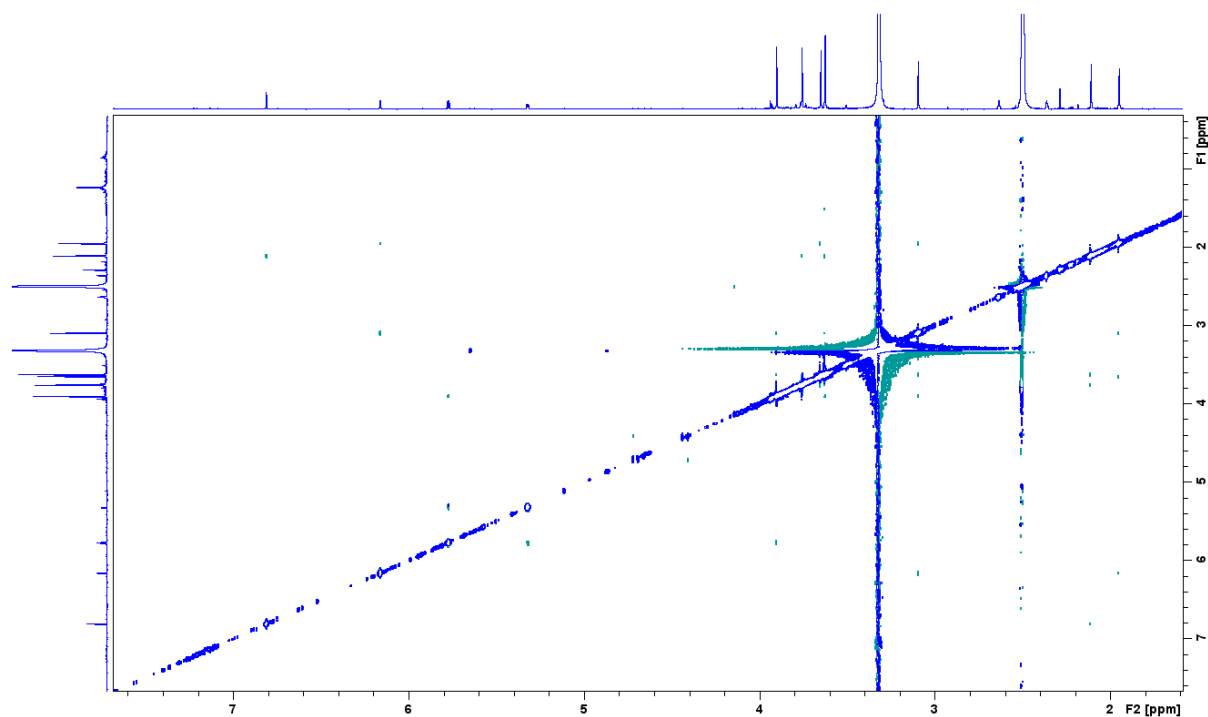
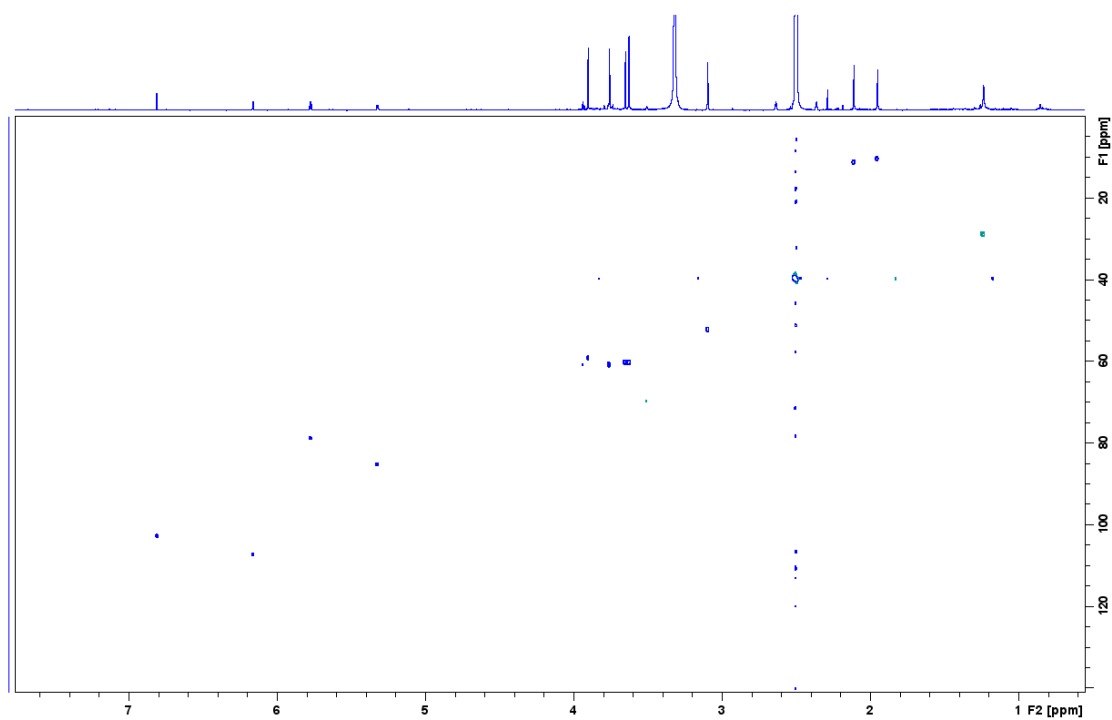
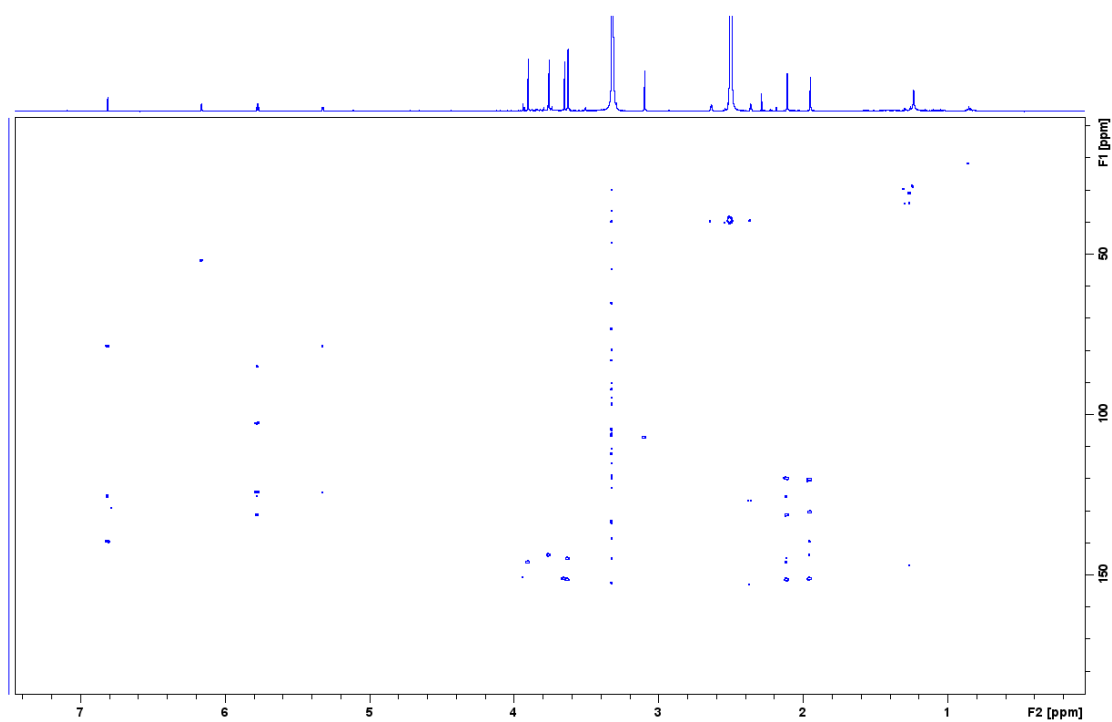
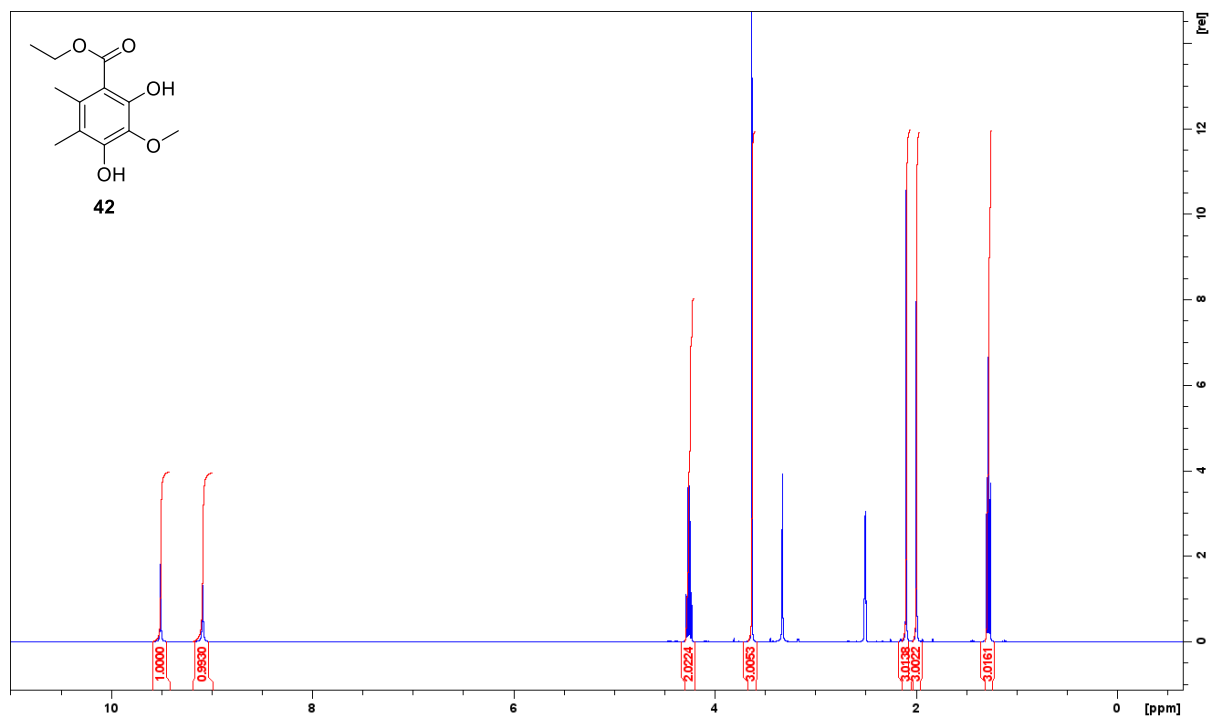
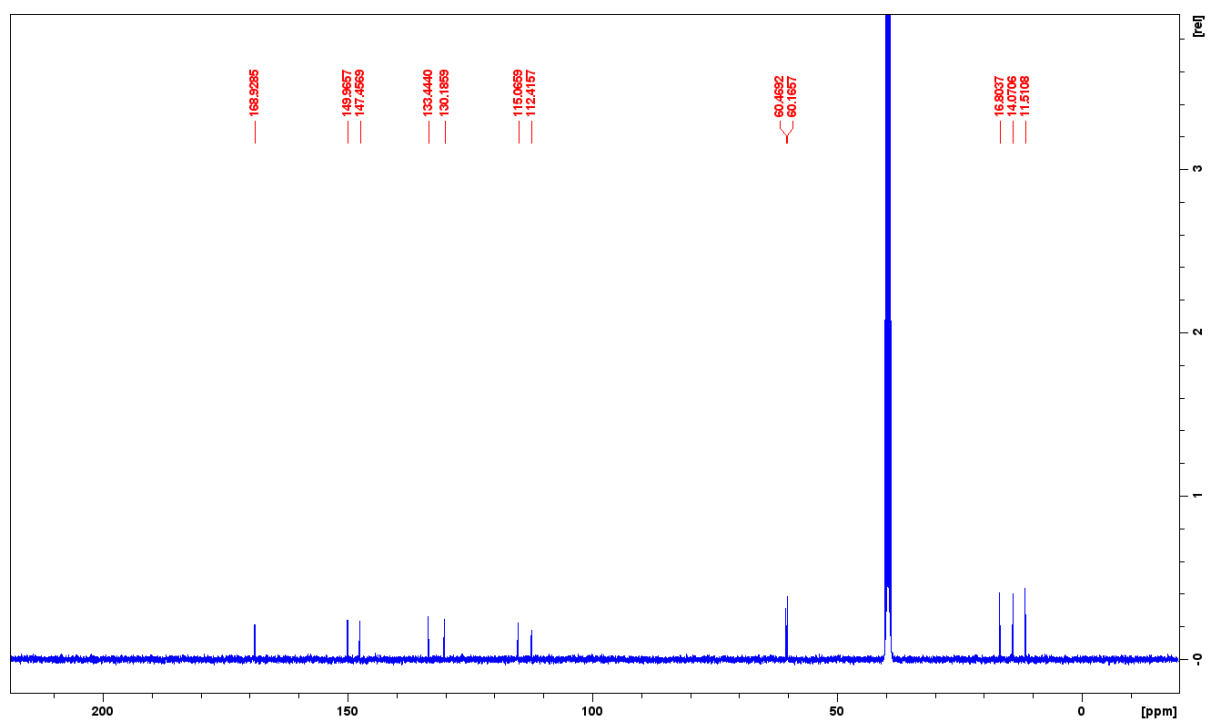


Fig. S65: 1H -NMR (500 MHz, $DMSO-d_6$) of **29b**.

Fig. S66: ^1H - ^1H COSY (500 MHz, $\text{DMSO}-d_6$) spectrum of **29b**.Fig. S67: ^1H - ^1H ROESY (500 MHz, $\text{DMSO}-d_6$) spectrum of **29b**.

Fig. S68: ^1H - ^{13}C HSQC (500 MHz, $\text{DMSO-}d_6$) spectrum of **29b**.Fig. S69: ^1H - ^{13}C HMBC (500 MHz, $\text{DMSO-}d_6$) spectrum of **29b**.

Fig. S70: ¹H-NMR (400 MHz, DMSO-*d*₆) of 42.Fig. S71: ¹³C-NMR (101 MHz, DMSO-*d*₆) of 42.

8.2 Oxazoline-containing Madurastatins from *Actinomadura* sp. ST100801

8.2.1 Dereplication of Madurastatins

8.2.1.1 MS/MS spectra

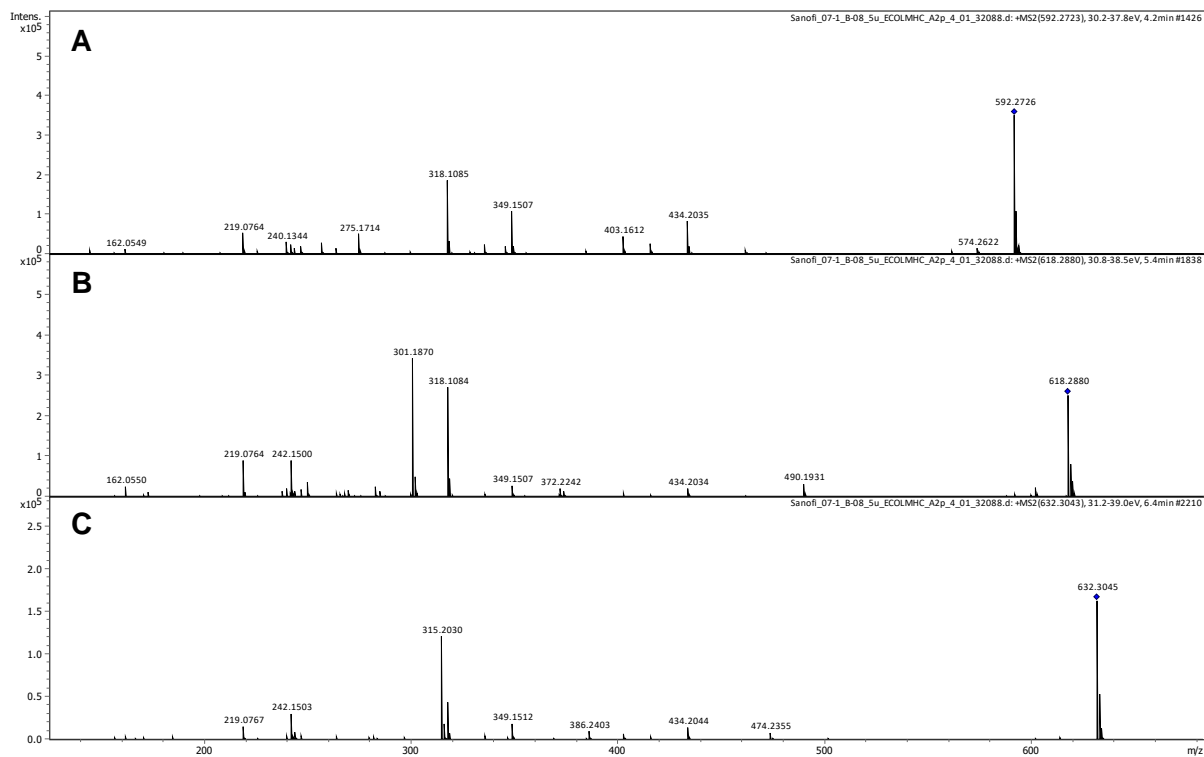


Fig. S72: MS/MS spectra of A: **48** (m/z 592.2726 \pm 0.005, $[M+H]^+$), B: **53** (m/z 618.2882 \pm 0.005, $[M+H]^+$) and C: **54** (m/z 632.3039 \pm 0.005, $[M+H]^+$).

8.1.1.2 Molecular Networking

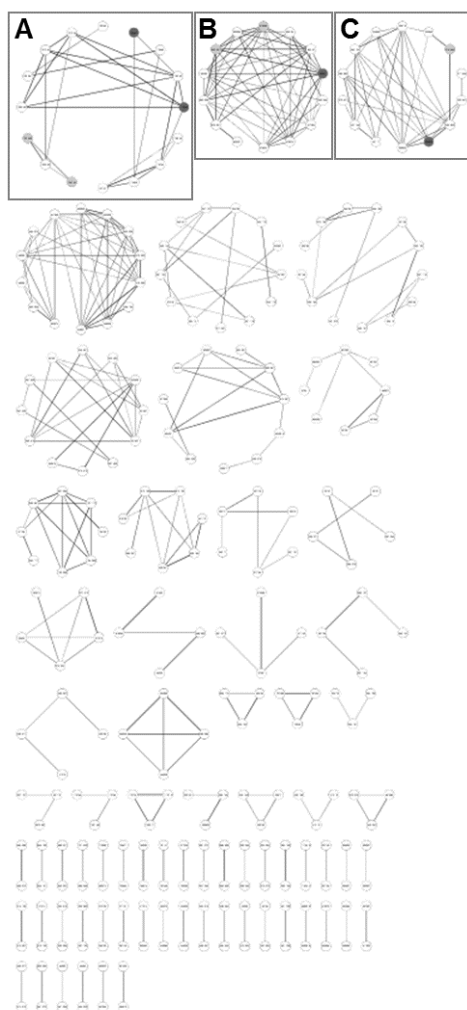


Fig. S73: Molecular Network of *Actinomadura* sp. ST100801. Madurastatin clusters are labelled; A: $[2M+H/2M+Na]^+$ cluster, B: $[M+H]^+$ cluster, C: $[M+2H]^{2+}$ cluster.

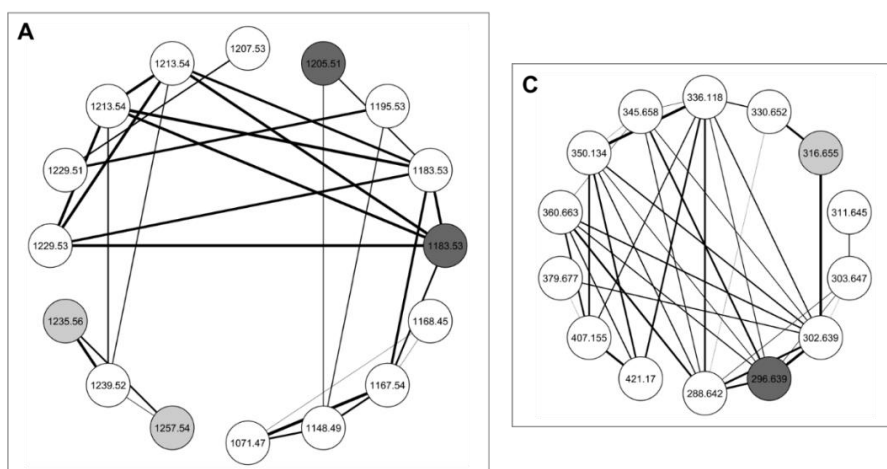
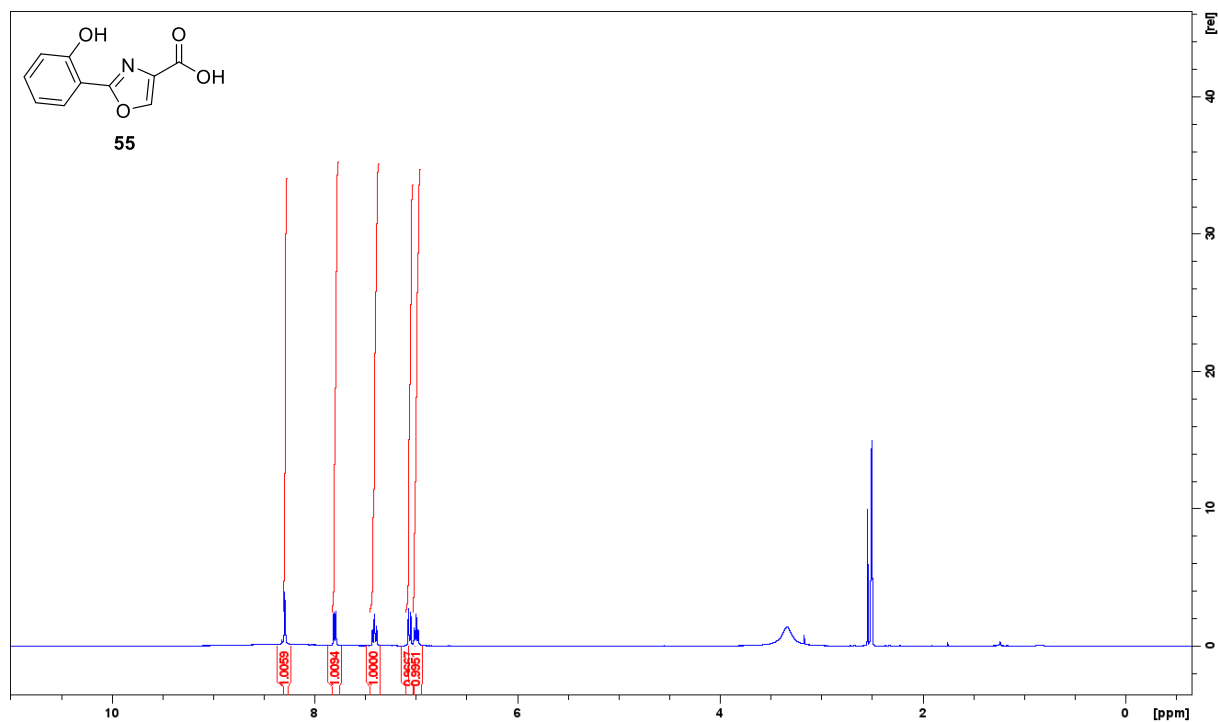
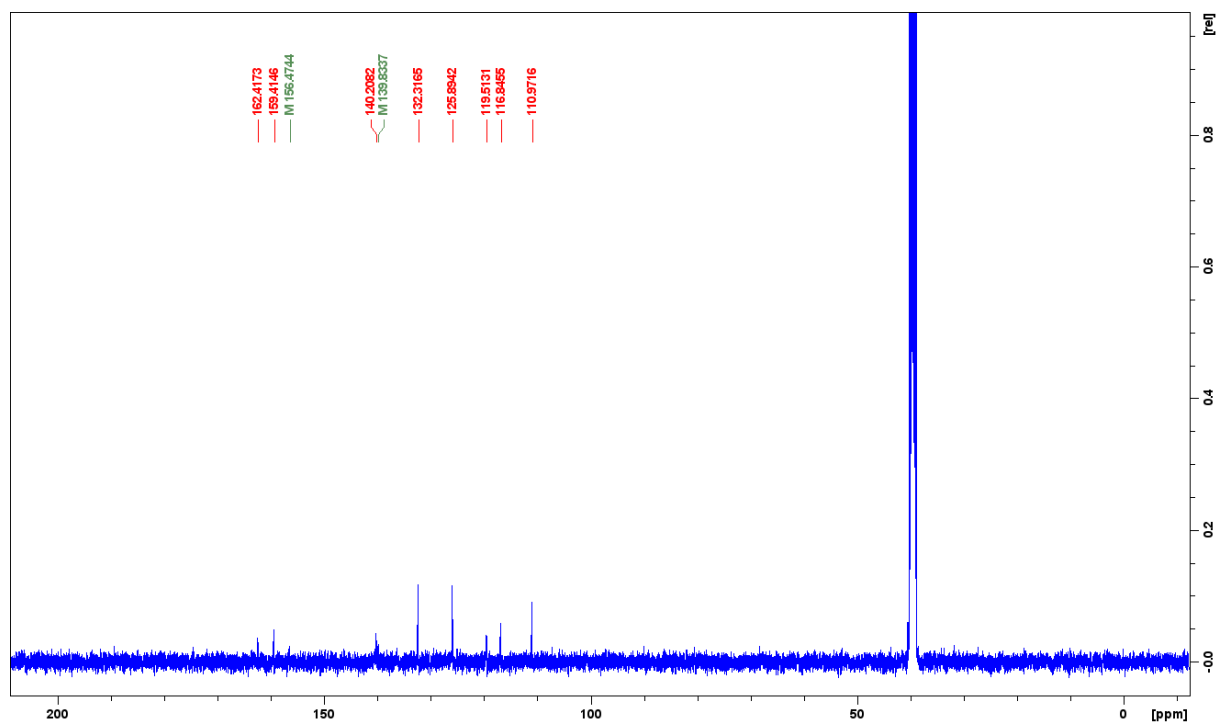
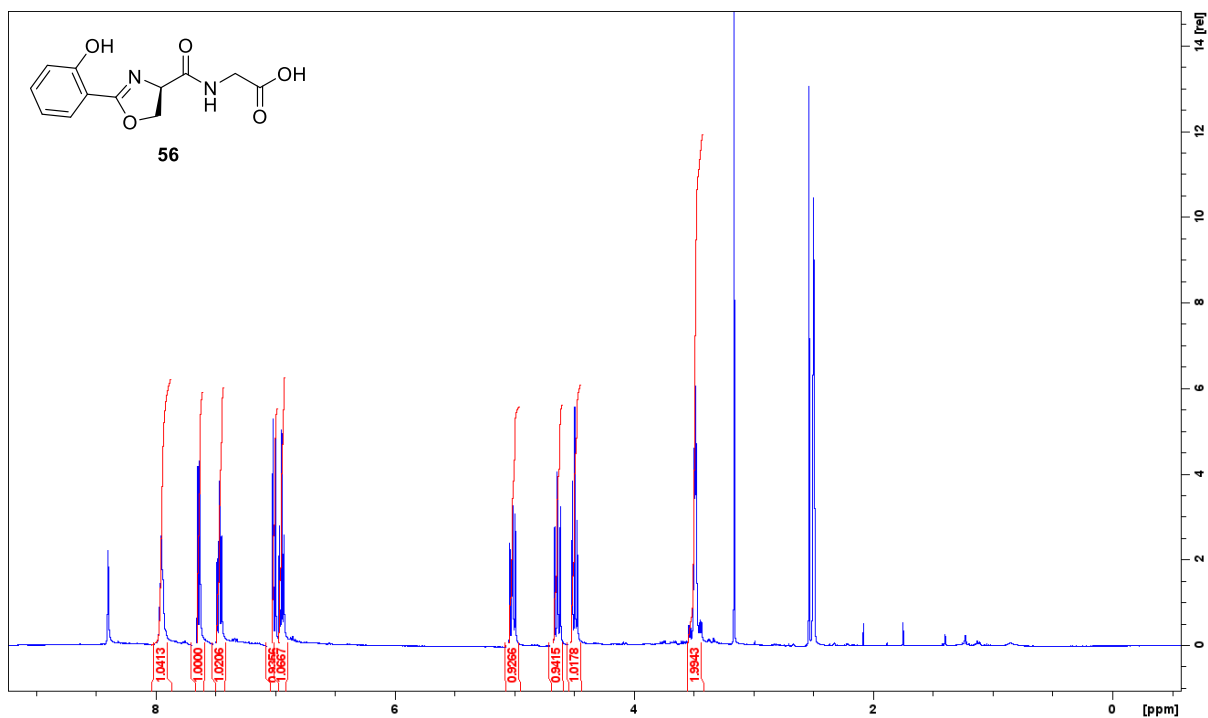
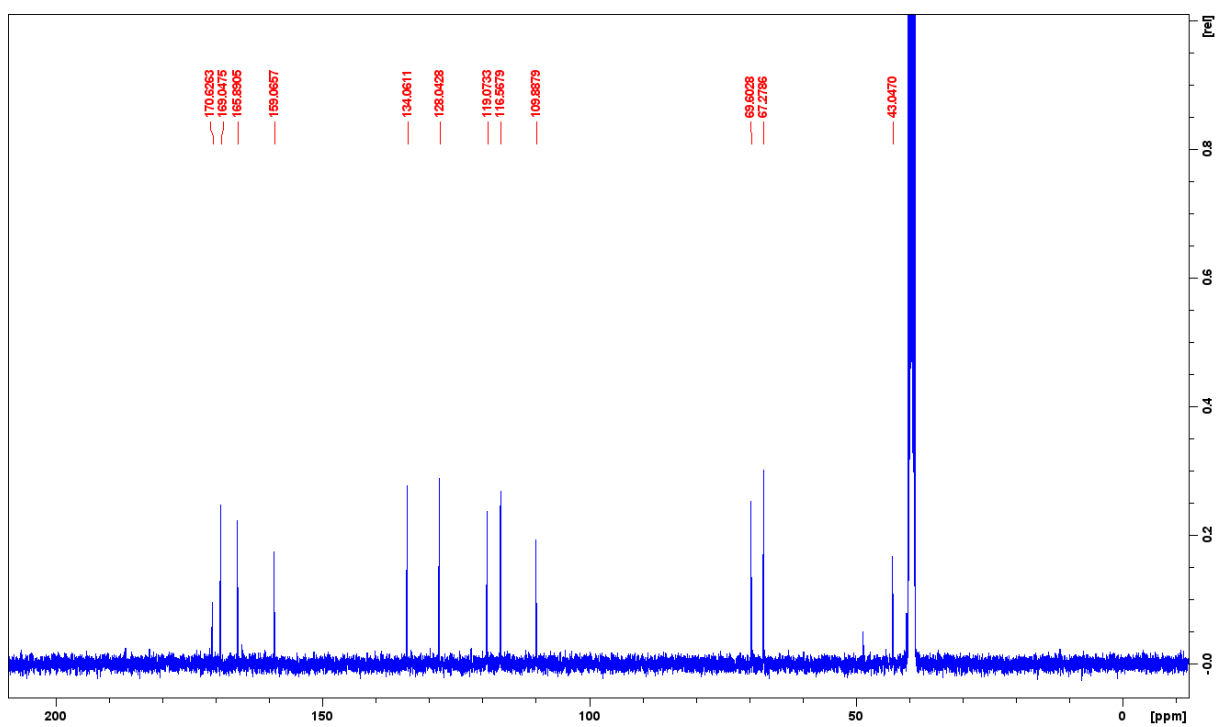


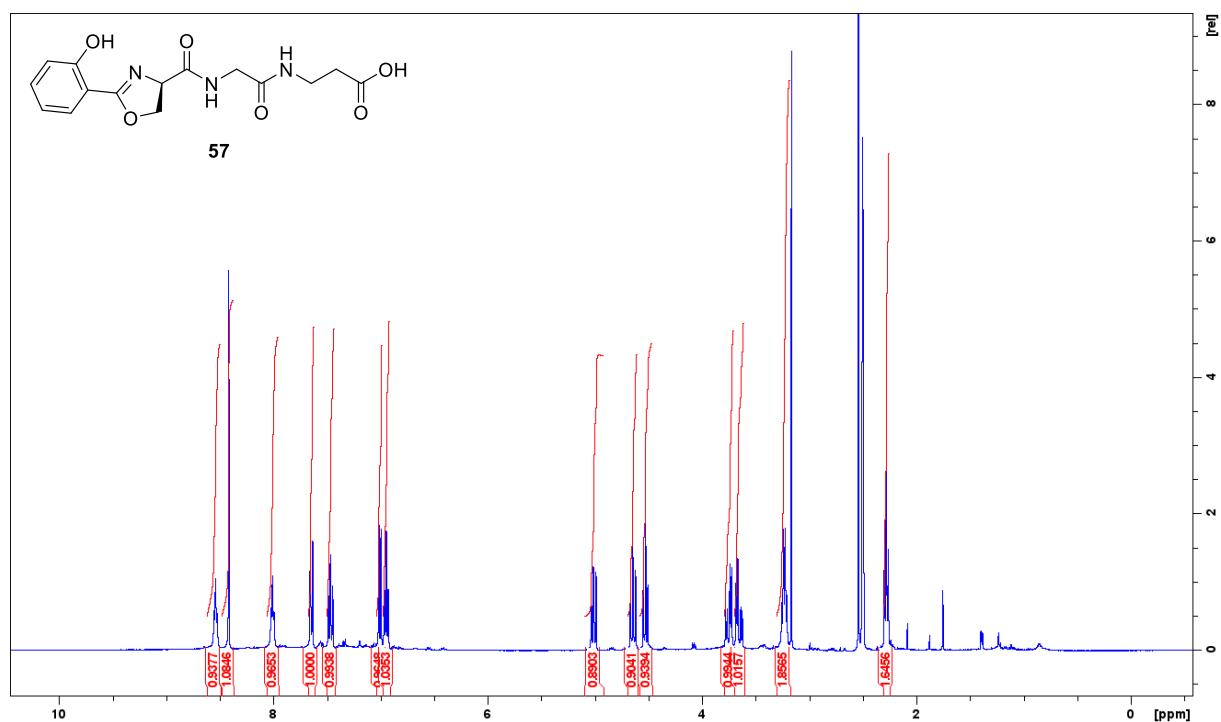
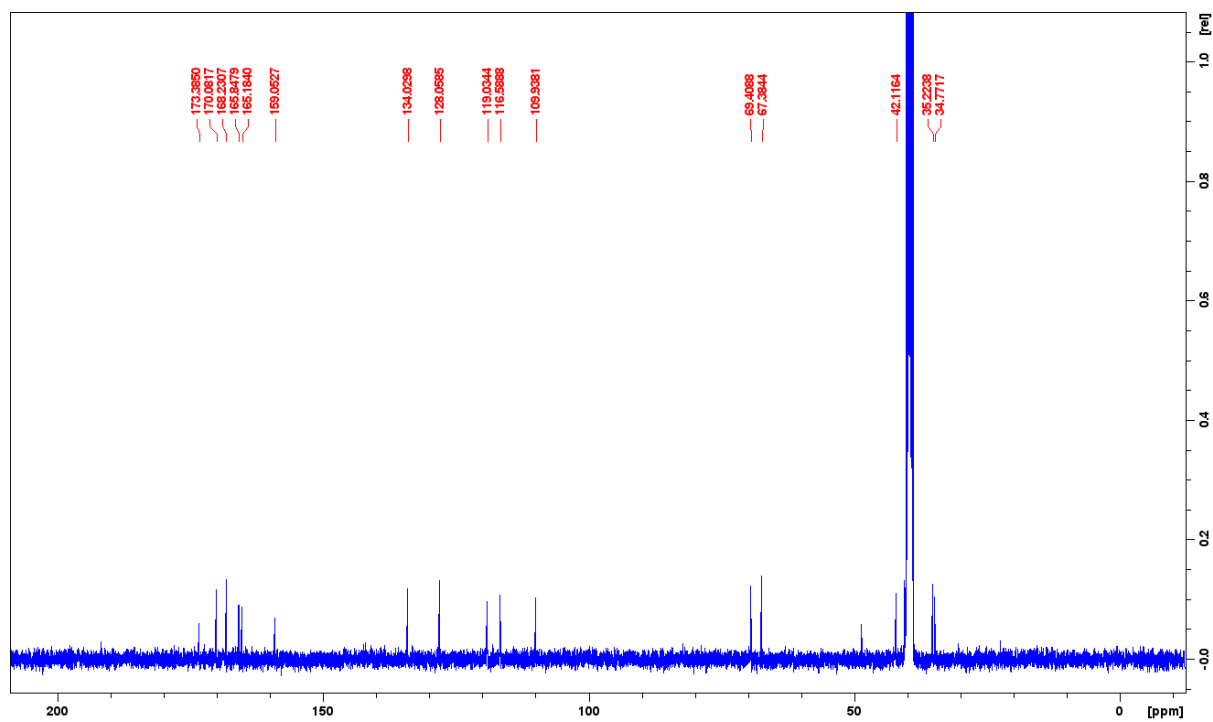
Fig. S74: A: $[2M+H/2M+Na]^+$ madurastatin cluster; dark grey: madurastatin C1 (**48**), $[2M+H]^+$ m/z 1183.5378, $[2M+Na]^+$ m/z 1205.5198; light grey: dereplicated madurastatin **53** with molecular formula $C_{28}H_{39}N_7O_9$, $[2M+H]^+$ m/z 1235.5691, $[2M+Na]^+$ m/z 1257.5511. B: $[M+2H]^{2+}$ madurastatin cluster; dark grey: madurastatin C1 (**48**), $[M+2H]^{2+}$ m/z 296.6399; light grey: dereplicated madurastatin **54** with molecular formula $C_{29}H_{41}N_7O_9$, $[M+2H]^{2+}$ m/z 316.6556.

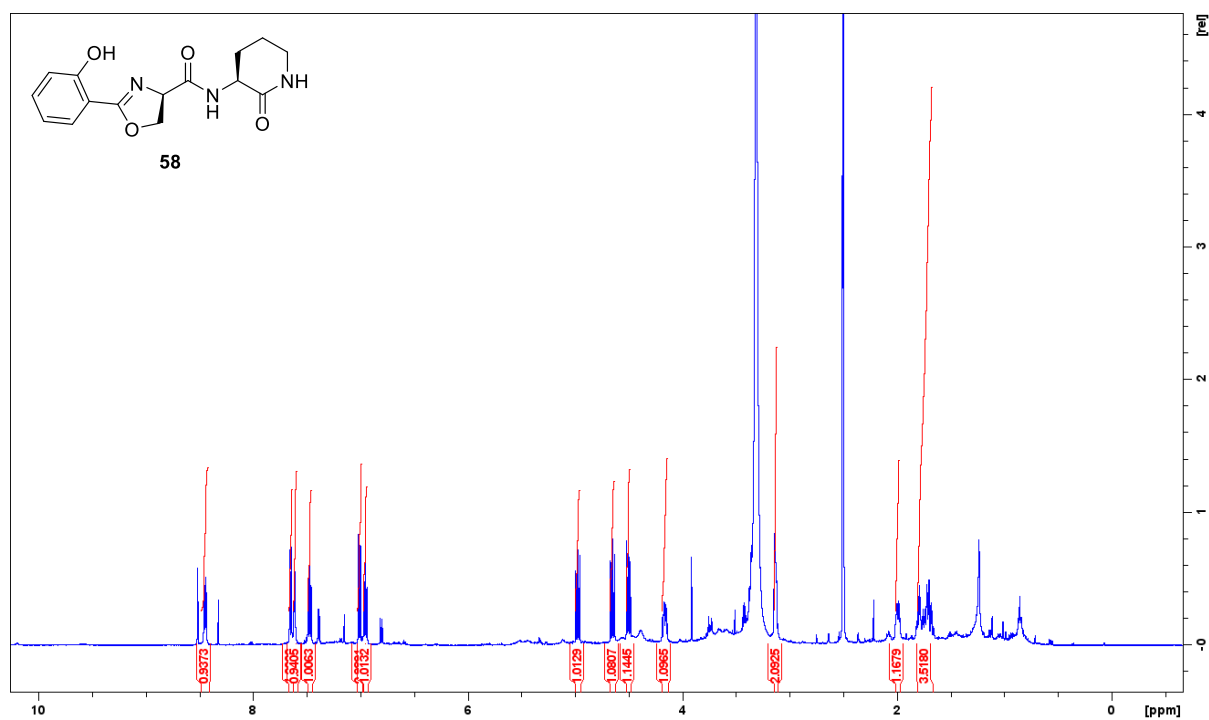
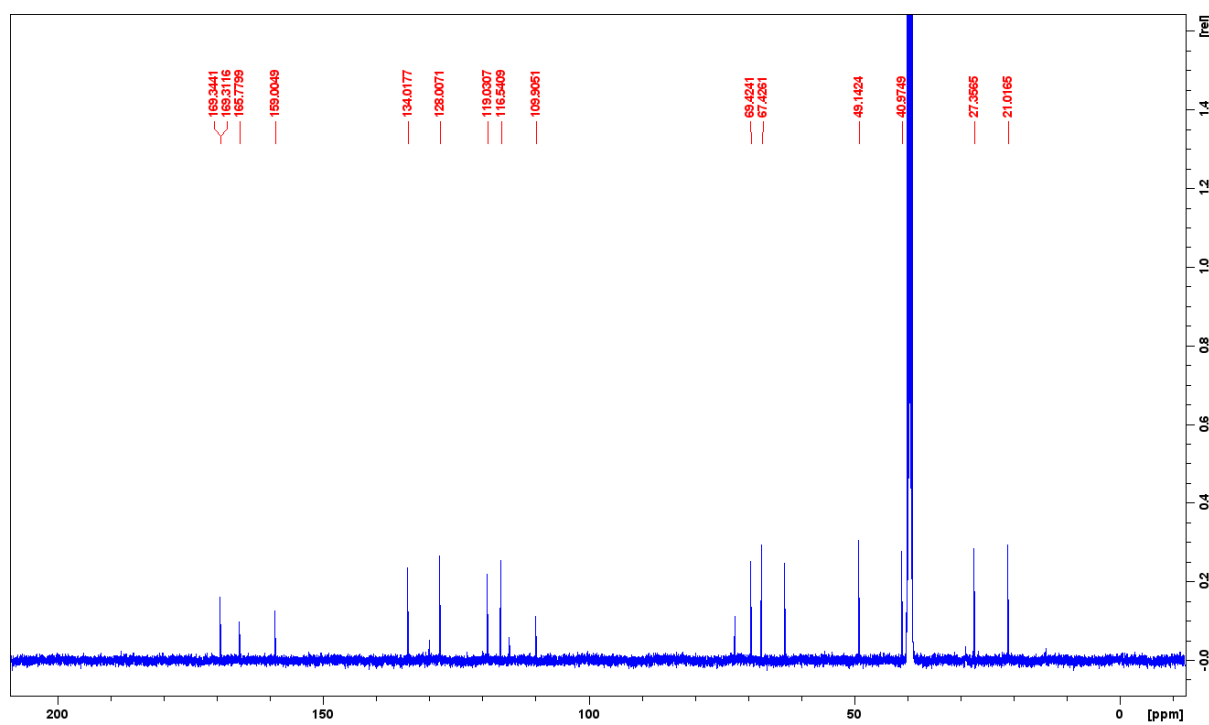
8.2.2 Structure Elucidation

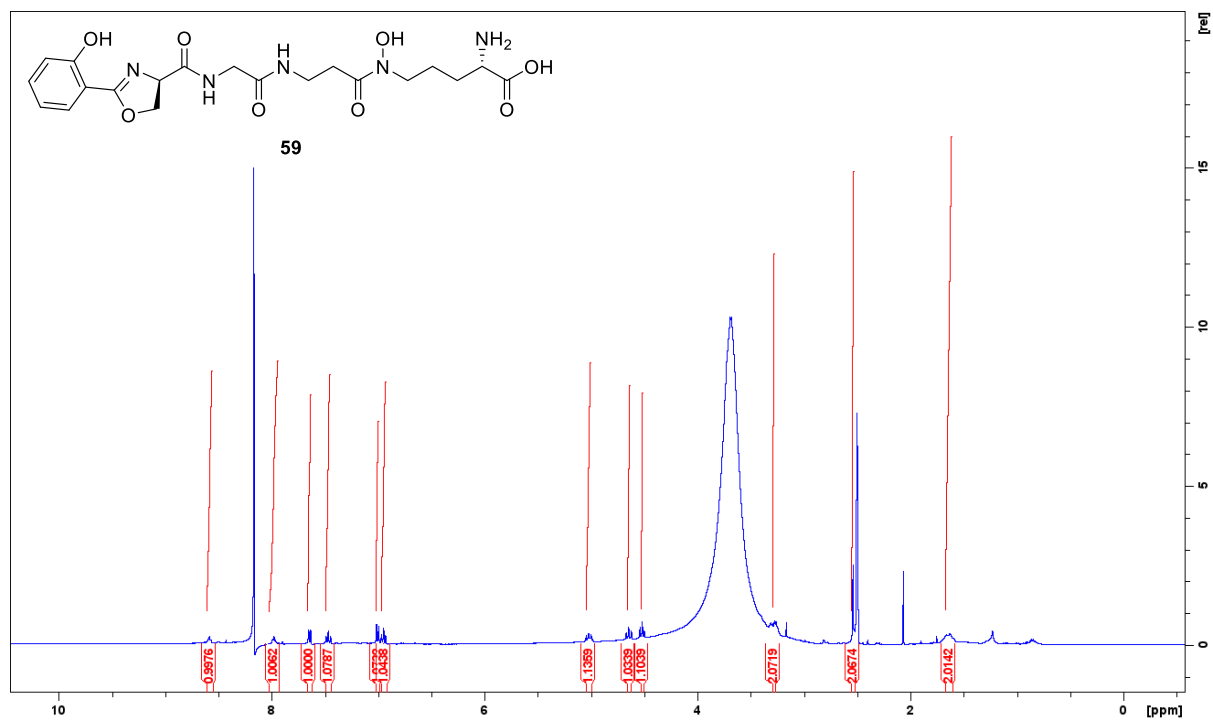
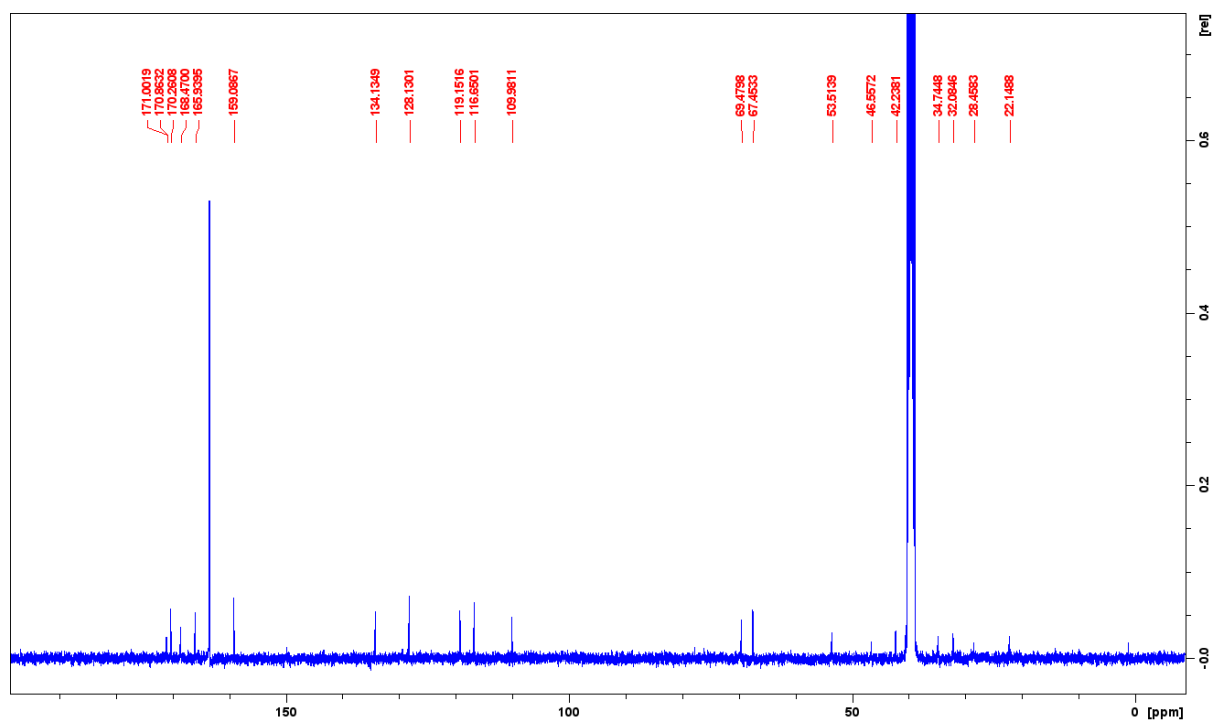
8.2.2.1 NMR spectra

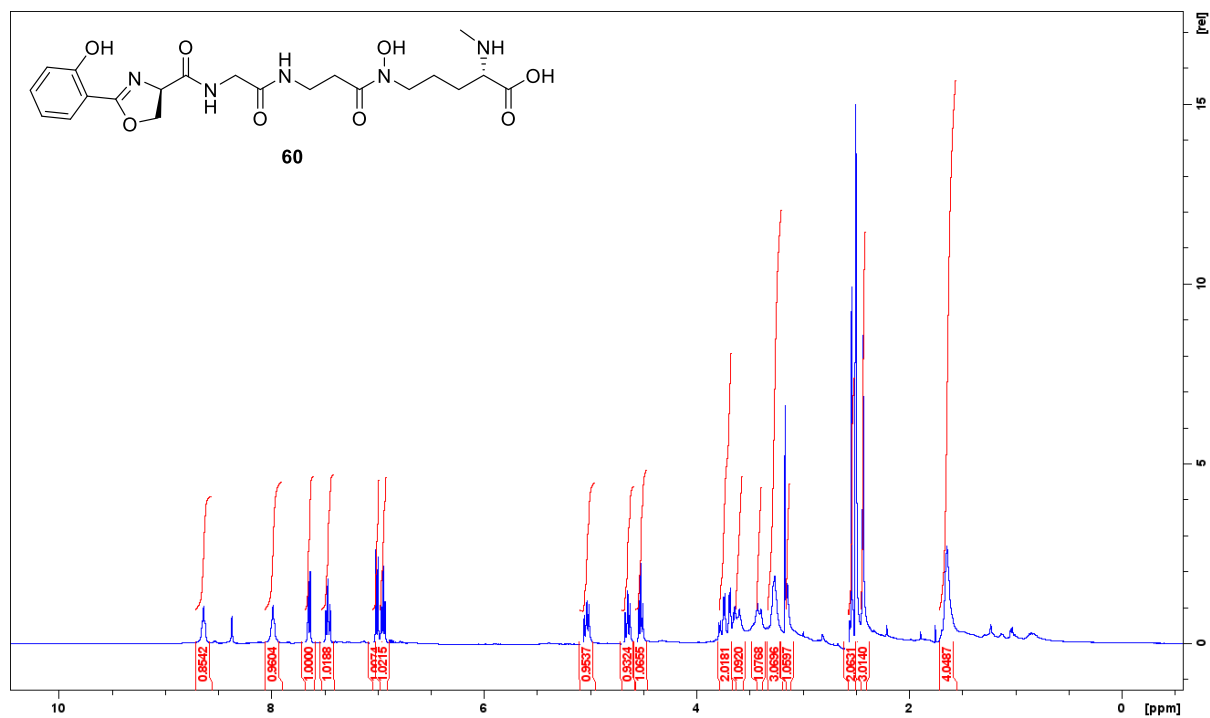
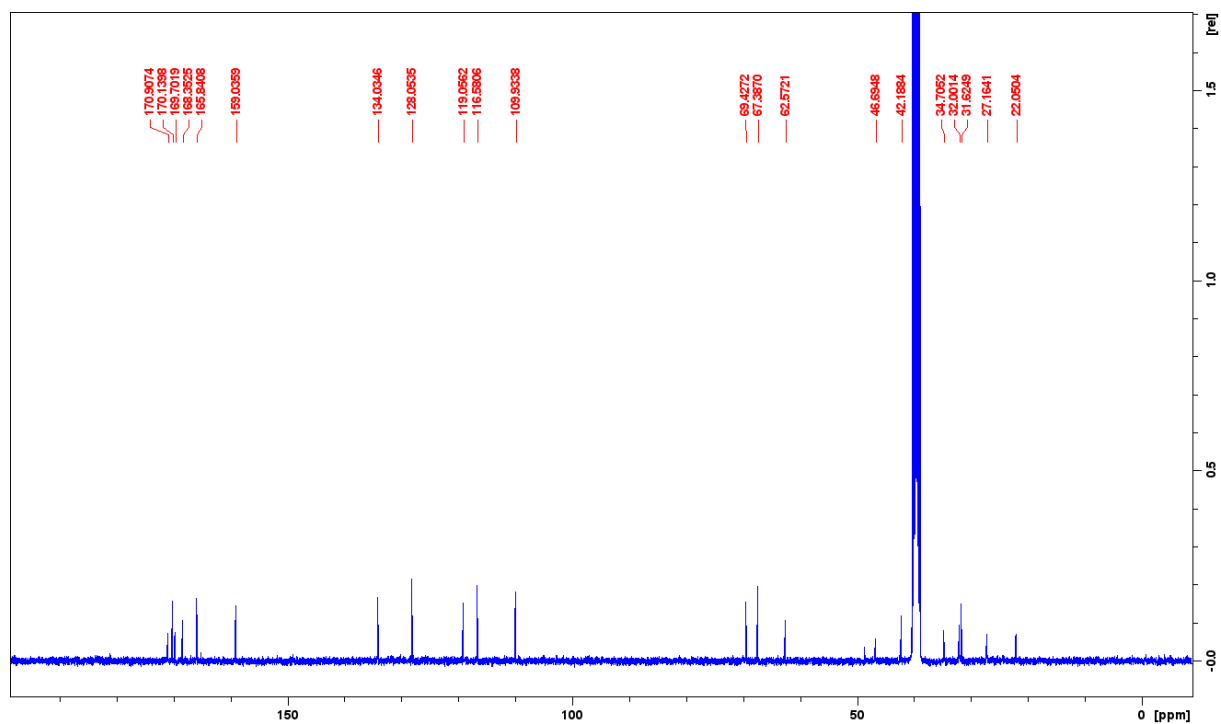
Fig. S75: ¹H-NMR (400 MHz, DMSO-*d*₆) of madurastatin B4 (55).Fig. S76: ¹³C-NMR (101 MHz, DMSO-*d*₆) of madurastatin B4 (55).

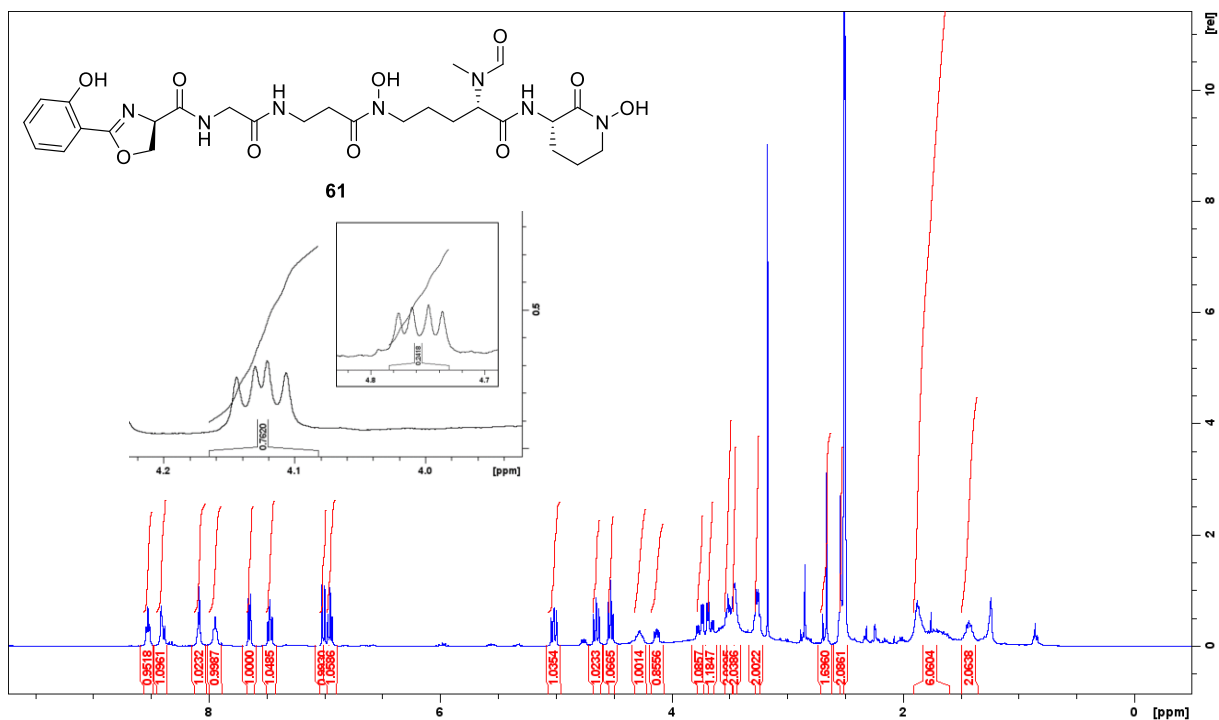
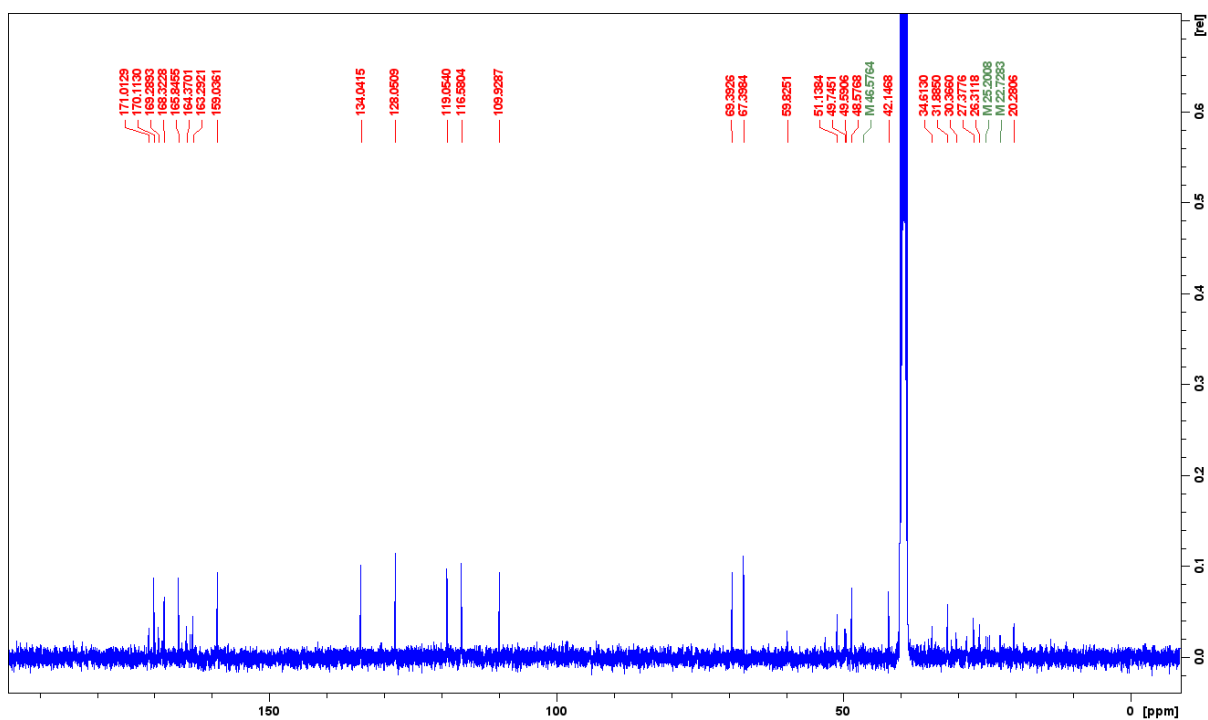
Fig. S77: ¹H-NMR (400 MHz, DMSO-*d*₆) of madurastatin E1 (56).Fig. S78: ¹³C-NMR (101 MHz, DMSO-*d*₆) of madurastatin E1 (56).

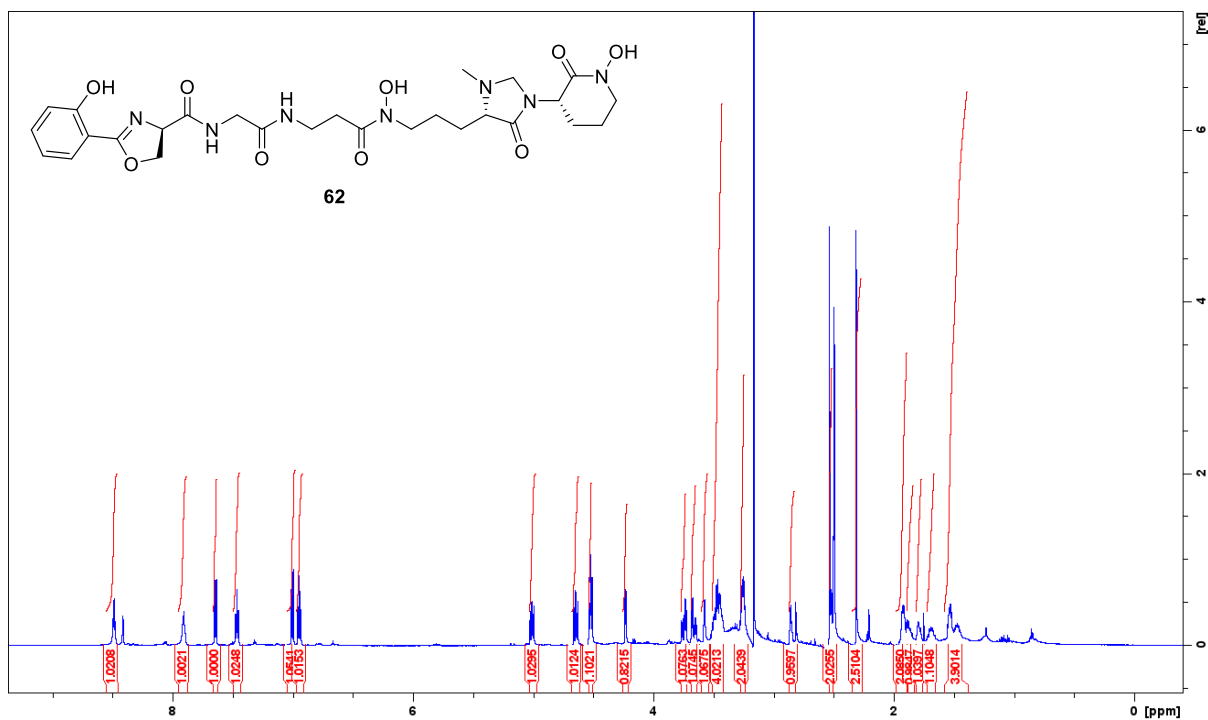
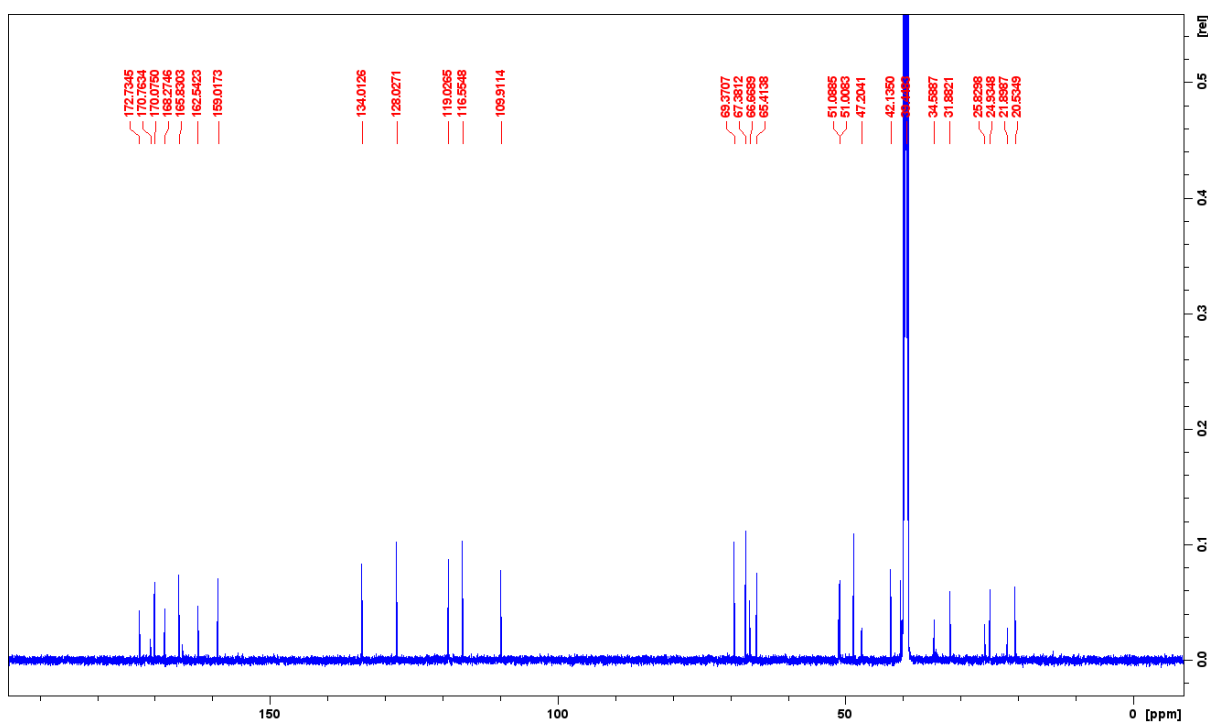
Fig. S79: ¹H-NMR (400 MHz, DMSO-*d*₆) of madurastatin F1 (57).Fig. S80: ¹³C-NMR (101 MHz, DMSO-*d*₆) of madurastatin F1 (57).

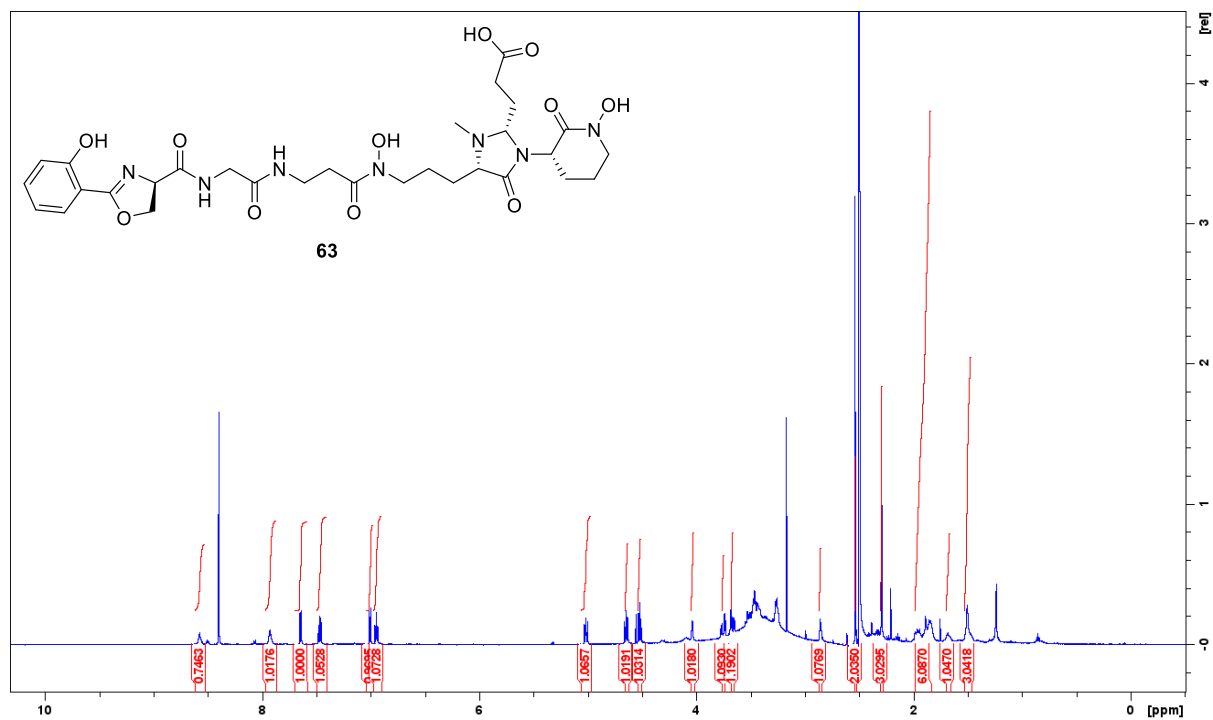
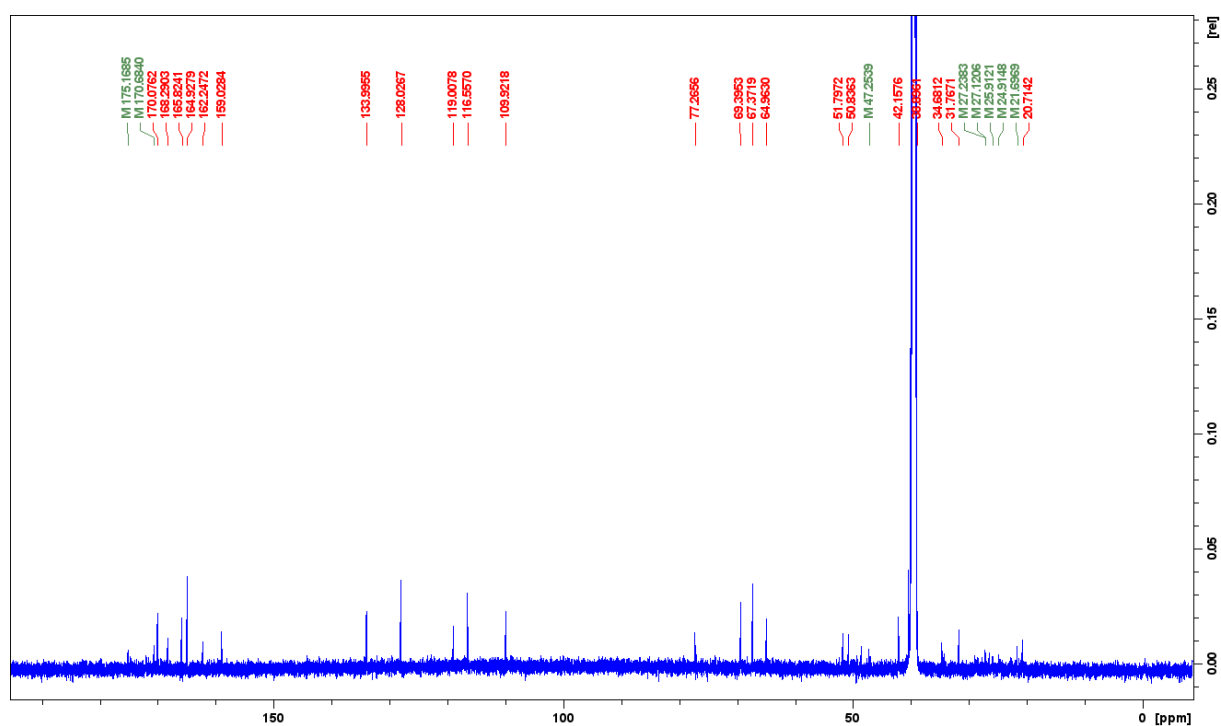
Fig. S81: ¹H-NMR (500 MHz, DMSO-*d*₆) of madurastatin E2 (58).Fig. S82: ¹³C-NMR (126 MHz, DMSO-*d*₆) of madurastatin E2 (58).

Fig. S83: $^1\text{H-NMR}$ (400 MHz, $\text{DMSO-}d_6$) of madurastatin G1 (59).Fig. S84: $^{13}\text{C-NMR}$ (101 MHz, $\text{DMSO-}d_6$) of madurastatin G1 (59).

Fig. S85: ¹H-NMR (400 MHz, DMSO-*d*₆) of madurastatin G2 (60).Fig. S86: ¹³C-NMR (101 MHz, DMSO-*d*₆) of madurastatin G2 (60).

Fig. S87: ¹H-NMR (400 MHz, DMSO-*d*₆) of madurastatin C2 (61).Fig. S88: ¹³C-NMR (101 MHz, DMSO-*d*₆) of madurastatin C2 (61).

Fig. S89: ¹H-NMR (600 MHz, DMSO-*d*₆) of madurastatin D3 (62).Fig. S90: ¹³C-NMR (151 MHz, DMSO-*d*₆) of madurastatin D3 (62).

Fig. S91: $^1\text{H-NMR}$ (600 MHz, $\text{DMSO-}d_6$) of madurastatin D4 (63).Fig. S92: $^{13}\text{C-NMR}$ (151 MHz, $\text{DMSO-}d_6$) of madurastatin D4 (63).

8.2.2.2 LC-MS/MS Chromatograms of Potential Madurastatins

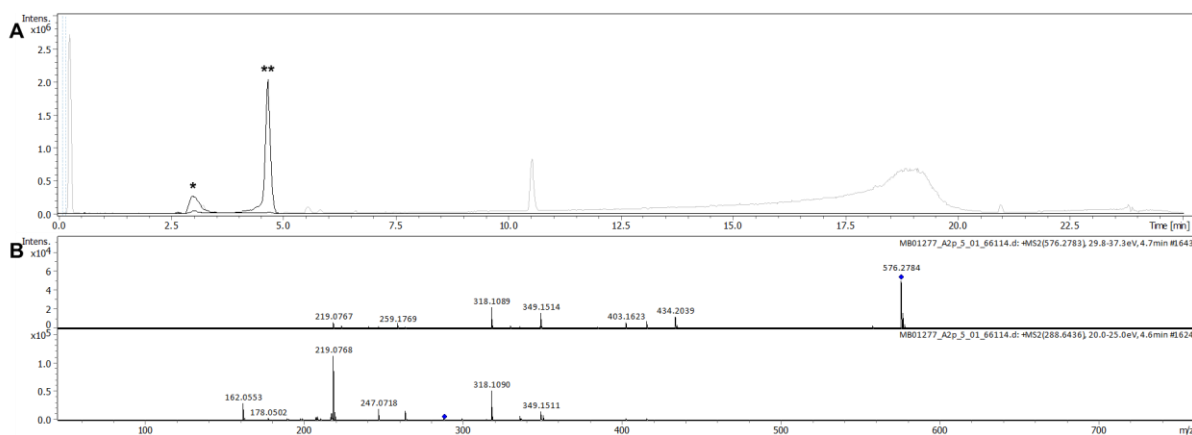


Fig. S93: LC-MS chromatogram of potential madurastatin with molecular formula $C_{26}H_{37}N_7O_8$. A: BPC (grey), EIC (black) of * m/z 315.0982 \pm 0.005 $[M-H+Fe]^{2+}$ and ** m/z 288.6425 \pm 0.005 $[M+2H]^{2+}$; B: MS/MS spectrum of m/z 576.2783 $[M+H]^+$ (top) and m/z 288.6436 $[M+2H]^{2+}$ (bottom).

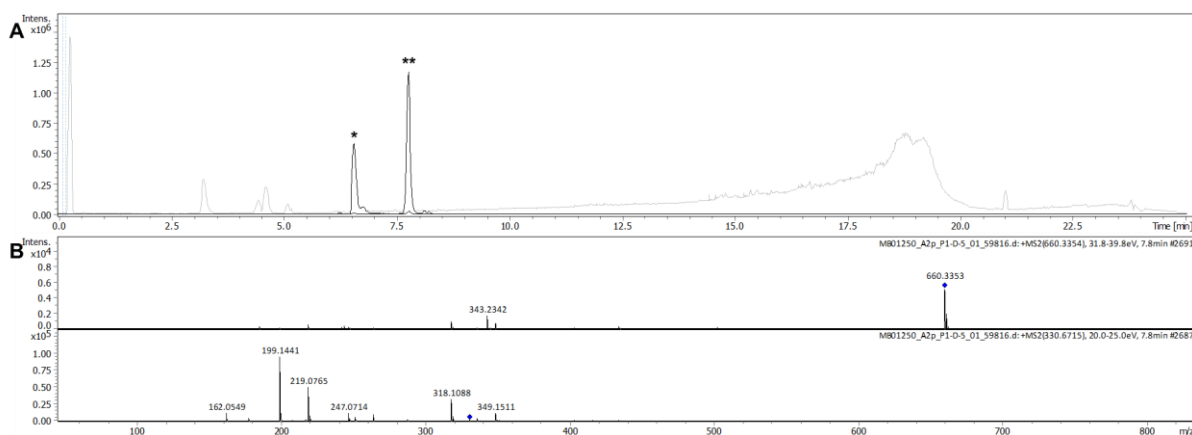


Fig. S94: LC-MS chromatogram of potential madurastatin with molecular formula $C_{31}H_{45}N_7O_9$. A: BPC (grey), EIC (black) of * m/z 357.1270 \pm 0.005 $[M-H+Fe]^{2+}$ and ** m/z 330.6712 \pm 0.005 $[M+2H]^{2+}$; B: MS/MS spectrum of m/z 660.3354 $[M+H]^+$ (top) and m/z 330.6715 $[M+2H]^{2+}$ (bottom).

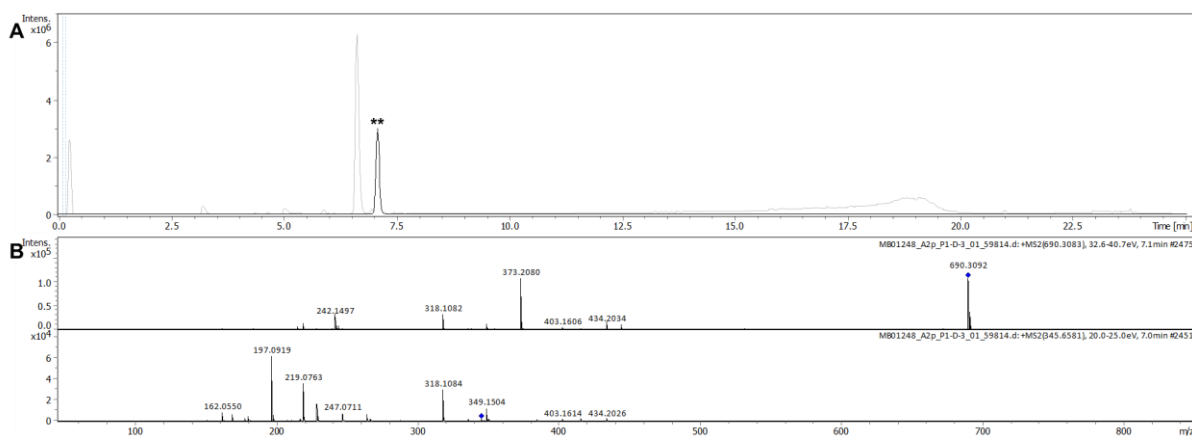


Fig. S95: LC-MS chromatogram of potential madurastatin with molecular formula $C_{31}H_{43}N_7O_{11}$. A: BPC (grey), EIC (black) of ** m/z 345.6583 \pm 0.005 $[M+2H]^{2+}$; B: MS/MS spectrum of m/z 690.3083 $[M+H]^+$ (top) and m/z 345.6582 $[M+2H]^{2+}$ (bottom).

8.2.2.3 Marfey's Analysis

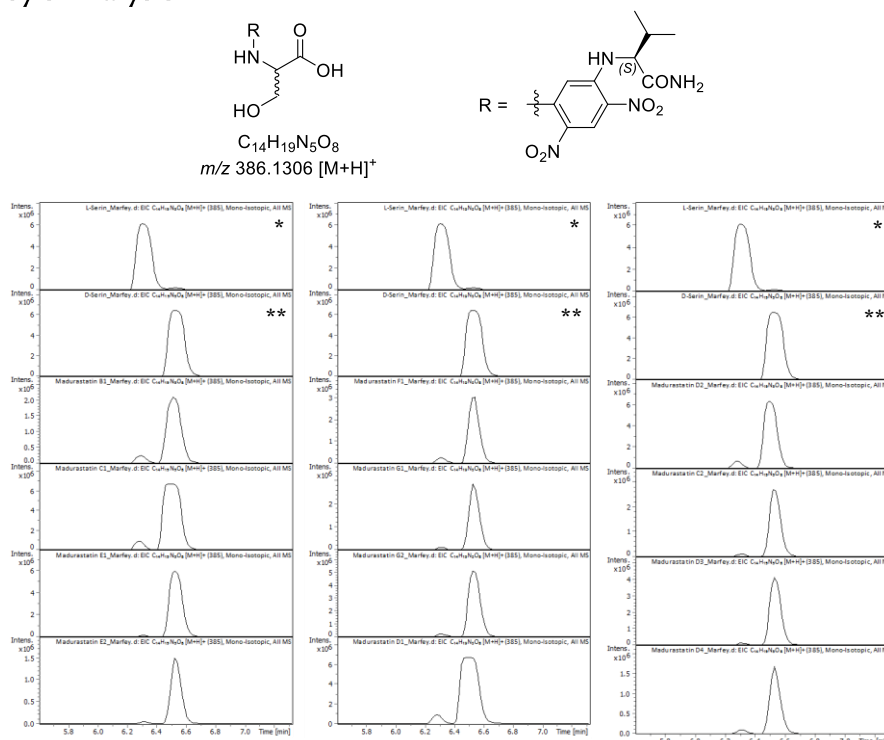
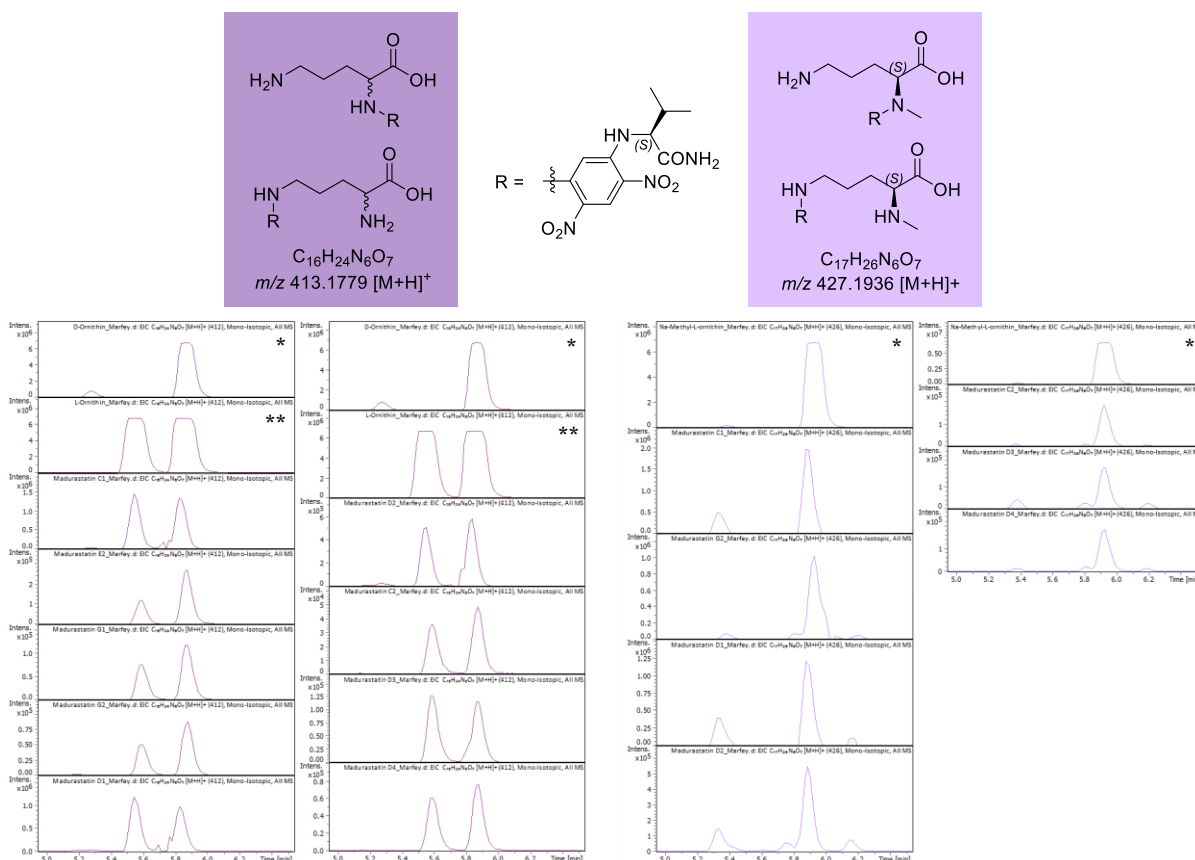


Fig. S96: L-FDVA adducts of serine; references: L-serine* and D-serine**.

Fig. S97: Left: L-FDVA adducts of ornithine; references: D-ornithine* and L-ornithine**. Right: L-FDVA adducts of α -methyl-ornithine; reference: α -methyl-L-ornithine*.

8. Appendix

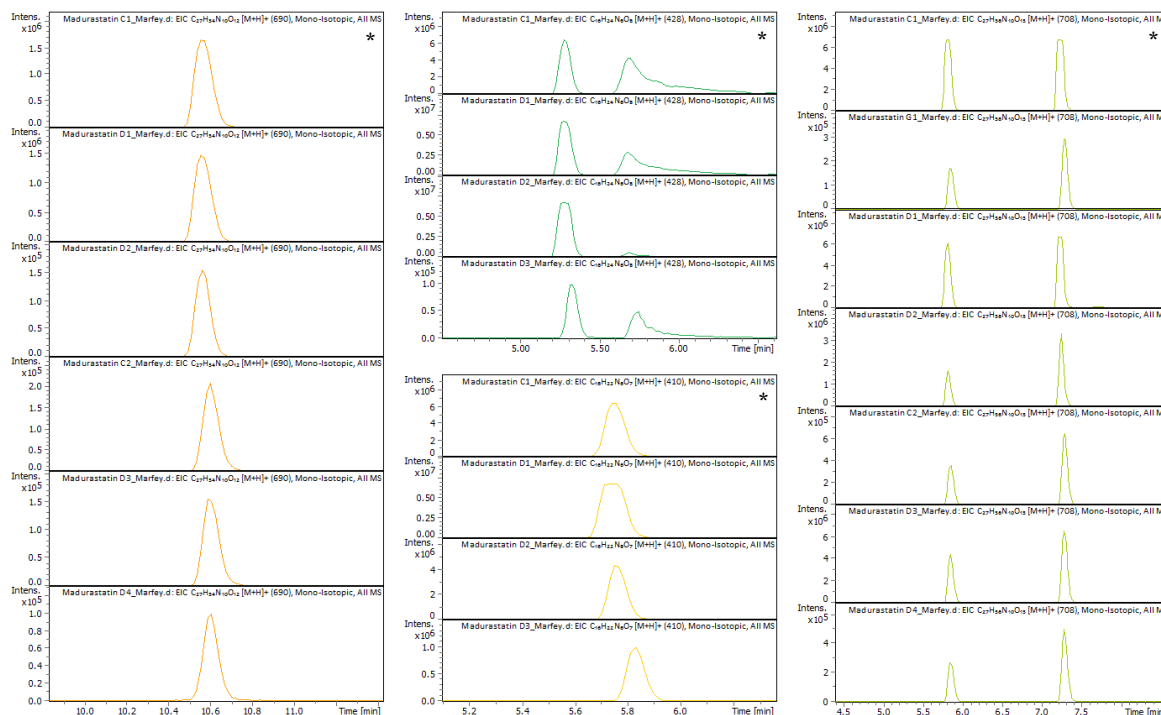
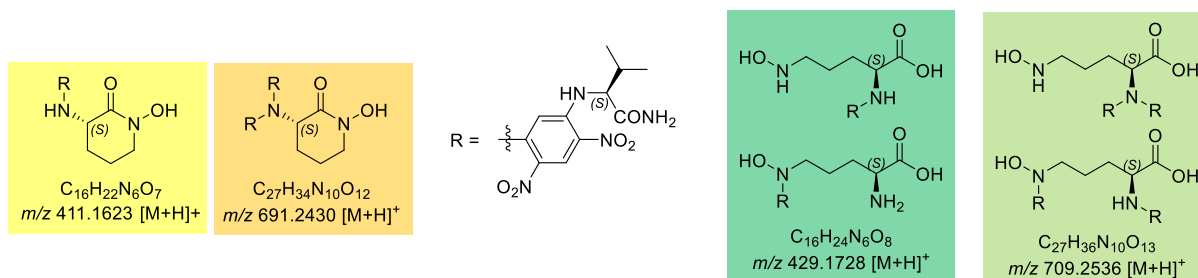


Fig. S98: Left/middle (bottom): single/double L-FDVA adducts of cyclic L-ornithine; reference: madurastatin C1*. Right/middle (top): single/double L-FDVA adducts of *N*δ-hydroxyl-L-ornithine; reference: madurastatin C1*.

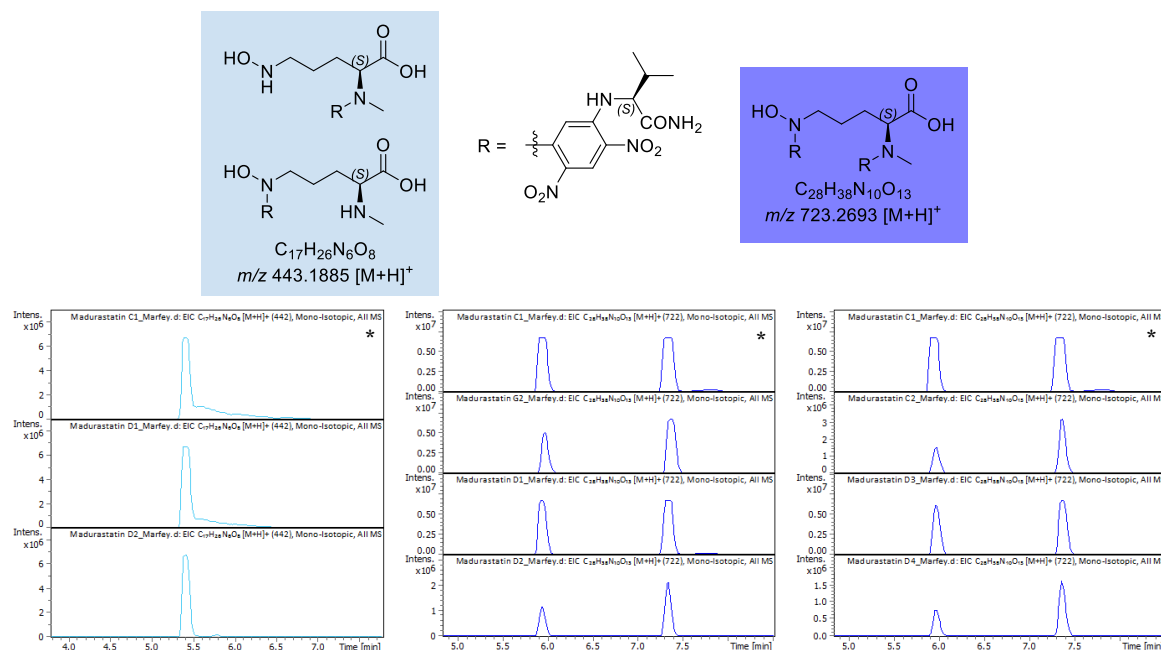


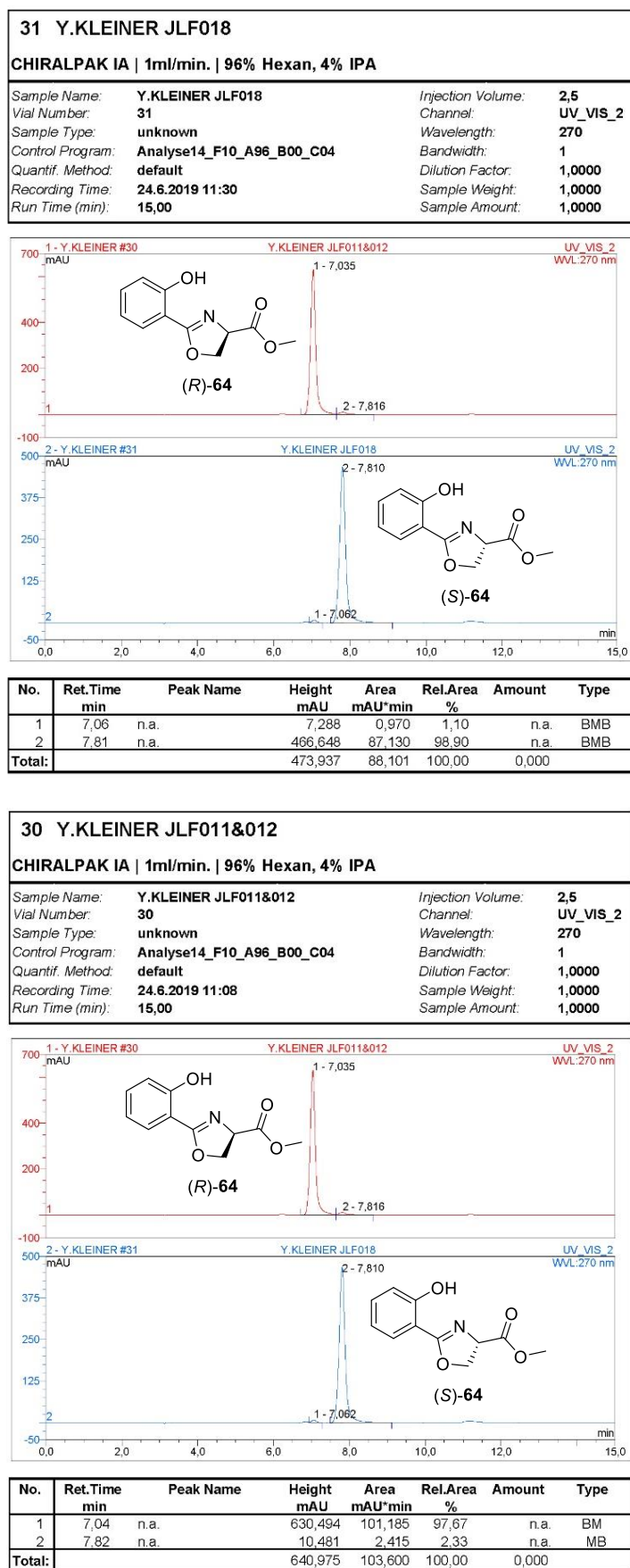
Fig. S99: Single (left) and double (middle/right) L-FDVA adducts of cyclic *N*α-methyl-*N*δ-hydroxyl-L-ornithine; reference: madurastatin C1*.

8.2.3 Stereoselective Synthesis of Madurastatin B1 and Derivatives

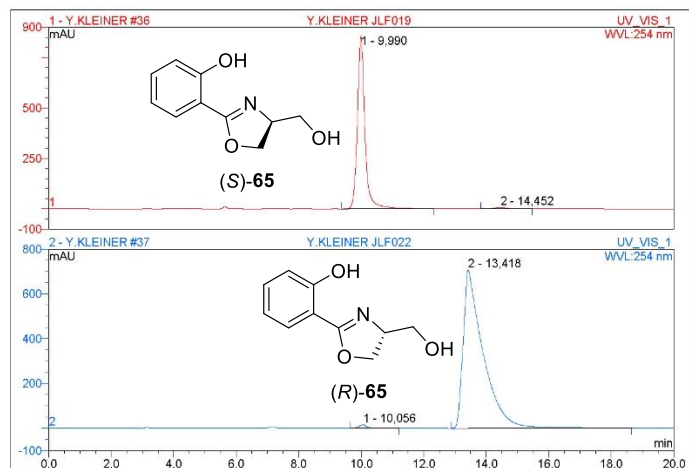
8.2.3.1 Comparison of Specific Rotation Values

Table S27: Specific rotation values of natural products described in literature in comparison to synthesized references.

NP (literature)	Synthetic Reference		NP (literature)
Madurastatin B1 ^[105]	(R)-50	(S)-50	-
$[\alpha]_D^{27} = -5.6$ (c 0.1, MeOH)	$[\alpha]_D^{25} = -48.0$ (c 0.4, DMSO)	$[\alpha]_D^{23} = +72.8$ (c 0.1, DMSO)	
(R)-64 ^[120]	(R)-64	(S)-64	-
$[\alpha]_D^{20} = -50.1$ (c 1.5, CHCl ₃ /MeOH)	$[\alpha]_D^{25} = -38.8$ (c 0.5, CHCl ₃)	$[\alpha]_D^{25} = +27.9$ (c 0.4, CHCl ₃)	
Nocazoline A ^[123]	(R)-65	(S)-65	Yanglingmycin ^[121]
$[\alpha]_D^{25} = +15.0$ (c 0.1, CHCl ₃)	$[\alpha]_D^{25} = +24.3$ (c 0.5, CHCl ₃)	$[\alpha]_D^{25} = -23.7$ (c 0.5, CHCl ₃)	$[\alpha]_D^{28} = -16.2$ (c 0.1, MeOH)
Spoxazomicin C ^[122]			Madurastatin B3 ^[108]
$[\alpha]_D^{25} = +7.4$ (c 0.1, MeOH)			$[\alpha]_D^{25} = -11.0$ (c 0.1, MeOH)
-	(R)-66	(S)-66	Spoxazomicin D ^[109]
	$[\alpha]_D^{25} = -28.5$ (c 1.1, MeOH/DMSO)	$[\alpha]_D^{25} = +34.4$ (c 1.1, MeOH/DMSO)	$[\alpha]_D^{25} = +62.0$ (c 1.0, MeOH/DMSO)

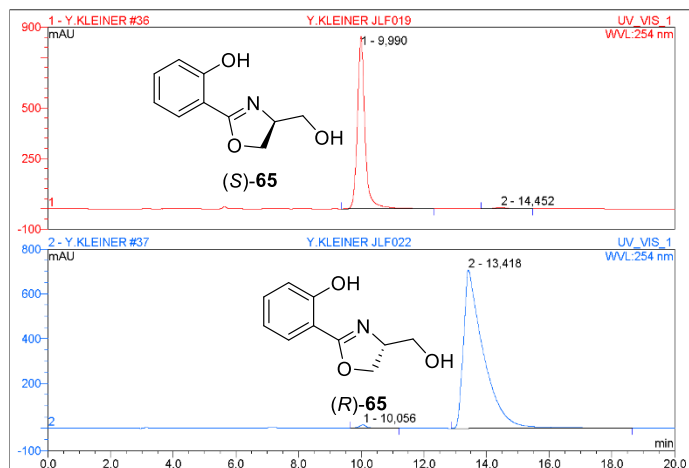
8.2.3.2 Determination of the Enantiomeric Excesses (*ee*)Fig. S100: Determination of *ee* for (S)-64 (top) and (R)-64 (bottom) by chiral HPLC.

37 Y.KLEINER JLF022		
CHIRALPAK IA 1ml/min. 90% Hexan, 10% IPA		
Sample Name:	Y.KLEINER JLF022	Injection Volume: 5,0
Vial Number:	37	Channel: UV_VIS_1
Sample Type:	unknown	Wavelength: 254
Control Program:	Analyse04_F10_A90_B00_C10	Bandwidth: 1
Quantif. Method:	default	Dilution Factor: 1,0000
Recording Time:	25.6.2019 9:06	Sample Weight: 1,0000
Run Time (min):	20,00	Sample Amount: 1,0000



No.	Ret.Time min	Peak Name	Height mAU	Area mAU*min	Rel.Area %	Amount	Type
1	10,06	n.a.	15,027	4,761	0,91	n.a.	BMB
2	13,42	n.a.	706,134	517,859	99,09	n.a.	BMB
Total:			721,162	522,621	100,00	0,000	

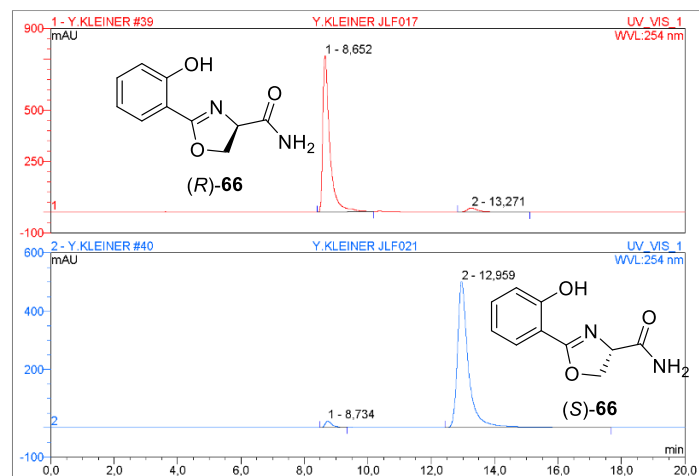
36 Y.KLEINER JLF019		
CHIRALPAK IA 1ml/min. 90% Hexan, 10% IPA		
Sample Name:	Y.KLEINER JLF019	Injection Volume: 5,0
Vial Number:	36	Channel: UV_VIS_1
Sample Type:	unknown	Wavelength: 254
Control Program:	Analyse04_F10_A90_B00_C10	Bandwidth: 1
Quantif. Method:	default	Dilution Factor: 1,0000
Recording Time:	25.6.2019 8:44	Sample Weight: 1,0000
Run Time (min):	20,00	Sample Amount: 1,0000



No.	Ret.Time min	Peak Name	Height mAU	Area mAU*min	Rel.Area %	Amount	Type
1	9,99	n.a.	854,532	238,282	98,63	n.a.	BMB
2	14,45	n.a.	7,274	3,311	1,37	n.a.	BMB
Total:			861,806	241,593	100,00	0,000	

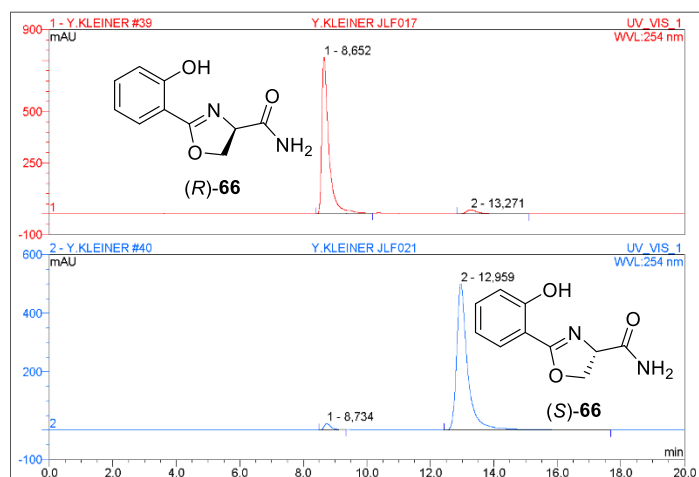
Fig. S101: Determination of *ee* for (*R*)-65 (top) and (*S*)-65 (bottom) by chiral HPLC.

40 Y.KLEINER JLF021		
CHIRALPAK IA 1ml/min. 85% Hexan, 15% IPA		
Sample Name:	Y.KLEINER JLF021	Injection Volume: 5,0
Vial Number:	40	Channel: UV_VIS_1
Sample Type:	unknown	Wavelength: 254
Control Program:	Analyse03_F10_A85_B00_C15	Bandwidth: 1
Quantif. Method:	default	Dilution Factor: 1,0000
Recording Time:	25.6.2019 11:31	Sample Weight: 1,0000
Run Time (min):	20,00	Sample Amount: 1,0000



No.	Ret.Time min	Peak Name	Height mAU	Area mAU*min	Rel.Area %	Amount	Type
1	8,73	n.a.	22,004	5,450	2,67	n.a.	BMB
2	12,96	n.a.	500,985	198,280	97,33	n.a.	BMB
Total:			522,989	203,730	100,00	0,000	

39 Y.KLEINER JLF017		
CHIRALPAK IA 1ml/min. 85% Hexan, 15% IPA		
Sample Name:	Y.KLEINER JLF017	Injection Volume: 5,0
Vial Number:	39	Channel: UV_VIS_1
Sample Type:	unknown	Wavelength: 254
Control Program:	Analyse03_F10_A85_B00_C15	Bandwidth: 1
Quantif. Method:	default	Dilution Factor: 1,0000
Recording Time:	25.6.2019 10:50	Sample Weight: 1,0000
Run Time (min):	20,00	Sample Amount: 1,0000



No.	Ret.Time min	Peak Name	Height mAU	Area mAU*min	Rel.Area %	Amount	Type
1	8,65	n.a.	766,156	194,196	96,03	n.a.	BMB
2	13,27	n.a.	19,755	8,038	3,97	n.a.	BMB
Total:			785,911	202,234	100,00	0,000	

Fig. S102: Determination of ee for (*S*)-66 (top) and (*R*)-66 (bottom) by chiral HPLC.

8.2.4 Iron Chelating Properties

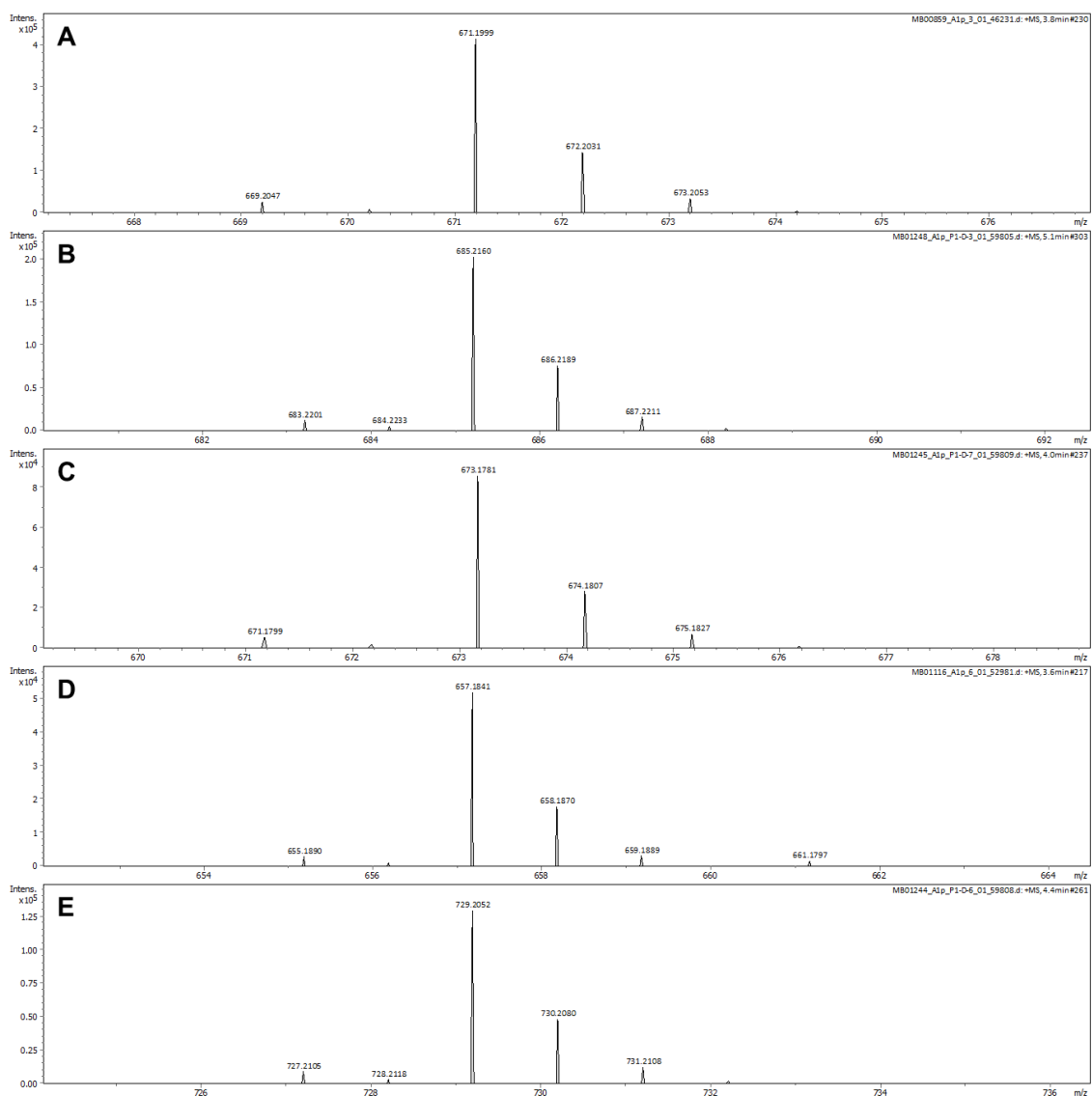


Fig. S103: Isotope pattern of positive HRESIMS $[M-2H+Fe]^+$ adduct ion of A: madurastatin D1 (*ent*-53a), B: madurastatin D2 (*ent*-54a), C: madurastatin C2 (**61**), D: madurastatin D3 (**62**) and E: madurastatin D4 (**63**).

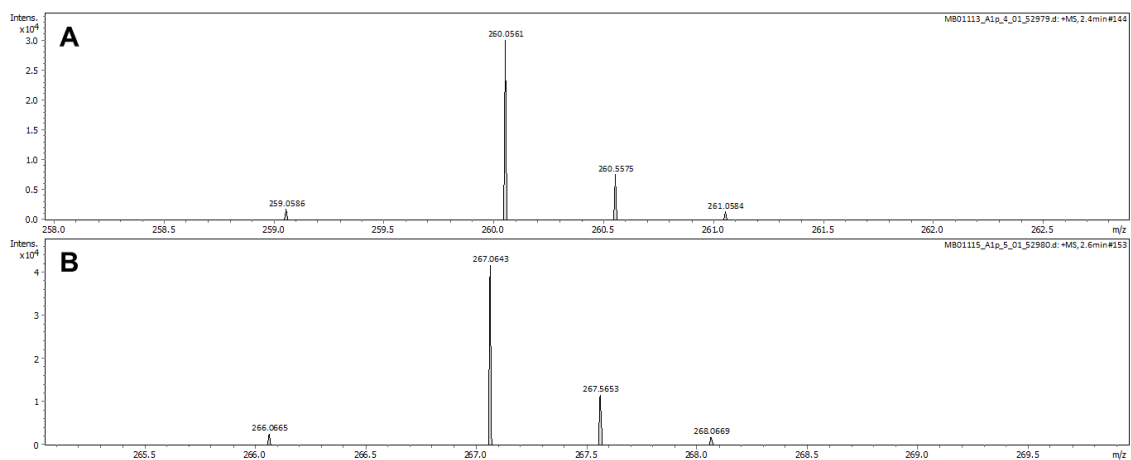


Fig. S104: Isotope pattern of positive HRESIMS $[M-H+Fe]^{2+}$ adduct ion of A: madurastatin G1 (**59**) and B: madurastatin G2 (**60**).

8.3 Amino- and Phospholipids from *Olivibacter* sp. FHG000416

8.3.1 Dereplication

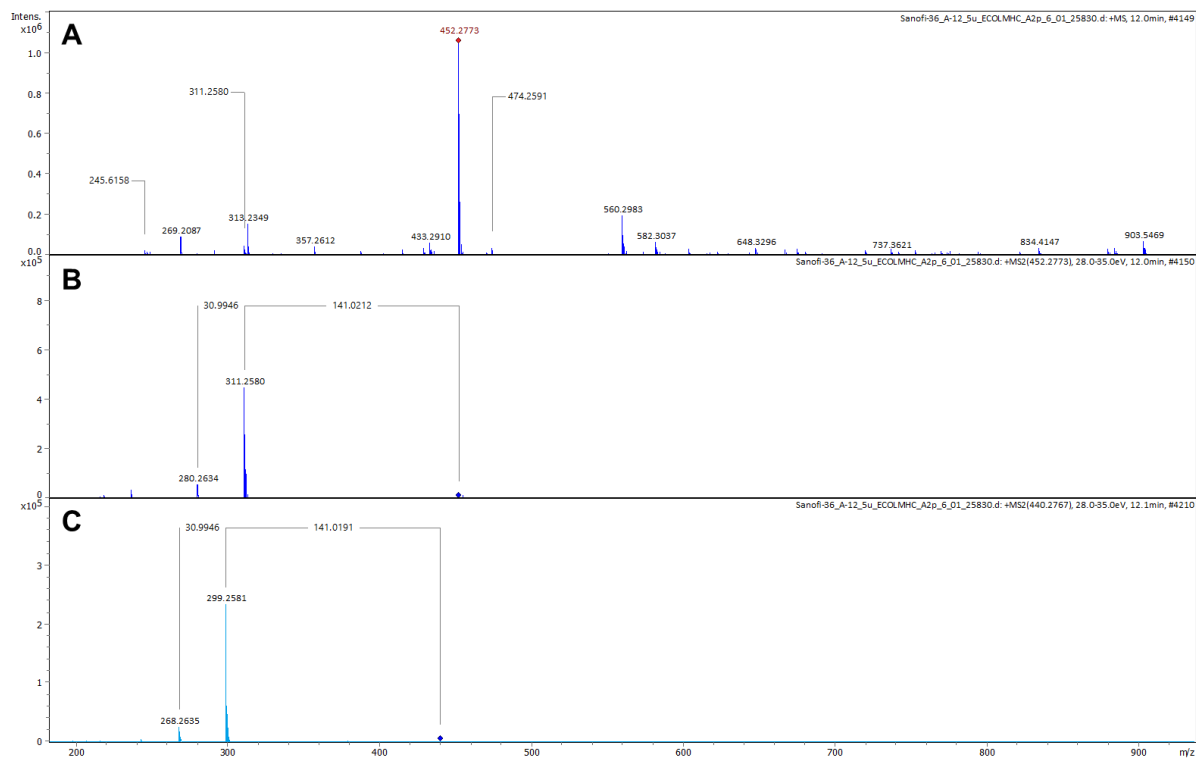
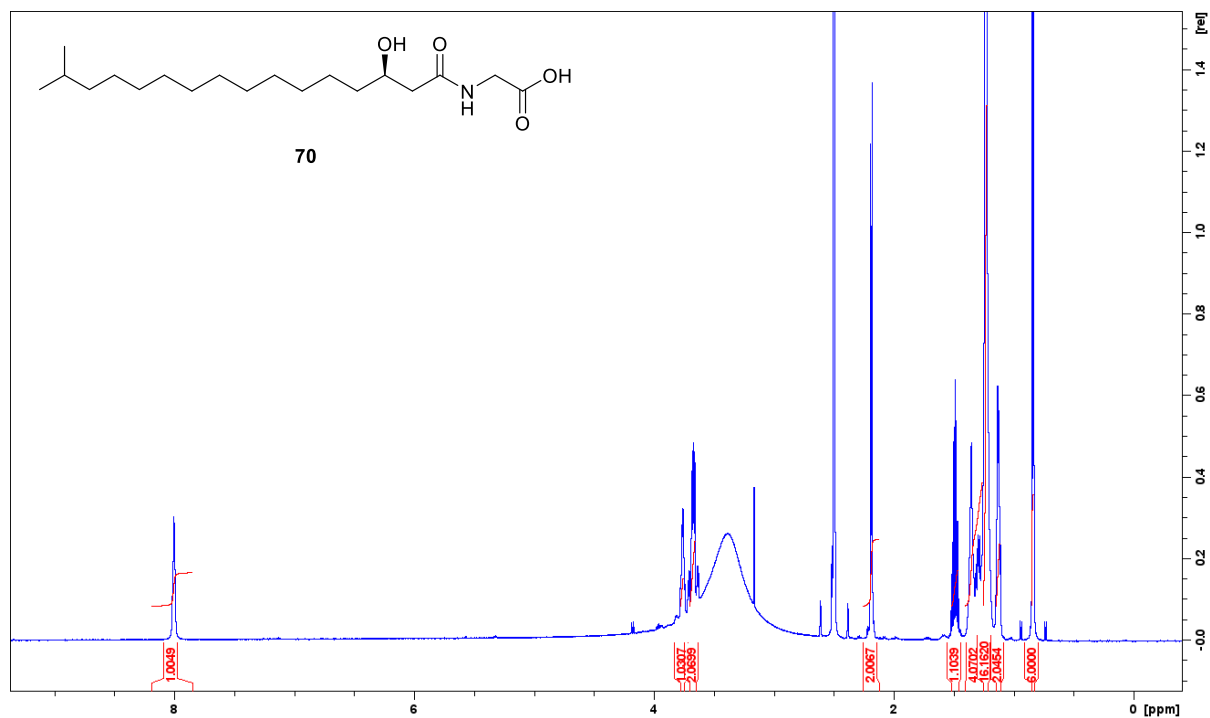
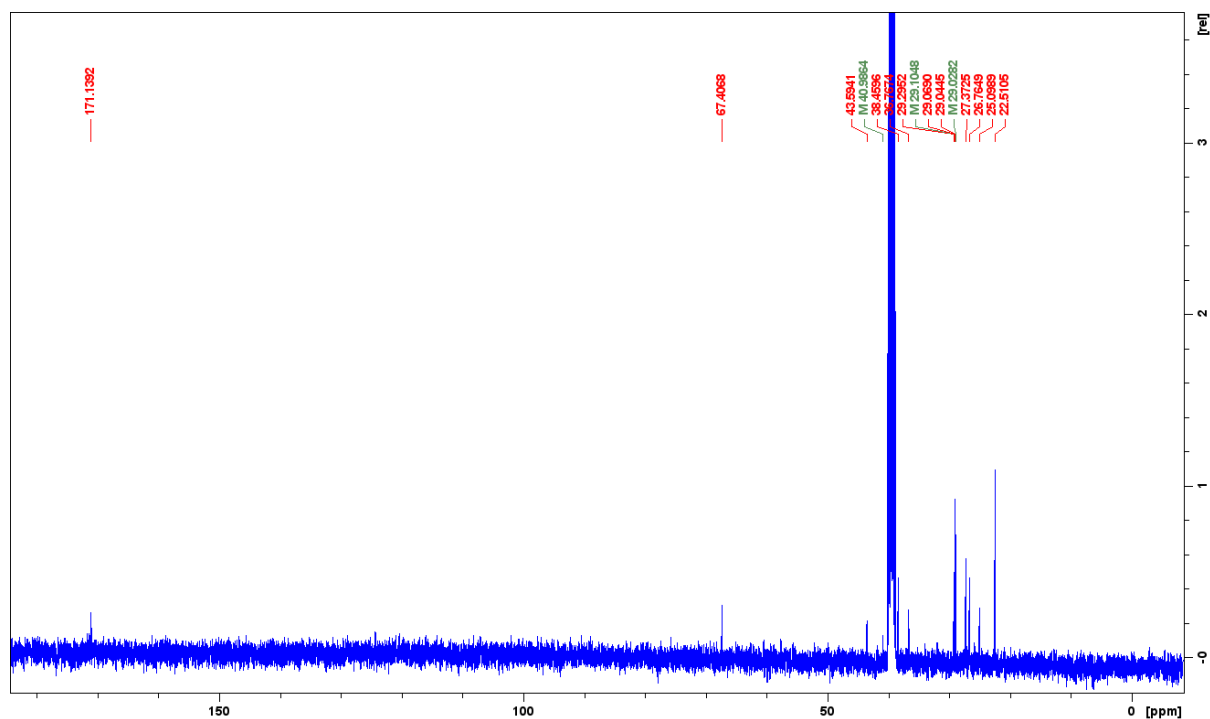
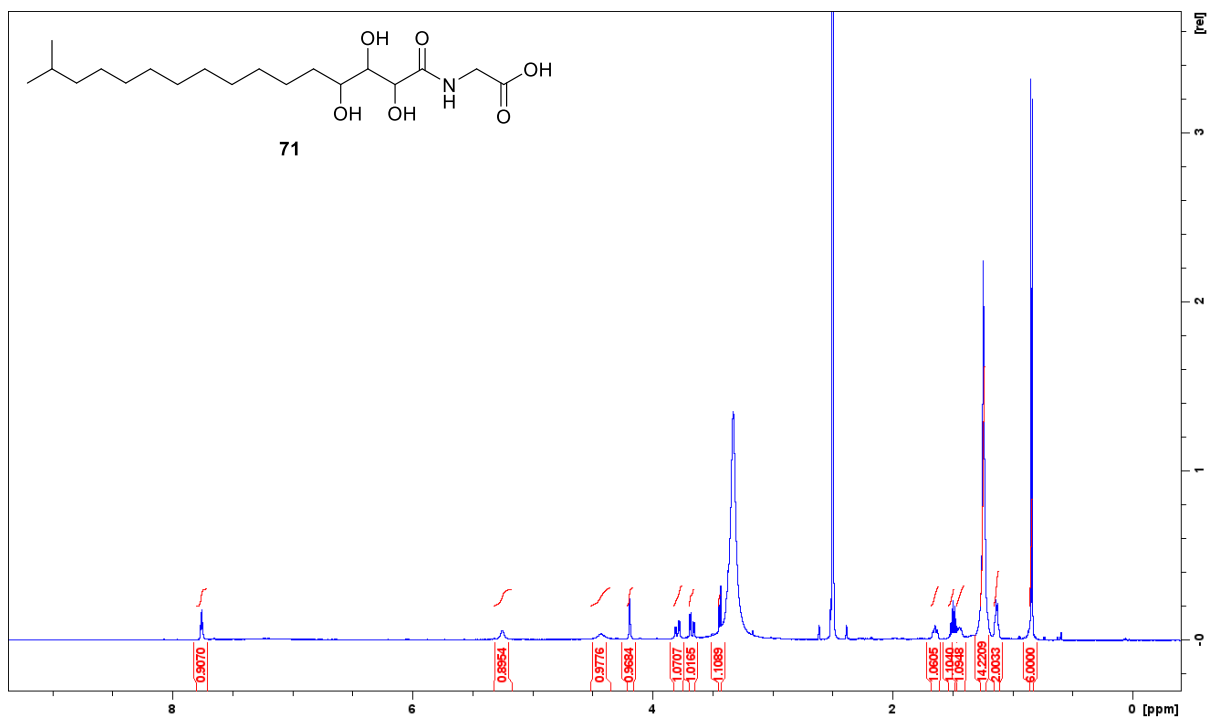
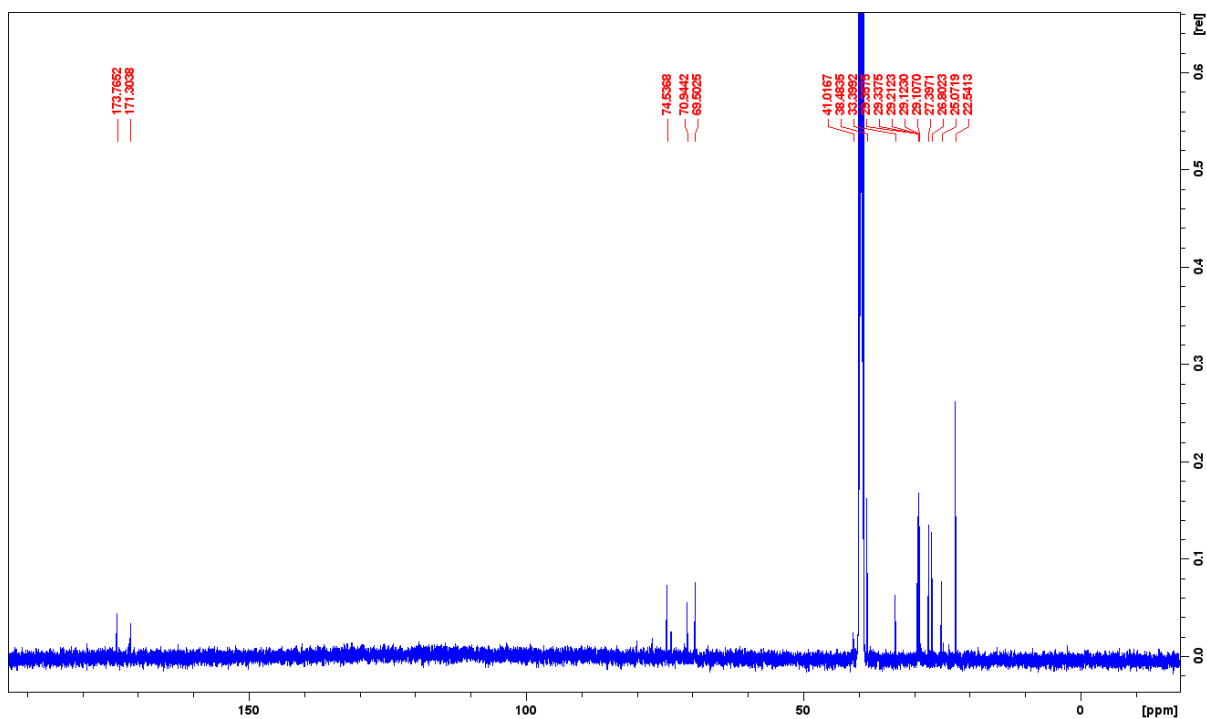


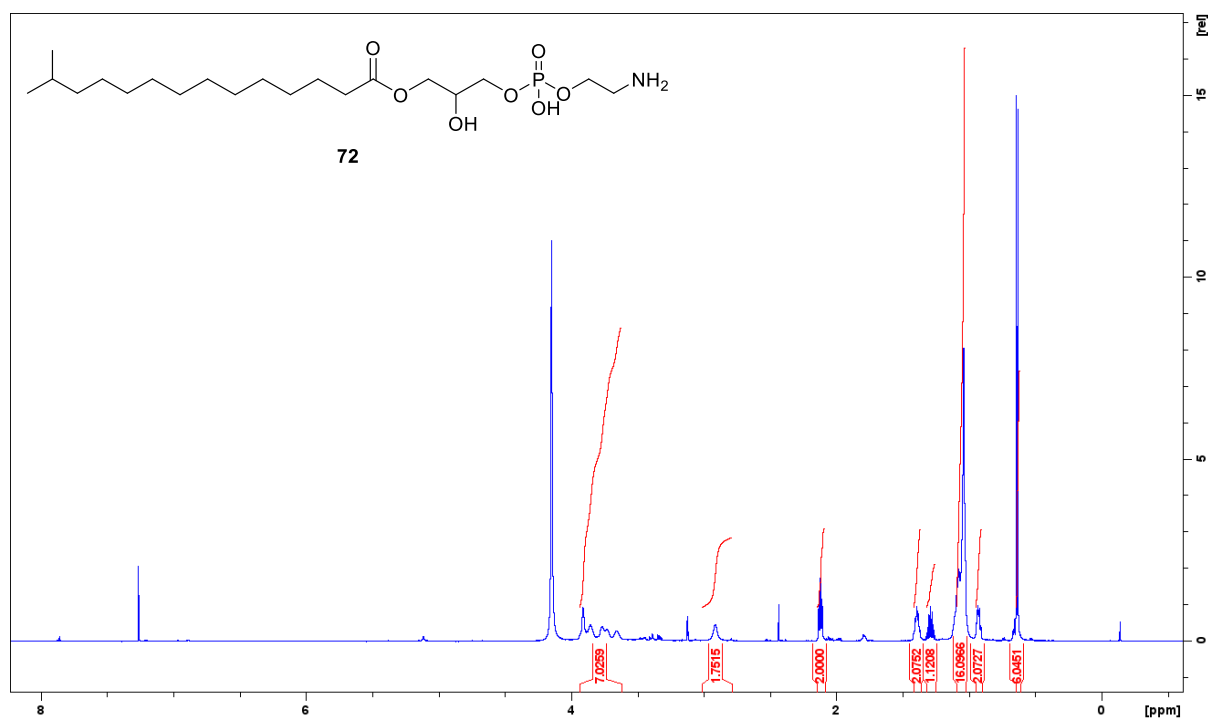
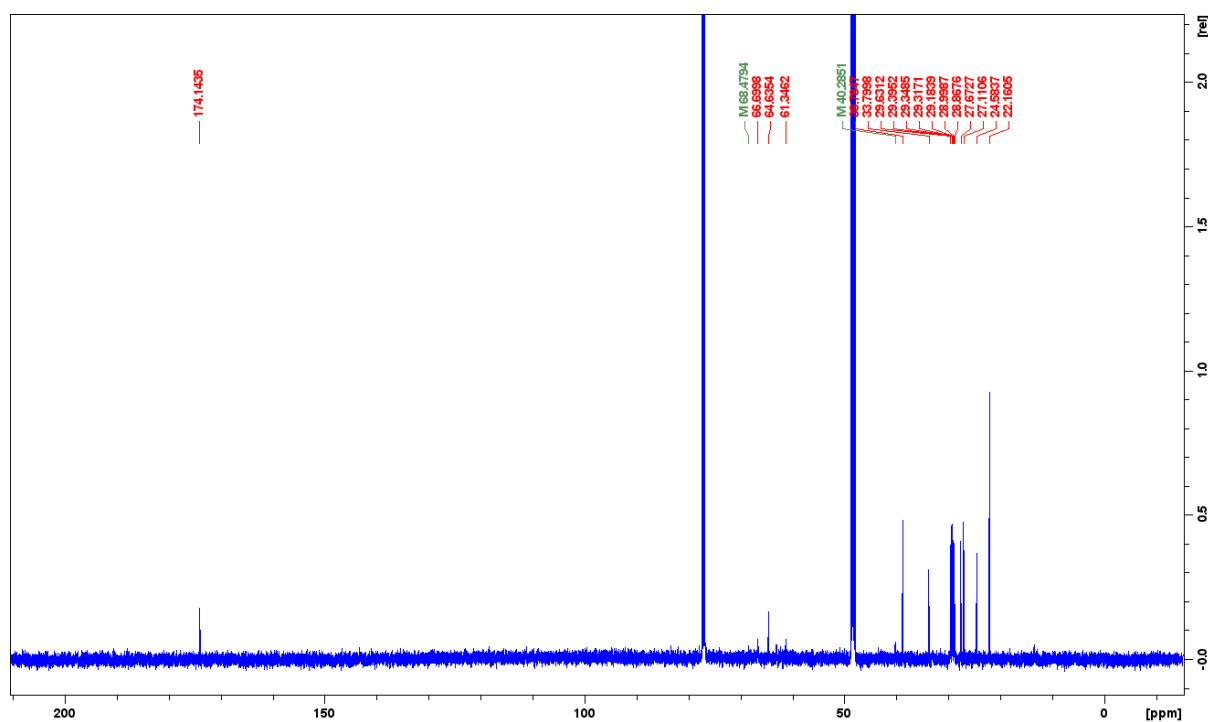
Fig. S105: Lysophosphatidylethanolamines in the crude extract of FHG000416. A: MS spectrum of FE006 (73) at $t_R=12.0$ min; B: MS/MS spectrum of m/z 452.2773 ($[M+H]^+$ parent ion of FE006 (73)); C: MS/MS spectrum of m/z 440.2767 ($[M+H]^+$ parent ion of FE005 (72)).

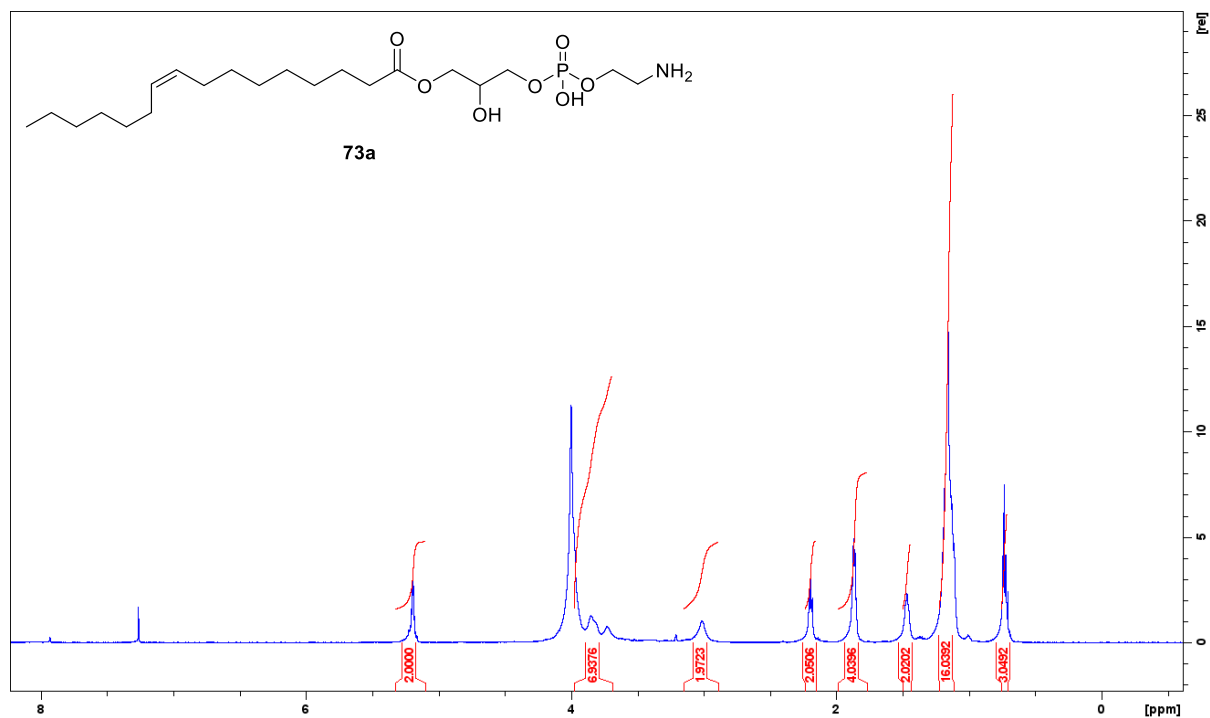
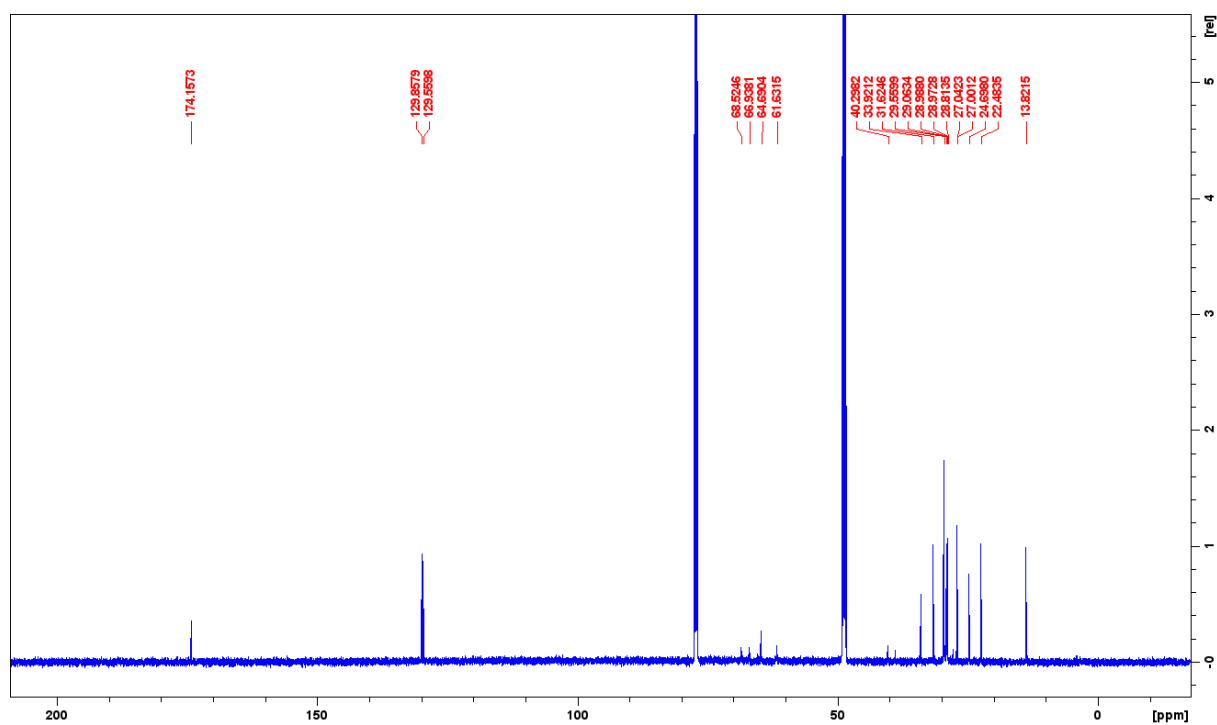
8.3.2 Structure Elucidation

8.3.2.1 NMR Spectra

Fig. S106: ¹H-NMR (600 MHz, DMSO-*d*₆) of FE003 (70).Fig. S107: ¹³C-NMR (151 MHz, DMSO-*d*₆) of FE003 (70).

Fig. S108: ¹H-NMR (600 MHz, DMSO-*d*₆) of FE004 (71).Fig. S109: ¹³C-NMR (151 MHz, DMSO-*d*₆) of FE004 (71).

Fig. S110: ¹H-NMR (600 MHz, CDCl₃/MeOD-*d*₄ 2:1) of FE005 (72).Fig. S111: ¹³C-NMR (151 MHz, CDCl₃/MeOD-*d*₄ 2:1) of FE005 (72).

Fig. S112: $^1\text{H-NMR}$ (600 MHz, $\text{CDCl}_3/\text{MeOD-}d_4$ 2:1) of FE006 (73a).Fig. S113: $^{13}\text{C-NMR}$ (151 MHz, $\text{CDCl}_3/\text{MeOD-}d_4$ 2:1) of FE006 (73a).

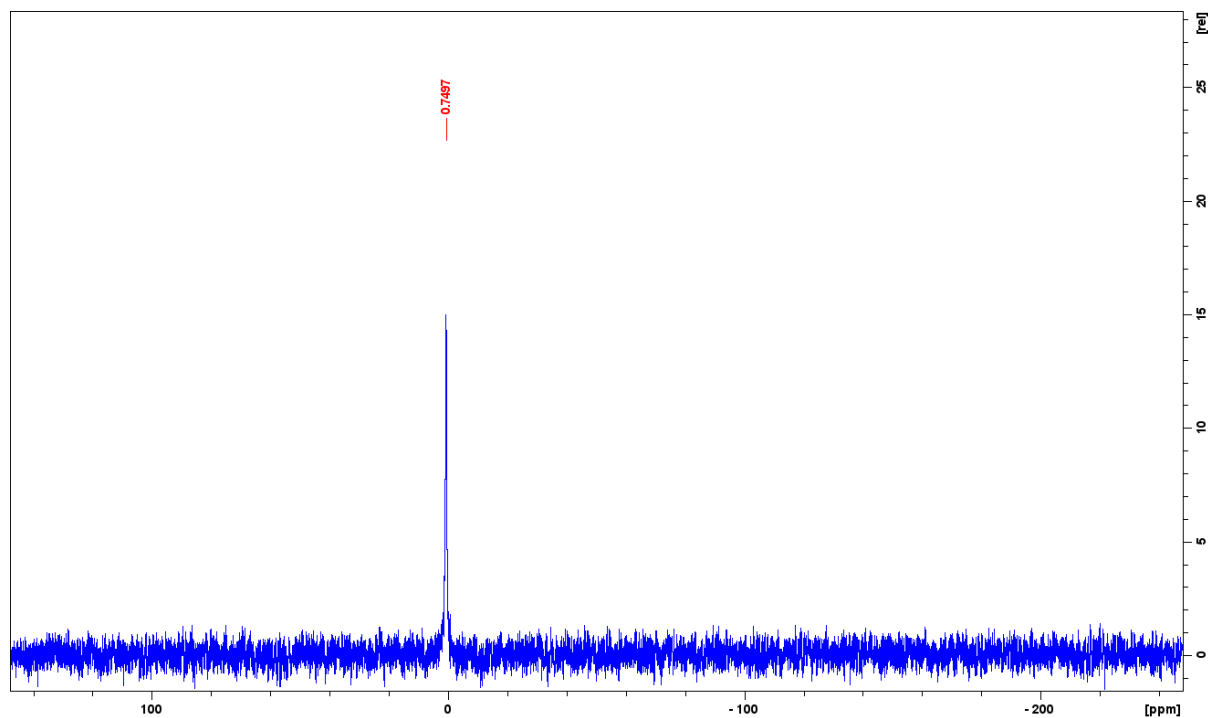


Fig. S114: ^{31}P -NMR (243 MHz, $\text{CDCl}_3/\text{MeOD}-d_4$ 2:1) of FE005 (72).

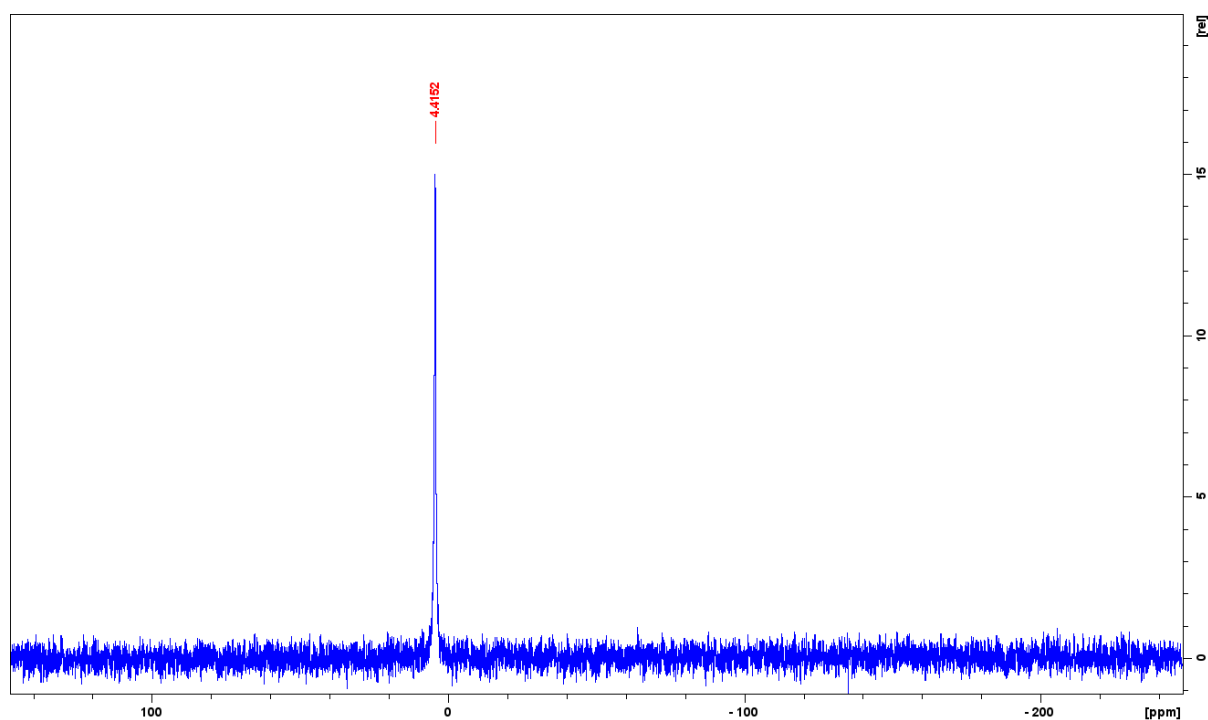
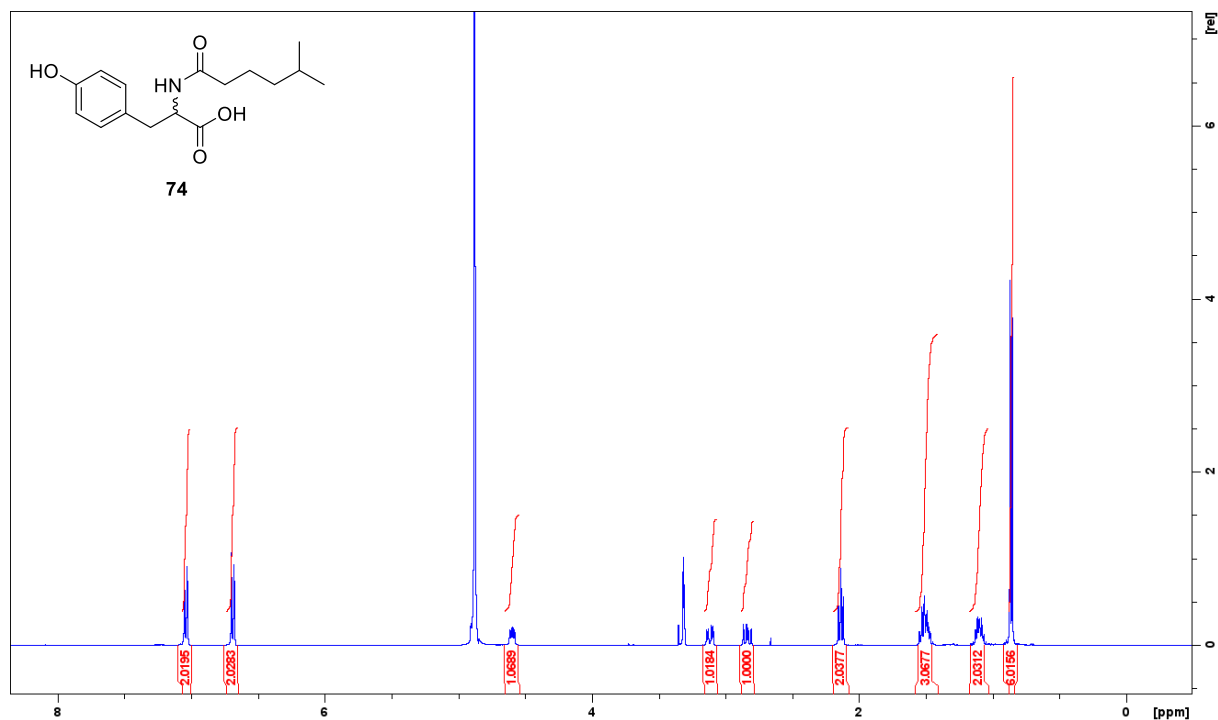
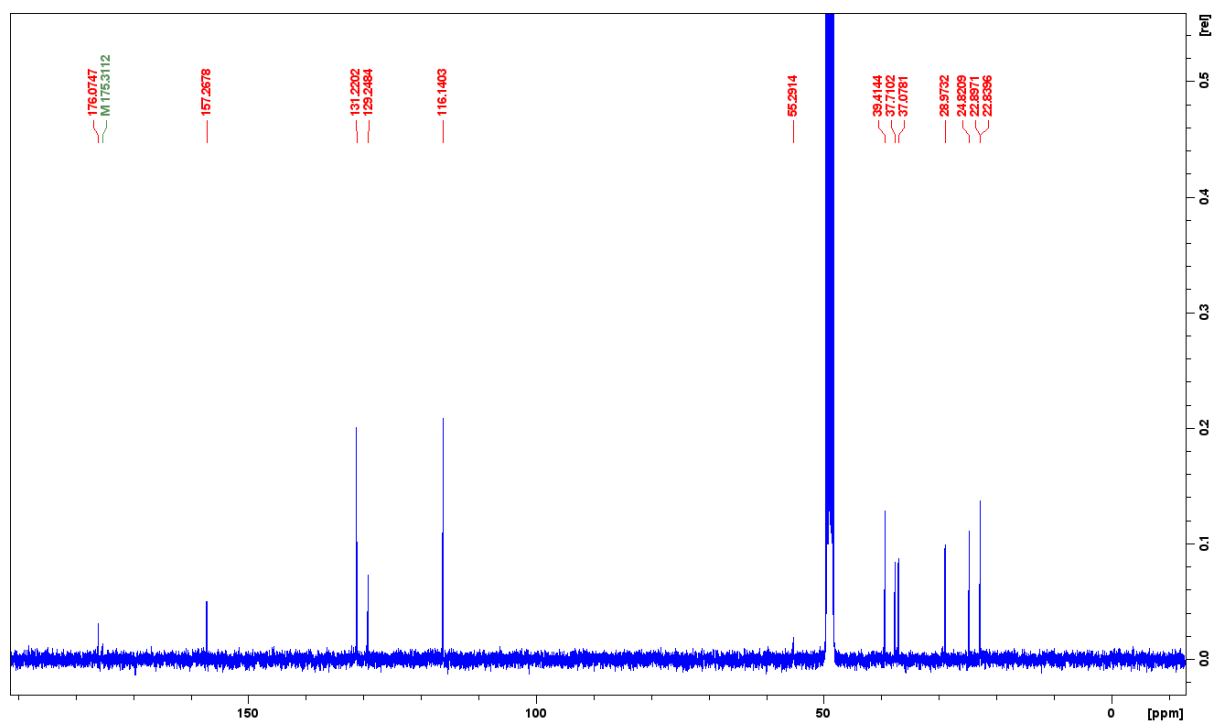
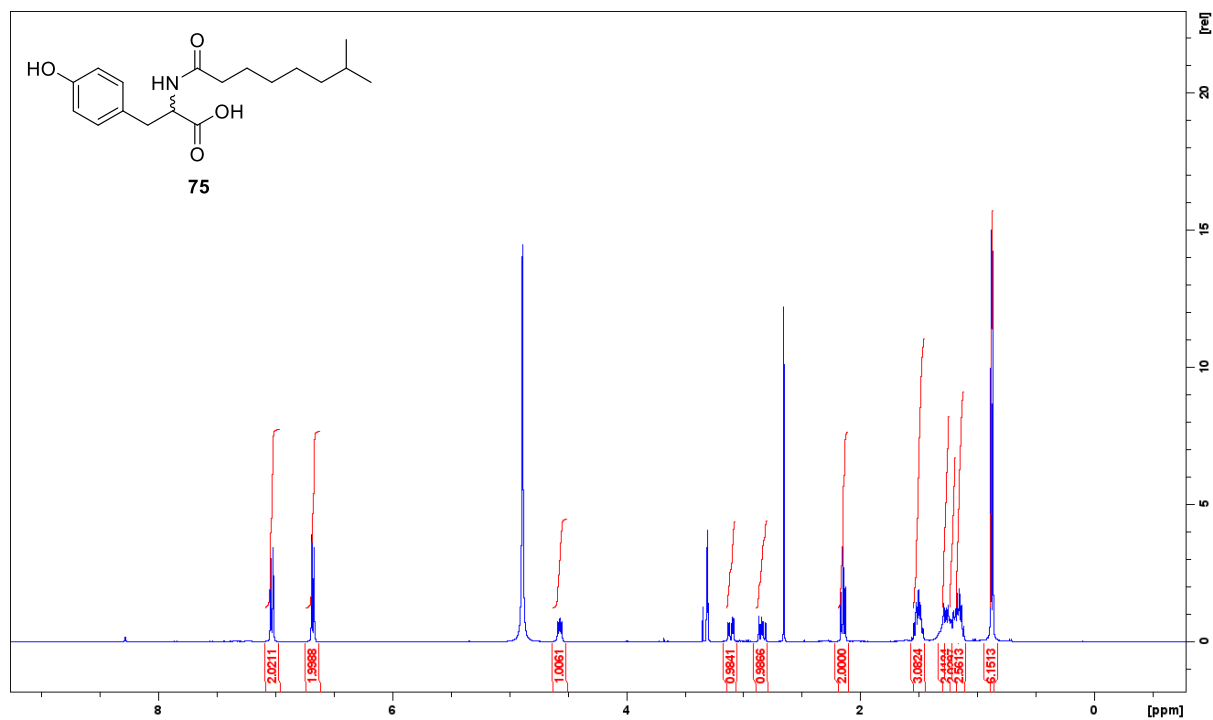
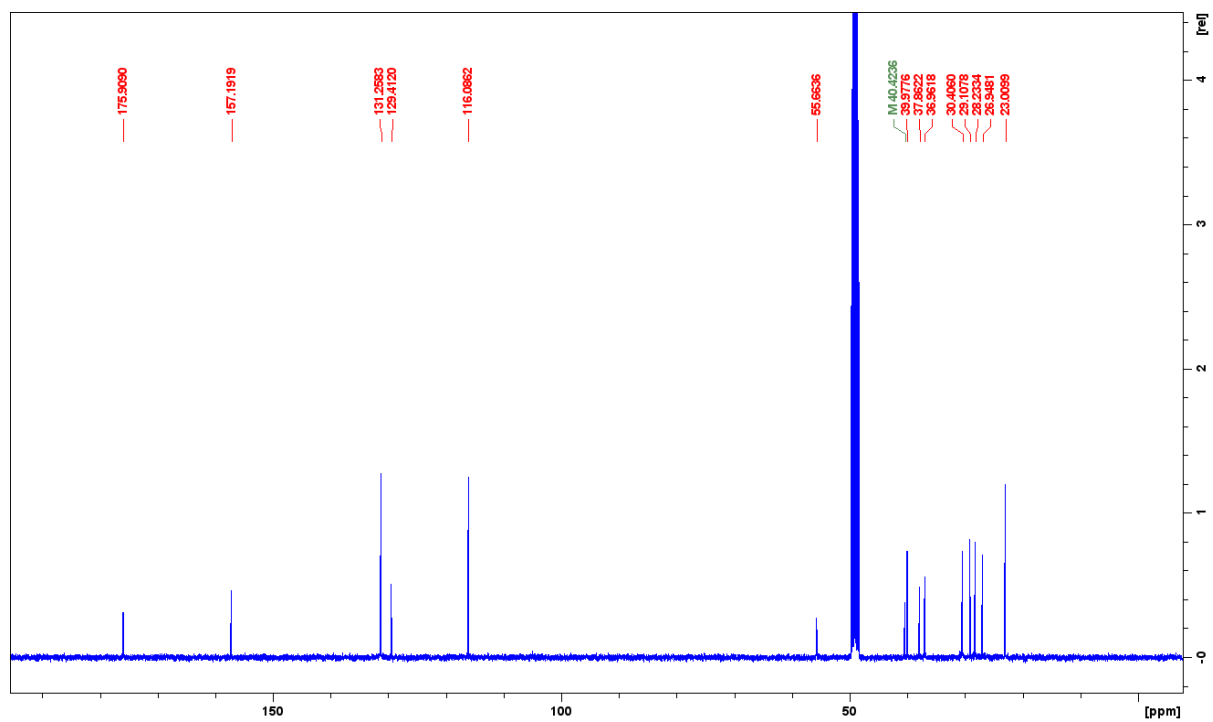
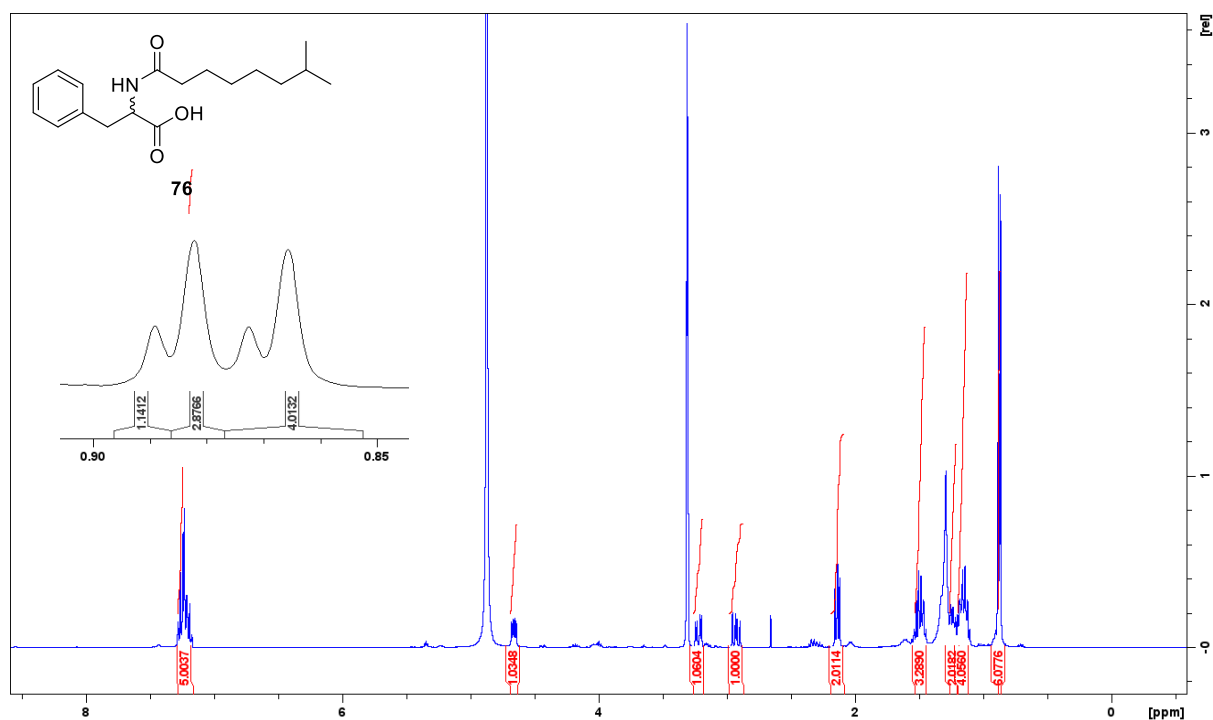
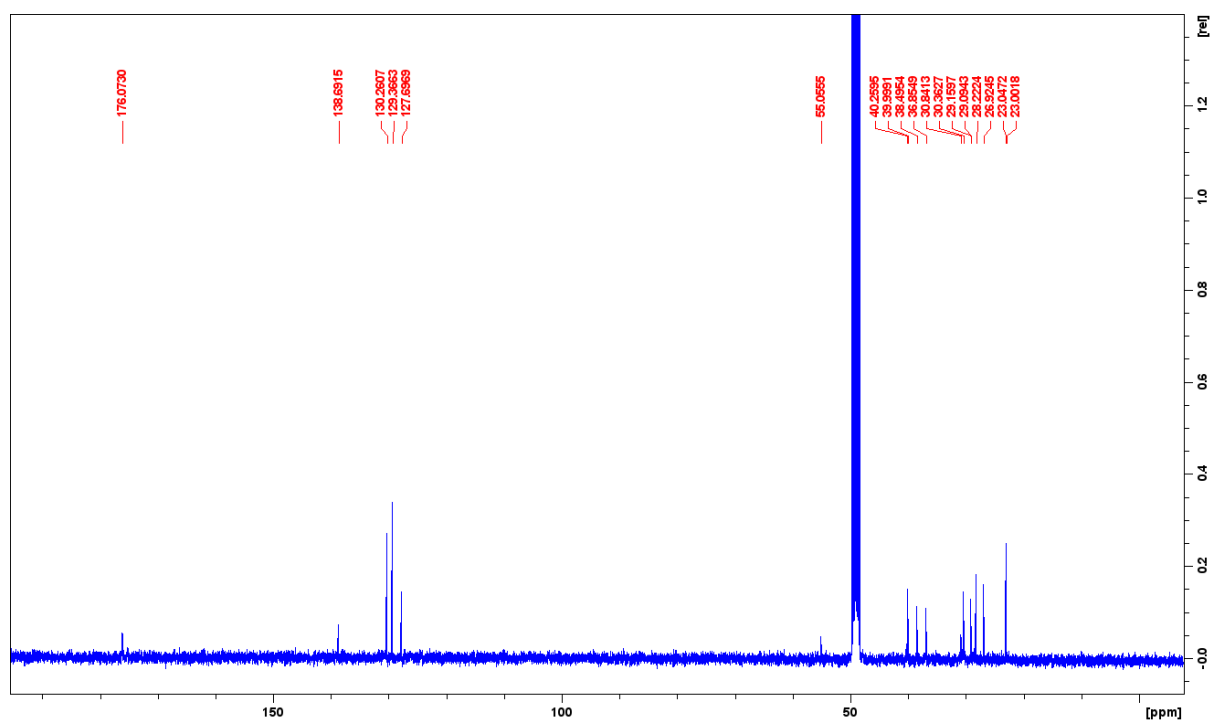
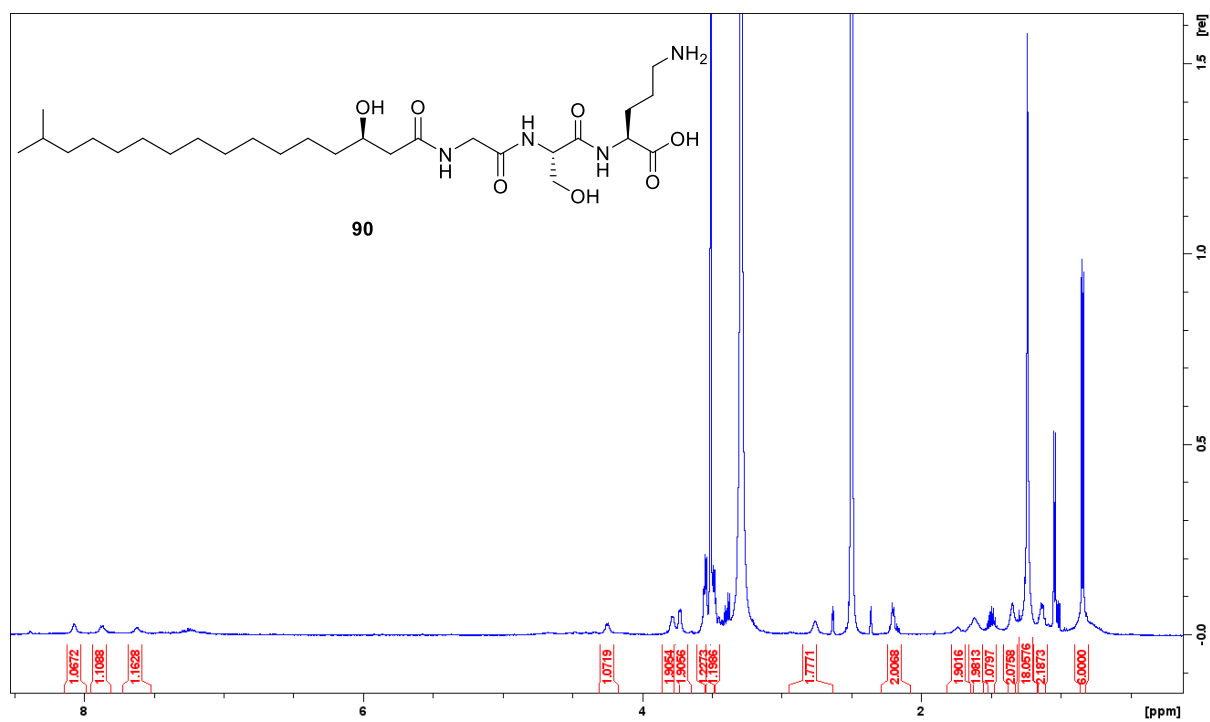
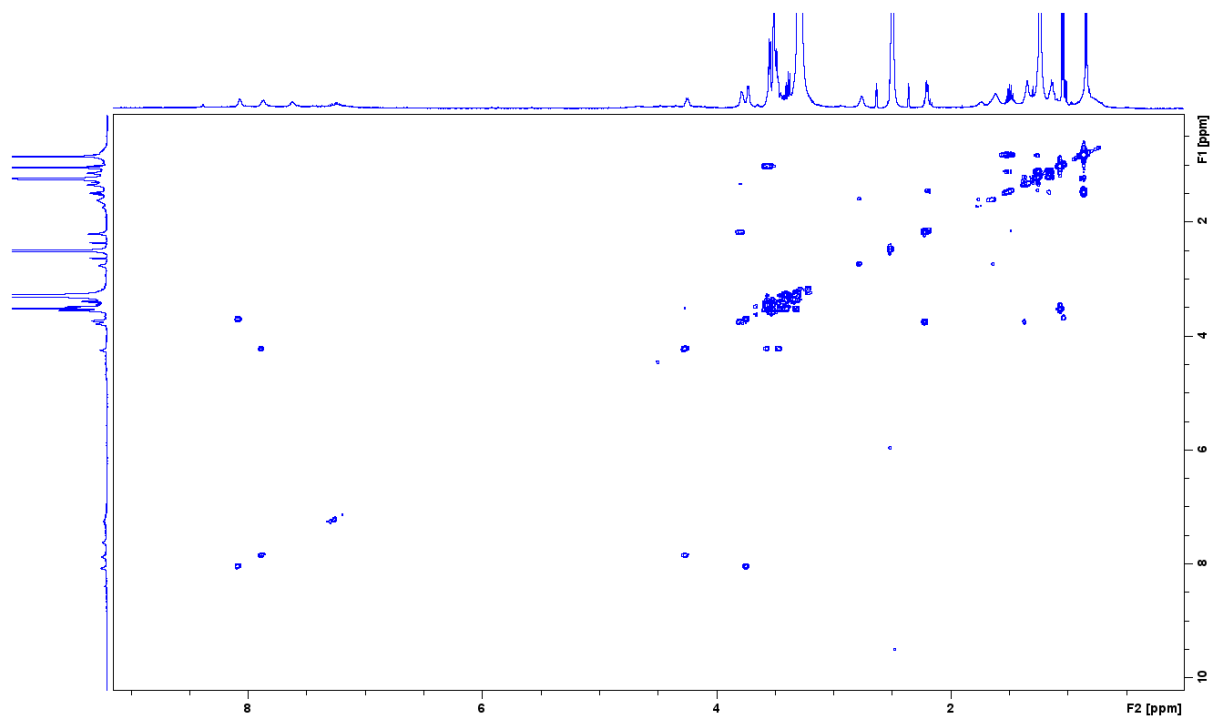


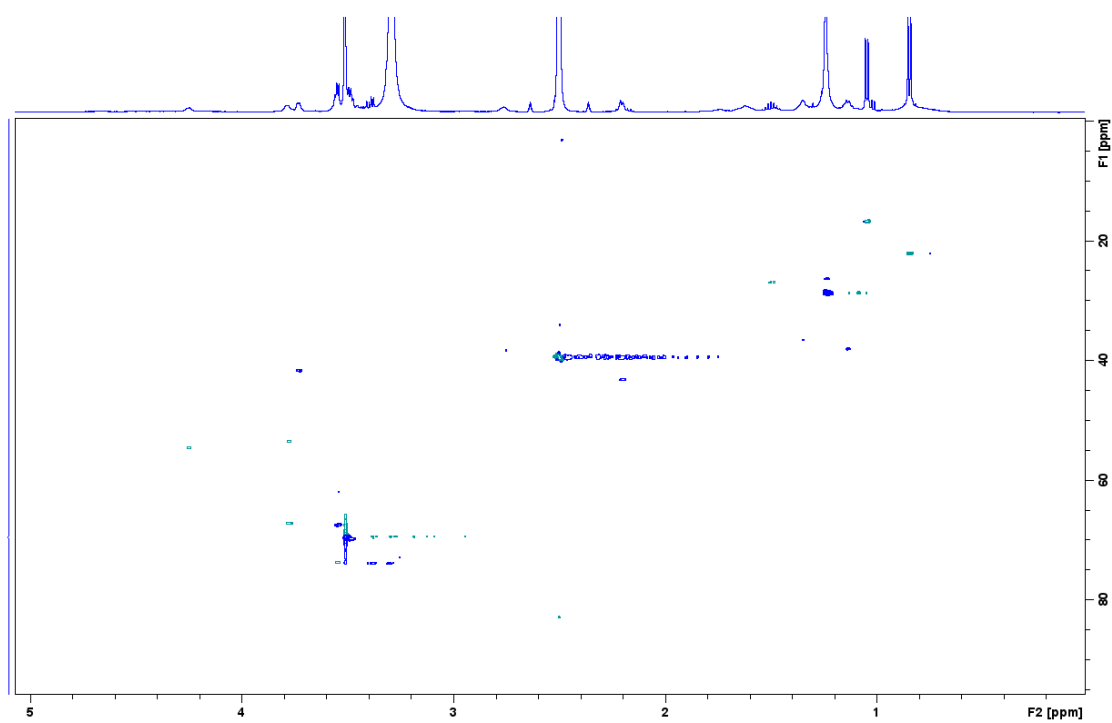
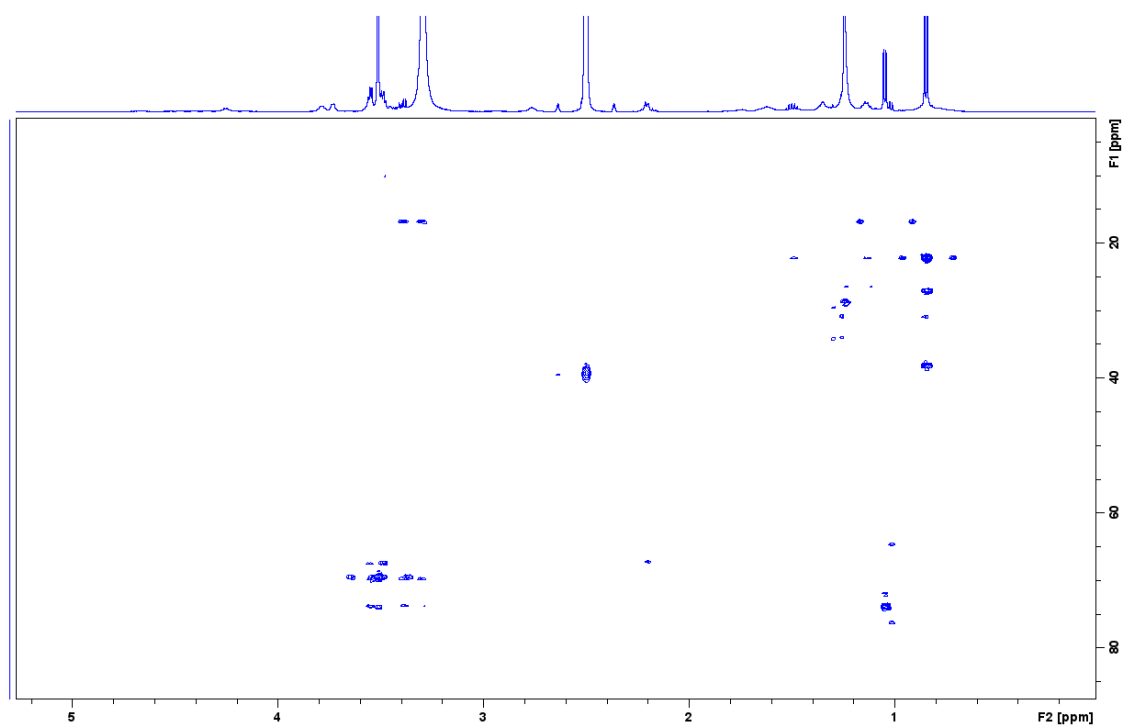
Fig. S115: ^{31}P -NMR (243 MHz, $\text{CDCl}_3/\text{MeOD}-d_4$ 2:1) of FE006 (73a).

Fig. S116: ¹H-NMR (400 MHz, MeOD-*d*₄) of FE008 (74).Fig. S117: ¹³C-NMR (101 MHz, MeOD-*d*₄) of FE008 (74).

Fig. S118: ¹H-NMR (400 MHz, MeOD-*d*₄) of FE009 (75).Fig. S119: ¹³C-NMR (101 MHz, MeOD-*d*₄) of FE009 (75).

Fig. S120: ¹H-NMR (400 MHz, MeOD-*d*₄) of FE10 (76).Fig. S121: ¹³C-NMR (101 MHz, MeOD-*d*₄) of FE10 (76).

Fig. S122: $^1\text{H-NMR}$ (500 MHz, $\text{DMSO-}d_6$) of FE002 (**90**).Fig. S123: $^1\text{H-}^1\text{H}$ COSY (500 MHz, $\text{DMSO-}d_6$) spectrum of FE002 (**90**).

Fig. S124: ^1H - ^{13}C HSQC (500 MHz, $\text{DMSO}-d_6$) spectrum of FE002 (**90**).Fig. S125: ^1H - ^{13}C HMBC (500 MHz, $\text{DMSO}-d_6$) spectrum of FE002 (**90**).

8.3.2.2 MS/MS Spectra

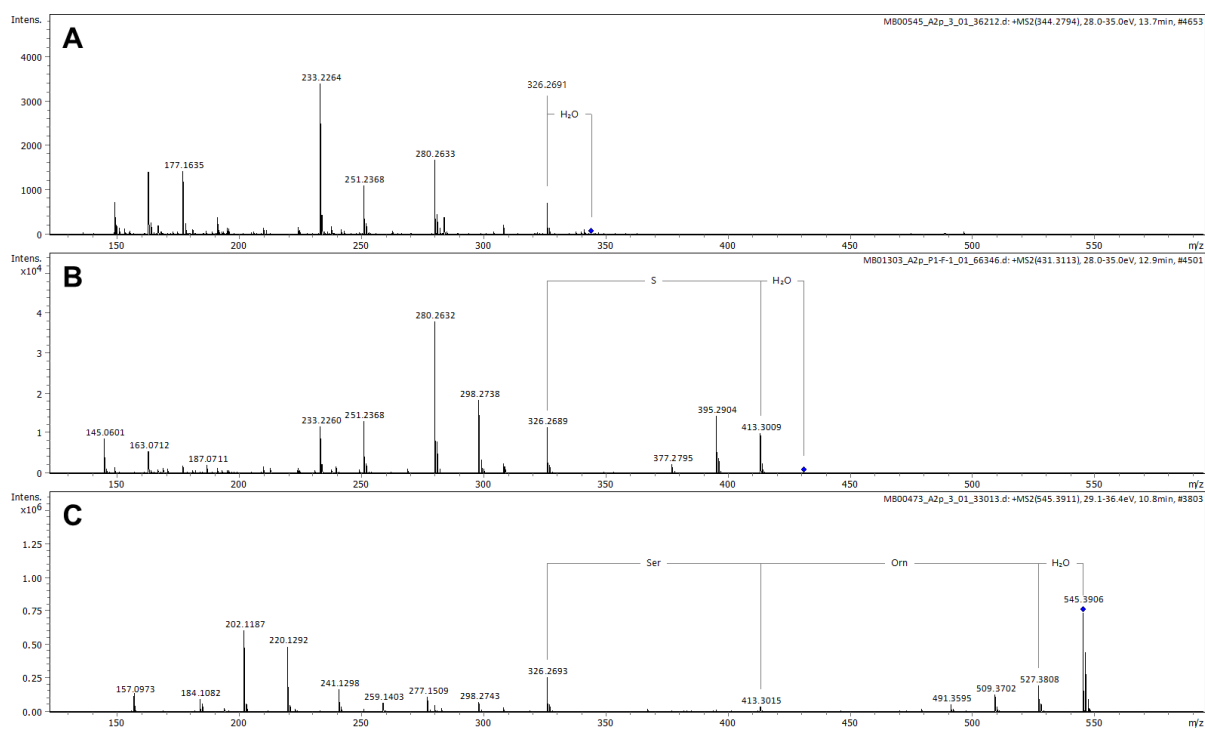


Fig. S126: MS/MS spectra of A: FE003 (**70**), B: Lipid 430 (**87**) and FE002 (**90**). Neutral losses are annotated leading to shared fragment ion of m/z 326.2693 (correlating to $C_{19}H_{36}NO_3^+$).

8.3.2.3 Marfey's Analysis

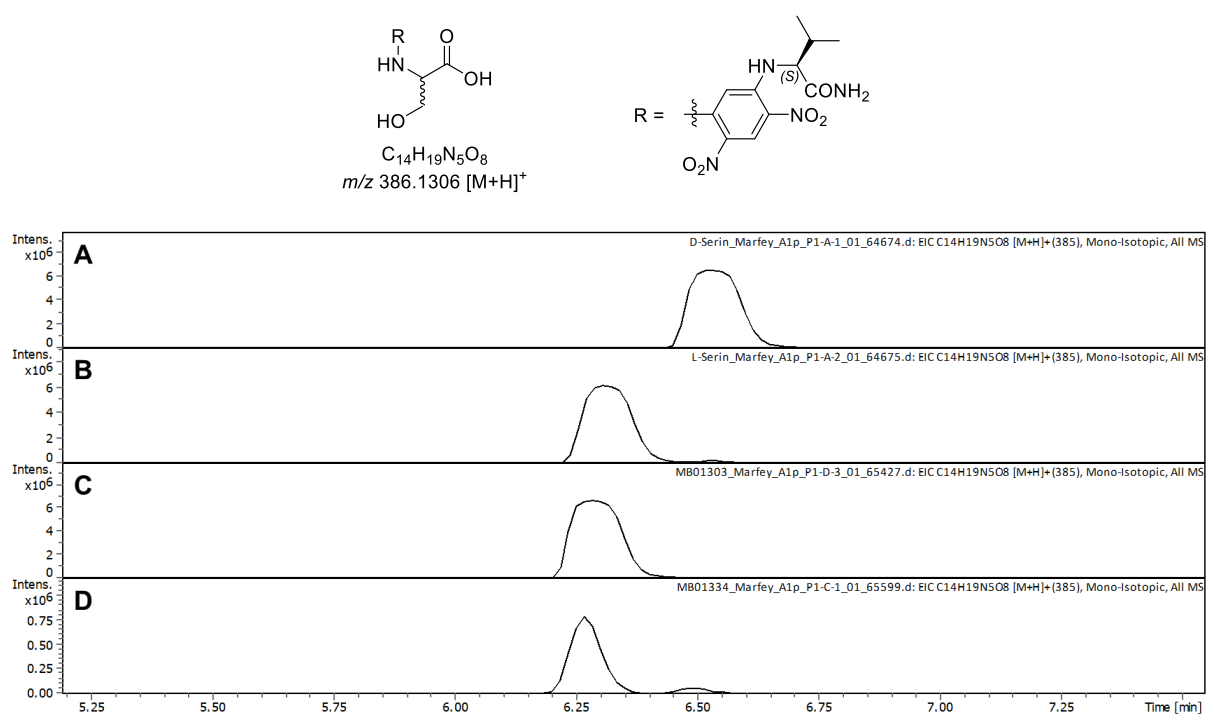


Fig. S127: L-FDVA adducts of serine. EICs (m/z 386.1306 \pm 0.005, $C_{14}H_{19}N_5O_8$, $[M+H]^+$) for A: D-serine reference, B: L-serine reference, C: hydrolyzed Lipid 430 (**87**) and D: hydrolyzed FE002 (**90**).

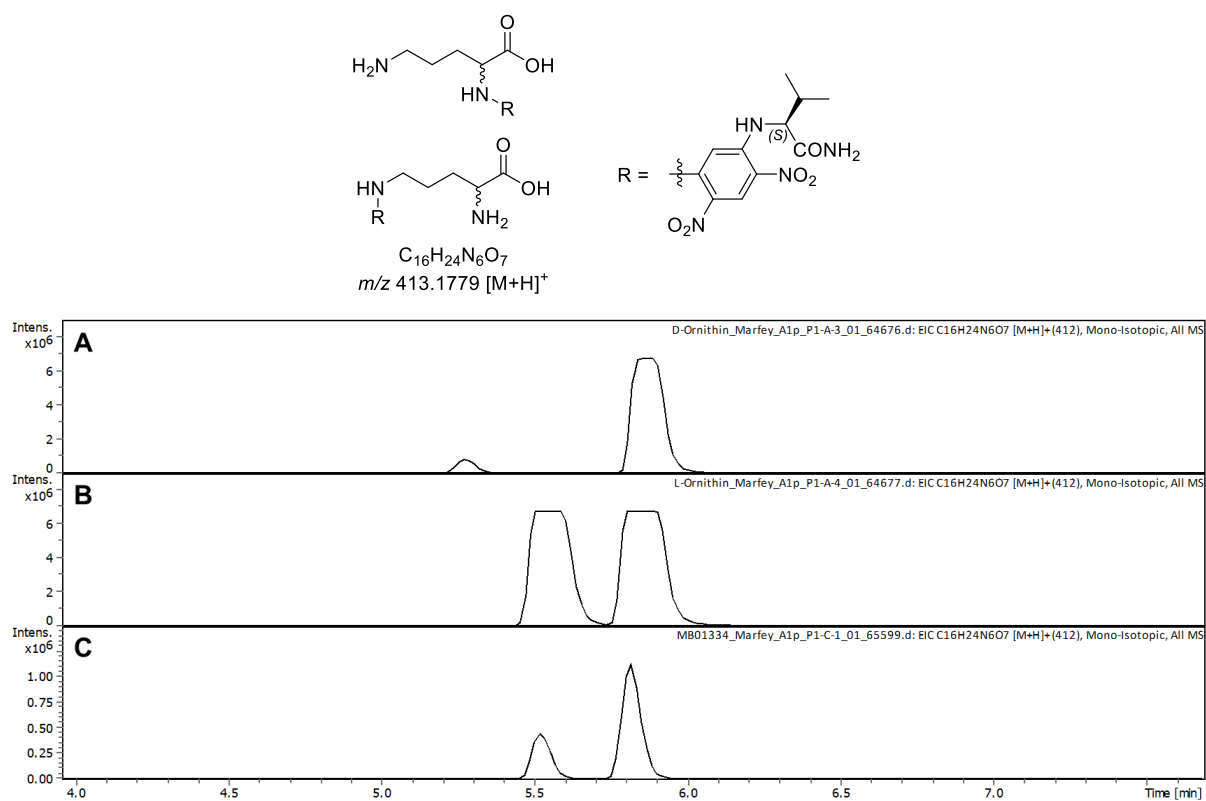


Fig. S128: L-FDVA adducts of ornithine. EICs (m/z 413.1779 \pm 0.005, $C_{16}H_{24}N_6O_7$, $[M+H]^+$) for A: D-ornithine reference, B: L-ornithine reference, C: hydrolyzed FE002 (**90**).

8. Appendix

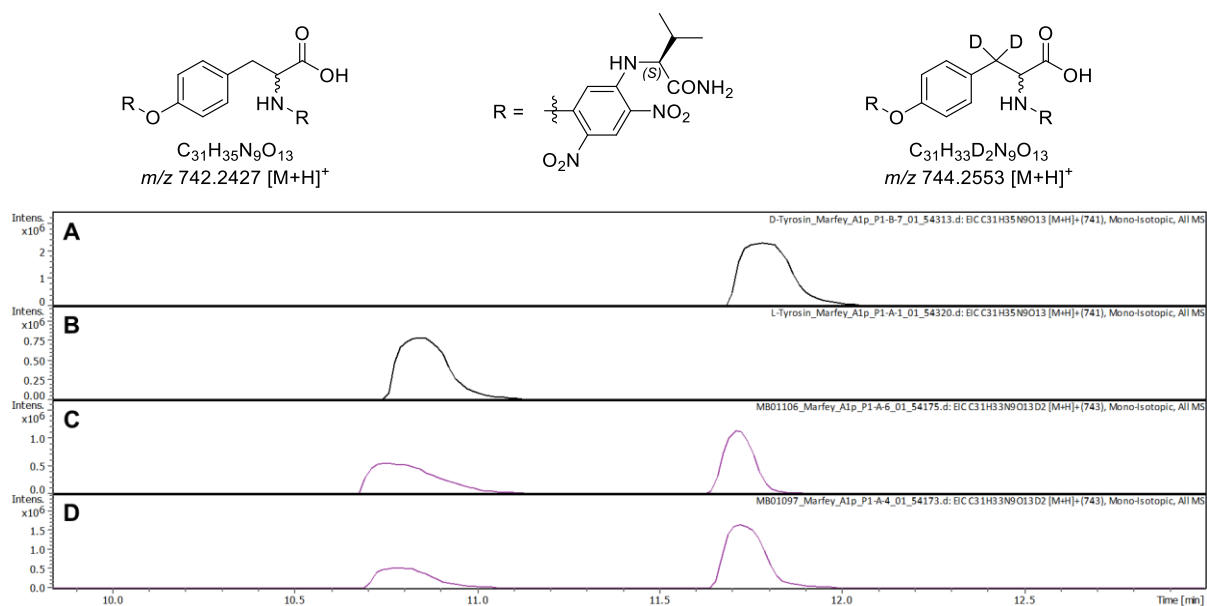


Fig. S129: Double L-FDVA adducts of tyrosine. EICs (m/z 742.2427 ± 0.005, $C_{31}H_{35}N_9O_{13}$, $[M+H]^+$) for A: D-tyrosine reference, B: L-tyrosine reference and EICs (m/z 744.2553 ± 0.005, $C_{31}H_{33}D_2N_9O_{13}$, $[M+H]^+$) for C: hydrolyzed FE008 (74) and D: hydrolyzed FE009 (75).

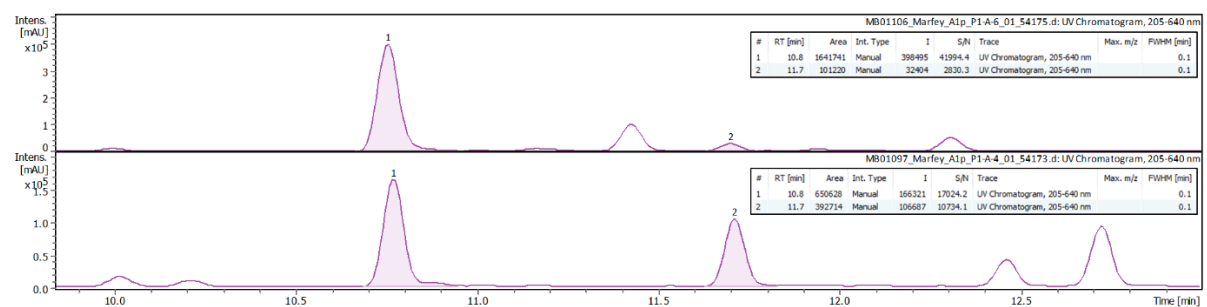


Fig. S130: Integrated UV signals corresponding to double L-FDVA adducts of tyrosine for hydrolyzed FE008 (74) (top) and hydrolyzed FE009 (75) (bottom).

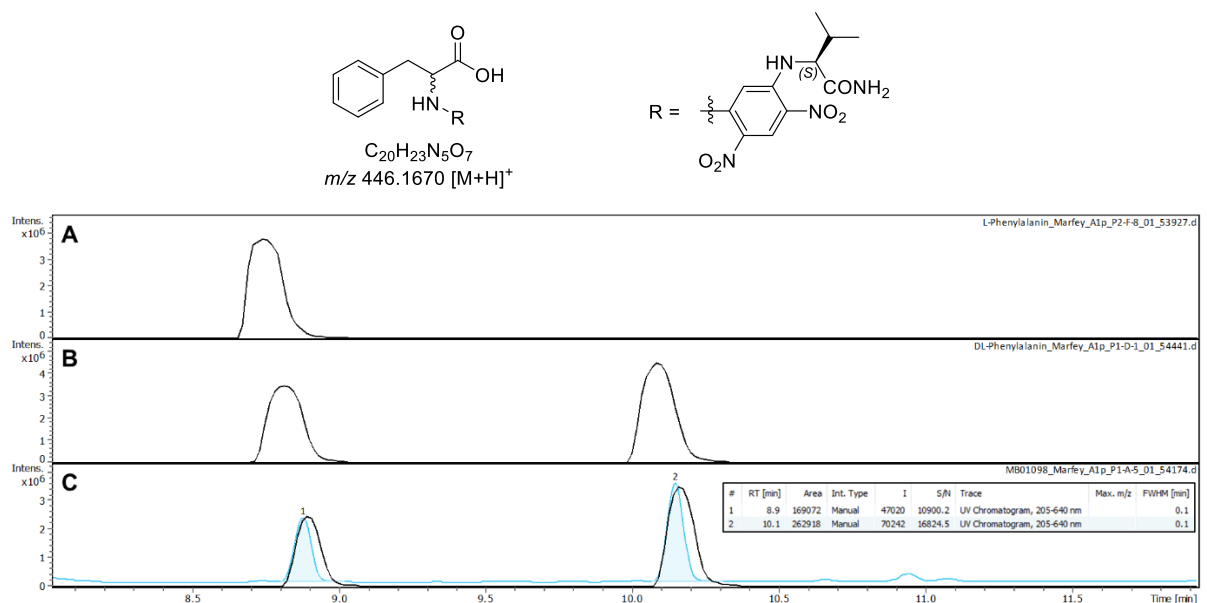


Fig. S131: L-FDVA adducts of phenylalanine. EICs (m/z 446.1670 ± 0.005, $C_{20}H_{23}N_5O_7$, $[M+H]^+$) for A: L-phenylalanine reference, B: DL-phenylalanine reference and C: hydrolyzed FE010 (76) (including integrated UV signals).

8.3.2.4 Antimicrobial Activity

Table S28: MICs [$\mu\text{g}/\text{mL}$] of compound 74–76.

	FE008 (74)	FE009 (75)	FE010 (76)
<i>Escherichia coli</i> ATCC 35218 (MH-II)	> 64	> 64	> 64
<i>Escherichia coli</i> ATCC 35218 (MHC)	> 64	> 64	> 64
<i>Escheria coli</i> ATCC 25922 (ΔToIC)	> 64	> 64	> 64
<i>Klebsiella pneumoniae</i> ATCC 13883	> 64	> 64	> 64
<i>Moraxella catarrhalis</i> ATCC 25238	64	> 64	> 64
<i>Pseudomonas aeruginosa</i> ATCC 27853	> 64	> 64	> 64
<i>Mycobacterium smegmatis</i> ATCC 607	> 64	> 64	> 64
<i>Bacillus subtilis</i> DSM 10	> 64	> 64	> 64
<i>Staphylococcus aureus</i> ATCC 25923	> 64	> 64	> 64
<i>Micrococcus luteus</i> DSM 20030	64	> 64	> 64
<i>Candida albicans</i> FH 2173	> 64	> 64	> 64

8.3.2.5 TLR2/TLR4 Activity

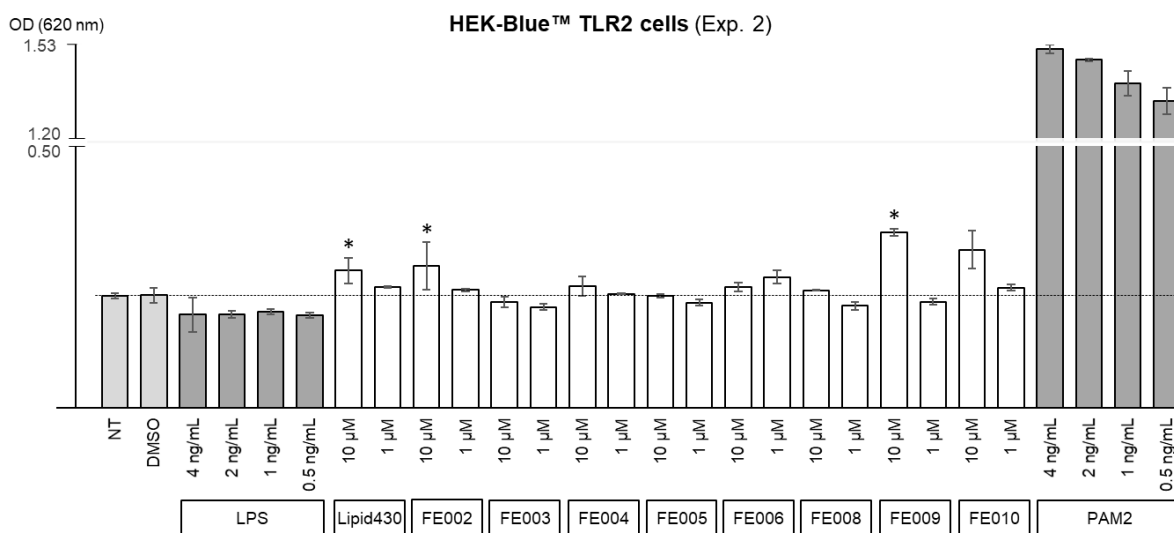


Fig. S132: HEK-Blue™ TLR2 cell activation, experiment 2. Cell activation levels are expressed as optical density (OD) at 620 nm. Assays were validated by the specific positive controls (dark grey) PAM2 (TLR2) and LPS (TLR4) as well as untreated (NT) and DMSO-treated (DMSO) negative controls (light grey). Taking standard deviations into account, response levels of compounds (white) elevated over the DMSO negative control in both experiments are marked (*).

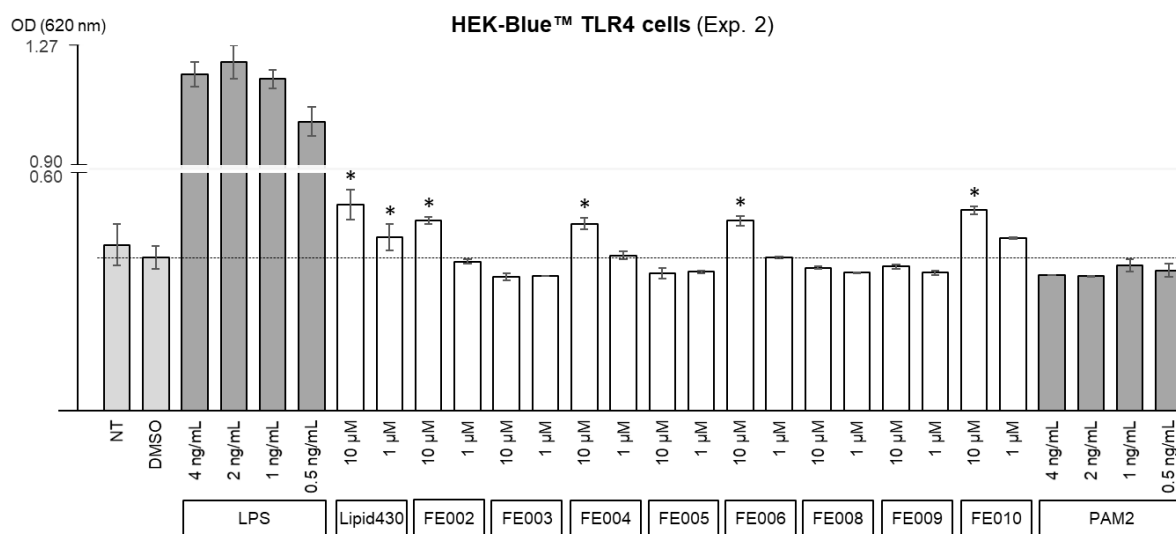
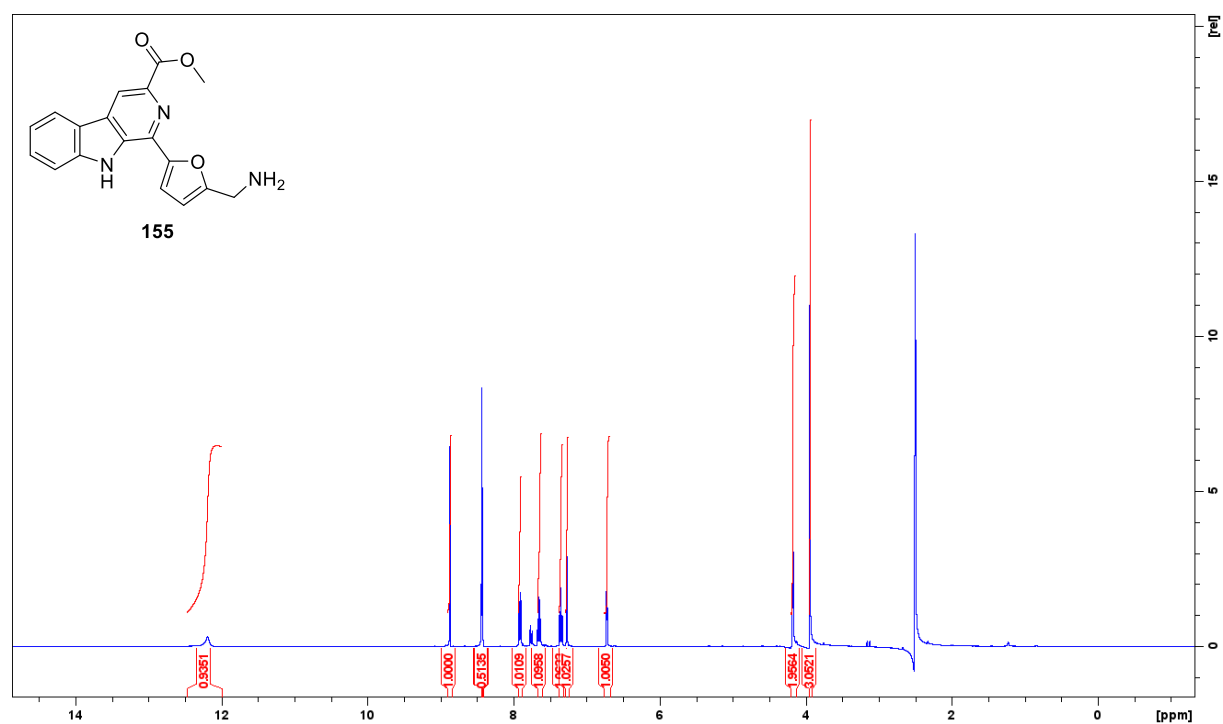
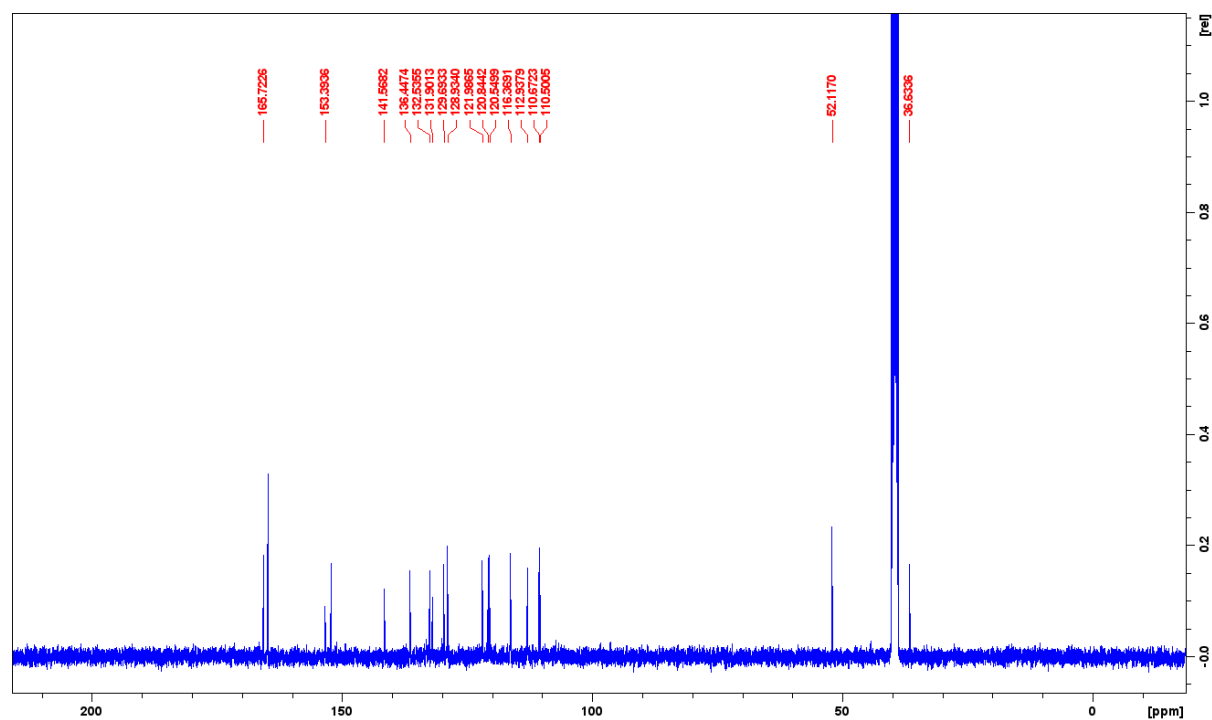
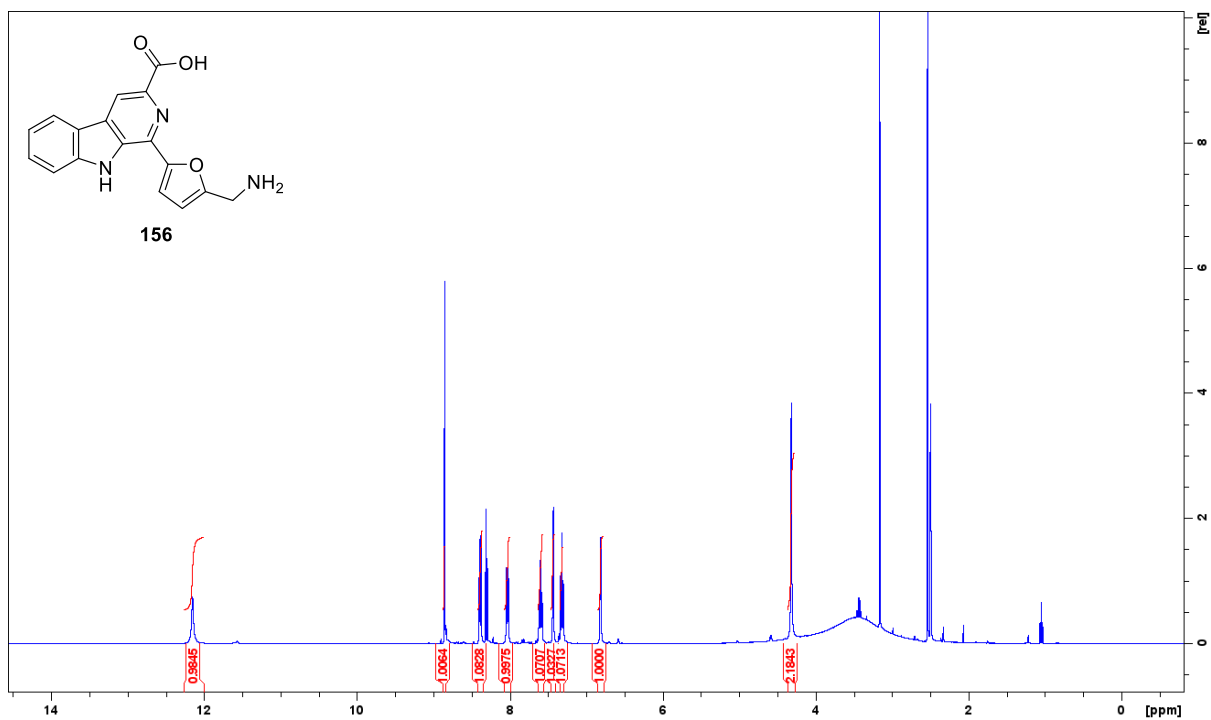
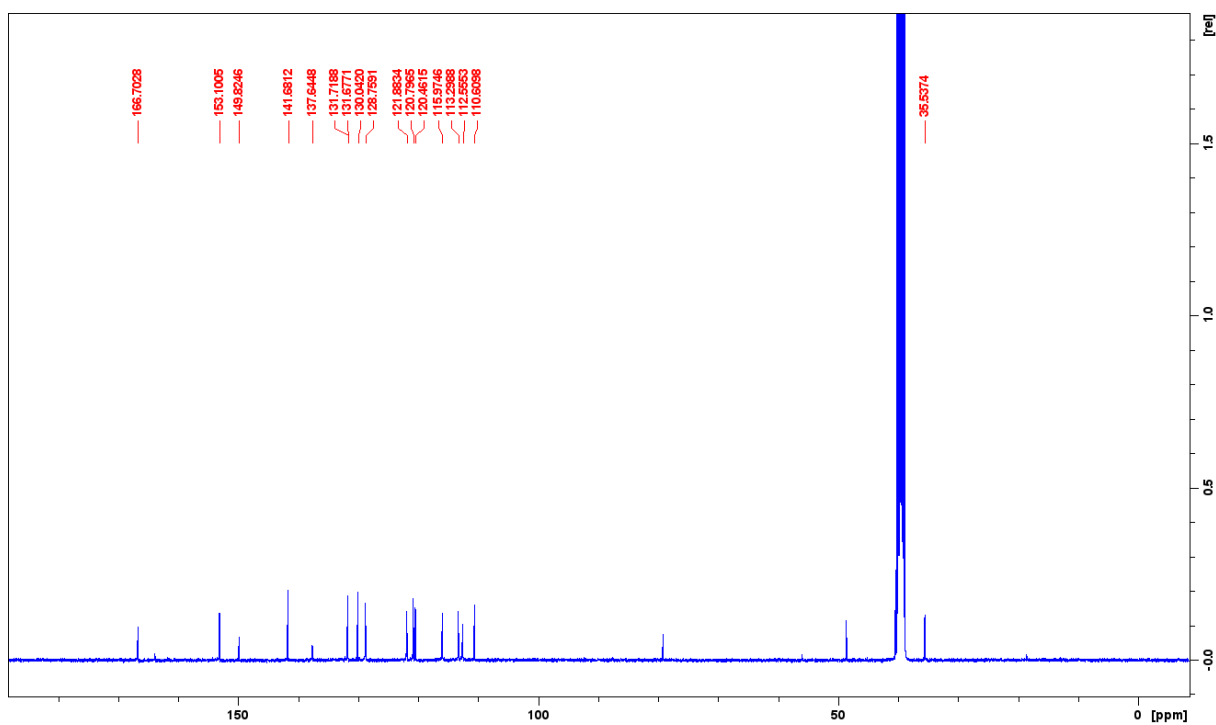


Fig. S133: HEK-Blue™ TLR4 cell activation, experiment 2. Cell activation levels are expressed as optical density (OD) at 620 nm. Assays were validated by the specific positive controls (dark grey) LPS (TLR4) and PAM2 (TLR2) as well as untreated (NT) and DMSO-treated (DMSO) negative controls (light grey). Taking standard deviations into account, response levels of compounds (white) elevated over the DMSO negative control in both experiments are marked (*).

8.4 Antimycobacterial activity of *Streptomyces* sp. HAG010336

8.4.1 Total Synthesis of SF009 and Derivatives: NMR Spectra

Fig. S134: $^1\text{H-NMR}$ (400 MHz, $\text{DMSO-}d_6$) flazin methyl ester amine (155).Fig. S135: $^{13}\text{C-NMR}$ (101 MHz, $\text{DMSO-}d_6$) of flazin methyl ester amine (155).

Fig. S136: ¹H-NMR (400 MHz, DMSO-*d*₆) flazin amine (**156**).Fig. S137: ¹³C-NMR (101 MHz, DMSO-*d*₆) of flazin amine (**156**).

8.4.2 Bioactivity Profiling

8.4.2.1 Dereplication

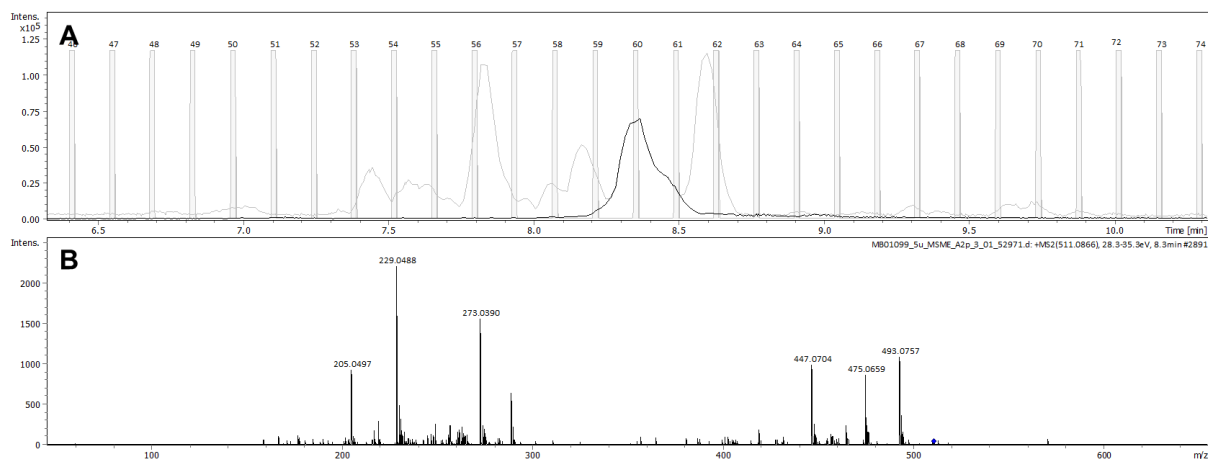


Fig. S138: MS/MS-guided UPLC fractionation of sample A. Relative growth inhibition of *M. smegmatis* ATCC 607 $\geq 85\%$: fractions F-58–F-61. A: BPC (grey), EIC (black) of m/z 511.0871 \pm 0.005, C₂₅H₁₈O₁₂ [M+H]⁺. B: MS/MS spectrum of m/z 511.0866.

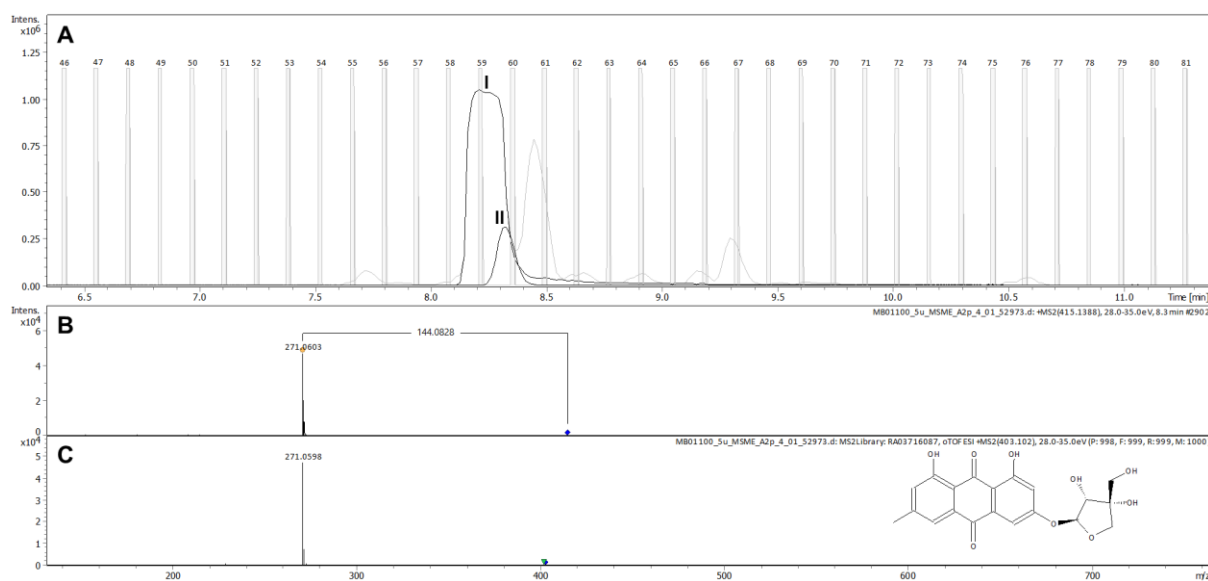


Fig. S139: MS/MS-guided UPLC fractionation of sample B. Relative growth inhibition of *M. smegmatis* ATCC 607 $\geq 85\%$: fraction F-59. A: BPC (grey), EICs (black) of I: m/z 323.1026 \pm 0.005, C₁₈H₁₄N₂O₄, [M+H]⁺ and II: m/z 415.1387 \pm 0.005, C₂₂H₂₂O₈, [M+H]⁺. B: MS/MS spectrum of m/z 415.1388; neutral loss is annotated. C: hit in Sanofi legacy MS/MS database: RA037xxx (166); MS/MS spectrum of m/z 403.102.

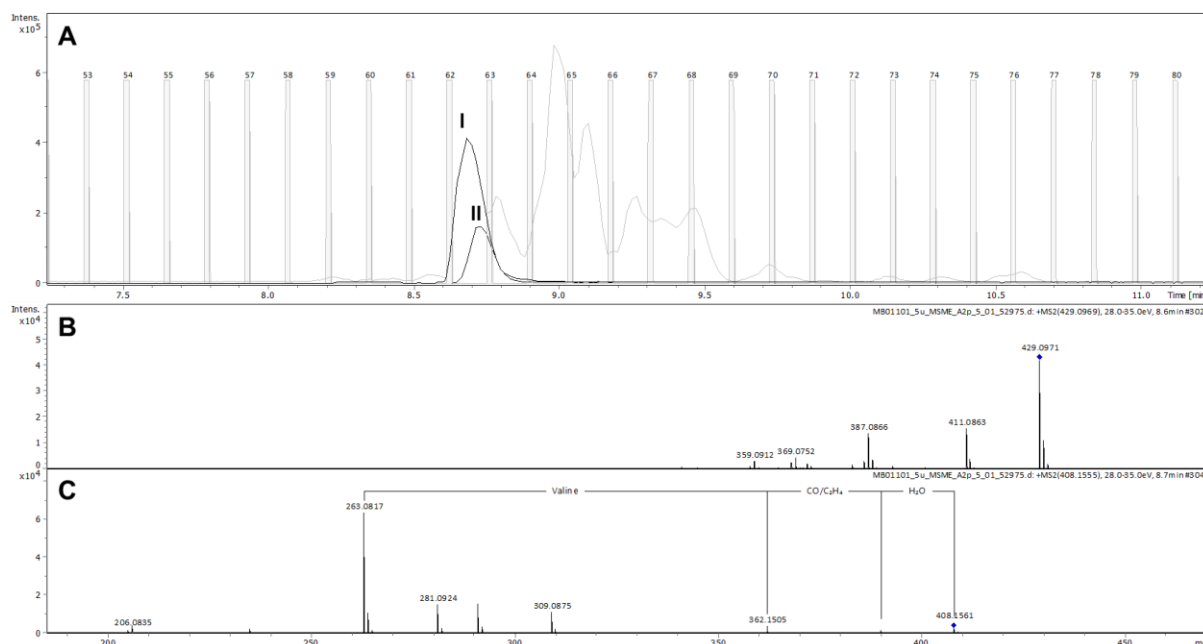


Fig. S140: MS/MS-guided UPLC fractionation of sample C. Relative growth inhibition of *M. smegmatis* ATCC 607 $\geq 85\%$: fraction F-62. A: BPC (grey); EICs (black) of I: m/z 429.0969 \pm 0.005, C₂₅H₁₆O₇, [M+H]⁺ and II: m/z 408.1554 \pm 0.005, C₂₂H₂₁N₃O₅, [M+H]⁺. B: MS/MS spectrum of m/z 429.0969. C: MS/MS spectrum of m/z 408.1555; selected neutral losses are annotated.

8.4.2.2 IC₈₀ Determination: *M. tuberculosis* H37Rv

Table S29: IC₈₀ of flazin methyl ester amine (155) (EOAI10001858) against *M. tuberculosis* H37Rv.

Compound ID	Batch ID	n=1		n=2		n=3		
		Status	C _{max}	Main CE80rel	Status	Main CE80rel	Status	Main CE80rel
EOAI10001858	EV-CHI001-183-001	A	3,00E-05	2.79E-05	A	2.56E-05	A	2.21E-05
RIFAMPICIN	RIFAMPICIN	A	3,00E-05	9.44E-08	A	7.87E-08	A	7.32E-08
ISONIAZIDE	ISONIAZIDE	A	3,00E-05	2.37E-07	A	2.35E-07	A	2.52E-07

8.4.2.3 Cytotoxicity Assay

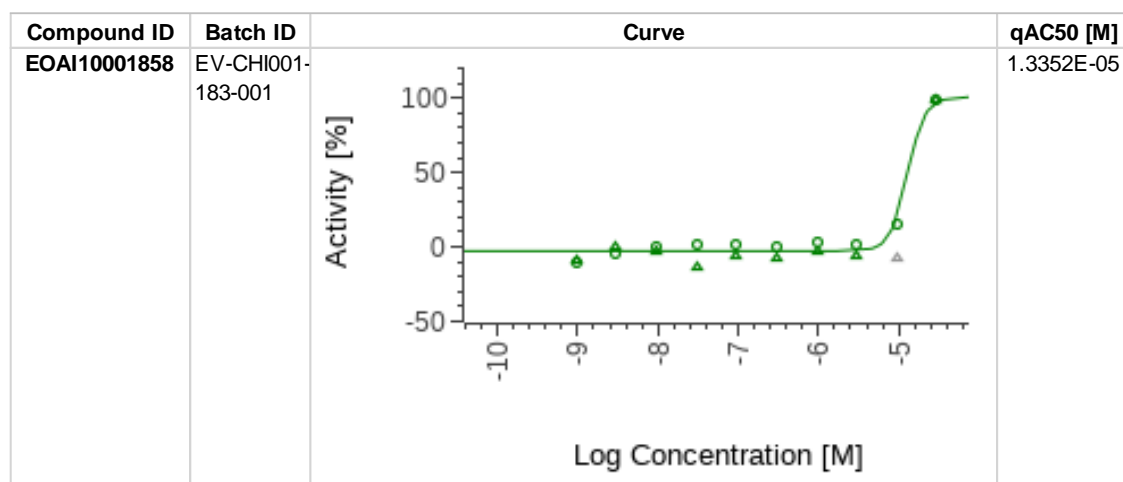


Fig. S141: Cytotoxicity assay of flazin methyl ester amine (155) (EOAI10001858) against THP-1 cell line.

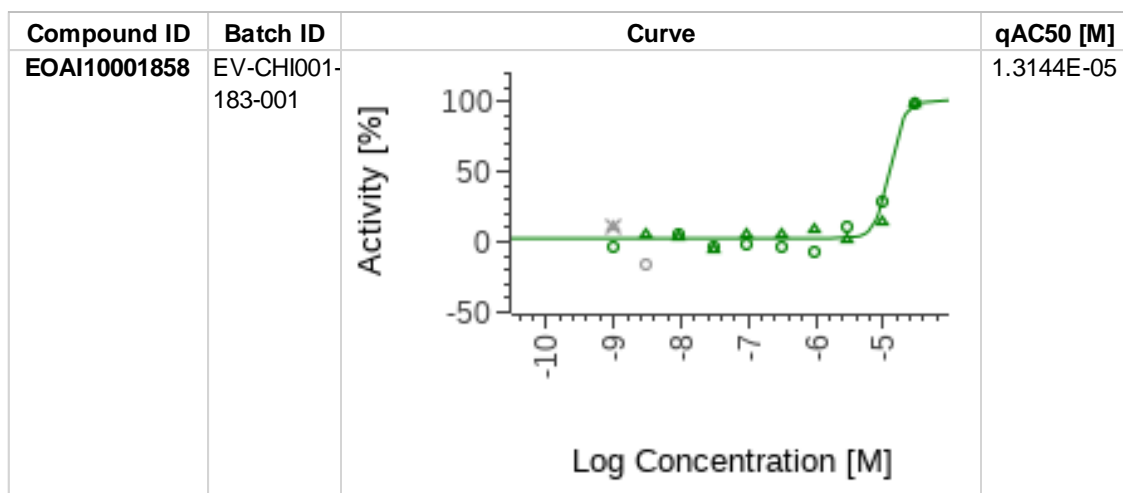


Fig. S142: Cytotoxicity assay of flazin methyl ester amine (155) (EOAI10001858) against HepG2 cell line.

9. References

- [1] Gaynes, R. *Emerg. Infect. Dis.* **2017**, *23*, 849-853.
- [2] Lakemeyer, M.; Zhao, W.; Mandl, F. A.; Hammann, P.; Sieber, S. A. *Angew. Chem. Int. Ed.* **2018**, *57*, 14440–14475.
- [3] Zucca, M.; Savoia, D. *Int. J. Biomed. Sci.* **2010**, *6*, 77–86.
- [4] Bill, M.-K.; Schuler, S.; Vilcinskas, A.; Hammann, P. “Tackling the resistance crisis: What does the antibiotic pipeline look like?”, 9th HIPS symposium, Saarbrücken, Germany, **2019** (short talk/poster).
- [5] Davies, J.; Davies, D. *Microbiol. Mol. Biol. Rev.* **2010**, *74*, 417–433.
- [6] Mulani, M. S.; Kamble, E. E.; Kumkar, S. N.; Tawre, M. S.; Pardesi, K. R. *Front. Microbiol.* **2019**, *10*, 539.
- [7] Munita, J. M.; Arias, C. A. *Microbiol Spectr.* **2016**, *4*, 10.
- [8] Bush, K.; Bradford, P. A. *Cold Spring Harb. Perspect. Med.* **2016**, *6*, a025247.
- [9] Tooke, C. L.; Hinchliffe, P.; Bragginton, E. C.; Colenso, C. K.; Hirvonen, V.; Takebayashi, Y.; Spencer, J. *J. Mol. Biol.* **2019**, *431*, 3472–3500.
- [10] Hutchings, M. I.; Truman, A. W.; Wilkinson, B. *Curr. Opin. Microbiol.* **2019**, *51*, 72–80.
- [11] Tacic, A.; Nikolic, V.; Nikolic, L.; Savic, I. *Adv. Technol.* **2017**, *6*, 58–71.
- [12] U.S. Food and Drug Administration (FDA). *New Drugs at FDA: CDER’s New Molecular Entities and New Therapeutic Biological Products* Silver Spring, Maryland, USA: FDA; **2021** [cited: 2021 February 19]. Retrieved from: <https://www.fda.gov/drugs/development-approval-process-drugs/new-drugs-fda-cders-new-molecular-entities-and-new-therapeutic-biological-products>.
- [13] Butler, M. S.; Paterson, D. L. *J. Antibiot.* **2020**, *73*, 329–364.
- [14] Heil, E. L.; Tamma, P. D. *Lancet Infect. Dis.* **2021**, *21*, 153–155.
- [15] European Centre for Disease Prevention and Control (ECDC). *Surveillance Atlas of Infectious Diseases*. Stockholm, Schweden: ECDC; **2020** [cited: 2020 September 18]. Retrieved from: <https://www.ecdc.europa.eu/en/surveillance-atlas-infectious-diseases>.
- [16] Singh, S.; Singh, S. K.; Chowdhury, I.; Singh, R. *Open Microbiol. J.* **2017**, *11*, 53–62.
- [17] Nigo, M.; Munita, J. M.; Arias, C. A. *Curr. Infect. Dis. Rep.* **2014**, *16*, 431.
- [18] Hirsch, E. B., Tam, V. H. *Expert Rev. Pharmacoecon. Outcomes Res.* **2010**, *10*, 441–451.

- [19] Yarrington, M.; Anderson, D.; Dodds Ashley, E.; Jones, T.; Davis, A.; Johnson, M.; Moehring, R. *Infect. Control Hosp. Epidemiol.* **2019**, *40*, 1297–1300.
- [20] Newman, D. J.; Cragg, G. M. *J. Nat. Prod.* **2012**, *75*, 311–335.
- [21] Luo, Y.; Cobb, R. E.; Zhao, H. *Curr. Opin. Biotechnol.* **2014**, *0*, 230–237.
- [22] Bérdy, J. *J. Antibiot.* **2012**, *65*, 385–395.
- [23] Strobel, G.; Daisy, B.; Castillo, U.; Harper, J. *J. Nat. Prod.* **2004**, *67*, 257–268.
- [24] Crawford, J. M.; Clardy, J. *Chem. Commun.* **2011**, *47*, 7559–7566.
- [25] Pan, R.; Bai, X.; Chen, J.; Zhang, H.; Wang, H. *Front. Microbiol.* **2019**, *10*, 294.
- [26] Stewart, E. J. *J. Bacteriol.* **2012**, *194*, 4151–4160.
- [27] Solden, L.; Lloyd, K.; Wrighton, K. *Curr. Opin. Microbiol.* **2016**, *31*, 217–226.
- [28] Zengler, K.; Toledo, G.; Rappé, M.; Elkins, J.; Mathur, E. J.; Short, J. M.; Keller, M. *PNAS* **2002**, *99*, 15681–15686.
- [29] Farha, M. A.; Brown, E. D. *Ann. N.Y. Acad. Sci.* **2015**, *1354*, 54–66.
- [30] Harvey, A. L.; Edrada-Ebel, R.; Quinn, R. J. *Nat. Rev. Drug Discov.* **2015**, *14*, 111–129.
- [31] Thomford, N. E.; Senthebane, D. A.; Rowe, A.; Munro, D.; Seele, P.; Maroyi, A.; Dzobo, K. *Int. J. Mol. Sci.* **2018**, *19*, 1578.
- [32] Ersoy, S. C.; Heithoff, D. M.; Barnes, L.; Tripp, G. K.; House, J. K.; Marth, J. D.; Smith, J. W.; Mahan, M. J. *EBioMedicine* **2017**, *20*, 173–181.
- [33] Farha, M. A.; French, S.; Stokes, J. M.; Brown E. D. *ACS Infect. Dis.* **2018**, *4*, 382–390.
- [34] Constant, H. L.; Beecher, C. W. W. *Nat. Prod. Lett.* **1995**, *6*, 193–196.
- [35] Nielsen, K. F.; Månsson, M.; Rank, C.; Frisvad, J. C.; Larsen, T. O. *J. Nat. Prod.* **2011**, *74*, 2338–2348.
- [36] Ito, T.; Masubuchi, M. *J. Antibiot.* **2014**, *67*, 353–360.
- [37] Lang, G.; Mayhudin, N. A.; Mitova, M. I.; Sun, L.; van der Sar, S.; Blunt, J. W.; Cole, A. L. J.; Ellis, G.; Laatsch, H.; Munro, M. H. G. *J. Nat. Prod.* **2008**, *71*, 1595–1599.
- [38] Whitehouse, C. M.; Dreyer, R. N.; Yamashita, M.; Fenn, J. B. *Anal. Chem.* **1985**, *57*, 675–679.
- [39] Remane, D.; Meyer, M. R.; Wissenbach, D. K.; Maurer, H. H. *Rapid Commun. Mass Spectrom.* **2010**, *24*, 3103–3108.

- [40] Yang, J. Y.; Sanchez, L. M.; Rath, C. M.; Liu, X.; Boudreau, P. D.; Bruns, N.; Glukhov, E.; Wodtke, A.; de Felicio, R.; Fenner, A.; Wong, W. R.; Linington, R. G.; Zhang, L.; Debonsi, H. M.; Gerwick, W. H.; Dorrestein, P. C. *J. Nat. Prod.* **2013**, *76*, 1686–1699.
- [41] Quinn, R. A.; Nothias, L. F.; Vining, O.; Meehan, M.; Esquenazi, E.; Dorrestein, P. C. *Trends Pharmacol. Sci.* **2017**, *38*, 143–154.
- [42] Frank, A. M.; Bandeira, N.; Shen, Z.; Tanner, S.; Briggs, S. P.; Smith, R. D.; Pevzner, P. A. *J. Proteome Res.* **2008**, *7*, 113–122.
- [43] Watrous, J.; Roach, P.; Alexandrov, T.; Heath, B. S.; Yang, J. Y.; Kersten, R. D.; van der Voort, M.; Pogliano, K.; Gross, H.; Raaijmakers, J. M.; Moore, B. S.; Laskin, J.; Bandeira, N.; Dorrestein, P. C. *PNAS* **2012**, *109*, E1743–E1752.
- [44] Aron, A. T.; Gentry, E. C.; McPhail, K. L. *et al. Nat. Protoc.* **2020**, *15*, 1954–1991.
- [45] Boudreau, P. D.; Monroe, E. A.; Mehrotra, S.; Desfor, S.; Korobeynikov, A.; Sherman, D. H.; Murray, T. F.; Gerwick, L.; Dorrestein, P. C.; Gerwick, W. H. *PLoS ONE* **2015**, *10*, e0133297.
- [46] Sarker, S. D.; Nahar, L., (eds) *Natural product isolation* (3rd ed.). Humana Press, **2012**.
- [47] Reddy, N. G.; Ramakrishna, D. P. N.; Rajagopal, S. V. *Egypt. J. Biol.* **2011**, *13*, 21–29.
- [48] Zhang, Q. W.; Lin, L. G.; Ye, W. C. *Chin. Med.* **2018**, *13*, 1–26.
- [49] Malviya, N.; Malviya, S. *Int. J. Hosp. Pharm.* **2017**, *2*, 5.
- [50] Molinski, T. F. *Curr. Opin. Biotechnol.* **2010**, *21*, 819–826.
- [51] Bross-Walch, N.; Kühn, T.; Moskau, D.; Zerbe, O. *Chem. Biodivers.* **2005**, *2*, 147–177.
- [52] Molinski, T. F. *Nat. Prod. Rep.* **2010**, *27*, 321–329.
- [53] Hatzakis, E. *Compr. Rev. Food Sci. Food Saf.* **2019**, *18*, 189–220.
- [54] Kwan, E.; Huang, S. G. *Eur. J. Org. Chem.* **2008**, 2671–2688.
- [55] Reynolds, W. F.; Mazolla, E. P. *Prog. Chem. Nat. Prod.* **2015**, *100*, 223–309.
- [56] Bifulco, G.; Dambruoso, P.; Gomez-Paloma, L.; Riccio, R. *Chem. Rev.* **2007**, *107*, 3744–3779.
- [57] Menna, M.; Imperatore, C.; Mangoni, A.; Della Sala, G.; Tagliatela-Scafati, O. *Nat. Prod. Rep.* **2019**, *36*, 476–489.
- [58] Williamson, M. P.; Williams, D. H. *J. Am. Chem. Soc.* **1981**, *103*, 6580–6585.
- [59] Doost, A. S.; Akbari, M.; Stevens, C. V.; Setiowati, A. D.; Van der Meeren, P. *Trends Food Sci. Tech.* **2019**, *86*, 16–24.

- [60] Williams, A. J.; Martin, G. E.; Rovnyak, D. (eds) *Modern NMR Approaches to the Structure Elucidation of Natural Products. Volume 2: Data Acquisition and Applications to Compound Classes*. Royal Society of Chemistry, **2016**.
- [61] Karunakaran, C.; Santharamn, P.; Balamurugan, M. (eds) *Spin Resonance Spectroscopy: Principles and Applications. Chapter 2: ¹H and ¹³C Nuclear Magnetic Resonance Spectroscopy*. Elsevier. **2018**, 49–110.
- [62] Kurz, M.; Schmieder, P.; Kessler, H. *Angew. Chem. Int. Ed. Engl.* **1991**, *30*, 1329–1331.
- [63] Ling-Yi, K.; Peng, W. *Chin. J. Nat. Med.* **2013**, *11*, 0193–0198.
- [64] Seco, J. M.; Quiñoá, E.; Riguera, R. *Chem. Rev.* **2004**, *104*, 17–117.
- [65] Li, X. C.; Ferreira, D.; Ding, Y. *Curr Org. Chem.* **2010**, *14*, 1678–1697.
- [66] Vijayasathy, S.; Prasad, P.; Fremlin, L. J.; Ratnayake, R.; Salim, A. A.; Khalil, Z.; Capon, R. J. *J. Nat. Prod.* **2016**, *79*, 421–427.
- [67] B'Hymer, C.; Montes-Bayon, M.; Caruso, J.A. *J. Sep. Sci.* **2003**, *26*, 7–19.
- [68] Bhushan, R.; Brückner, H. *Amino Acids* **2004**, *27*, 231–247.
- [69] Fujii, K.; Ikai, Y.; Mayumi, T.; Oka, H.; Suzuki, M.; Harada, K. *Anal. Chem.* **1997**, *69*, 3346–3352.
- [70] Oberpaul, M.; Zumkeller, C. M.; Culver, T.; Spohn, M.; Mihajlovic, S.; Leis, B.; Glaeser, S. P.; Plarre, R.; McMahan, D. P.; Hammann, P.; Schäberle, T. F.; Glaeser, J.; Vilcinskas, A. *Front. Microbiol.* **2020**, *11*, 597628.
- [71] Singh, A. K.; Rana, H. K.; Pandey, A. K. *Fungal Derived Natural Product: Synthesis, Function and Applications*. In: *Recent Advancement in White Biotechnology Throungh Fungi. Vol. 2: Perspective for Value-Added Products and Environments*. Yadav, A. N.; Singh, S.; Mishra, S.; Gupta, A. (eds.), Springer Nature Switzerland AG, **2019**, 229–248.
- [72] Hawksworth, D. L. *Mycol. Res.* **2001**, *105*, 1422–1432.
- [73] Hyde, K. D.; Xu, J.; Rapior, S. *et al. Fungal Diversity* **2019**, *97*, 1–136.
- [74] Karwehl, S.; Stadler, M. *Curr. Top. Microbiol. Immunol.* **2016**, *398*, 303–338.
- [75] Jakubczyk, D.; Dussart, F. *Molecules* **2020**, *25*, 911.
- [76] Shinde, Y.; Sproules, S.; Kathawate, L.; Pal, S.; Badireenath Konkimalla, V.; Salunke-Gawali, S. *J. Chem. Sci.* **2014**, *126*, 213–225.
- [77] Luan, Y.; Wei, H.; Zhang, Z.; Che, Q.; Liu, Y.; Zhu, T.; Mándi, A.; Kurtán, T.; Gu, Q.; Li, D. *J. Nat. Prod.* **2014**, *77*, 1718–1723.
- [78] Kwon, Y.-J.; Sohn, M.-J.; Kim, C.-J.; Koshino, H.; Kim, W.-G. *J. Nat. Prod.* **2012**, *75*, 271–274.

- [79] Cornella, J.; Zarate, C.; Martin, R. *Org. Synth.* **2014**, *91*, 260–272.
- [80] Torres, A.; Gutierrez, P.; Alvarez-Manzaneda, R.; Chahboun, R.; Alvarez-Manzaneda, E. *Org. Biomol. Chem.* **2016**, *14*, 9836–9845.
- [81] More, A. A.; Ramana, C. V. *Org. Lett.* **2016**, *18*, 1458–1461.
- [82] Irie, T.; Izawa, M.; Kurosawa, E. *Tetrahedron Lett.* **1968**, *9*, 2091–2096.
- [83] Kiriya, N.; Nitta, K.; Sakaguchi, Y.; Taguchi, Y.; Yamamoto, Y. *Chem. Pharm. Bull.* **1977**, *25*, 2593–2601.
- [84] Nitta, K.; Fujita, N.; Yoshimura, T.; Arai, K.; Yamamoto, Y. *Chem. Pharm. Bull.* **1983**, *31*, 1528–1533.
- [85] Haritakun, R.; Rachtawee, P.; Chanthaket, R.; Boonyuen, N.; Isaka, M. *Chem. Pharm. Bull.* **2010**, *58*, 1545–1548.
- [86] Rao, K. V.; Sadhukhan, A. K.; Veerender, M.; Ravikumar, V.; Mohan, E. V.; Dhanvantri, S. D.; Sitaramkumar, M.; Babu, J. M.; Vyas, K.; Reddy, G. O. *Chem. Pharm. Bull.* **2000**, *48*, 559–562.
- [87] Luo, Y.; Ma, H.; Zhang, X.; He, X.; Wang, W.; Gang, C.; Wang, H.; Pei, Y.-H. *Chem. Nat. Compd.* **2018**, *54*, 1035–1037.
- [88] Bamford, P. C.; Norris, G. L. F.; Ward, G. *Trans. Br. Mycol. Soc.* **1961**, *44*, 354–356.
- [89] Nitao, J. K.; Meyer, S. L. F.; Oliver, J. E.; Schmidt, W. F.; Chitwood, D. J. *Nematology* **2002**, *4*, 55–63.
- [90] Burge, W. R.; Buckley, L. J.; Sullivan, J. D.; McGrattan, C. J.; Ikawa, M. *J. Agric. Food Chem.* **1976**, *24*, 555–559.
- [91] Brown, A. E.; Finlay, R.; Ward, J. S. *Soil Biol. Biochem.* **1987**, *19*, 657–664.
- [92] Raistrick, H.; Rudman, P. *Biochem. J.* **1956**, *63*, 395–406.
- [93] Madrigal, C.; Tadeo, J. L.; Melgarejo, P. *Mycol. Res.* **1991**, *95*, 1375–1381.
- [94] Elkhateeb, W. A.; Daba, G. M. *Biomed. J. Sci. Tech. Res.* **2019**, *14*, 10616–10620.
- [95] Talontsi, F. M.; Dittrich, B.; Schüffler, A.; Sun, H.; Laatsch, H. *Eur. J. Chem.* **2013**, *2013*, 3174–3180.
- [96] El Amrani, M.; Lai, D.; Debbab, A.; Aly, A. H.; Siems, K.; Seidel, C.; Schnekenburger, M.; Gaigneaux, A.; Diederich, M.; Feger, D.; Lin, W.; Proksch, P. *J. Nat. Prod.* **2014**, *77*, 49–56.
- [97] Brill, G. M.; Premachandran, U.; Karwowski, J. P.; Henry, R.; Cwik, D. K.; Traphagen, L. M.; Humphrey, P. E.; Jackson, M.; Clement, J. J.; Burren, N. S.; Kadam, S.; Chen, R. H.; McAlpine, J. B. *J. Antibiot.* **1996**, *49*, 124–128.

- [98] Silva, G. H.; Teles, H. L.; Trevisan, H. C.; Bolzani, V. S.; Young, M. C. M.; Pfenning, L. H.; Eberlind, M. N.; Haddad, R.; Costa-Netoe, C. M.; Araújo, A. R. *J. Braz. Chem. Soc.* **2005**, *16*, 1463–1466.
- [99] Hinder, R. C.; Kong, X. *Nat. Prod. Rep.* **2010**, *27*, 637–657.
- [100] Miethka, M.M Marahiel, M. A. *Microbiol. Mol. Biol. Rev.* **2007**, *71*, 413–451.
- [101] Snow, G. A. *Bacteriol. Rev.* **1970**, *34*, 99–125.
- [102] Jin, Z. *Nat. Prod. Rep.* **2009**, *26*, 382–445.
- [103] Mitchell, J. M.; Shaw, J. T. *Org. Lett.* **2007**, *9*, 1679–1681.
- [104] Sontag, B.; Gerlitz, M.; Paululat, T.; Rasser, H. F.; Grun-Wollny, I.; Hansske, F. G. *J. Antibiot.* **2006**, *59*, 659–663.
- [105] Harada, K.; Tomita, K.; Fujii, K.; Masuda, K.; Mikami, Y.; Yazawa, K.; Komaki, H. *J. Antibiot.* **2004**, *57*, 125–135.
- [106] Mazzei, E.; Iorio, M.; Maffioli, S.; Sosio, M.; Donadio, S. *J. Antibiot.* **2012**, *65*, 267–269.
- [107] Kawahara, T., Itoh, M., Izumikawa, M.; Sakata, N.; Tsuchida, T.; Shin-ya, K. *J. Antibiot.* **2014**, *67*, 577–580.
- [108] Zhang, X.; He, H.; Ma, R.; Ji, Z.; Wei, Q.; Dai, H.; Zhang, L.; Song, F. *J. Ind. Microbiol. Biotechnol.* **2017**, *44*, 589–594.
- [109] Shaaban, K. A.; Saunders, M. A.; Zhang, Y.; Tran, T.; Elshahawi, S. I.; Ponomareva, L. V.; Wang, X.; Zhang, J.; Copley, G. C.; Sunkara, M.; Kharel, M. K.; Morris, A. J.; Hower, J. C.; Tremblay, M. S.; Prendergast, M. A.; Thorson, J. S. *J. Nat. Prod.* **2017**, *80*, 2–11.
- [110] Tyler, A. R.; Mosaei, H.; Morton, S.; Waddell, P. G.; Wills, C.; McFarlane, W.; Gray, J.; Goodfellow, M.; Errington, J.; Allenby, N.; Zenkin, N.; Hall, M. J. *J. Nat. Prod.* **2017**, *80*, 1558–1562.
- [111] Saha, M.; Sarkar, S.; Sarkar, B.; Sharma, B. K.; Bhattacharjee, S.; Tribedi, P. *Environ. Sci. Pollut. Res.* **2016**, *23*, 3984–3999.
- [112] Lin, Y.-M.; Ghosh, M.; Miller, P. A.; Möllmann, U.; Miller, M. J. *Biometals* **2019**, *32*, 425–451.
- [113] Marner, M.; Patras, M. A.; Kurz, M.; Zubeil, F.; Förster, F.; Schuler, S.; Bauer, A.; Hammann, P.; Vilcinskas, A.; Schäberle, T. F.; Glaeser, J. *J. Nat. Prod.* **2020**, *83*, 2607–2617.
- [114] Fry, E. M. *J. Org. Chem.* **1950**, *15*, 802–806.
- [115] Yan, J.-X.; Chevrette, M. G.; Braun, D. R.; Harper, M. K.; Currie, C. R.; Bugni, T. S. *Org. Lett.* **2019**, *21*, 6275–6279.
- [116] Kessler, H. *Angew. Chem.* **1968**, *80*, 201.
- [117] Bhushan, R.; Brückner, H. *Amino Acids* **2004**, *27*, 231–247.

- [118] O'Shea, R.; Moser, H. E. *J. Med. Chem.* **2008**, *51*, 2871–2878.
- [119] Walter, T.; Collenburg, L.; Japtok, L.; Kleuser, B.; Schneider-Schaulies, S.; Müller, N.; Becam, J.; Schubert-Unkneir, A.; Kong, J. N.; Bieberich, E.; Seibel, *J. Chem. Commun.* **2016**, *52*, 8612–8614.
- [120] Sasaki, T.; Otani, T.; Yoshida, K.-I.; Unemi, N. *J. Antibiot.* **1997**, *50*, 881–883.
- [121] Zhang, J.-W.; Zhang, W.-J.; Wie, S.-P.; Wu, W.-J. *Heterocycles.* **2014**, *89*, 1656–1661.
- [122] Inahashi, Y.; Iwatsuki, M.; Ishiyama, A.; Namatame, M.; Nishihara-Tsukashima, A.; Matsumoto, A.; Hirose, T.; Sunazuka, T.; Yamada, H.; Otaguro, K.; Takahashi, Y.; Omura, S.; Shiomi, K. *J. Antibiot.* **2011**, *64*, 303–307.
- [123] Fu, P.; Liu, P.; Qu, H.; Wang, Y.; Chen, D.; Wang, H.; Li, J.; Zhu, W. *J. Nat. Prod.* **2011**, *74*, 2219–2223.
- [124] Li, L. B.; Dan, W. J.; Tan, F. F.; Cui, L. H.; Yuan, Z. P.; Wu, W. J.; Zhang, J. W. *Chem. Pharm. Bull.* **2015**, *63*, 33–37.
- [125] Carmi, R.; Carmeli, S.; Levy, E.; Gough, F. J. *J. Nat. Prod.* **1994**, *57*, 1200–1205.
- [126] Lacava, P. T.; Silva-Stenico, M. E.; Araújo, W. L.; Simionato, A. V. C.; Carrilho, E.; Tsai, S. M.; Azevedo, J. L. *Pesq. Agropec. Bras.* **2008**, *43*, 521–528.
- [127] Goh, K. M.; Shahar, S.; Chan, K.-G.; Chong, C. S.; Amran, S. I.; Sani, M. H.; Zakaria, I. I.; Kahar, U. M. *Microorganisms* **2019**, *7*, 468–492.
- [128] Thomas, F.; Hehemann, J.-H.; Rebuffet, E.; Czjzek, M.; Michel, G. *Front. Microbiol.* **2011**, *2*, 93.
- [129] Gupta, R. S. *Crit. Rev. Microbiol.* **2004**, *30*, 123–143.
- [130] Nord, C.; Bjerketorp, J.; Levenfors, J. J.; Cao, S.; Strömstedt, A. A.; Guss, B.; Larsson, R.; Hughes, D.; Öberg, B.; Broberg, A. *ACS Chem. Biol.* **2020**, *15*, 2937–2944.
- [131] Okanya, P. W.; Mohr, K. I.; Gerth, K.; Jansen, R.; Müller, R. *J. Nat. Prod.* **2011**, *74*, 603–608.
- [132] Katayama, N.; Nozaki, Y.; Okonogi, K.; Ono, H.; Harada, S.; Okazaki, H. *J. Antibiot.* **1985**, *38*, 1117–1127.
- [133] Mohr, K. I.; Volz, C.; Jansen, R.; Wray, V.; Hoffmann, J.; Bernecker, S.; Wink, J.; Gerth, K.; Stadler, M.; Müller, R. *Angew. Chem. Int. Ed. Engl.* **2015**, *54*, 11254–11258.
- [134] Katayama, N.; Fukusumi, S.; Funabashi, Y.; Iwahi, T.; Ono, H. *J. Antibiot.* **1993**, *46*, 606–613.
- [135] Steinmetz, H.; Gerth, K.; Jansen, R.; Schläger, N.; Dehn, R.; Reinecke, S.; Kirschning, A.; Müller, R. *Angew. Chem., Int. Ed.* **2011**, *50*, 532–536.
- [136] Vaz-Moreira, I.; Nobre, M. F.; Nunes, O. C.; Manaiá, C. M. *Int. J. Syst. Evol. Microbiol.* **2007**, *57*, 1535–1538.

- [137] Siddiqi, M. Z.; Liu, Q.; Lee, S. Y.; Choi, K. D.; Im, W.-T. *Int. J. Syst. Evol. Microbiol.* **2018**, *68*, 2509–2514.
- [138] Woznica, A.; Cantley, A. M.; Beemelmans, C.; Freinkman, E.; Clardy, J.; King, N. *PNAS* **2016**, *113*, 7894–7899.
- [139] Matyash, V.; Liebisch, G.; Kurzchalia, T. V.; Shevchenko, A.; Schwudke, D. *J. Lipid Res.* **2008**, *49*, 1137–1146.
- [140] Shahina, M.; Hameed, A.; Lin, S. Y.; Lai, W. A.; Liu, Y. C.; Hsu, Y. H.; Young, C. C. *Int. J. Syst. Evol. Microbiol.* **2013**, *63*, 4765–4770.
- [141] Nedashkovskaya, O.I.; Kim, S. G.; Zhukova, N. V.; Mikhailov, V. V. *Int. J. Syst. Evol. Microbiol.* **2017**, *67*, 2205–2210.
- [142] Lv, Y. Y.; Wang, C. L.; Feng, G. D.; Yao, Q.; Su, B. L.; Li, A. Z.; Zhu, H. H. *Int. J. Syst. Evol. Microbiol.* **2019**, *69*, 625–630.
- [143] Vaz-Moreira, I.; Nobre, M. F.; Nunes, O. C.; Manaia, C. M. *Int. J. Syst. Evol. Microbiol.* **2007**, *57*, 1535–1538.
- [144] Kawai, Y.; Akagawa, K. *Infect. Immun.* **1989**, *57*, 2086–2091.
- [145] Kawai, Y.; Yano, I.; Kaneda, K. *Eur. J. Biochem.* **1988**, *171*, 73–80.
- [146] Chianese, G.; Esposito, F.P.; Parrot, D.; Ingham, C.; De Pascale, D.; Tasdemir, D. *Mar. Drugs* **2018**, *16*, 187.
- [147] Kawazowe, R.; Okuyama, H.; Reichardt, W.; Sasaki, S. *J. Bacteriol.* **1991**, *173*, 5470–5475.
- [148] Batrakov, S.G.; Nikitin, D.I.; Mosezhnyi, A.E.; Ruzhitsky, A.O. *Chem. Phys. Lipids* **1999**, *99*, 139–143.
- [149] Morishita, T.; Sato, A.; Hisamoto, M.; Oda, T.; Matsuda, K.; Ishii, A.; Kodama, K. *J. Antibiot.* **1997**, *50*, 457–468.
- [150] Nemoto, T.; Ojika, M.; Takahata, Y.; Andoh, T.; Sakagami, Y. *Tetrahedron* **1998**, *54*, 2683–2690.
- [151] Yoshida, K.; Iwami, M.; Umehara, Y.; Nishikawa, M.; Uchida, I.; Kohsaka, M.; Aoki, H.; Imanaka, H. *J. Antibiot.* **1985**, *38*, 1469–1475.
- [152] Shiozaki, M.; Deguchi, N.; Mochizuki, T.; Wakabayashi, T.; Ishikawa, T.; Haruyama, H.; Kawai, Y.; Nishijima, M. *Tetrahedron* **1998**, *54*, 11861–11876.
- [153] Shioiri, T.; Terao, Y.; Irako, N.; Aoyama, T. *Tetrahedron*, **1998**, *54*, 15701–15710.
- [154] Nemati, R.; Dietz, C.; Anstadt, E. J.; Cervantes, J.; Liu, Y.; Dewhirst, F. E.; Clark, R. B.; Finegold, S.; Gallagher, J. J.; Smith, M. B.; Yao, X.; Nichols, F. C. *J. Lipid Res.* **2017**, *58*, 1999–2007.

- [155] Clark, R. B.; Cervantes, J. L.; Maciejewski, M. W.; Farrokhi, V.; Nemati, R.; Yao, X.; Anstadt, E.; Fujiwara, M.; Wright, K. T.; Riddle, C.; La Vake, C. J.; Salazar, J. C.; Finegold, S.; Nichols, F. C. *Infect. Immun.* **2013**, *81*, 3479–3489.
- [156] Schneider, Y.K.-H.; Hansen, K.; Isaksson, J.; Ullsten, S.; Hansen, E. H.; Hammer Andersen, J. *Molecules* **2019**, *24*, 3991.
- [157] Meylaers, K.; Clynen, E.; Daloze, D.; DeLoof, A.; Schoofs, L. *Insect Biochem. Mol. Biol.* **2004**, *34*, 43–49.
- [158] Makide, K.; Kitamura, H.; Sato, Y.; Okutani, M.; Aoki, J. *Prostaglandins Other Lipid Mediat.* **2009**, *89*, 135–139.
- [159] Hou, Q.; Ufer, G.; Bartels, D. *Plant Cell Environ.* **2016**, *39*, 1029–1048.
- [160] Thakkar, B. S.; Svendsen, J. S. M.; Engh, R. A. *Molecules* **2018**, *23*, 2455.
- [161] Brady, S. F.; Clardy, J. *J. Am. Chem. Soc.* **2000**, *122*, 12903–12904.
- [162] Brady, S. F.; Chao, C. J.; Clardy, J. *Appl. Environ. Microbiol.* **2004**, *70*, 6865–6870.
- [163] Brady, S. F.; Clardy, J. *Org. Lett.* **2005**, *7*, 3613–3616.
- [164] Phoon, C. W.; Somanadhan, B.; Heng, S. C. H.; Ngo, A.; Ng, S. B.; Butler, M. S.; Buss, A. D.; Sim, M. M. *Tetrahedron* **2004**, *60*, 11619–11628.
- [165] Uchida, I.; Yoshida, K.; Kawai, Y.; Takase, S.; Itoh, Y.; Tanaka, H.; Kohsaka, M.; Imanaka, H. *J. Antibiot.* **1985**, *38*, 1476–1486.
- [166] Nemati, R.; Dietz, C.; Anstadt, E. J.; Cervantes, J.; Liu, Y.; Dewhirst, F. E.; Clark, R. B.; Finegold, S.; Gallagher, J. J.; Smith, M. B.; Yao, X.; Nichols, F. C. *J. Lipid Res.* **2017**, *58*, 1999–2007.
- [167] Jenske, R.; Vetter, W. *J. Agric. Food Chem.* **2008**, *56*, 11578–11583.
- [168] Tareq, F. S.; Lee, M. A.; Lee, H.-S.; Lee, J.-S.; Lee, Y.-J.; Shin, H. *J. Mar. Drugs* **2014**, *12*, 871–885.
- [169] Moon, K.; Lim, C.; Kim, S.; Oh, D. C. *J. Chromatogr. A* **2013**, *1272*, 141–144.
- [170] Van Rensburg, C.E.; Joone, G.K.; O’Sullivan, J.F.; Anderson, R. *Antimicrob. Agents and Chemother.* **1992**, *36*, 2729–2735.
- [171] Li, J. W.-H.; Vederas, J. C. *Science* **2009**, *325*, 161–165.
- [172] Lu, B. L.; Williams, G. M.; Brimble, M. A. *Org. Biomol. Chem.* **2020**, *18*, 5073–5094.
- [173] Rychnovsky, S. D.; Rogers, B. N.; Richardson, T. I. *Acc. Chem. Res.* **1998**, *31*, 9–17.
- [174] Iwamori, M.; Costello, C.; Moser, H. W. *J. Lipid Res.* **1979**, *20*, 86–96.
- [175] Shing, T. K. M.; Wong, A. W. F.; Ikeno, T.; Yamada, T. *J. Org. Chem.* **2006**, *71*, 3253–3263.

- [176] Batra, H.; Moriarty, R. M.; Penmasta, R.; Sharma, V.; Stanciuc, G.; Staszewski, J. P.; Tuladhar, S. M.; Walsh, D. A.; Datta, S.; Krishnaswamy, S. *Org. Process Res. Dev.* **2006**, *10*, 484–486.
- [177] Jayakanthan, K.; Johnston, B. D.; Pinto, B. M. *Carbohydr. Res.* **2008**, *343*, 1790–1800.
- [178] Ji, Y.; Xin, Z.; He, H.; Gao, S. *J. Am. Chem. Soc.* **2019**, *141*, 16208–16212.
- [179] Mun, J.; Onorato, A.; Nichols, F. C.; Morton, M. D.; Saleh, A. I.; Welzel, M.; Smith, M. B. *Org. Biomol. Chem.* **2007**, *5*, 3826–3833.
- [180] Taber, D. F.; Zhang, Z. *J. Org. Chem.* **2006**, *71*, 926–933.
- [181] Blakemore, P. R.; Cole, W. J.; Kociński, P. J.; Morley, A. *Synlett* **1998**, *1998*, 26–28.
- [182] Ayers, B. J.; Ngo, N.; Jenkinson, S. F.; Martínez, R. F.; Shimada, Y.; Adachi, I.; Weymouth-Wilson, A. C.; Kato, A.; Fleet, G. W. J. *J. Org. Chem.* **2012**, *77*, 7777–7792.
- [183] Estevez, J. C.; Fairbanks, A. J.; Fleet, G. W. J. *Tetrahedron* **1998**, *54*, 13591–13620.
- [184] Mitra, R. N.; Show, K.; Barman, D.; Sarkar, S.; Maiti, D. K. *J. Org. Chem.* **2019**, *84*, 42–52.
- [185] Jad, Y. E.; Khattab, S. N.; de la Torre, B. G.; Govender, T.; Kruger, H. G.; El-Faham, A.; Albericio, F. *Eur. J. Org. Chem.* **2015**, 3116–3120.
- [186] Takano, D.; Nagamitsu, T.; Ui, H.; Shiomi, K.; Yamaguchi, Y.; Masuma, R.; Kuwajima, I.; Ōmura, S. *Org. Lett.* **2001**, *3*, 2289–2291.
- [187] Zhao, M. M.; Li, J.; Mano, E.; Song, Z. J.; Tschaen, D. M. *Org. Synth.* **2005**, *81*, 195–203.
- [188] Cheng, J. M. H.; Chee, S. H.; Knight, D. A.; Acha-Orbea, H.; Hermans, I. F.; Timmer, M. S. M.; Stocker, B. L. *Carbohydr. Res.* **2011**, *346*, 914–926.
- [189] Park, J. K.; McQuade, D. T. *Angew. Chem. Int. Ed.* **2012**, *51*, 2717–2721.
- [190] Tiefenbacher, K.; Arion, V. B.; Mulzer, J. *Angew. Chem. Int. Ed.* **2007**, *46*, 2690–2693.
- [191] Fukase, H.; Satoshi, H. *J. Org. Chem.* **1992**, *57*, 3642–3650.
- [192] Sun, Z.-F.; Zhou, L.-N.; Zhang, T.; Du, Z.-T. *Chin. Chem. Lett.* **2017**, *28*, 558–562.
- [193] World Health Organization. *Global tuberculosis report 2020*, **2020**. [cited: 2020 December 01]. Retrieved from: <https://apps.who.int/iris/bitstream/handle/10665/336069/9789240013131-eng.pdf>.
- [194] Ma, Z.; Lienhardt, C.; McIlleron, H.; Nunn, A. J.; Wang, X. *Lancet* **2010**, *375*, 2100–2109.
- [195] Garrido-Cardenas, J. A.; de Lamo-Sevilla, C.; Cabezas-Fernández, M. T.; Manzano-Agugliaro, F.; Martínez-Lirola, M. *Tuberculosis* **2020**, *121*, 101917.
- [196] Yuan, T., Sampson, N. S. *Chem. Rev.* **2018**, *118*, 1887–1916.
- [197] Mabhula, A.; Singh, V. *Med. Chem. Commun.* **2019**, *10*, 1342–1360.

- [198] World Health Organization. *Global tuberculosis report 2018*, 2018. [cited: 2020 November 30]. Retrieved from: <https://apps.who.int/iris/bitstream/handle/10665/274453/9789241565646-eng.pdf?sequence=1&isAllowed=y>.
- [199] Deoghare, S. *Indian J. Pharmacol.* **2013**, *45*, 536–537.
- [200] Munsiff, S. S.; Kambili, C.; Ahuja, S. D. *Clinical Infectious Diseases* **2006**, *43*, 1468–1475.
- [201] Nueremberger, E.; Kendall, E. *Delamanid and pretomanid*. In: Kucers the Use of Antibiotics: A Clinical Review of Antibacterial, Antifungal, Antiparasitic, and Antiviral Drugs (7th ed.). CRC Press, **2017**, 2550-2558.
- [202] Mariani, R.; Granata, G.; Maffioli, S. I.; Serina, S.; Brunati, C.; Sosio, M.; Marazzi, A.; Vannini, A.; Patel, D.; White, R.; Ciabatti, R. *Bioorg. Med. Chem. Lett.* **2005**, *15*, 3748–3752.
- [203] Su, C.-C.; Klenotic, P. A.; Bolla, J. R.; Purdy, G. E.; Robinson, C. V.; Yu, E. W. *PNAS* **2019**, *116*, 11241–11246.
- [204] Pethe, K.; Bifani, P.; Jang, J. *et al. Nature medicine* **2013**, *19*, 1157–1160.
- [205] Tenero, D.; Derimanov, G.; Carlton, A.; Tonkyn, J.; Davies, M.; Cozens, S.; Gresham, S.; Gaudion, A.; Puri, A.; Muliaditan, M.; Rullas-Trincado, J.; Mendoza-Losana, A.; Skingsley, A.; Barros-Aguirre, D. *Antimicrob. Agents Chemother.* **2019**, *63*, e00240–00259.
- [206] Grant, A.; Gothard, P.; Thwaites, G. *BMJ* **2008**, *337*, a1110.
- [207] Lelovic, N.; Mitachi, K.; Yang, J.; Lemieux, M. R.; Kurosu, M. *J. Antibiot.* **2020**, *73*, 780–789.
- [208] Corbaz, R.; Ettliger, L.; Gäumann, E.; Keller-Schierlein, W.; Kradolfer, F.; Neipp, L.; Prelog, V.; Zähler, H. *Helv. Chim. Acta* **1955**, *38*, 1445–1448.
- [209] Woo, A. J.; Strohl, W. R.; Priestley, N. D. *Antimicrob. Agents Chemother.* **1999**, *43*, 1662–1668.
- [210] Nakatsuka, S.; Feng, B.; Goto, T.; Kihara, K. *Tetrahedron Lett.* **1986**, *27*, 3399–3402.
- [211] Zheng, B.; Trieu, T. H.; Meng, T.-Z.; Lu, X.; Dong, J.; Zhang, Q.; Shi, X.-X. *RSC Adv.* **2018**, *8*, 6834–6839.
- [212] Shiomi, K.; Hatae, K.; Hatano, H.; Matsumoto, A.; Takahashi, Y.; Jiang, C.-L.; Tomoda, H.; Kobayashi, S.; Tanaka, H.; Omura, S. *J. Antibiot.* **2005**, *58*, 74–78.
- [213] Li, Y.; Zhao, M.; Parkin, K. L. *J. Agric. Food Chem.* **2011**, *59*, 2332–2340.
- [214] Tang, J.-G.; Wang, Y.-H.; Wang, R.-R.; Dong, Z.-J.; Yang, L.-M.; Zheng, Y.-T.; Liu, J.-K. *Chem. Biodiversity* **2008**, *5*, 447–460.
- [215] Wang, Y.-H.; Tang, J.-G.; Wang, R.-R.; Yang, L.-M.; Dong, Z.-J.; Du, L.; Shen, X.; Liu, J.-K.; Zheng, Y.-T. *Biochem. Biophys. Res. Commun.* **2007**, *355*, 1091–1095.

- [216] Richter, M. F.; Drown, B. S.; Riley, A. P.; Garcia, A.; Shirai, T.; Svec, R. L.; Hergenrother, P. J. *Nature* **2017**, *545*, 299–304.
- [217] Cox, E. C.; Cook, J. M. *Chem. Rev.* **1995**, *95*, 1797–1842.
- [218] Badland, M.; Crook, R.; Delayre, B.; Fussell, S. J.; Gladwell, I.; Hawksworth, M.; Howard, R. M.; Walton, R.; Weisenburger, G. A. *Tetrahedron Lett.* **2017**, *58*, 4391–4394.
- [219] Saxon, E.; Bertozzi, C. R. *Science* **2000**, *287*, 2007–2010.
- [220] Eckhardt, K.; Thrum, H.; Bradler, G.; Fuegner, R. *Antibiotiki* **1965**, *10*, 603–612.
- [221] Stroshane, R. M.; Chan, J. A.; Rubalcaba, E. A.; Garretson, A. L.; Aszalos, A. A.; Roller, P. P. *J. Antibiot.* **1979**, *32*, 197–204.
- [222] Lin, Z.; Zachariah, M. M.; Marett, L.; Huguen, R. W.; Teichert, R. W.; Concepcion, G. P.; Haygood, M. G.; Olivera, B. M.; Light, A. R.; Schmidt, E. W. *J. Nat. Prod.* **2014**, *77*, 1224–1230.
- [223] Ortega, H. E.; Batista, J. M.; Melo, W. G. P.; Clardy, J.; Pupo, M. T. *Tetrahedron Lett.* **2017**, *58*, 4721–4723.
- [224] Atkinson, D. J.; Furkert, D. P.; Brimble, M. A. *Tetrahedron* **2015**, *71*, 91–101.
- [225] Yang, J.; Fan, S.; Pei, H.; Zhu, B.; Xu, W.; Naganawa, H.; Hamada, M.; Takeuchi, T. *J. Antibiot.* **1991**, *44*, 1277–1279.
- [226] Panzone, G.; Trani, A.; Ferrari, P.; Gastaldo, L.; Colombo, L. *J. Antibiot.* **1997**, *50*, 665–670.
- [227] Yunt, Z.; Reinhardt, K.; Li, A.; Engeser, M.; Dahse, H.-M.; Gütschow, M.; Bruhn, T.; Bringmann, G.; Piel, J. *J. Am. Chem. Soc.* **2009**, *131*, 2297–2305.
- [228] Ueno, T.; Takahashi, H.; Oda, M.; Mizunuma, M.; Yokoyama, A.; Goto, Y.; Mizushima, Y.; Sakaguchi, K.; Hayashi, H. *Biochemistry* **2000**, *39*, 5995–6002.
- [229] Rosenthal, I.; Wolfram, E.; Peter, S.; Meier, B. *J. Nat. Prod.* **2014**, *77*, 3, 489–496.
- [230] Omosa, L. K.; Midiwo, J. O.; Mbaveng, A. T.; Tankeo, S. B.; Seukep, J. A.; Voukeng, I. K.; Dzotam, J. K.; Isemeki, J.; Derese, S.; Omolle, R. A.; Efferth, T.; Kuete, V. *SpringerPlus* **2016**, *5*, 901.
- [231] Mukne, A. P.; Viswanathan, V.; Phadatare, A. G. *Pharmacogn. Rev.* **2011**, *5*, 13–18.
- [232] Shaaban, M.; El-Metwally, M. M.; Nasr, H. *Nat. Prod. Res.* **2014**, *28*, 86–94.
- [233] Netz, N.; Opatz, T. *Mar. Drugs* **2015**, *13*, 4814–4914.
- [234] Harvey, A.; Edrada-Ebel, R.; Quinn, R. *Nat. Rev. Drug Discov.* **2015**, *14*, 111–129.
- [235] Atanasov, A. G.; Zotchev, S. B.; Dirsch, V. M.; Supuran, C. T. *et al. Nat. Rev. Drug Discov.* **2021**, 1–17 (online ahead of print: doi: 10.1038/s41573-020-00114-z).

- [236] Walter, T.; Collenburg, L.; Japtok, L.; Kleuser, B.; Schneider-Schaulies, S.; Müller, N.; Becam, J.; Schubert-Unkmeir, A.; Kong, J. N.; Bieberich, E.; Seibel, J. *Chem. Commun.* **2016**, 52, 8612–8614.
- [237] Chen, Y. K.; Joen, S.-J.; Walsh, P. J.; Nugent, W. A. *Org. Synth.* **2005**, 82, 75.
- [238] Batra, H.; Moriarty, R. M.; Penmasta, R.; Sharma, V.; Stanciuc, G.; Staszewski, J. P.; Tuladhar, S. M.; Walsh, D. A.; Datla, S.; Krishnaswamy, S. *Org. Process Res. Dev.* **2006**, 10, 484–486.
- [239] Fürstner, A.; Flügge, S.; Larionov, O.; Takahashi, Y.; Kubota, T.; Kobayashi, J. *Chem. Eur. J.* **2009**, 15, 4011–4029.
- [240] Collins, L.; Franzblau, S. G. *Antimicrob. Agents Chemother.* **1997**, 41, 1004–1009.

10. Project contributions

Dereplication was performed by Dr. FLORIAN ZUBEIL and Dr. MARIA A. PATRAS. Moreover, they contributed to this work by establishing the Molecular Networking platform and instructing its use, respectively.

JENNIFER KUHN and CHRISTINE WEHR (supervised by Dr. SANJA MIHAJLOVIC) performed the fermentation of all producer strains as well as the media variation.

NMR measurement and data interpretation regarding structure elucidation was performed or supported by MICHAEL KURZ¹² (Sanofi, Germany), MARC-PHILIPPE MAITRE¹³ (Sanofi Pasteur, France) and Dr. HEIKE HAUSMANN (JLU Gießen).

KIRSTEN BOMMERSHEIM, Dr. BENEDIKT LEIS and Dr. MICHAEL MARNER contributed by performing the in-house MIC determination.

Other bioassays were performed by Evotec (Lyon/Toulouse, France). This included: i) MIC determination against *M. tuberculosis* by STEPHANIE SANS, ii) cytotoxicity assays CORINNE LAFON and iii) TLR2/TLR4 assays PATRICIA LABOUDIE and their teams.

The total synthesis of FE004 was carried out in cooperation with YOLANDA KLEINER. Furthermore, Dr. CHRISTOPH PÖVERLEIN (Sanofi, Germany) contributed to this project by providing synthesized building blocks and performing certain reaction steps besides technical support.

¹² Compound **29b**, **39**, **40**, *ent*-**53a**, **58**, **61**, **63** and **150**

¹³ Compound **71** and **90**

